Technical Transactions

Czasopismo Techniczne

Contents

Wiesława Gadomska orcid.org/0000-0002-0456-4837
wiga@uwm.edu.pl
Department of Landscape Architecture, University of Warmia and Mazury in Olsztyn

Modern park as a result of urban space recycling
– a review of new york city's developments

Współczesny park jako efekt recyklingu przestrzeni miejskiej
– przegląd nowojorskich realizacji

Abstract

The development of organized green areas in the specific circumstances of New York's "culture of concentration" [1, p. 10] takes place, among others, in areas whose original function has changed or found a new peripheral location. Many projects related to transport, storage, or freight forwarding have been completed in post-industrial areas. The issue of urban space *recycling*, besides the basic question of adapting the area to a new function, requires a particular reference to the cultural heritage of the place, including its material legacy, which is sometimes difficult to preserve and expose. This article presents characteristic examples of urban **recycling** in particular districts of New York where the new function of a city park has been overlaid on unused areas, while preserving their characteristic environmental circumstances and cultural identities.

Keywords: space *recycling*, revitalization, gentrification, city parks, cultural and environmental circumstances

Streszczenie

Rozwój terenów urządzonej zieleni miejskiej w szczególnych uwarunkowaniach „kultury zagęszczenia" Nowego Jorku [1, s.10] odbywa się między innymi w obszarach, których pierwotna funkcja wygasła lub znalazła nową, peryferyjną lokalizację. W wielu zrealizowanych przypadkach wykorzystano tereny poprzemysłowe, związane z transportem, magazynowaniem i spedycją.. Problematyka recyklingu przestrzeni miejskiej, poza podstawowym zagadnieniem adaptacji terenu do nowej funkcji, wymaga szczególnego odniesienia się do kulturowego dziedzictwa miejsca – w tym jego materialnej spuścizny, niejednokrotnie trudnej w zachowaniu i ekspozycji. Artykuł prezentuje charakterystyczne przykłady miejskiego recyklingu realizowanego w poszczególnych dzielnicach Nowego Jorku, prowadzącego do wpisania nowej funkcji parku miejskiego w zdewaluowaną przestrzeń z zachowaniem jej charakterystycznych środowiskowych uwarunkowań i kulturowej tożsamości.

Słowa kluczowe: recykling przestrzeni, rewitalizacja, gentryfikacja, park miejski, uwarunkowania kulturowe i środowiskowe

1. Introduction

The clear symptomatic trend of laying new functions over inactive parts of the city is exemplified by East River Park, located on the eastern shore of lower Manhattan. The park, which was completed along with the building of East River Drive (a large transport project) was opened in 1939; the 20-hectare area absorbed, among others, the 19th century docking ports and warehouses located along the East River [2, p. 187]. Despite its ambitious functional design, the enterprise, financed from the federal budget, lacked any reference to the original function of the area, which was essential to the life of the district and the city. The realized development effectively diluted the scale, spatial system, and the characteristic artefacts of the waterfront part of the Lower East Side, which now can only be deduced through an analysis of historical maps and iconographic materials [3, p. 132]. From the point of view that was common at the beginning of the 20th century, such a development went well with the overall planning strategy of the city [2], but the results became evident much later[1].

A contemporary comparative analysis of the west and east shore of lower Manhattan can easily identify the differences in the attitudes towards the *recycling* of unused urban spaces which took place nearly a century apart. The development of Hudson River Park, a nearly 10-kilometer-long linear park marked out along the west shore of lower and mid-town Manhattan, set a specific standard in the reuse of exploited, degraded urban space, whilst preserving its cultural origins [5, 175]. The Master Plan, elaborated in 1997, provided for division of the development into seven segments that made up a coherent whole; however, the project took into account the local diversity and uniqueness of the district [6]. The first segment of the park was opened in 2003; the others were completed in subsequent years. As a result of consistent investment, the inactive areas of ports and warehouses acquired the new, attractive function of a park that complemented the local urban fabric [7]. Preserving the cultural heritage of the area and its identity in the city landscape was crucial to the entire development; these conditions included a characteristic spatial layout with a sequence of nearly one hundred port jetties, some of which acquired new recreational functions, while others underwent a process of controlled entropy, introducing the dimension of time into these new urban spaces. As of 2015, the total development was 70 per cent complete, creating an undisputed standard of excellence in the process of green area development and urban space *recycling* [8].

2. Recycling, revitalization, and gentrification of urban space

By way of *recycling* inactive areas of the city, their spaces assume new functions and forms of use[2]. Significant transformations of post-industrial areas of New York into parks appeared in the city landscape at the end of the 20th century [10]. The scale of recycling in the urban space of New York is remarkable. Along with the successful recycling of the space recovered for public

---

[1]   A comprehensive criticism of urban planning which ignores the local character of the area can be found in Jane Jacob's book "The Death and Life of Great American Cities", published in 1961 [4].

[2]   Apart from frequent commercial and residential investments, it also includes a city park [9].

green areas of New York, there was an intense revitalization of inactive areas of the city, together with an evident gentrification of the surroundings [11] and improvements in environmental conditions[3]. The very positive evaluation of the completed projects remains closely related to improving the quality of urban spaces, which acquire a new, attractive function, an image based on the cultural identity of the area, as well as better operating conditions[4]. It should be noted that the projects designed by public sector architects were of high quality [13].

3. Parks in the process of urban space recycling – characteristic examples in manhattan and its close vicinity

▶ MANHATTAN, Governors Island – a park in the former military zone.

Governors Island, nearly a kilometre away from the southern tip of Manhattan[5], used to constitute a strategic point of New York's military defence. Between 1800 and 1996[6] the nearly 70-hectare area of the island was a closed zone serving as an administrative and logistical base for the US army and finally as a local base for the US Coast Guard. The interesting cultural accumulations (mainly in the former fortifications and the historical spatial system of the housing base) led to the granting of National Historic Landmark status to a significant part of the island.

At the end of the 20th century, the final termination of the island's defensive function and the decentralization of the administrative structures inside this closed, inaccessible area led to interesting investment opportunities[7] in this attractively located city area[8] and its efficient ferry connection (Fig. 1). The final character of the island's development was determined by way of

---

[3] Including, for instance, the improvement in the water and soil quality, reduction of noise, retention of rainwater.

[4] New park projects are often the winners of architecture competitions; it is also a common practice to commission project designs to landscape architects with acknowledged work experience [12].

[5] In the administrative sense, Governors Island belongs to Manhattan.

[6] In 1800, the state of New York ceded the island to the federal government; in subsequent years important military objects and an administrative base for the American military were located on the island. During the First World War it served as a logistical base for troops dispatched to Europe. During WWII it was mainly an administrative center and a recruitment point. In 1966 the military importance of the island expired when the US Department of State decided to reduce the military installations. The specific location of the island was still utilized – this time as a base for the US Coast Guard. After 30 years in operation, the base was closed in 1996 [14].

[7] The Van Allen Institute offered a broad open contest entitled "Public property" in 1996. The aim was to examine the potential of the island in its broad urban, cultural, and eco-physiographic context. Proposals submitted by 200 participants from 14 countries proved to be deeply absorptive of the place and flexible as to its future function. The major value of the contest, however, was sparking off a debate on open, public access to the island and giving the place an active recreational, cultural and innovative character [15].

[8] In 2005, Santiago Calatrava, at the request of New York's mayor, prepared a draft project to connect Governors Island to Manhattan and Brooklyn with a cable car. The objective was to efficiently connect the island to the rest of the city; a visually light structure based on three structural pylons was planned to introduce an interesting, lapidary spatial form into the landscape of New York Bay. This bold proposal was never realized, one of the reasons being the high projected cost of the investment [15].

a closed design contest in 2006 by the non-profit Trust for Governors Island[9] organization; the master plan was elaborated in 2010 and covered the southern part of the island, which was free of historical buildings and valuable cultural accumulations.[10] The plan covered an area of over 35 hectares, or nearly half of the island's area. Half of this space was allocated to a park; the remaining area became a development zone with hotel, conference, and education functions in mind. The key element of the project was the synthetic inclusion of the planned park into the existing cultural space of the island, with regard to the many circumstances determined by its location, including the potential threat of flooding from New York Bay.[11]

The composition of the park was based on a nodal point in the geometric centre of the island where the historical urban interior permeated the projected terrain of a contemporary park. In a manner symptomatic of the newly created urban landscapes of New York [17], the key issues of natural and cultural circumstances of the proposed space were treated synergistically. A far-reaching intervention into the original flat landscape of the island led to the elevation of the terrain [12]; this provided shelter against high winds and potential flooding of the park, and, at the same time improved the landscape value of the surrounding area (Fig. 2).

The two-phase development of the park was completed in the middle of 2016. The tourist turnout since then suggests a high level of acceptance of the idea of creating a new public space in the specific context of a satellite area away from the urbanized core of the city.[13] The process of the island's revitalization will be finally finished when the new investment in the designated development zones is completed.

---

9   The short list of finalists: Field Operation / Wilkinson Eyre Architects *New York, USA / London, United Kingdom*; Hargreaves Associates / Michael Maltzan Architecture, Inc. *New York, USA / Los Angeles, USA*; Ramus Ella Architects (REX) / Michel Desvigne Paysagistes (MPD) *New York, USA / Paris, France*; West 8 urban design landscape architecture b.v. / Rogers Marvel Architects / Diller Scofidio + Renfro *Rotterdam, The Netherlands / New York, USA*; WRT LLC / Weiss / Manfredi / Urban Strategies. Inc. *Philadelphia, USA / New York, USA / Toronto, Canada* [14].
    In December 2007, the contest winner was announced: the international design studio West 8 Urban Design Landscape Architecture, which was set up in 1987. It is an international studio specializing in designs for urban planning and landscape architecture; apart from its headquarters in Holland, it has an office in Belgium, and, upon winning the contest, also in New York. It is worth noting that, among the studio's many projects realized in Europe, West 8 took part in the "City of Tomorrow" exhibition in Malmö in 2001, which placed emphasis on the issues of ecology and sustainable development and the identity of the local landscape [16].

10 In 2001, the northern, nearly 9-hectare side of the park, where the most valuable historical buildings (for example, Fort Jay and Castle Williams) are located, was granted the status of Governors Island National Monument and brought under the federal administration of the National Park Service.

11 New York lies in a hurricane hazard zone and is susceptible to possible consequences such as the flooding of low-lying coastal areas; since the 17th century New York has suffered from over 80 hurricanes; the last one, Hurricane Sandy in 2012, caused catastrophic damage, flooding the area of lower Manhattan; this threat is of a recurring and escalating character.

12 As a result of macro-levelling measures, the central part of the park was elevated, while the terrain slopes down toward the shoreline. In the southern part, a zone of controlled flood retention was established and complemented with plants of naturally high water retention. To protect the area against high winds, four artificially built hills were constructed in the windward part of the island. These hills, with their vast bases and heights between 7 and 21 meters, constitute a sort of breakwater defense that protects the park and the island's interior [18].

13 When the military function expired, wider access to tourism was made possible in 2005, when it was visited by 8 thousand people. The park was opened to the public in May 2014 (first phase), which raised the number of visitors to 450 thousand in 2015 [19].

Fig. 1. Ferry harbour in Governors Island (photo by W. Gadomska)

Fig. 2. Shaped terrain elevations (photo by W. Gadomska)

▶ BROOKLYN – Brooklyn Bridge Park, adaptation of the waterfront and the closed port docks

Historically, the western shore of Brooklyn – an important port serving the majority of transatlantic and continental freight traffic – was part of an essential element of New York's metropolitan structure. The logistical value of the district followed from the favourable geographical location on the estuary of two important rivers (The Hudson River and the East River) into New York Bay and the open ocean. The area particularly predestined for the port and storage function was the stretch of the Brooklyn shore that is close to the southern tip of Manhattan; from 1814 a regular ferry connection between Manhattan and Brooklyn was in operation, and in 1883 both banks were connected with the Brooklyn Bridge. The turn of the century was a period of intense development of the port infrastructure and the land-based facilities which included warehouses, cold stores, factory buildings, etc., all of which exert a heavy influence on the characteristic shoreline, local landscape, and the evasive peculiarity of the place.[14]

The gradual termination of the port and the storage functions of New York's shores began in the 1980s and was, among other factors, a consequence of the consistent development of port and shipment infrastructure[15] in the neighbouring state of New Jersey. In 1984, the Port Authority, an interstate agency in charge of ports, [21] decided to sell a stretch of the shore together with six jetties and several buildings. A local community group, the Friends of Fulton Ferry Landing, which later developed into Brooklyn Bridge Park Conservancy, protected this attractive area from commercial use by developers.

The idea that the freed space could be filled with a park took shape [22] in the 1990s and the master plan was elaborated in 1998. The park project provided for the adaptation of the six port jetties and a connection – via a wide stretch of greenery – to a waterfront promenade of winding pathways and bicycle lanes [23]. As a result, an attractive linear park came to life (designed by landscape architect Michael Van Valkenburgh) of over 2 kilometres in length and an area of 34 hectares,[16] including interesting formal developments and rich functionalities.

Brooklyn Bridge Park exemplifies a holistic approach to urban recycling, operating at different scales and using various techniques of preserving the cultural uniqueness of the place. Besides the basic revitalization of the inactive area in the original port and dock configuration, the original profile of the port waterfront, created by characteristic saddle roofs, was well-preserved. On one of the jetties, the roof cover was adapted for a team sports area; on two other jetties the pillars of the steel structures were used as support for modern sun shading structures. In the construction, many architectural details used the existing elements of the park: the original timber from the demolished port warehouses was recycled [23], while stone blocks retrieved during the modernization of one of New York's bridges were built into some parts of the development. The designed reconfiguration of the land area of the park was completed using soil extracted in civil engineering projects in various parts of the city.

---

[14] Excerpt of Harvey Shapiro's poetry (1924–2013) "National Cold Storage Company" 1966.
[15] Container Transport System [20, p. 310–311].
[16] The park's completion was the largest enterprise in Brooklyn since the establishment of Prospect Park; opened in 1867, at 215 ha this is the largest park in the district [24, p. 286].
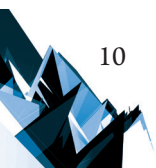
This new public space in Brooklyn has become part of the landscape relations in the city. The park arrangement and the reshaping of its terrain allow the lower Manhattan skyline to be viewed from a new perspective which has never been taken advantage of before[17] (Fig. 3). The value of the park as a vantage point is closely related to the evident changes in the city panorama, for example, in the area of the World Trade Center [25]. On the other hand, Brooklyn Park has established itself as a new, important element of the landscape as seen from southern Manhattan,[18] bringing the much-transformed port area into the urban space.

Fig. 3. Recreational lawn with a view of Manhattan (photo by W. Gadomska)

Besides the preservation and exposition of a culturally significant district of New York, the completion of the new project ushered in a new type of urban landscape with highly efficient sustainable functions in a metropolitan space. In addition to the basic preservation of the rich local biocenosis (Fig. 4), the park is also an area for rational rainwater management and solar energy production for its own use to offset the negative consequences of the city's development.[19]

---

[17] The views from high elevations have been possible since the middle of the last century thanks to the vast Brooklyn-Heights Promenade that runs above the Brooklyn-Queens Expressway, while the view from the level of the shore was limited due to difficult access to the shoreline.

[18] Among other points, Elevated Acre Park provides excellent observation conditions.

[19] They may include, among others, the negative influence of the transport system within New York, which was expanded in the first half of the 20th century and generates serious spatial and environmental consequences,

Fig. 4. Biodiversity of the coastal part of the park (photo by W. Gadomska)

▶ QUEENS – Gantry Plaza State park, adaptation of a former trans-shipment hub

In the 19th century, the neighbourhood of Hunters Point[20] (the western side of Queens on the East River) was a convenient area for the district's industrial development. The well-developed shoreline of the East River, the Queensboro Bridge[21] (raised in 1909) connection to Manhattan, and the close vicinity of the industrially advanced Brooklyn predisposed this place for storage and production functions. The expansion of the Long Island Rail Road[22] made the area an important freight forwarding point. The favourable conditions stimulated the growth of the district over the decades, which saw the development of multi-industrial sweat shops, factories, and warehouses. The character of the district began to change in the last decades of the 20th century due to the global shift in economic geography and the

including noise. The shape of the park in the form of an elevated embankment running parallel to the three-level Brooklyn-Queens Expressway artery helps reduce the level of noise by a noticeable margin.

[20] Historically, Hunters Point was a part of Long Island City, which until 1898 was an autonomous settlement independent of New York City.

[21] Since 2011, the official name of the bridge is Ed Koch Bridge (Edward Irwin Koch was the mayor of New York from 1978–1989).

[22] Modified several times, The Long Island Rail Road has been in operation since 1834.

consistent relocation of the industrial and logistic centres of American cities to outside of their boundaries.[23] The industrial shore of Queens lost its economic character. The high-rise Citicorp office at Court Square [26] (designed in 1989) and the New York home of the PS 1 Contemporary Art Center (now MoMA PS 1) [27, p. 293] in an empty public-school building in a desolated area were local landmarks. At the same time, the close vicinity of Manhattan and the good connections with other city boroughs opened up new opportunities for real estate development on a large scale.

Clear signals of the search for new functions to redefine the spatial character of Queen's western shore appeared in the last decade of the 20th century. First, the Master Plan was elaborated in 1993–1995, then the Gantry Plaza State Park project was designed to become the first phase of the development of the nearly 8-hectare area along the East River (designed by landscape architect Thomas Balsley) [10, p. 17–27]. The first stretch of the park was completed in 1998; the interesting utility program[24] and the attention paid to take into account the cultural context of the location set a high standard for a new public space.

Fig. 5. Historical cranes bearing witness to the area's tradition (photo by W. Gadomska)

---

[23]   A. Toffler in his works characterized the origin, scale and consequences of the phenomenon, e.g. in "The Third Wave".

[24]   Designed on the four jetties were characteristic seats, crab fishing stands, a table for cleaning fish, etc.
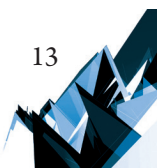
Gantry Plaza State Park's composition was determined by two clear directions in the local space: its direction parallel to the shoreline defined the course of the multi-track foot promenade, while the direction perpendicular to the shoreline was determined by the remains of the tracks of the former rail branch line. The central area of the park adapted the former cargo shipment square (previously located where the land meets the river) and its historical technical infrastructure, dominated by two high dockside gantry cranes from 1925 that enabled the transfer of cargo (Fig. 5). The artefacts of the former cranes were used to create new landscape relations in the place and their frame structures create attractive views of the skyline of midtown Manhattan. (Fig. 6). Besides the conservation role of the adaptation of the old industrial space for the needs of the park, the former function of the area was symbolically preserved: the water transport tradition of the city is continued by the terminal for water taxis and ferries on one of the four jetties flanking the massive pillars of the cranes.

Starting at the end of the 20th century, the process of the post-industrial recycling of Queens' shores led to the structural exchange of local functions, which exerted an influence over a wide spatial context. In 2013, the new Hunter's Point South Park became a natural extension of Gantry Plaza State Park. This newly-created green area is the foundation for a spatial composition of a 30-hectare multi-function neighbourhood, including residential areas complemented with educational, commercial, and service functions [28].

Fig. 6. Skyline of Manhattan exposed from the recreational jetties (photo by W. Gadomska)

4. Recycling in urban space – second plan developments

the interesting results of turning inactive urban areas into active park areas are also discernible in former industrial districts outside the city centre[25]. For the presented secondary developments, the original conditions included the peripheral location, the definitely worse transport links to the city, and the more frequent degradation of the area as a result of its industrial function. The key factor, however, was the landscape context, which exerts a heavy influence on the local space and is dominated by post-industrial forms and technical artefacts of a significant scale.[26] Through urban recycling, post-industrial areas whose locations are less amenable to adaptation have acquired a new function as parks, which are much desired in metropolitan circumstances and which preserve and expose the well-defined cultural landscape.

▶ BROOKLYN – Erie Basin Park, revitalization of historical shipyard areas

The park opened in 2008 in a historical harbour of Brooklyn port, which until the beginning of the 20th century was the most important point of freight shipment on the east coast of the USA. Apart from being a harbour, the areas close to Red Hook peninsula, on the waters of New York Bay, used to be home to shipyard plants, warehouses, storage areas and housing estates for shipyard workers. This rapidly growing section of Brooklyn began to lose its importance in the second half of the 20th century as its primary port function was marginalized by the containerization of freight shipments. The former area of intense port and industrial activity underwent gradual economic, social, and visual degradation. Despite the marginalization, the ship-repair yard, with its valuable 19th-century dry dock and well-preserved shipyard infrastructure, survived the transformation [30]. This area attracted a large investor who is planning to build a department store for a global retail network.

The park project,[27] initiated in 2002, was an indispensable part of the negotiations and changes to the local zoning plan, which enabled the realization of a controversial investment enterprise on a scale that would dominate the local landscape. Of the planned public-private partnership of the 9 hectares of land for development, nearly 30 per cent would be occupied by the park. On such conditions, the city sold the area of the former shipyard to a private investor [30].

The park's composition was based on the industrially shaped shore, including the characteristic remains of the shipyard's past: technical jetties, the repair dock gate, and the mooring infrastructure. The development of the two-kilometre shore created a characteristic linear park, spatially defined by the four port cranes that dominate the landscape with their height (Fig. 7). The artefacts of the technical equipment on the shore were clearly exposed and

---

[25]   In the case of New York, defining a traditional downtown area is difficult: "*Manhattan has no center… if you asked a New Yorker for directions to ´the center of town´, he would be bewildered".* James Traub, 2011.

[26]   This daring adaptation of the post-industrial landscape to the needs of a modern park was made by Richard Haag, *Gas Works Park*, Seattle, 1975 [29].

[27]   The project authors: Lee Weintraub Landscape Architecture , LLC, New York [30].

combined in theme blocks: the port rigging, shipyard devices, and mooring lines. The park area was also complemented with an interesting detail: customized steel daybeds (Fig. 8.), sets of benches, lettering with the park's name, and lighting. The reminiscent character of the park is complemented with a narration layer that corresponds with the spatial context: iconographic materials, shipyard worker's memories, and names of repaired vessels recorded on boards and reliefs. A characteristic motive which distinguishes the park area is the diagonal textured lines in the transport planes and in the vertical planes of the railings running along the preserved jetties, all of which constitute a clear reference to the rigging of ships when the shipyard was prosperous.

The park's development plan took into account some critical landscape issues related to both its location in the New York metropolis and in the local neighbourhood. The north-western side of the park was designed as a rectangular, green plain of elevated terrain; it is part of the attractive landscape exposition which accentuates the unique panorama of the industrial landscape of Red Hook against the characteristic skyline of southern Manhattan. On the other hand, the consistently designed green area and a sequence of screens which sets this section of the park apart compose an idiosyncratic vantage filter which limits the view of the large-scale commercial building.

The park, which has been open for 8 years, has clearly raised the standard of the marginalized post-industrial zone, contributing to its revitalization and gentrification. What turned out to

Fig. 7. Port cranes of the former ship-repair yard (photo by W. Gadomska)

Fig. 8. Steel daybeds (photo by W. Gadomska)

be a crucial factor was the creation of an alternative water transport route that links southern Manhattan to the mooring jetty which is now part of the park. In the designer's intention, the park was supposed to spur reflection on the global changes that are causing irreversible relocation of production to outside of the homeland, which, in consequence, leads to the termination of traditionally American industries. Besides the consumers who purchase goods in the retail centre, the park serves the local community[28] and makes an attractive place to visit for New Yorkers and tourists who appreciate the cultural dimension of the enterprise.

▸ BRONX – Concrete Plant Park, recycling of the degraded cement production plant

The main parks of the Bronx are concentrated in the northern[29] and central[30] parts of the district, marking a noticeable disproportion in the number, area, and access to organized green areas in the southern neighbourhoods. To address this, new parks are being established

---

[28]   The park made it possible for the residents of the neighboring housing estates to access the shoreline, previously inaccessible for decades [30].
[29]   Pelham Bay Park, an area of 1122ha, the largest park in New York (over three times the size of Central Park) [24, p. 281].
[30]   The centrally located 290ha Bronx Park includes, among others, the New York Botanical Garden and Bronx Zoo International Wildlife Conservation Park.

in the south of the Bronx.[31] To generate synergy, it is necessary to implement a consistent system of parks and connecting green corridors that provide better access and create parity for the southern part of the district. A natural greenway corridor would be the riverbed of the Bronx River, which used to be important to the development of New York's industry. Right next to its western bank, the Concrete Plant park was opened in 2009.

The area of the new park had been in industrial use for decades. In 1987, the concrete production plant went bankrupt and the land became the property of the municipality. Apart from the profound degradation[32] of the area, the history of the place made a specific mark on the local landscape, with characteristic elements of the technical infrastructure of the old concrete mixing plant dominating the area. As a result of the efficient activities of the well-organized local communities,[33] a contemporary park came to life which preserves the raw heritage of the Bronx River's post-industrial neighbourhoods.

Fig. 9. The Bronx River bank with elements of small architecture (photo by W. Gadomska)

---

[31] e.g. the Ferry Point Waterfront Park, designed in 2008 to complement the area of the Ferry Point Park, set up in 1937 [31, p. 62].
[32] For example, 10 thousand car tires were removed from the river bank; nearly 32 thousand tons of oil-contaminated soil (leaking underground tanks) were replaced [32].
[33] Quote: '… an example of what happens when the community leads and the government is smart enough to follow' [24, p. 123].

The over half-kilometre-long linear park[34] with a nearly 3-hectare area introduced a subtly marked foot and cycle path that runs north–south along the riverbed into the transformed space. In a good part of the waterfront, a geometrical edge on the shore was recreated, making a boulevard waterfront that allows easy access to the river (Fig. 9). Exposed in the central sector of the park are the dominating artefacts of the former technical infrastructure (cement silos, aggregate tanks, fragments of technological infrastructure), all in a monochromatic red-lead colour (Fig. 10) with evident signs of long-term use. In a clear reference to the area's tradition, concrete was deliberately used as the prime building material for architectural details: the retaining wall by the river and the transport planes in the park area. The whole space was made decisively greener: lawns were surrounded with local plants and ornamental grass, and clusters of trees were planted to provide the desired shade in the future.

Fig. 10. Technical infrastructure exposed in the park space (photo by W. Gadomska)

The park has been a well-functioning element of the local landscape for seven years; it is an area of recreation and contact with the river that serves the residents of the dense neighbouring housing development, which itself has poor green infrastructure. However,

---

[34]   The project's author: James Mituzas, New York City Department of Parks and Recreation [24, p. 126]
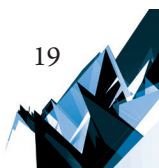
the potential role of the park goes well beyond the neighbouring area: it will become part of a large-scale sequence of green areas known as the Bronx River Greenway. The Master Plan designed in 2005 provides for consistency and continuity of green areas along a nearly 40-km stretch, running north–south along the Bronx River and including parks of various scale and character [33].

5. Conclusion

the observed development of green areas facilitated in the specific conditions of New York's "concentration culture" takes place, among others, by means of the recycling of urban areas which have become inactive and deprived of their original functions. Besides the improvement of the overall balance of urban greenery, the completed investments have led to the revitalization and gentrification of significant areas and upgraded their environmental conditions. The resulting appreciation of the standard of these public spaces is due to the high quality of the realized projects, the individual formal solutions, and the clear references to the cultural past and identity of these places. The principle of respect for the cultural context of redeveloped urban spaces is present both in the well-exposed, downtown locations and in peripheral locations which have difficult local, cultural, and spatial conditions.

References

[1] Koolhaas R., *Deliryczny Nowy Jork*, Karakter, Kraków 2013.
[2] Ballon H., Jackson K., *Robert Moses and the modern city: the transformation of New York*, W.W. Norton &Company, New York London 2007.
[3] Homberger E., *The historical atlas of New York City*, St. Martin's Griffin, New York 2016.
[4] Jacobs J., Śmierć i życie wielkich miasta Ameryki, Fundacja Centrum Architektury, Warszawa 2014.
[5] Kosiński W., *Sixty parks in Manhattan – the network of social life*, Technical Transactions, 7-A/2012, 163–151.
[6] Ulam A., *New west side story*, Landscape Architecture, 8, 2007, 88–99.
[7] Gadomska W., *Hudson River Park - współczesny park nad rzeką*, [in:] Horyzonty architektury krajobrazu – język architektury krajobrazu, Wieś Jutra, Warszawa 2010, 116–121.
[8] Reut J., *The leading edge*, Landscape Architecture Magazine, 4, 2015, 119–125.
[9] Greenstein R., Sungu-Eryilmaz Y., *Recycling the City*, Lincoln Institute of Land Policy, Cambridge, Massachusetts 2004.
[10] Balsley T., Muschamp H., *Thomas Balsley: the urban landscape*, Spacemaker Press, Berkeley CA 2000.
[11] Gadomska W., Gadomski W., *The High Line Park - public space as a result of post-industrial heritage of western Manhattan revitalisation*, Przestrzeń i Forma, 21, 2014, 273–284.

[12] Thomas Balsley Associates, *Thomas Balsley Uncommon Ground*, ORO Editions 2015.

[13] Thompson J. W., *Land matters*, Landscape. Architecture 12, 2006.

[14] Gadomska W., *Governors Island: a new park in New York*, Technical Transactions 4-A/2017, 15–26.

[15] Jodidio P., *Calatrava Complete Works 1979–2007*, Taschen, Köln 2007, 501–509.

[16] Betsky A., *Landscrapers: Building with the Land*, Thames & Hudson, London 2002, 46–47.

[17] Jost D., *Gotham goes green* Landscape Architecture, 7, 2010, 54–59.

[18] Lerner J., *Treasure Island*, Landscape Architecture Magazine, 6, 2015, 102–123.

[19] https://govisland.com/history (access: 10.11.2017).

[20] Wielka Encyklopedia PWN, tom 14, Wydawnictwo Naukowe PWN, Warszawa 2003.

[21] https://www.panynj.gov/about/history-port-authority.html (access: 10.11.2017).

[22] Lynn R., Morrone F., *Guide to New York City Urban Landscapes*, W.W. Norton & Company, New York-London 2013, 100–102.

[23] Larsen K., *Wood that could and should*, Landscape Architecture Magazine, 8, 2013, 102–111.

[24] Berner N., Lowry S., *Garden Guide: New York City*, W. W. Norton & Company, New York-London 2010.

[25] Pawłowska K., *Wieżowiec i park publiczny – relacje funkcjonalne i krajobrazowe cz. I*, Architektura krajobrazu 2/2009, 4–10.

[26] Sirefman S., *New York. A guide to recent architecture*, Ellipsis, London 2001, 15.12.

[27] Luna I., *New New York. Architecture of the City*, Rizzoli, New York 2004, 292–296.

[28] Lerner J., *The amphibious edge*, Landscape Architecture Magazine, 2, 2014, 88–106.

[29] Nicolin P., Repishti F., *Dictionary of Today´s landscape Designers*, Skira Editore S.p.A, Milano 2003, 139.

[30] Ulam A., *The Park IKEA Built*, Landscape Architecture, 11, 2008, 110–117.

[31] Wantuch-Matla D., *Under the bridge*, Architektura & Biznes, 7/8, 2011, 50–65.

[32] Mclntyre L., *The Bronx blooming*, Landscape Architecture, 11, 2010, 66–77.

[33] http://www.bronxriver.org/puma/images/usersubmitted/greenway_plan/ (access: 05.01.2018).

If you want to quote this article, its proper bibliographic entry is as follow: Gadomska W., *Modern park as a result of urban space recycling – a review of new york city's developments*, Technical Transactions, Vol. 10/2018, pp. 5–22.

21
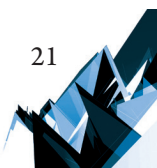
Anna Franta ⓘD orcid.org/0000-0001-6351-8622
    Institute of Urban Design, Faculty of Architecture, Cracow University of Technology

Agnieszka Bojarowicz ⓘD orcid.org/0000-0003-3924-9260
agnieszkabojarowicz@gmail.com
    Chair of Architecture and Urban Planning, Faculty of Civil Engineering and Architecture,
    Kielce University of Technology

From slums to a model example of revitalisation: overcoming a difficult identity in the renewal process of the district of Hulme in Manchester

Od slumsu do wzorcowego przykładu rewitalizacji: przełamanie trudnej tożsamości w procesie odnowy dzielnicy Hulme w Manchesterze

Abstract

The paper is devoted to the renewal of inner city districts, burdened with a difficult identity. The analysis focuses on the case study of the district of Hulme in Manchester. Within the perimeter of Hulme the attempts to revitalise the area burdened with bad reputation of the biggest slum in Manchester have been made twice. The paper presents the genesis of the bad reputation of the district, its effect on the degradation of the district, as well as it describes the strategies undertaken during both attempts of the revitalisation of Hulme.

Keywords: identity, revitalisation of inner city districts, difficult identity of the place, revitalisation of Hulme

Streszczenie

Artykuł podejmuje tematykę odnowy dzielnic śródmiejskich obarczonych trudną tożsamością. Analizie poddano studium przypadku dzielnicy Hulme w Manchesterze. Na obszarze Hulme dwukrotnie podjęto próbę rewitalizacji obszaru obarczonego złą reputacją największego slumsu Manchesteru. Artykuł przedstawia genezę złej tożsamości dzielnicy, jej wpływ na degradację dzielnicy oraz opisuje podjęte strategie działania w trakcie obu prób rewitalizacji Hulme.

Słowa kluczowe: tożsamość, rewitalizacja dzielnic śródmiejskich, trudna tożsamość miejsca, rewitalizacja Hulme

1. On identity

Identity – the spirit of a place – belongs to the sphere of human consciousness and sub-consciousness. It also has its material carrier: spatial identity reflected by the state of a space – its features and the manner of managing it. Spatial identity is characterised by a collection of noticeable properties fixed in memory and typical of a given place or area – distinguishing this place or area from other locations. It consists of natural features – hardly changeable – expressed visually in the natural landscape, and of anthropogenic properties – with various degrees of changeability – visually interpreted as a cultural landscape, a result of human activity. The features of places and areas can be positive – then they should be maintained, emphasised and continued creatively (inspirations in accordance with the principle of good continuation), while some new ones can be added. However, there are also negative features which require removing, transforming and moderating.

It all happens in the permanent process of spatial management whose desirable objective is to increase its quality consistently and progressively.

Thus, identity is determined by what is there and what is characteristic – characteristically valuable. At the same time, identity is 'slowly changeable' which means that certain features come and certain features go. Sometimes the loss of distinguishing features is intense. The carrier of identity – urban and architectural space – is destroyed in fires, floods, wars… Then, by accident, its positive and negative features get lost, whereas identity is difficult to reconstruct. Sometimes the image of a city changes radically – a new identity comes into being. Sometimes changes, even the radical ones, produce a new identity intentionally reconstructing and maintaining values acknowledged as valuable – then the new identity becomes a continuator of the old identity. Sometimes, while reviving a city, it makes mistakes which deform the values. The identity of a place is distorted – it can be annihilated. Whether the process of shaping a space is professional and consistent depends on the level of the cultural awareness of the community of a given city (place) and its authorities. If it is not, it leads to the regress of identity, which changes negatively as it has worse architectural carriers.

Violent (even though rarely total) damage to the architectural carrier of identity clearly shows the loss of values to the community of a place (a city, its separating fragment) which did not always notice or appreciate them before destruction. It means the loss of material values, also sensed as this community's identity: characteristic features fixed in the collective memory. If the sensation of loss concerns a significant part of the community, the need to save, reconstruct and maintain these values for the future generations is strong and commonplace. Public opinion is conducive to their reconstruction – it demands it. The authorities and the society entrust it to professionals without hesitation and 'in full'. They appoint professional, competent, authorised institutions which are not subject to democratic procedures and the pressure of the market – architectural and urban quality is crucial here. It concerned all the destroyed or severely damaged cities that were rebuilt successfully (Warsaw, Gdansk, London etc.). It was professional work in the atmosphere of trust which was reflected in good legislation and organisation without corruption, lawlessness or destructive anarchy.

Without the shock of loss, these values are unnoticed and unappreciated again, sometimes associated with poverty and a low civilisation standard... they disappear slowly. In our surroundings, the mass of 'the new universal' dominates quantitatively over the old or acknowledged carriers of identity. Whether they are oppressed and eliminated becoming 'islands' of values in the sea of randomness and imitation depends on the degree of the commonness of the social awareness that identity i s a v a l u e – undoubted and desirable – and that it must be protected and developed. The matter of identity is delicate. It is easy to neglect and lose the values. It is often infeasible to recreate them and difficult to repair the deformed ones. It is equally hard to create new values which build identity.

New needs bring new programmatic requirements and frequently a larger scale. New technologies bring a new distinguishing feature for a place but also uniformisation – similarity to 'the rest of the world'. This results in a thesis on blurred differences – characteristic features of given areas important for their identity.

History, destruction and redevelopment influence identity. However, there is something special in it which causes the characteristics of a form, its specificity. It is a peculiar 'cultural record' related to the psychics of a cultural formation influencing a space. This record has an impact on the manner of distributing its elements, on the preferences of proportions, the way of accentuating, on detail, the degree of rigour while putting the elements of space in order. This record is fixed in man – in the creator. However, if it is absent in consciousness, only the subconscious remains: the source of particular preferences, the stimulation of the construction of a specific form.

If this factor is fixed in the subconscious, it should result from free creation concurrent with the times of architecture. In order to show it in its unique 'peculiarity', however, the creator must be filled with it. It is attainable through education where the knowledge of the history of a country and works of art from various domains – getting used to them, absorbing them in 'a self' – plays an important role. This art must be valued highly; its existence in the subconscious should be treated emotionally; what is important, one ought to work on it consciously. Being a well-educated architect is not enough – one also has to be a c o n s c i o u s 'carrier' of unrealised features forming identity within creative freedom.

Architecture is the art of the harmony of a place. Its basis is order – then creation should aim at the perfection of this harmony in a defined place. Every place (city) includes the impacts of all the cultures which played the dominating role in its area at various times leaving their trace in the identity of the place. The community which inhabits the place currently takes over these c o m b i n e d features as its identical properties. In the name of cultural pluralism – human achievements – it is necessary to transfer cultural autonomies into the future maintaining and developing them. The assimilating influence of technology and fashion is inevitable. An architect must know the world, the richness of its opportunities and autonomies, shaping his own separateness and being rooted in the achievements of the native culture and tradition. So, he will transfer all the shared features uniformising the world; it is the question of the pressure of information. However, only he can transfer the characteristic features into the future through t h e s u b c o n s c i o u s g u i d e d t o w a r d s i d e n t i t y – a chance for creative continuation of the autonomy of cultural identities.
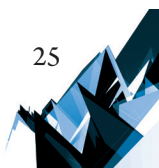
The creative result – 'original individuality' or correct (sometimes attractive) imitation – depends on the suitable proportions of the consolidation of these components of 'encoded identity' and 'worldwide orientation'.

Art has its material, financial aspect – someone pays for it (it is noncommercial by nature in spite of its quality). First and foremost, it has its spiritual aspect: communing with it, somebody b e n e f i t s spiritually, intellectually and emotionally, which means the best possible social profit and an investment for the future. Education in the cult of valuable art leads to the activation of a recipient, who is looking for contact with quality professional art. At the same time, being sensitive to cultural values, he begins cultivating artistic values, protecting them and creating them apart from his professional activities for pleasure, for the development of his personality and sensitivity – identity. He becomes an interactive partner for professional creators who expects high quality, being able to appreciate and evaluate it.

"The city is the people" (J. Jakobs). A social environment works in 'the space of a city' – its urban and architectural shape being a n e c e s s a r y processor facilitating (among other things) the democratic flow of ideas and meanings characteristic of the community (or rather communities since their changeability is obvious) of the city. On one hand, the creation of 'the image of a city' depends on the identity and individual character of its public spaces; on the other hand, it is the local community's p r i d e of the statement that 'we are different', treating this 'otherness' and 'distinguishableness' as a positive value which still searches for its expressiveness – again in the shape of a public space.

In order to be itself – high culture protecting and connecting the values of the past with those created at present for the sake of enriching the future, culture should shine with its own instead of reflected light. Confrontation of cultures – in defiance of aggressiveness associated with the word 'confrontation' – serves to compare and study, to learn each other's 'specificities' and individualities. Its sense is inspiration and enrichment of one's own creative potency. It is senseless to reject and depreciate other values as well as imitate them uncritically ('mimicry'). "The development of one's own architectural expression is the crucial part of man's cultural obligations […] and requires much more care, attention and effort than repeating previous achievements" (E. Saarinen).

Because of the informational openness of the world, contemporary man wants to live in two cultures: his local homeland, and the global one. In the past, identity was protected by physical borders: difficult access, distance, the slow flow of patterns (information) which were easily modified at the local level. In the contemporary world, it is only protected by the limits of consciousness: the awareness of the need for it and its value. It concerns every member of a local community.

We are all obliged to serve elementary beauty. The measure of the maturity of local self-governments is the realisation that the public space of a city is 'common' and that 'common' does not mean 'no-one's' but 'ours'.

"Our grasp of being is pre-conceptual comprehension; our comprehension is of the character of a design. It means that we d e s i g n, i.e. bring certain possibilities out of ourselves and realise them" (M. Heidegger). As a society, we design the conditions which influence the quality of life in general as well as the quality of the space that surrounds us.

Sometimes the identity of a specific urban structure can be a difficult one, burdened with negative connotations in the social reception, although ones that identify a place and its local community.

This paper is devoted to the revitalisation of inner city districts, burdened with a difficult identity[1]. The analysis of the renewal process of the city area is predominantly directed towards issues relating to overcoming of a difficult identity, which contributes to enhancing the degradation of the district.

The case study of the district of Hulme in Manchester discusses the effectiveness of the renewal of the district burdened with a difficult identity, identifies and emphasises errors and effective methods, with an intention to formulate good practices possible to be transferred, also in the Polish reality.

The revitalisation of Hulme is a particularly valuable example, as it demonstrates a double attempt to revitalise the district, the first being a broadly discussed failure, whereas the strategy adopted in the second one seems to have positive effects and lead to achieving the planned goals. In both revitalisation plans one of the main problems in the district that had to be tackled was the 'bad reputation', 'bad identity' of Hulme.

2. District of hulme – effects of development conditions and the first revitalisation

By the mid-19th century Manchester reached the status of one of the main urban and industrial centres in England: "new social forces were created thanks to the advent of the industrial era, and Manchester became a symbol of new ways of living and working" [9, p. 5]. The development of Manchester as an industrial, trade, banking, and transport centre generated increased migration of people to the city. An enormous pace of the population growth resulted in the overpopulation of hastily built residential districts and the continuous deterioration of the living conditions of their residents. The population of the city increased four times over the first decade of the 19th century, reaching the level of one million by 1851. The immigrant population caused such a great concentration of people in the inner city of Manchester that by 1914 80,000 out of 180,000 houses and apartments in the inner city gained the status of "slums" [9, p. 5].

One of Manchester's inner city districts, Hulme, grew very rapidly over the span of the 19th century as well, due to the labour migration. It was quickly dubbed the worse slums in the world, often affected by epidemics of cholera and other infectious diseases. In 1924, when the average population density in Manchester was 34 persons per acre, in Hulme

---

[1] Research on the issue of difficult identity is conducted as a part of Ph.D. thesis ent.: *Overcoming the difficult identity of a place in the process of revitalization of historical downtown areas. On the example of the Nowe Miasto district in Kielce*, by M.Sc. Eng. Arch. Agnieszka Bojarowicz, Kielce University of Technology, Faculty of Civil Engineering and Architecture, Chair of Architecture and Urban Planning, under the scientific supervision of DSc. Ph.D. Eng. Arch., Professor of CUT Anna Franta, Cracow University of Technology, Faculty of Architecture, Institute of Urban Design.

it was 136 persons per acre on average, and this ratio grew to 196 persons per acre in the northern part of the district, closer to the centre of Manchester. In 1934 Hulme was officially dubbed England's largest clearance area [1, p. 30]. This meant not only a complete removal of the existing architecture, classified as 'uninhabitable', but also the destruction of the local community. The previous residents of Hulme were gradually relocated to new council estates, such as Wythenshawe.

Fig. 1. A still from a film *Hulme, What Went Wrong* (source: [16])

Fig. 2. Bird's eye view of Hulme, 1930 (source: [17])

Fig. 4. Celebrations in honour of the coronation of Queen Elisabeth in a street in Hulme, 1953 (source: [19])

Fig. 3. A street in Hulme, early 20th century (source: [18])

Fig. 5. A street in Hulme 1956 (source: [20])

Fig. 6. Terraced houses in Hulme, 1965 (source: [21])

The most extensive demolition of the degraded architecture, very intense, although rather low and 'urban' in its essence and urban patterns (including a street as a space for social life and interaction) in Hulme took place in the 1960s.

One of the main assumptions of the urban solution that emerged in this area after the removal of the old structure was the separation of the pedestrian and vehicle traffic. Stretford Road, the main traffic axis of the area, was excluded from the car traffic in 1965. The leading vision of the new project was to replace the traditional street life with a new model: elevating the pedestrian traffic and social interactions above the ground level. According to the designing assumptions, this measure was to guarantee residents' safety, eliminating collisions with the car traffic. Another measure was the introduction of a new typology of development: tall and large-scale modern residential buildings. Apartments located in the designed buildings were accessible from open galleries, individual buildings where linked with a grid of walking paths. 5000 new apartments were built in five gallery buildings and in 13 skyscrapers during the reconstruction of the district. The central point of the new urban plan, which was to build a new, positive identity of the district, were enormous Crescent Blocks, inspired by the Victorian architecture of Bath [9, p. 31].

Therefore, the urban structure of Hulme was drastically changed during the reconstruction. The population of the district dropped to 12,000 out of 130,000 people who lived there in the 1930s. The floor area ratio was reduced from 150 residential units per hectare to 37 residential units per hectare [9, p. 32].

Only several years after introducing new residents to the districts problems started to emerge. They resulted from wrong assumptions of the revitalisation programme in both social and urban aspect. Designing and workmanship errors were made when building the blocks, as well.

A considerable reduction of the population of Hulme destroyed the existing social relations and deprived the residents of the sense of identification with their place of residence. When allocating apartments, no attention was paid to the diversification of residents in terms of their economic situation and social position. Once again a big concentration of poor, often unemployed people came into being in Hulme.

The design idea of the gallery buildings was not adjusted to the cold and wet climate of Manchester. The galleries – streets never worked as places of neighbours' gatherings and social interactions. They were even dangerous, e.g. in 1974 a child playing there fell out. The green areas between the buildings were too big, as if belonging to no one. They were not designed and developed in a way that would be attractive for residents.

Another drawback of this architecture was its expensive maintenance, high heating costs, frequent failures of its installations. Structural and workmanship defect of the buildings were revealed, as well.

The utopia imposed by central planning was not approved by residents. Better-off families were gradually moving out from Hulme. The apartments were getting cheaper, and their standard was quickly dropping. A huge problem was the growing crime, also organised crime. The multi-level passageways made it difficult to patrol the area and to maintain safety.

Once again Hulme was dubbed a slum, a district with a bad identity. The problem of social exclusion of its residents was growing, once again the area became one of the poorest

and most problematic places in Manchester. The level of the community's participation in the social and economic life was going down. Seventeen years after the new development of Hulme had come into being, it was decided to demolish it yet again.

Fig. 7. Bird's eye view of the project of Crescent Blocks (source: [22])

Fig. 8. Architecture of Hulme – project of multi-level, gallery passages between the buildings (source: [23])

Fig. 9. Hulme, the space between the buildings of Crescent Blocks (source [24])

3. City challenge programme – the second revitalisation of hulme

The task of rebuilding the integration with the centre of Manchester became one of the foundations of the plan for another revitalisation of Hulme. The Hulme City Challenge Programme was developed with the view of the urban transformation of this big part of Manchester comprising 3000 residential units, the infrastructure development, and subsidising the newly erected buildings. Upon the commission of Hulme Regeneration – City Challenge Company, a handbook of good designing practices was written, too: "A Guide to Development – Hulme Manchester", where rules for designing top-quality urban environment were formulated.

In 1991 the State Secretary Michael Heseltine announced the City Challenge programme. Its goals focused on overcoming the bad identity of Hulme on many planes, its complex revitalisation instead of focusing merely on the physical reconstruction. Naturally, City Challenge aimed to create a new urban design, although it also made use of the experience from the reconstruction carried out in the 1960s, which demonstrated that a new design would not solve all issues in this area. In order to create a well-functioning local community it is equally important to take social and economic aspects into account. Within the scheme of the programme strategies engaging local organisations and the private sector were developed so as to link the solutions implemented with the needs of the local community and of the city as a whole.

The City Challenge programme was financed from the Single Regeneration Budget (SRB), a national revitalisation programme engaging five government departments. City Challenge was granted 7.5 million pounds annually for a period of five years for the purposes of the revitalisation of Hulme. A joint venture was set up in order to secure funds for the construction of residential houses, the network of roads, and the extension of the underground. Over 110 million pounds was collected from the public and private sector for the purposes of regeneration and reconstruction of the entire Hulme community [9, p 33].

Within the scheme of the City Challenge initiative the following institutions cooperated with each other: Hulme Community Homes, Manchester City Council, Hulme Community and Hulme Regeneration Ltd. The structure of the established partnership is depicted in the diagram (Fig. 10).

Strategic goals of the established partnership were as follows:
- Strengthening the local economy,
- Increasing the accessibility of different forms of employment for residents,
- Improving the situation on the local real estate market,
- Increasing the diversity of apartments and homes available on the market,
- Constant improvement of the quality of the housing environment.

Integration of the social, economic, urban, and architectural renewal via cooperation within the scheme of the partnership increased the probability of wielding durable positive influence not only on Hulme as a district, but also on Manchester as a city. The main goal of the strategy was to create relations between the renewal, education, social policy preventing unemployment, and improvement of the housing conditions. Table No. 1 demonstrates the effects achieved thanks to City Challenge in four key fields.
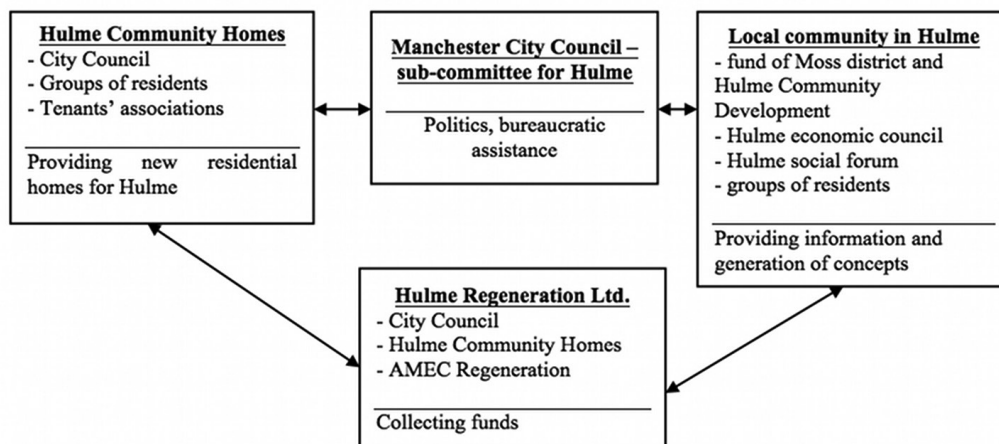
Fig. 10. City Challenge Development Strategy. Cooperation between organisations and institutions within the partnership (source: [1, p. 48])

Table 1. City Challenge Programme. Key effects of the renewal of Hulme, data as of 1996 (source: [1, p. 48])

ECONOMIC DEVELOPMENT	
New jobs	725
Initiatives stimulating the increase in the employment level	75
Number of the unemployed who benefitted from assistance	8000
Number of the disabled who benefitted from assistance in looking for jobs	500
HOUSING	
State sector, mixed ownership	1000
Private sector	1000
Number of residents who received support within the scheme of the social benefit programme	5500
ENVIRONMENT	
Open space	10 ha
Open space covered with the renewal programme	7,4 ha
SOCIAL EFFECTS	
New childcare places	1000
Newly built community centres	2

Hulme Regeneration, one of the companies established within the scheme of City Challenge, decided to employ a representative of the local community, architect Charlie Baker, to write a designing guidebook for the district of Hulme. Charlie Baker was an activist of local organisations of residents and one of the most ardent critics of the previous restructuring of Hulme. Baker and his colleague, David Rudlin, studied the literature devoted to good practices in designing cities, and next travelled around, analysing cities and districts in search of inspiring examples of urban solutions. Guided by the knowledge and experience they gained, they formulated a set of rules which were the foundation for the urban design code in Hulme.

In 1994 "A Guide to Development – Hulme Manchester" was published, a document describing 53 rules of urban design, classified into the following ten parts:

- **Streets:** they are to fulfil the role of a road to move around and a space for social interaction. Fronts of buildings should face the street and the main access to them should be directly from the street.
- **Integration:** integration of different forms of use of buildings and land within the district, introduction of diversified ownership forms.
- **Development density:** it was assumed that the optimum ratio is 90 residential units per hectare (35 per acre).
- **Patency:** the design of the network of roads - they need to be arranged in a specific hierarchy, it is forbidden to design dead-end streets.
- **Roads and transport:** parking along the street is a preferred option, it is not recommended to build multi-level car parks.
- **Reference points, openings, and landmarks:** the significance of top-quality spaces of the city were emphasised: open views, taller buildings in corners.
- **Definition of space:** it was required that buildings should be built along a defined frontage. Urban interiors should be arranged in sequences of streets, squares, and parks.
- **Identity:** buildings and the space around them should have individual features, it was recommended to apply diversified materials and design solutions.
- **Sustainable development:** a considerable part of the rules relates to the introduction of greenery, waste management, the use of alternative energy sources
- **Hierarchy:** the final section sets forth a five-level hierarchy of streets, starting from transit roads, through collective and local roads, to private roads.

The principles specified in the guidebook were applied during negotiations and talks with investors, the police, engineers, and planners. The city council appointed a planning sub-committee, engaged in the analysis of the investments planned in Hulme. Members of the sub-committee analysed in detail the projects presented to them, comparing them with the rules described above. Developers were told to introduce changes in the designs many times. Such decisions of the city authorities built respect for the rules contained in the guidebook amongst designers and developers.

The guidebook did not refer to the quality of architecture as such, but it rather set the directions of reasoning, it determined the height and orientation of buildings so as to make sure they were harmoniously inscribed in the urban context. The leading objective was creating a friendly urban space, bustling with life.

4. Hulme today – effects of city challenge in the context of overcoming the trend of difficult identity

It has been over 20 years since the completion of the Hulme City Challenge programme in 1997. These over two decades allow us to evaluate whether the measures undertaken by the City Council and the partner organisations helped to achieve the initial goals of the revitalisation programme of the district.

The evaluation of Hulme City Challenge was carried out twice: in 1999 and 2002 by the SURF Centre (Centre for Sustainable Urban and Regional Futures) at Salford University. The research methods adopted were a comprehensive programme of interviews and a statistic analysis.

150 DWELLINGS/HA   37 DWELLINGS/HA   75-87 DWELLINGS/HA

Fig. 11. Stages of the urban transformation of Hulme. To the left – development from the 19th/20th century, in the centre - development from the 1960s, to the right – the quarter development proposed in the 1990s. (source: [10, p. 16])
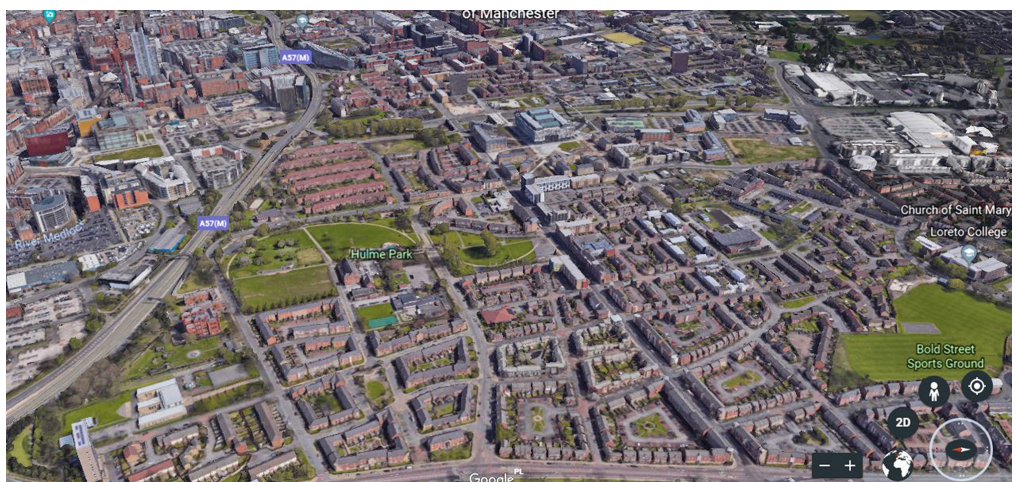
Fig. 12. Bird's eye view of Hulme (source: [25])

In compliance with the report of the SURF Centre, in the period 1999-2002 the total value of the investments implemented in Hulme and Moss Side by the public and private sector was 400 million pounds. Projects given support were connected with the development of the local economy, improvement of the urban environment and quality of development, improvement of the quality of life, construction and development of public utility buildings. These activities gave measurable results in the form of a bigger number of jobs, a broader access to education, development of infrastructure; new commercial and public buildings appeared.

A large green area, Hulme Park, was arranged in the northern part of the district. In the south-western part of the district there is a local shopping centre.

The housing resources in Hulme got considerably diversified compared to 1992. It had its effect on the much more rapid increase of prices of new private houses than the average increase observed in the same period for the entire city. The attractiveness of Hulme as a place of residence increased, the population of the district rose by 3.3%, whereas the average rise in the population of the entire city in the same period was 0.2%. A considerable part of the housing development of Hulme is social housing, which translates into the image of Hulme still as 'the poorer district', but equipped with high-quality urban and architectural space. According to the data from 2010, 47.5% of the population of the district lived in social houses [26].

What is remarkable is a big drop in unemployment from 32% in 1989 to 6% in 2010. The market of minor services and services connected with entertainment developed much more than expected. Another element that emerged was big concentration of public sector entities and voluntary services.

Although the level of poverty improved when compared with other areas of Manchester, it is still high against the background of the rest of the country. The reports from 2002 and 2006 mention also the issue of the still high level of crime in Hulme, especially a big number of petty thefts and car thefts.
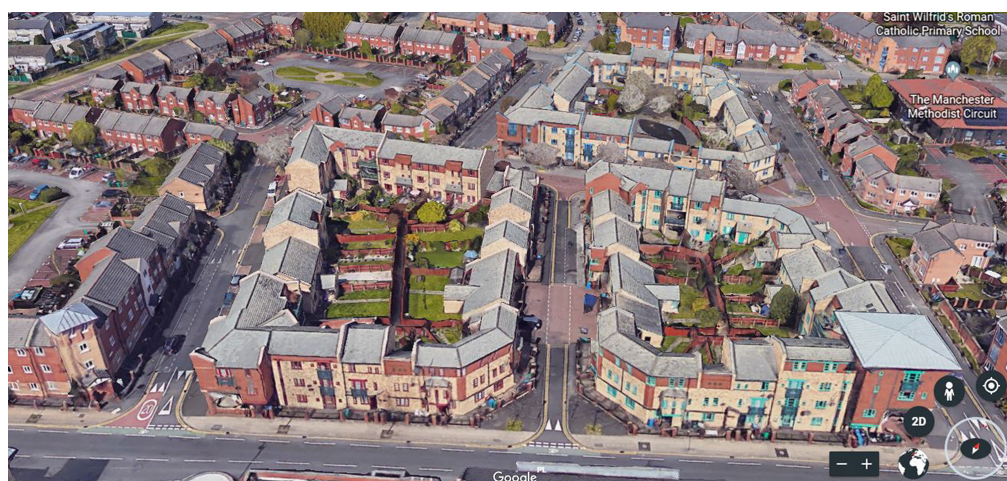
Fig. 13. Residential development quarter in the north-western part of the district (source: [25])

Fig. 14. Residential development quarter in the north-western part of the district (source: [25])

Fig. 15. Development quarters in the central part of the district (source: [25])
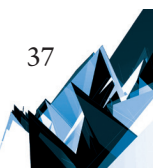
Fig. 16. High Street – a part of the southern commercial part of Hulme (source: [25])

Fig. 17. Hulme, Hunmaby Ave – an urban interior of the street between residential development quarters (source: [25])

Fig. 18. Contemporary residential architecture in Hulme (source: [27])

Over the last 10 years several architecturally interesting investments were implemented in the district. The most significant of them is Birley Fields Campus Manchester Metropolitan University. The main building of the campus, Brooks Building, was erected at Bonsall Street. The university edifice is one of the most advanced facilities of the type in the United Kingdom. The entire complex comprises also student dormitories, the Energy Centre, and a multi-level car park.

Fig. 19. Bird's eye view of Birley Fields Campus (source: [25])

Fig. 20. Brook Building (source: [28])

Fig. 21. Multi-level car park (source: [29])

Fig. 22. Dunham House (source: [29])

Fig. 23. Urban interior of a residential street of a part of Hulme and a view of a backyard inside the quarter. Visible regional, characteristic for Manchester character of development, the 'human' scale of development, and proportions of the street interior (photo by B. Kwiatkowski)

The Manchester Evening News characterises this district in the following way: "it is a residential district, popular among students, young professionals, and families. It is a place with a flourishing artistic scene and creative people. The newly erected theatre centre Z Arts at Stretford Road, the renovation of the old hippodrome, and the extension of the Community Garden Centre – all this charges us with positive energy" [14].

On the basis of the analysis of the revitalisation process implemented in Hulme, several important conclusions can be drawn. What is necessary to ensure a sustainable process of regeneration of a given area is the commitment of the local community. The revitalisation programme must also respect the local specificity of the area, transform it so as to eliminate problems, but not destroying its socially and spatially valuable features.

Fig. 24. Example of designing facades of residential buildings. Visible individual features of buildings emphasising the composition of the urban interior: emphasis of the entrance zone, the corner, a detail in the form of a relief (photo by: B. Kwiatkowski)

Fig. 25. Contemporary multi-family architecture in Hulme. Visible care of maintaining the 'human' scale. Brick used in the facades as a finishing material characteristic for the district (photo by: B. Kwiatkowski)
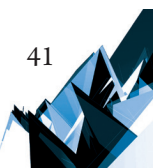
Fig. 26. Hulme Park – recreational green area in the district. Despite a certain degree of degradation and neglect, the care for interesting street furniture elements is well visible (photo by: B. Kwiatkowski)

The comparison of two action plans in Hulme demonstrates an advantage of a comprehensive approach to the regeneration plan developed, of the ability to overcome discipline-related limits, offering potential explanations for essential problems, which for a long time have been nagging experts and bureaucrats perceiving them only fragmentarily.

Prior to the central intervention there usually exists a potential, an earlier 'resilient' reality, characteristic for this particular area of the city, and an effective intervention is a function of how well the transformation programme is synchronised with the existing conditions.

An element of key importance for the success of the revitalisation programme is also the participation of national and local authorities, stimulating and supervising the activities undertaken by the private sector. Good results are reached by the cooperation of state and private entities in this respect within the scheme of the public-private partnership. A role of the administration and planning units is to create a coherent master plan for the revitalised area, as well as to formulate a set of rules for the new development, and subsequently to establish effective mechanisms of supervision and control over the planned investments.

The example of the revitalisation of Hulme clearly demonstrates how important for the area revitalisation the social aspect is. Revitalisation will be ineffective if we ignore the needs of local residents and the way in which the local community operates.

The district of Hulme has been subjected to the regeneration process twice. In both cases it was necessary to face its bad identity, to overcome the bad reputation of Hulme. The activities commenced in the 1990s have been bringing positive results. It seems that the key to success in this respect is to perceive the district as a neighbourhood, and not as a property to be developed. Following clearly established rules for the entire area, their consequent enforcement, and monitoring of the results of the process allowing to verify all errors and strengthen the measures offering the best effects – this is a specific and effective 'guideline', helping to overcome the difficult identity and to create a new one, making use of its positive features, in the recognition of and respect for continuity.

References

[1] Dickson G., Rendek K., *Urban Regeneration: City of Manchester* in: *Urban Regeneration, Learning from British Experience*, ed. S. Tsenkowa, Faculty of Environmental Design, University of Calgary, Calgary 2002, pp. 35–50.

[2] Franta A., *Reżyseria przestrzeni. O doskonaleniu przestrzeni publicznej miast*, Monografia, Wydawnictwo PK, Kraków 2004.

[3] Franta A., *Mieszkać w mieście – mieszkać w centrum miasta*, Czasopismo Techniczne, 3-A/2007, pp. 59–69.

[4] Franta A., *Rola restrukturyzacji obszarów postindustrialnych w kreowaniu nowych rodzajów przestrzeni publicznych metropolii – stymulująca funkcja regulacji*, Czasopismo Techniczne, 1-A/2007, pp. 35–43.

[5] Guzik R., *Rewitalizacja miast w Wielkiej Brytanii*, collective work, Institute of Urban Development, Kraków 2009.

[6] Jacobs J., *Śmierć i życie wielkich miast Ameryki*, "Centrum Architektury" Foundation, Warszawa 2014.

[7] Lynch K., *Obraz miasta*, "Archivolta" Publishing House, Kraków 2011.

[8] Rudlin D., *The Hulme and Manchester Design Guides*, Built Environment, vol. 25, Alexandrine Press, 1999, pp. 317–324.

[9] Williams G., *Metropolitan Governance and Strategic Planning: a Review of Experience in Manchester, Melbourne and Toronto,* Progress in Planning, vol. 52, Pergamon 1999, pp. 1–100.

[10] *A Guide to Development. Hulme Manchester*, Manchester City Council, 1994.

[11] http://manchesterhistory.net/manchester/gone/crescents.html (access: 2.07.2018).

[12] https://www.manchestereveningnews.co.uk/news/greater-manchester-news/hulme-sweet-film-project-history-10573357 (access: 3.07.2018).

[13] VIVACITY 2020 Evaluation of the Regeneration of Hulme, Manchester, http://www.vivacity2020.co.uk (access: 5.07.2018).

[14] https://www.manchestereveningnews.co.uk/all-about/hulme (access: 5.08.2018).

[15] https://www.manchester.gov.uk/download/.../id/.../hulme_10_years_on.pdf (access: 4.08.2018).

[16] https://www.youtube.com/watch?v=a-y05b40eMs (access: 2.07.2018).

[17] https://www.google.pl/maps (access: 5.07.2018).

[18] source: httpschorltonhistory.blogspot.com201510britannia-emery-mills-down-at-hulme.html (access: 13.08.2018).

[19] https://pl.pinterest.com (access: 5.07.2018).

[20] https://www.manchestereveningnews.co.uk/incoming/gallery/in-pictures-archiving-hulmes-past-779619 (access: 5.07.2018).

[21] https://www.flickr.com/photos/manchesterarchiveplus/5453484652/in/photostream (access: 13.08.2018).

[22] https://www.express.co.uk/pictures/pics/3067/Manchester-slums-street-life-1960s-pictures (access: 13.08.2018).

[23] http://manchesterhistory.net/manchester/gone/crescents.html (access: 2.07.2018).

[24] http://www.halcyonmag.com/article/Hulme+Estate%3A+The+Best+of+Times%2C+ The+Worst+of+Times (access: 13.08.2018).

[25] https://www.manchestereveningnews.co.uk/news/greater-manchester-news/hulme- sweet-film-project-history-10573357 (access: 18.08.2018).

[26] Google Earth (access: 13.08.2018).

[27] https://www.brainscape.com/flashcards/hulme-manchester-city-challenge-partnersh- 3826694/packs/5681567 (access: 5.08.2018).

[28] http://history.aboutmanchester.co.uk/hulme-three-times-regenerated (access: 13.08.2018).

[29] https://www.gillespies.co.uk/projects/mmu-birley-fields-campus (access: 6.08.2018).

[30] http://manchesterhistory.net/manchester/outside/birley.html (access: 13.08.2018).

Jacek Gyurkovich ⒾⒹ orcid.org/0000-0003-2167-6424
jgyurkovich@pk.edu.pl
Institute of Urban Design, Faculty of Architecture, Cracow University of Technology

New forms in a historical context. Contemporary architectural interventions in the landscape of the Oder river's riverfronts in Wrocław's city centre

Nowe formy w historycznym kontekście. Współczesne interwencje architektoniczne w krajobrazie nadbrzeży Odry w śródmieściu Wrocławia

Abstract

The author analyses selected examples of contemporary built residential development projects in locations close to the historical city centre of Wrocław that create a new architectural frame around the waterfronts of the Oder River. The ambitious works of architecture, constituting a contemporary interpretation of the atmosphere and tradition of the place, introduce new values into the unique space of the waterfronts, remaining in accord with the new philosophy of cultural heritage.

Keywords: Wroclaw, cultural landscape, contemporary architectural interventions

Streszczenie

Autor analizuje wybrane przykłady współczesnych realizacji inwestycji mieszkaniowych, w lokalizacjach usytuowanych w pobliżu historycznego śródmieścia Wrocławia, tworzących nową oprawę architektoniczną nadbrzeży Odry. Ambitne kreacje architektoniczne stanowiące współczesną interpretację klimatu i tradycji miejsca, wnoszą nowe wartości do unikalnej przestrzeni frontów wodnych, pozostając w zgodzie z nową filozofią dziedzictwa kulturowego.

Słowa kluczowe: Wroclaw, krajobraz kulturowy, współczesne interwencje architektoniczne

Contemporary cities are subjected to a constant process of transformation – the adaptation of their spatial and functional structure to the changing needs and requirements of contemporary life. The elements undergoing transformation include transport systems and infrastructure, while the tissue of urban built-up areas is being infilled or replaced. Historical downtown urban complexes in cities with ages-old histories are characterised by the unique properties of their urban cultural landscape. The building substance of these complexes – both the individual historical buildings that are essential to the culture and identity of a place, just as the entire scope of the cultural landscape, are subjected to architectural conservation. However, in protected areas, as well as in their immediate vicinity, it is still possible to introduce contemporary architectural interventions – subjected to specific precepts of the design of the composition of urban tissue, conducive to the maintaining of existing qualities and the adding of new values to them.

Andrzej Tomaszewski in the chapter *The cultural landscape as a protected good* wrote: "Just as we have agreed with the fact that a historical city is a living organism and cannot be merely a relic of the past and must evolve, we must acknowledge that the cultural landscape is a living organism to an even greater degree". He also further stated: This is about an intelligent compromise between the past and the present. Often a very difficult compromise..." [1, p. 85–86].

The economic condition of the country and a much great degree of affluence of many citizens provides development opportunities associated with European Union aid – creating potentially advantageous conditions for the creation of new values, which is particularly essential in the case of unique areas of the urban cultural landscape.

* * *

Wrocław's Oder River waterfronts increasingly attract real estate developers – the direct contact of buildings and their users with the river, the expansive views that open up thanks to this and that are not limited by the close proximity of other buildings – these are the great advantages of waterfront locations. The dense network of waterways within the city – the numerous branches of the Oder River and the Old Oder, the Oława, the Sailing Channel, the Opatowski Channel or the City Moat – have created sequences of numerous areas of various size that are surrounded by water, setting up the unique qualities of the urban landscape. Wrocław's waterway node creates an original spatial and landscape structure that plays an important role in the shaping of the identity of the city [2]. The historical city centre, surrounded by the waters of the main channel of the Oder River from the north and cut off from the south by the City Moat, Wyspa Piasek and Ostrów Tumski – are areas of particularly precious cultural and spatial values. They are under strict protection due to their cultural value and historical architectural substance [4]. Numerous historical relics have been either preserved or rebuilt in the area after the destruction wrought by the Second World War. The attractiveness of areas in the vicinity of historical downtown areas for new development projects can constitute a threat to the urban cultural landscape. However, it can also be an opportunity to enrich urban tissue with new cultural values – both spatial and aesthetic.

In the views from the southern bank and the western tip of Wyspa Słodowa, as well as across the University Bridge, new tall buildings located on the waterfront of the Oder River in the vicinity of the Władysław Sikorski bridge near Podwale and Generała Sikorskiego streets – the Odra Tower and ATAL Tower buildings – were visible for a number of years in the panorama of the northern edge of the Old Town in the context of the historical buildings forming the frontage of the southern bank of the Oder River. The buildings visible in this frame on the first plane are historical structures – the Baroque Church of the Holiest Name of Jesus, which is currently a university church, as well as the grand, almost two-hundred-metres-long building of the Wrocław University, also from the Baroque period, near Grodzka street, which has a local landmark – the Mathematical Tower. On the subsequent plane in this view we can see the massing of the roof of the Gothic-period Basilica of St. Elisabeth of Hungary and the tall tower with a Renaissance-era dome that stands above it (91,46 m) [9]. Initially, the tower had a pointed dome from the middle of the fifteenth century, with a height of 130,5 metres, which made it the tallest building in Lower Silesia. This tradition is perhaps associated with contemporary yearnings and concepts of pursuing prestige for the city by constructing tall and high-rise buildings.

The view described above has been completely altered – the Odra Tower and ATAL Towers have been covered by a new complex of eight and nine-storey residential buildings with commercial spaces in their ground floors that are being built near the Pomeranian Bridge, on its western side, near the eastern tip of Kępa Mieszczańska and near Księcia Witolda Street.

The second observation point from which the aforementioned buildings are visible in the context of the panorama of the Old Town is a short section of the southern waterfront of the Oder River below the intersection of Długa and Rybacka streets near the Romana Dmowskiego Bridge. However, from this spot we can only see the tower of the Basilica of St. Elisabeth of Hungary – which will still be playing the part of a well-exposed local landmark from this perspective. The remaining buildings of the Old Town, including the tower of the Town Hall, are obscured by rows of trees and existing buildings that are located between the site in question and the urban tissue of the Old Town.

The **Odra Tower** residential and service building, built in the years 2011–2013 (Generała Sikorskiego Street/Podwale, Wrocław – Old Town: developer – GNT Development from Legnica; designer – Biuro Projektów i Realizacji Inwestycji M.Z. Walas; completed between 2011–2013) [5], which is qualified as a high-rise building due to its height reaching 61 metres, was the first tall structure located at this site, at a relatively close distance away from the historical buildings of the Old Town – around 500 metres away from the tower of the Basilica of St. Elisabeth of Hungary when measured in a straight line and 700 metres away from the aforementioned Mathematical Tower of the university building. From the observation point located in an open public space on the western tip of Wyspa Słodowa, from which the Odra Tower building was visible in the context of the previously described historical buildings of the Old Town – it remained in good relations with them, preserving an appropriate scale, one that neither collided nor competed with the landmarks of the Old Town. It is unfortunate that this structure, although properly placed within the spatial structure of the city – accentuating
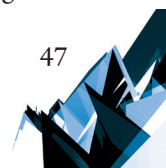
Fig. 1. ATAL Towers – Part I – eight-storey buildings, view towards the west from Generała Sikorskiego Street

the exit point from the Generała Sikorskiego Bridge – does not, however, introduce any new values into the cultural landscape.

The existing Odra Tower building was built in place of a previously planned high-rise – which was to have 35 stories and be 140 metres high [10]. Placed on a four-storey orthogonal base with an oval floor plan, its architectural concept was characterised by a dynamic massing with a contemporary expression. The different geometry of the form, one that did not refer to historical buildings, had probably been meant to ensure its neutrality. However, it appears that the placement of the planned building so close to the unique historical buildings and the disproportion in terms of scale would be detrimental to the perception of the downtown urban complex.

The construction of the **ATAL Towers** building complex (Generała Sikorskiego Street, Wrocław – Old Town: developer: ATAL S.A.; designer – AP Szczepaniak, Wrocław; design – 2014–2015; construction – part I (urban blocks I–II) – 2017; part II – 2018 [6, 12, 13] in the direct vicinity of the previously discussed building made it possible to create a waterfront frontage with better proportions and a contemporary architectural atmosphere. The complex is composed of two parts – to the west is part I (MW19) – with lower buildings featuring seven storeys, from the side of the Oder River, and eight storeys from the side of Generała Sikorskiego Street, with a floor plan in the shape of the letter "L" – along with the existing buildings at Sikorskiego Street, in accordance with the guidelines of the local spatial development plan (Resolution of the City Council of Wrocław No. IV/48/07, Official Journal

of the Lower Silesian Voivodship of the 26th of March 2007, iss. 80, pos. 911) [11] it forms an urban block with a relatively expansive internal courtyard and features service spaces on the ground floors. Along the course of former Sokolnicza Street a twenty-metre-wide belt was designed, attractively developed with preserved tall greenery, forming a pedestrian public space. It separates two compositionally integrated complexes of buildings which are being built as a part of this project. Part II of the complex (MWU 2) has also been shaped in the form of an urban block, cut open by a narrow internal courtyard, open towards the river. Two eighteen-storey (55 metres tall) towers have been connected from the side of Sikorskiego Street with a lower, five and eight-storey segment. There are service spaces on the ground floors, accessible from open public spaces. The underground part of the building includes parking garages. Vertical cracks – cuts in the towers divide them into narrower, more dynamic forms. The slight slants and deviations from the vertical direction, highlighted in the lower buildings by narrow, vertical belts of silvery openwork covers from cut and stretched steel sheets interchangeably connecting several storeys of belt-like terraces each, cause the architecture to become dynamic, as if it was in motion. The slender segments of narrow white towers with horizontal belts of terraces surrounding the buildings, encircled with the same openwork material, through subtle deviations of the facades from the vertical direction and black cracks – also participate in this dynamism as well.

From the side of the river a pedestrian promenade was created – attractively arranged, conducive to rest and recreation, with both low-lying and tall greenery, street furniture and

Fig. 2. ATAL Towers – Part II – eighteen-storey towers with a lower, eight-storey base, view towards the east from Generała Sikorskiego Street

Fig. 3. ATAL Towers – pedestrian zone at Sokolnicza street between Parts I and II of ATAL Towers, view from Generała Sikorskiego Street

Fig. 4. ATAL Towers – Part I – view of the frontage of Oder River's riverfront with a pedestrian promenade above the river

five terraces over the Oder River supported by cantilevers. This project enriches the entire layout, introducing a contemporary, attractive atmosphere of architectural forms. The ATAL Towers complex meets the conditions outlined in the local detailed plan in terms of the principles of shaping space and the size of the buildings – by creatively adapting them (Fig. 1–6).

The close proximity of the historical downtown urban complex, particularly the possibility of placing a residential building in direct contact with water, attracts developers who are expecting high-standard projects to be successful. The prices of dwellings – apartments in such locations are sometimes many times higher, however, it is the market that will verify the economic success and rate of return of such projects. In terms of urban space, the possibility of building architecture with unique qualities and a high quality standard, one that blends in with original, modern design into a cultural landscape with such exceptional qualities – that has not yet been vandalised by standard commercial buildings that do not introduce any new aesthetic value to the unique spatial environment – is particularly valuable.

Completed projects with high aesthetic qualities undoubtedly include the residential and service **Rezydencja Piasek** building (Wrocław – Old Town, Wyspa Piasek, Staromłyńska Street; developer – Emmerson S.A.; designers – Pracownia Projektowa Dziewoński Łukaszewicz

Architekci S.C. and +48 Pracownia Projektowa; completion 2010–2015) [7, 14] – a four-storey apartment building that utilises the space of the attics and features a reception space and services on the ground floors and two underground levels with parking garages. The building is located near the northern waterfront of the Oder River and compositionally constitutes a continuation of one of the two surviving buildings of the former mill – which is currently awaiting adaptation. The preserved historical complex of buildings in the central part of the island, including the Gothic Church of Mary the Mother of God at Piasek and the Baroque monastic buildings – is a demanding neighbourhood of high cultural and spatial value, essential to the history and identity of the place. Another of the location's advantages is the attractive development of the open green spaces of the island, with pedestrian pathways and a picturesque connection through its seven bridges with the Old Town and four other islands, as well as Ostrów Tumski. The contemporary, creative interpretation of the traditional form of the building with a gabled roof covered in red ceramic tiles and with red ceramic cladding on the walls criss-crossed by black belts of aluminium and glass facades with oriels, glass railings and the exotic timber cladding of the terraces and balconies – is the high standard that makes itself evident in the finishes and that announces the quality of the interior. As a result, the designers and the developer created a building that has achieved a unique form and contemporary expression, integrally connected with the historical context of the place (Fig. 7).

Fig. 5. ATAL Towers – Part II – residential towers, view from the pedestrian promenade

Fig. 6. Pedestrian promenade above the Oder River – ATAL Towers, with the Odra Tower in the background, at Podwale/Generała Sikorskiego streets, as well as Sikorskiego Bridge

The **Marina III** apartment building is also a completed project with exceptional spatial quality, while at the same time being placed literally "on the water" (Wyspa Pomorska, Wrocław – Old Town; developer – Topacz Investment sp. z o.o.; designers – Major Architekci – Pracownia Projektowa; design – 2014; completion – 2016 – 2018) [8, 15]. It is located on Wyspa Pomorska – on a narrow belt of land between the main outline of a branch of the Oder river and the so-called Śluza Mieszczańska – on the eastern side of the Pomeranian Bridge. The Marina III complex is composed of two buildings separated by a visual opening with a width of around 8–10 metres – which opens the view of the Mathematical Tower of the Wrocław University building from the Pomeranian Bridge and the eastern part of Księcia Witolda Street. The buildings occupy the entire surface of the eastern tip of the island, with a width of around 30 metres, providing an actual impression of living on water. The buildings are five storeys high (15 metres) – with a ground floor with commercial spaces (shops, gastronomy) and two underground levels with a parking garage. The two-hundred-years-old oak tree that grows right near the bridge was exposed from the direction of the entry hall leading to one of the buildings. The simple, geometric forms of the buildings covered with a flat roof feature transparent glass facades – which open up to views of the surroundings, primarily including the historical building of the Wrocław University. The glass facades are hidden beneath movable wooden blinds in the colour of black coffee, as well as the graphite black of a concrete grate, both of which constitute the "external skin" of the buildings, fulfilling both structural and aesthetic functions – creating the distinct climate of this architecture – which is peaceful, neutral and simultaneously immensely expressive. The mobile blinds dynamise the calm facades of the buildings. Marina III is an example of inscribing an architecture with contemporary aesthetic qualities into an urban space with unique, historical values in a good manner (Fig. 8).

Fig. 7. Rezydencja Piasek – view from the south

Fig. 8. Marina III – view from Księcia Józefa Street

An earlier project in the immediate vicinity of Marina III is the cameral, three-storey building with a gabled roof and distinct, two-storey oriels – the Marina I. It is a building that can also be presented as a successful project on a good scale, which also constitutes a contemporary interpretation of tradition. The building, with a residential function, offers services on the ground floor – restaurants, a coffee shop and a gallery. The public function, in combination with an accessible public space – the restaurant garden, with a jetty for yachts nearby – creates a good atmosphere of the place [3].

* * *

The completed projects that have been discussed implement the postulate of shaping new aesthetic values into the spatial environment of Wrocław's urban areas to a varying degree, as defined in the text of the article. However, there are numerous places that still wait for successful redevelopment interventions. New structures that will fill the gaps in the waterfront buildings of the southern edge of Kępa Mieszczańska will have a decidedly important role in the perception of this urban landscape. In this location it is necessary to preserve the appropriate scale of the buildings that create the new riverfront, as well as the pursuit of a contemporary architecture that introduces new aesthetic values into the urban cultural landscape.

Translated by K. Barnaś

53

References

[1] Tomaszewski A., *Ku nowej filozofii dziedzictwa*, E. Święcka (ed.), Międzynarodowe Centrum Kultury, Kraków 2012.

[2] Januchta-Szostak A., *Rola architektury w kształtowaniu tożsamości miejskich frontów wodnych*, „Zeszyty Naukowe Politechniki Poznańskiej", Poznań 2009, iss. 19, 119–127.

[3] Horn P., *Fenomen relacji miasto – rzeka w nowych formach przestrzeni publicznej we Wrocławiu / Phenomenon of relationship City – River in new forms of public space in Wroclaw*, „Czasopismo Techniczne" 1-A/1/2012, 269–280.

[4] Netczuk Ł.K., *Zmiany w krajobrazie nadrzecznym centrum Wrocławia – zagrożenia i szanse na rozwój*, [in:] *Miasto w Kulturze*, E. Trocka-Leszczyńska, E.Przesmycka (eds.), Oficyna Wydawnicza Politechniki Wrocławskiej, Wrocław 2012, 237–253.

[5] https://www.urbanity.pl/dolnoslaskie/wroclaw/odra-tower,b378 (access: 22.08.2018).

[6] http://www.apsz.com.pl/pl-projekt-atal-towers.html (access: 22.08.2018).

[7] https://investmap.pl/artykul/artykuly,wroclaw-wroclawian-nie-stac-na-mieszkanie-na-wyspie-piasek,62263 (access: 25.08.2018).

[8] https://www.urbanity.pl/dolnoslaskie/wroclaw/marina-iii,b8420 (access: 27.07.2018).

[9] https://pl.wikipedia.org/wiki/Bazylika_św._Elżbiety_we_Wrocławiu (access: 24.07.2018).

[10] http://www.bryla.pl/bryla/1,85301,5987786,Czy_powstanie_Odra_Tower_.html (access: 24.07.2018).

[11] http://uchwaly.um.wroc.pl/uchwala.aspx?numer=IV/48/07 (access: 2.08.2018).

[12] https://www.urbanity.pl/dolnoslaskie/wroclaw/atal-towers-we-wroclawiu-juz-gotowy,w16325 (access: 24.07.2018).

[13] https://architektura.info/index.php/architektura/polska_i_swiat/atal_towers_we_wroclawiu (access: 22.08.2018).

[14] http://www.bryla.pl/bryla/1,85301,18330507,rezydencja-piasek-we-wroclawiu.html (access: 22.08.2018).

[15] http://sztuka-architektury.pl/article/3198/nowy-apartamentowiec-od-major-architekci (access: 27.07.2018).

Małgorzata Hryniewicz ⬤ orcid.org/0000-0002-8034-1520
malgorzata.hryniewicz@pk.edu.pl
Institute of History of Architecture and Monument Preservation, Faculty of Architecture,
Cracow University of Technology

Royal residence in Lobzow. Transformations from the 13'th
to the 20'th century against the background
of the research state analysis in chronological order

Królewska rezydencja w Łobzowie. Przekształcenia
od XIII do XX wieku na tle analizy stanu badań
w ujęciu chronologicznym

Abstract

700 years of the former royal palace in Lobzow's history is a period of reconstruction and adaptation. Time faded traces of a representative residence and the nineteenth century brought her down. Reconstruction for the Austrian Kadetten Institut replaced the charming ruin with the barracks. Sources regarding the history of Krakow's Officer Cadet School are very diverse and largely unrecognized. They cover both the architectural object and the entire town where it was located. They concern its ownership status, topography of the area, natural properties and urban values in relation to the capital city of Krakow. The author of this article attempted to characterize the transformation of the royal palace in Lobzow over the centuries, based on an analysis of its state of research.

Keywords: Łobzów, rezydencja królewska, zamek, pałac królewski, przekształcenie zabytku, historia pomnika, historia Łobzowa

Streszczenie

700 lat historii dawnego królewskiego pałacu w Łobzowie to okres przebudów i adaptacji. Czas zatarł ślady reprezentacyjnej rezydencji, a XIX wiek przyniósł jej upadek. Przebudowa dla austriackiego Kadetten Institut zastąpiła urokliwą ruinę koszarami. Źródła dotyczące dziejów krakowskiej Podchorążówki są bardzo zróżnicowane i w dużej mierze mało rozpoznane. Obejmują one zarówno obiekt architektoniczny, jak i całą miejscowość, w której został on zlokalizowany. Dotyczą jej statusu własnościowego, topografii terenu, właściwości naturalno-przyrodniczych oraz walorów urbanistycznych w odniesieniu do stołecznego Krakowa. Autorka niniejszego artykułu podjęła próbę scharakteryzowania przekształceń łobzowskiego pałacu królewskiego na przestrzeni wieku na podstawie analizy stanu jego badań.

Słowa kluczowe: Lobzow, royal residence, castle, royal palac, transformation of the monument, history of the monument, history of Lobzow

Palace in Lobzow (Fig. 1 [4]) is the second most important royal residence in Krakow after Wawel. During the course of its almost seven-hundred-year-old history, the complex had undergone several stages of thorough reconstructions and adaptations.

One could say that it was doomed to constant changes: a fine royal residence ended up as scenic ruins just to get completely transformed into a military facility. As Zygmunt Kieszkowski wrote about the adaptation done by Kadetten Institut, "Austrian barracks took place of an old royal castle and with them, the charm was gone and the memories faded away" [14, pp. 6–25].
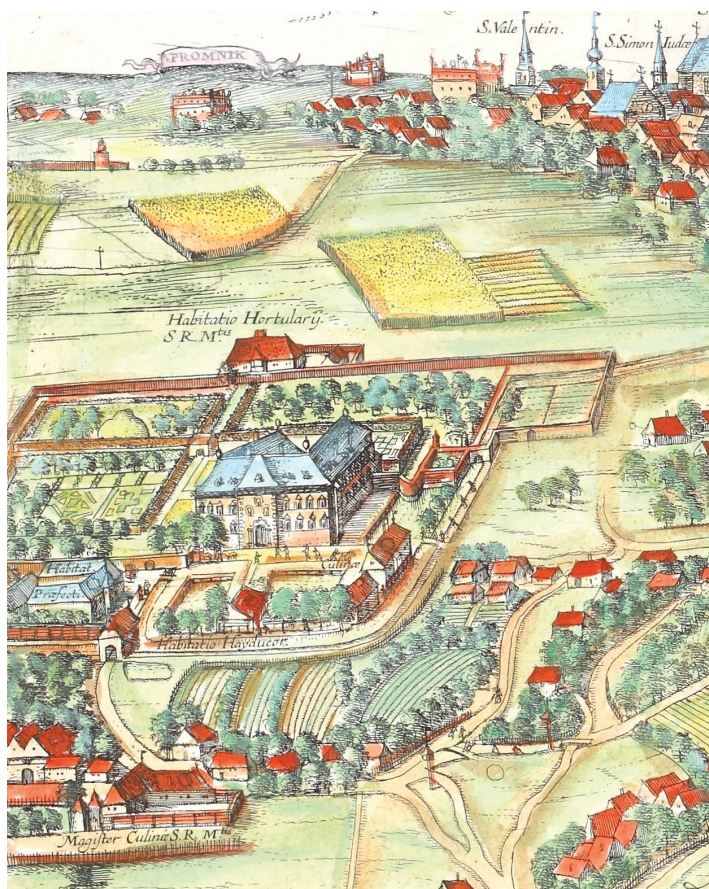
Fig. 1. A section of the view of Krakow in the work of G. Braun and F. Hogenberg Civitates orbis terrarum with the palace complex in Lobzow (soruce: [4])

1. The Middle Ages

It seems that because of its location, Lobzow was of vital significance for the development of the entire region, including the adjacent city: this is where the basis of settlement for the pre-incorporation Krakow. Its expansion was triggered by natural conditions [21, pp. 1–28], topography [2, pp. 138–172], distance from the overflowing Vistula [15], abundance of

56

groundwater, and local stretches of loess cover [14, p. 13]. Furthermore, thanks to erosion and geological processes, this land was enriched with fertile soil (as reflected in local nomenclature, e.g. "Czarna Wieś" which means "Black Village") that resulted in the common in historical literature opinions about the utility of acreage in Lobzow [25, pp. 24–25].

In political and economic terms, this area was also described as of the utmost importance for Krakow, as mentioned in the Incorporatioen Charter for the City of Krakow from 1257 that granted the office of Krakow borough the ownership of land on the western side – from Brama Szewska to Lobzow [30, pp. 236–237]. Most probably, this land had already belonged to knights, as it was exchanged for the village of Bosowice in the vicinity of Wislica that belonged to a duke[1] [12].

Analysis of the Diplomatic Code of the City of Krakow confirmed the significance of Lobzow as royal province: Władysław I the Elbow-high had Rudawa under his strict control, as proven by the document from 1306. This indicates to the need to obtain commune head's permission for the construction of mills that were located less than half a mile from Krakow, except for the already constructed and operating buildings [20, p. 304]. Thus, the river was of strategic importance as an inflow to the system of fortifications of the city. This was probably connected with the ruler's efforts to reclaim former capital of the Piasts and to complete the process of unification of the Kingdom of Poland. All these valuable lands were confiscated from the Krakow borough and incorporated into the royal province [20, p. 305]. This was a breakthrough moment. Sources confirm that already in 1317–1319 Rudawa existed and was called Młynówka Królewska.

Settlement there could have developed thank to the efforts of Casimir the Great who started and completed the establishment of royal jurydyki.

W 1357 Lobzow was divided which led to the demarcation of royal manor. This was where the out-of-town residence of the ruler was to be erected. Two villages were incorporated on the remaining part of the royal land, Czarna Wies in 1358 and Nowa Wies in 1367.

According to Jan W. Raczka, the construction of castle in 1367 in Lobzow in the reign of Casimir the Great is confirmed by the stone foundation relief with the Piasts' crowned eagle (Fig. 2 [28]) inscribed:

SUB ANNO D(OMI)NI MCCCLXVII INCEP(T)U(M) E(ST) (A)EDIFICARI HOC FORTALICIUM (P)ER DO(MIN)UM KAZ(IMIRUM) REGEM POLONIAE.

However, the hypothesis concerning the origin of the relief needs to verified due to: the partial destruction of the text; inconsistency with the date given by Maciej Miechowita; opinions of several art historians who connect this detail with a sculpture of the Silesian origin [10, pp. 305–307], even though some researchers support Jan Raczka's opinion [34].

---

[1]   Dzierżko (Deresław, Dzierzysław) bearing Janina coat of arms, knight of Malopolska and crusader from Chotla, a village in Ponidzie that nowadays belongs to Wislica district; according to Dlugosz, it was the oldest parish. Dzierżko, later the owner of Busko, founded a church and a Premonstratensian monastery there. Wit, the bishop of Plock, was his brother and co-founder. He was also from Chotla. According to Dzierżko's will written in 1190 before his departure for the 3rd crusade, he did not leave anything for his children, if he had them then. The village of Bosowice (according to Dlugosz, Bossowicze) was granted by Bolesław V the Chaste to Falkon, son of Dzierżko, in 1255, i.e. only two years before the incorporation of Krakow. If these are the same historical figures, Falek or Falkon could have been born after Dzierżko's return from the crusade around 1192.

Fig. 2. Stone foundation of Casimir the Great (1367) (source: [28])

The first Polish chronicle by Janko from Czarnkow that was created soon after Gallus Anonymus' text does not describe any defensive investments connected with Lobzow, not to mention the castle. The chronicle was written between 1370 and 1384, i.e. soon after death of Casimir the Great. One can find a description of the general activities of the king as translated by August Bielowski in 1907 when he wrote, "he [the king] surrounded all these cities and castles with very strong walls, deep moats, and towers for decoration of the state and to shelter and protect the kingdom of Poland" [19, p. 4].

An indicator of the existence of the fortified royal residence[2] [26, pp. 282, 284] might be an expression *Curia regalis Lobzow* from 1420 that was used in the Diplomatic Code of the Jagiellonian University as well as *curia regalis* from 1517 included in the same text [18, pp. 28–29].

In his *Annales*, Jan Dlugosz included in 1356 king's unfaithfulness to his wife, Adelaida, whom he abandoned for Rokiczana, townswoman from Prague. He left her later in order to start a relationship with Esterke, his Jewish mistress[3] [7, p. 277]. She was supposed to live in Lobzow. However, historians consider this fact to be unverified.

Without doubt, the oldest and the most convincing reference to Casimir the Great's castle there mentioning year 1357 dates at the beginning of the 14th century. It was written by Maciej of Miechow, called Miechowita, who included it in his historical work entitled *Chronica Polonorum* and issued in 1519 [1, pp. 43-67]. In the margin of a single-column Latin text on page 240 there is a remark: "Lobzow castrum erigitur", meaning: "Erection of the Lobzow castle". This event was elaborated on in the main text. The author reports the date (1357) and brief description of the complex that suggests that the castle had at least two elements: a tower and living chambers. According to the text, "Anno domini 1357 turrim & mansiunculas rex Kazimirus in villagio Lobzow iuxta Craccovia ad occidente construxit",

---

[2] The author believes that Casimir the Great's establishment in Lobzow was a form of out-of-city „curia", i.e. a complex of reduced defensive capabilities.

[3] "ad preces quoque praefatae Ester judeae et concubinae, exorbitantes praerogativas et libertates per literas singulis judaeis in regno Poloniae habitantibus, quae falso scriptae ab aliquibus insimulabantur, et quibus divina majestas contumeliatur et offenditur, concessit, quarum factor olidus etiam in hane diem perseverat".

which might be translated as, "In 1357 Anno Domini, king Casimir built a tower and chambers in the western part of the village of Lobzow near Krakow" [23, p. 240].

The above-mentioned quotation reveals the existence of a small *castrum* that included a defensive tower or gate and a building with living chambers. It is very probable that inside the defensive courtyard there were smaller and presumably wooden outbuildings, a well, stables, and rooms for troops.

Plural form of the word "mansiunculas" might suggest that there were at least several chambers serving different purposes. It is important that they might have been located on several stories[4]. Furthermore, there must have been a defensive wall around the castle courtyard.

It is worth mentioning that Dlugosz who most probably witnessed the erection of the royal residence in Lobzow did not mention this fact even once and yet meticulously listed all the other investments of Casimir. The first work to do so was *Kronika wszytkiego świata* by Marcin Bielski that was published for the first time in 1551 [3, pp. 414, 962–963]. It describes the castle as king's dwelling place and the complex where he would meet with consecutive mistresses.

Despite the fact that legends about Esterke's stay in the residence together with her bastard children until her suicide survived until the 18th century, the researchers consider this lover to lack authentication.

It is true that until the 1950s there was a mysterious mound in Lobzow's gardens that some considered to be her grave. Even **Stanislaw II Augustus** visited this place in 1787. Neither analyses of the mound conducted then nor any of the later analyses did reveal any human remains which is probably the reason why this royal mistress is believed to be fictional.

Looking at amatory conquests of the king, one can suspect confabulations about his stays in Lobzow. However, one cannot question the existence of *fortalicjum* from the Late Middle Ages. It is mentioned by Miechowit in *Chronica Polonorum* and cofirmed by the illustration prepared at the end of the 16th century by court clerks making an inventory. One can learn from it that there were still some elements of the Casimir the Great's fortress and that there were plans to convert it to a more modern complex. Stephen Báthory was behind this decision as at the beginning of 1585 he commissioned Santi Guci to erect him "a new home". The ruler was interested in the progress of construction works, as proven by numerous letters about the project and its implementation exchanged with Jacek Mlodziejowski, royal governor, who was responsible for an investment process conducted on behalf of the king [31, pp. 23–24].

2. Modern Times

Krystyna Sinko, author of the monograph on Santi Gucci's works [31, pp. 23–24], believes that the Palace in Lobzow as designed by the Italian (Fig. 4. [31]) was completed by Anna Jagiellon after Stephen Báthory's death and that the complex was "depicted in the famous panorama of Krakow from the first quarter of the 17th century created by Visscher de Jonge" [31, p. 25].

---

[4]   This version is supported by the analysis of similar solutions from the same period and especially defensive investments of Casimir the Great.

It is difficult to completely agree with this thesis but is should be emphasized that the author made an archival discovery in the Military Directorate [sic!] in Krakow. She found "plans of palace demolition… (from the 1850s) and a design for a new building with marked old parts that were to be included in the new building" [31, p. 26–27] which is of vital significance for future research on the modern complex and for the creation of scientific database of knowledge about its architectural past.

Two images of the royal castle in Lobzow from the Cracow panorama from the 17th century:
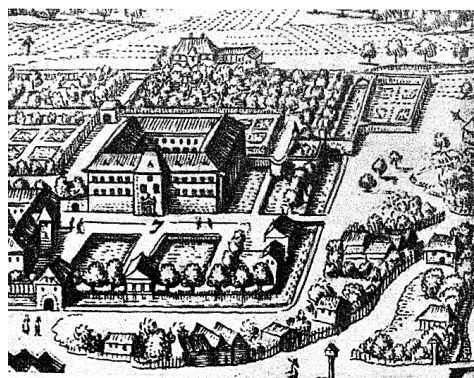
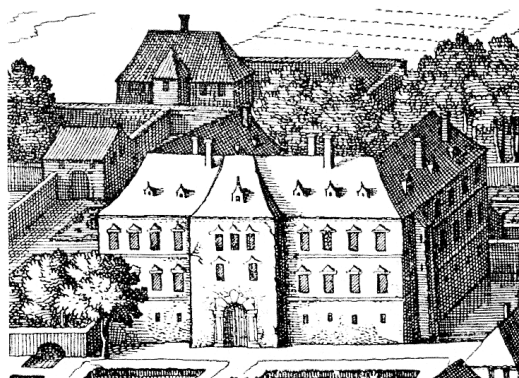Fig. 3. According to M. Merian's copper from 1619 (source: [25]) Fig. 4. According to copper from the 17th century (K. Sinko) (source: [31])

Unfortunately, the original was lost during World War Two and because of their poor quality, copy and microfilm make it difficult to verify the interpretation of these plans.

The researcher points out that Santi Gucci "never signed anything as a sculptor or a carver. It seems that he considered sculpture as an extra job and architecture as his main occupation and wanted to achieve fame as an architect" [31, p. 23]. Having in mind the above-mentioned quote and analyzing the certificate issued by Stephen Bathory in Niepolomice on July 8, 1585, one can deduct that Florentine builder was connected with the investment process before: "… thym listem naszym komu tho wiedzicz naliezi, Iześmy zuwily Santiego Gucciego sługe naszeo, ktorey się podyął swoją materią w lobzowie Nowey Dom Sfondamentu vedlie wizerąką y miary w niem naznaczoney zmurowacz…" (Old Polish; English translation: „we hereby declare to whom it may concern that we have hired our servant Santi Gucci who undertook to use his means to construct a new house in Lobzow from scratch abiding by plans and measurements set in them") [14, pp. 24–25].

Another well-known documents from the end of 1585 specifies that a construction of the new building had not reached the first floor level [31, p. 23] which led to the intervention of the ruler who worked on the designs himself. Thus, one can suspect that the delays in construction works were caused by his frequent trips outside the capital. However, it is safe to assume that Santi Gucci had to set about working beforehand, maybe even at the beginning of the 1580s, and prepare the designs.

It is also well-known that after king's death in 1586, Anna Jagiellon continued to work on the complex. Most probably, the goal was to achieve living conditions which did not mean full completion of her late husband's vision who *were striving for something greater* [31, p. 24].

K. Sinko believes that "palace in Lobzow depicted in the famous panorama of Krakow from the first quarter of the 17th century created by Visscher de Jonge must have an outline of S. Gucci's design even if His Majesty's Mason did not participate in any conversions after Anna Jagiellon's death" [31, p. 25]. She has no doubts that having at her disposal "plans of palace in Lobzow demolition (from the 1850s) a design for a new building with marked old parts that were to be included in the new building" that she discovered, [31, p. 27], she could have thought that "old plan of the building… corresponds visually with the external view of the palace in Visscher de Jonge's drawing" [31, p. 27].

Despite the fact that one should treat K. Sinko's work with reserve (given the state of knowledge she had at the beginning of the 1930s), it should be emphasized that her text represents a valuable contribution to the creation of a new field of research that was later expanded by Witold Kieszkowski with Jan Zachawatowicz and Andrzej Fischinger.

In his publication from 1935 entitled "Zamek królewski w Łobzowie", Witold Kieszkowski not only emphasized the multilayer stratigraphy of the complex and undertook and attempt at reconstructing the stage from Crisimir's times but also applied a new research method based on a simple comparison of written, iconographic, and cartographic sources.

The author admits that designs published in „Santi Gucci Fiorentino i jego szkoła" "constitute new and very valuable materials that led to the significant progress in the field of research" [14, p. 7] but he questioned a view that figure of a castle depicted on Mateusz Merian's drawing (Fig. 3. [25]) dated back to Stephen Bathory's times and presented work of an Italian architect. W. Kieszkowski has his own hypothesis "that Stephen Bathory's castle, including old buildings, probably dating back to Crisimir's times, had to be much smaller than the 18th century castle" [14, p. 11]. While interpreting the inventory from 1595 he decided that the new wing constructed by Sigismund III Vasa was added from the south along the entire length of Bathory's elevation.

However, this hypothesis does not withstand confrontation with archaeological investigation conducted much later. Even though it was incomplete and based on samples, it did not confirm this layout of the complex and can be considered as another proof of weakness of theoretical discussions that are not supported by the examination of the architectural structure of the given building.

Following Krystyna Sinko, Witold Kieszkowski conducted detailed analysis of sources and inventories from Báthory's and Sigismund III Vasa's times that include information about buildings belonging to the fortress of Casimir the Great: "Iześmy zmuwily Santego Gucceo sługe naszeo, ktorey się podjął swoią materią w lobzowie Nowey Dom Sfondamenta vedlie wizerąką i miary w niem naznaczoney zmurowacz… A od thego domu zobu stro mury na frambugach sgankami zasklepistemi… ktoremi Gankami ma bicz chodzenie stego noweo Domu zobu rogow do starey wieze… vedlug vizerąką do ktorey starey wieze ma fundamenti opatrzicz i now Filiari dlya umocznienia zmurowacz…" (Old Polish; English translation: "We hereby declare to whom it may concern that we have hired our servant Santi Gucci who undertook to use his means to construct a new house in Lobzow from scratch abiding by plans and measurements set in them… And from this house on both sides of the walls roofed over galleries… that can be used to walk to this new house from both corners to the old
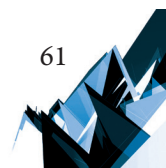
tower… According to the design, they are to restore foundations of this old tower and add new pillars to enhance it…")[5] [14, p. 24–25].

Inventory from the transfer of castle and the entire manor in Lobzow to the royal governor of Sigismund III Vasa includes an important confirmation that "kamienicza" (tenement) built by Santi Gucciego was completed just as "The second old renovated tenement was restored". This is without question information about the renovation of a construction built by the last royal from Piast dynasty commissioned by Stephen Bathory and called by Miechowita *mansiunculas.*

One can also find there crucial information about how the most important parts of the fortress are positioned towards each other and their relation in the context of adaptation proposed by the Italian architect: "Naprzod do zamku wchodzącz nad Brama Wielgą y przedniejszą do kthorey wiazd od sadzawek INSIGNIA troie Coronne… Pierwszey Czeszci zamku thego Kamienicza Athara kthora po prawey recze naweszcziu od sadzawek w dziecziniecz ku wschodu słoncza iesth postan-wiona…" (Old Polish; English translation: Coming to the castle from the front over the first great gate that can be entered from the ponds, the royal INSIGNIA… From the first part of this castle an old tenement that is built on the right next to the entrance to the ponds in the courtyard facing east…[6] [14, p. 25].

Witold Kieszkowski focused on the interpretation of documents published by K. Sinko and together with Jan Zachwatowicz tried to use that and iconography determine for the first time the outline of Casimir's designs. Findings concerning its fate after Anna Jagiellon's death were connected with activities of Giovanni Trevano who conducted another expansion of the palace for Sigismund III Vasa and redid it in the baroque manner [14, pp. 7–8].

Based on the comparison of this data with iconography and cartography from the 19th century, the above-mentioned researchers proposed the reconstruction (Fig. 4 [14] and Fig. 6 [14]): they visualized an „old tenement" described in the sources as a building on a rectangular plan with a surface area of just 9.5x19 meters. While the interpretation of the location of this building may not raise any doubts, neither its size nor the outline can be confirmed by archaeological examinations [12].

It is worth noticing that W. Kieszkowski describes the post-Casimirian complex as a habitable defensive tower standing in the unrecognized spatial context that was more of a *curia militaris* than a stronghold. Thus, the most probable would be the version with the defensive fortress (*castrum*) surrounded with a stone curtain-wall with a defensive gateway (*turrim*) and included in the curtain tower or rather, a residential tenement (*mansiunculas*) [33, pp. 119–124].

It is worth noticing that according to the sources, the gate was *first and great* and, most notably, was where the royal insignia were placed. One can assume that these are mentioned by Miechowita *turrim* and that this is where a stone royal coat of arms of Casimir the Great was displayed, as described by Jan W. Rączka [28, pp. 7–21].

---

[5]   Quotation from Annex no. 1.
[6]   Quotation from Annex no. 2.
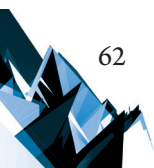
The publication of W. Kieszkowski and J. Zachwatowicz leads to important conclusions that are worth emphasizing: marking out an element that was a part of Casimir's *castrum*, i.e. an "old tower" that was absorbed by the buildings erected by Stephen Báthory and next, third stage created in times of Sigismund III Vasa that was described in the sources as "palacium sumptuosissimum … et hortus cultissimus" [14, p. 7] and finally destroyed during the Polish–Swedish wars and, despite John III Sobieski's efforts, never rebuilt.

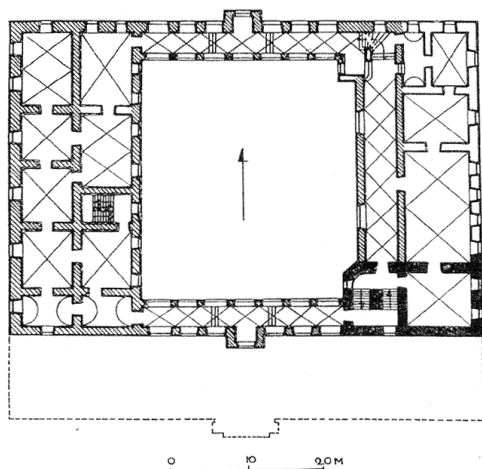Royal castle in Lobzow: reconstruction according to W. Kieszkowski and J. Zachwatowicz:

Fig. 5. Plan of the first floor after the reconstruction in the 1594–1595 (fortalice of the Casimir the Great marked in black, reconstruction by Stephen Báthory in szraf) (source: [14])
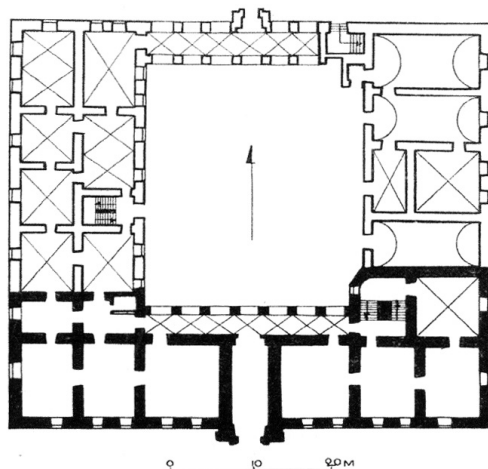
Fig. 6. Base plan, state from the 17th century (state of preservation of the ruins in the first half of the 19th century marked in black) (source: [14])

New post-war literature on the subject includes a number of outstanding researchers of Krakow's architecture who included royal palace in Lobzow, such as: Andrzej Fischinger [9], Helena Kozakiewiczowa [16], Janusz Bogdanowski [4], Bogusław Krasnowolski [18], or Jan Raczka [27]. Hypotheses proposed by the above-mentioned people are largely based on archival sources and are not supported by field research, especially archaeological and architectural, but are very useful when planning such research[7].

Work of A. Fischinger published in 1969 and focused on the works of Santi Gucci presented new original findings as it was based on new source materials that K. Sinko was unaware of [9].

Based on "numerous mentions in the archives" [9, p. 15] that were not discovered by the author's predecessor, he assumed that construction of the new manneristic palace conducted by the frequently mentioned, Florentine architect was finished in the spring of 1587 and that the "newly-erected palace" [9]. remained unharmed during the siege of Krakow in October 1587. His observations were based on the information that this was where Anna Jagiellon

---

[7] Archaeological research was conducted by: A. Filipowicz and M. Myszka (survey research); IHAiKZ team (excavation): under the direction of A. Kadłuczka, cooperation J. Czubiński, archaeology K. Kadłuczka, consultation Z. Pianowski.

displayed Stephen Bathory's body before the ceremonial funeral in the Wawel Cathedral. Based on the interpretation of royal inventories, A. Fischinger sees Báthory's layout like that (Fig. 7 [9] and Fig. 8 [9]): "Main residential building (new house) stood on the western side; there was an old residential „tower" from the east and most probably a gallery; from the south and the north the courtyard was enclosed by galleries with entrance gates in small towers. Conformity of the inventory description to the contract seems to indicate that during the erection of the palace the designs were not changed" [9, p. 17]. Thus, he assumes that the complex had a southern elevation (Fig. 9 [9]) shifted towards north compared to the subsequent southern wing of Sigismund III Vasa.
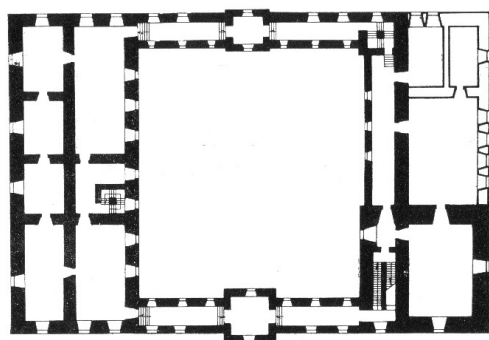

Royal castle in Lobzow: reconstruction according to A. Fischinger from 1595:

Fig. 7. Ground floor plan (source: [9])   Fig. 8. First floor plan (source: [9])
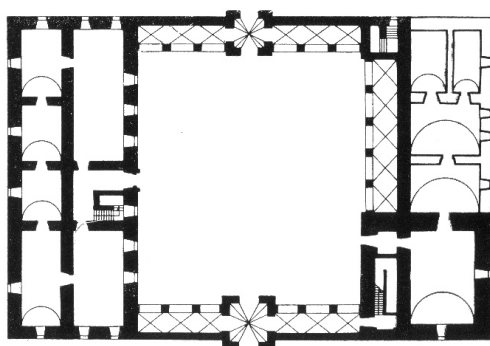
The postwar period resulted in axtensive research in the composition of royal gardens in Lobzow. Publications on that were published by such people as: Gerard Ciołek [6], Leszek Majdecki [22], Janusz Bogdanowski [4], etc.

Renaissance stage of conversion of residence in Lobzow including the layout of gardens was examined and reconstructed in theory by Janusz Bogdanowski in his work "Królewski ogród w Łobzowie" from 1997 [4] and by Jan Raczka in his study entitled "Królewska rezydencja cz. I–II" [28, pp. 7–21]. The author developed his concepts in the subsequent „Przemiany krajobrazu podkrakowskiej rezydencji Łobzów" [29, p. 16]. Nowadays, most up to date is a text by Boguslaw Krasnowolski and Jan W. Raczka prepared for a scientific session of Towarzystwo Milosnikόw Historii i Zabytkow Krakowa (TMHiZK) and published in 2007 [18]. It includes the state of research and review of sources, an attempt at reconstruction of changes in the complex, and a detailed calendar of events happening during the last 350 years.

3. Architectural and archaeological field research after 1945

The first archaeological research in a place of an old palace was conducted in 1960 on the initiative of the Archaeological Museum of Krakόw and Katedra Historii Architektury Polskiej at Politechnika Krakowska (Department of History of Polish Architecture at the University of Technology in Krakow). Results of this research were published only as a collective report
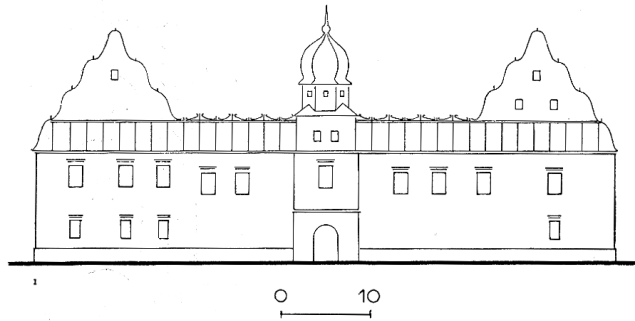
Fig. 9. Royal castle in Lobzow: south elevation's reconstruction according to A. Fischinger based on plans from 1595 (source: [9])

[27, pp. 245–246]. As Kazimierz Radwanski describes the excavations, "where the western wing and the northern gallery connected, confirmation of traditions was found, an extensive rubble, as well as the corner of a previous building, and at last, an architectural detail with the Vasas coat of arms".

Unfortunately, later on the research was not continued in the building itself.

Renovation works and adaptation needs after the takeover of the building of the old "Podchorazowka" by the WAPK authorities together with the provisional placement of the Voivodship Conservator of Monuments Office in the eastern part of the front wing made it possible to conduct survey architectural and archaeological research inside the building and limited research during the construction works aimed at securing foundations and adding fittings.

Archaeological research in the southeastern wing of an old palace (Fig. 10 [12]) were conducted by Klaudia Stala in 1999 [12]. As a result, a southeastern corner with stone facing of the pedestal were uncovered (Fig. 12 [32]), an extensive base of a corner pilaster strip in the southern wing (Fig. 11. [32]), identified as remains of the residence from Sigismund III Vasa times.

Fig. 10. Diagram of exposed walls of the royal palace in Lobzow during archaeological research in 1999, situational plan, ARCHECON drawing documentation (source: [12])

Photographs of excavations from 1999 (photos obtained thanks to the kindness of the author of research, K. Stal):

Fig. 11. The exposed corner's view of the palace of Zygmunt III Waza with a stone foundation and a corner lizen (source: [32])

Fig. 12. View of the stone pedestal associated with it, confirming the credibility of iconographic messages from the first half of the 19th century (source: [32])

Interpretation of this research that was expanded during archival studies was published by its author in 2015 [32, pp. 54–60].

Stratigraphy of the walls unveiled in 1999 in the south-eastern room of the "Podchorążówka" (photos obtained thanks to the kindness of the author of research, K. Stal):

Fig. 13. View of the brick floor from the turn of the 16th and 17th centuries (source: [32])

Fig. 14. A deep excavation confirming the lack of a basement in this part of the building (source: [31])

Remains of the preserved fragments of the southern and eastern wall (Fig. 13 [32]) were placed on strong foundation walls that could have been from Late Middle Ages. However, inside the walls there was no basement (Fig. 13 [32]) and no "traces of medieval relics or layers from this period which excluded the location of the supposed fortress in this part of the building" [32, p. 57]. What was discovered where free or re-used hand-made bricks of large, medieval sizes "which may suggest the existence of a medieval building within the palace building that was demolished completely or in part" [32, p. 60].

Recent research conducted in 2015/2015 in the south-eastern wing of the current WAPK building can shed some light on the matter of placement of a residential tower erected by the Casimir the Great as part of the defensive complex. It was conducted in the small room that was to be adapted for elevator shaft.

Archaeological survey led to the discovery of the continuation of a main wall that was known from previous research from 1999 (S-N direction).

The overground part of this wall is interpreted by the author of research [13] as a relic that may date back to the reconstruction of the palace by Santi Gucci at the end of the 16th century.

What is very mysterious and requires further research is a foundation wall of significant thickness that reaches 220 cm and has a deep-set base. It is very probable that this wall was a foundation of the courtain-wall of the fortress or a residential tower erected by Casimir the Great and located in this area [13, p. 14].

When concluding the analysis of the state of research, it is worth to mention the valuable and unpublished materials gathered during two editions of *Warsztaty Doktoranckie* (*Workshops for Doctoral Students*) conducted at IHAiKZ in WAPK. During the workshops, studies and analyses of selected known historical and obtained (undistributed before) sources were conducted and compared with field research completed after 1945.

Finally, one should mention the results obtained by Aleksander Filipowicz and Marian Myszka [8, pp. 21–32] in 2003 (Fig. 15 [8]). Even though their works were not directly related to the complex and its stratigraphy, they might be helpful as a comparative material for research based on the comparison of written, iconographic, and cartographic sources.

Their activities covered the area that used to be part of the old manor in Lobzow and were connected with an investment planned there (plots 475/124 and 475/125 to the south of the main elevation of the building at Podchorazych Street that belonged to KS Wawel Krakow).
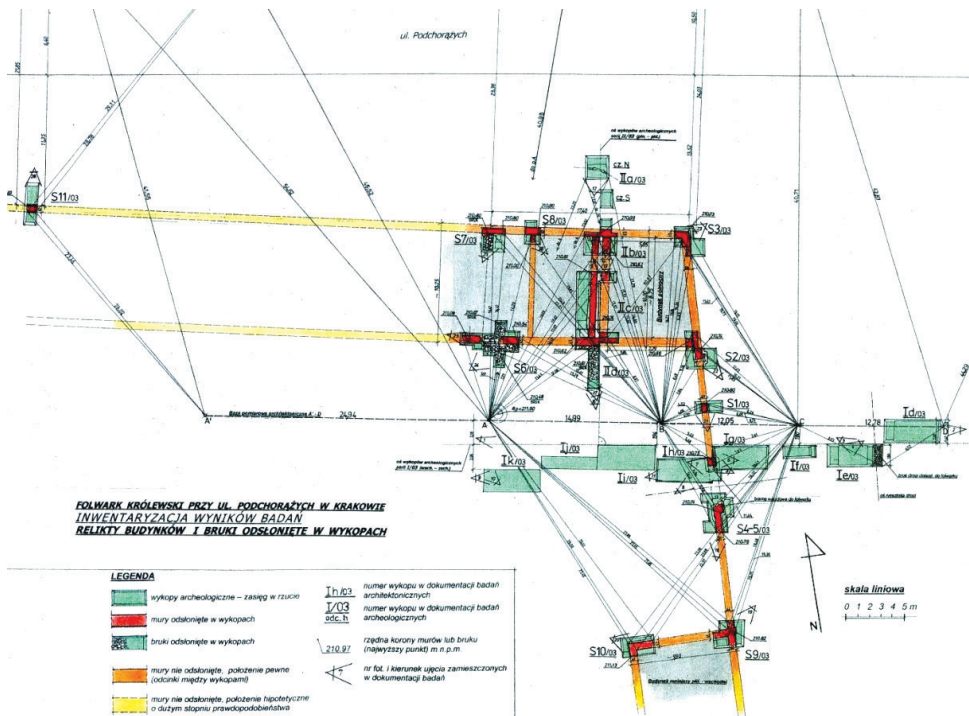
Fig. 15. Excavation plan with exposed walls and pavement (source: [8])

Their research revealed the relics of buildings (Fig. 16 [8]) that were described in the inspection from 1665. It was conducted after Swedish troops left Krakow [8, pp. 21–32].

Fig. 16. Relics of the north-eastern corner of the northern building, view from the south-east (source: [8])

4. Conclusions

Royal palace in Lobzow as a complex that has a reach architectonic history is a subject of many scientific studies. The building remains in the center of interest of many researchers. Its history is full of gaps that await filling. There are many unexplained issues that will undoubtedly lead to numerous debates and studies. It is certain that without grounding them in field research, it will be impossible to explain numerous secrets from the past. Analysis of historical sources and their subsequent studies clearly indicates that without architectural and archaeological research they will never be anything more than speculations and hypotheses.

Translated by Anna Oleszczuk.

References

[1]   Barycz H., *Życie i twórczość Macieja z Miechowa*, [in:] *Maciej z Miechowa 1457–1523*, Wrocław 1960.

[2]   Bąkowski K., *Dawne kierunki rzek pod Krakowem*, Rocznik Krakowski tom V, Kraków 1902, 138–172.

[3]   Bielski M., *Kronika polska*, Kraków 1597.

[4]   Bogdanowski J., *Królewski ogród w Łobzowie*, Towarzystwo Wydawnicze Historia Iagellonica, Kraków 1997.

[5]   Braun G. i Hogenberg F., *Civitates orbis terrarum,* Kolonia, 1617/ Muzeum Historyczne Miasta Krakowa, nr kat. MHK-905/VIII/1.

[6]   Ciołek G., *Ogrody polskie*, Warszawa 1954.

[7]   Długosz J., *ANNALES SEU CRONICAE INCLITI REGNI POLONIAE,* Państwowe Wydawnictwo Naukowe, Warszawa, 1978.

[8]   Filipowicz A., Myszka M., *Wyniki badań archeologiczno-architektonicznych dawnego folwarku królewskiego w Łobzowie, Krzysztofory,* nr 24, Kraków 2006.

[9]   Fischinger A., *Santi Gucci, architekt i rzeźbiarz królewski XVI wieku*, Biblioteka Wawelska, Kraków 1969.

[10] Gadomski J., *Funkcja kościołów fundacji Kazimierza Wielkiego w świetle heraldycznej rzeźby architektonicznej*, [in:] *Funkcja dzieła sztuki*, Materiały z Sesji SHS, Szczecin 1972, 105–107.

[11] Jurecki J., *Ponidzie: w świętokrzyskim stepie,* Wydawnictwo Bezdroża, Kraków 2007.

[12] Kadłuczka A., Kadłuczka K., Dokumentacja Techniczna: *Badania Historyczno-Konserwatorskie, Sprawozdanie 1999*, Kraków 1999.

[13] Kadłuczka A., Stala K., *Sprawozdanie z interwencyjnych badań architektoniczno-archeologicznych prowadzonych w południowo-wschodnim skrzydle budynku Wydziału Architektury PK (d. Pałac Królewski w Łobzowie) przy ul Podchorążych 1 w Krakowie*, 2016.

[14] Kieszkowski W., *Zamek Królewski w Łobzowie*, Biuletyn Historji Sztuki i Kultury, Kwartalnik wydawany przez Zakład Architektury Polskiej i Historji Sztuki Politechniki Warszawskiej, R. IV. Nr. 1, Warszawa 1935, 6–25.

[15] Kmietowicz-Drathowa I., *Zagadnienia starorzeczy na obszarze Krakowa*, Sprawozdanie z posiedzeń Komisji PAN w Krakowie, Kraków 1965.

[16] Kozakiewiczowa H., *Renesans w Polsce. Santi Gucci. Architekt i rzeźbiarz*, Wyd. Arkady, Warszawa 1983.

[17] Krasnowolski J., Rączka J. W*., Królewska rezydencja w Łobzowie*, [in:] *Pałace i wille podmiejskie Krakowa*, Materiały Sesji Naukowej TMHiZK, seria „Kraków w dziejach narodu" nr 24, Kraków 2007.

[18] Krasnowolski K., Rączka J. W., *Królewska rezydencja w Łobzowie*, [in:] Sesja Naukowa TMHiZK, Kraków 1999, 28-29.

[19] *Kronika Janka z Czarnkowa* wg tekstu Augusta Bielowskiego [in:] *Monumenta Poloniae Historica*, Lwów 1907.
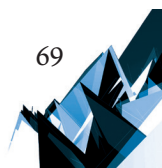
[19] Laberschek J., *Rozwój przestrzenny krakowskiego zespołu osadniczego extra muros w XIII–XVII wieku*, [in:] *Kraków. Nowe studia nad rozwojem miasta*, J. Wyrozumski (ed.), Biblioteka Krakowska nr 150, Wyd. TMHiZK, Kraków 2007, 304.

[20] Łuszczkiewicz W.*, Najstarszy Kraków na podstawie badania dawnej topografii*, Rocznik Krakowski t. II, Kraków 1899, 1–28.

[21] Majdecki L., *Rejestr ogrodów polskich*, z. 2, Warszawa 1965.

[22] Miechowita M., *Chronica Polonorum*, Wyd. H. Wietor, Kraków 1519.

[23] Muzeum Historyczne Miasta Krakowa, nr kat. MHK-906/VIII.

[24] Niezabitowski M., *Geografia a historia Krakowa. Warunki naturalne rozwoju Krakowa*, [in:] *Kraków. Nowe studia nad rozwojem miasta*, J. Wyrozumski (ed.), Biblioteka Krakowska nr 150, Wyd. TMHiZK, Kraków 2007, 24–25.

[25] Olszacki T., *Rezydencje królewskie prowincji małopolskiej – możliwości interpretacji*, Czasopismo Techniczne, 7-A/2011.

[26] Radwański K., *Konserwatorskie prace archeologiczne prowadzone w Krakowie w roku 1960*, Biuletyn Krakowski, T. III, Kraków 1961, 245–246.

[27] Rączka J. W., *Królewska rezydencja pałacowo-ogrodowa na Łobzowie. Stan badań i zachowane źródła archiwalne. Cz. 1–3*, [in:] *Teka Komisji Urbanistyki i Architektury T. XVI–XVIII*, Kraków 1982–1984, 7–21.

[28] J. Rączka, *Przemiany krajobrazu podkrakowskiej rezydencji Łobzów*, Wyd. PK, Kraków 1996.

[29] Reyman J., *Kraków. Zespół osadniczy, proces lokacji, mieszczanie do 1333 roku*, Kraków 2004.

[30] Sinko K., *Santi Gucci Fiorentino i jego szkoła*, Wydawnictwo Związku Kół Historyków Sztuki Studentów Uniwersytetów Rzeczypospolitej Polskiej, Gebethner i Wolff, Kraków 1933.

[31] Stala K., *Królewska rezydencja Zygmunta III Wazy w Łobzowie*, Wiadomości Konserwatorskie nr 42, Wydawnictwo ZG SKZ Warszawa, Warszawa 2015, 54–60.

[32] Stala K., *Najstarszy widok łobzowskiego castellum Kazimierza Wielkiego z 1536/1537 roku/The oldest view of the Łobzow castellum of Casimir the Great from 1536/1537, Wiadomości Konserwatorskie, nr 46, Kraków 2016, 119–124.*

[33] Walczak M., *Rzeźba architektoniczna w Małopolsce za czasów Kazimierza Wielkiego*, Kraków 2006.

[34] Wyrozumski J., *Dzieje Krakowa. Kraków do schyłku wieków średnich*, T. 1 Wydawnictwo Literackie, Kraków 1992.

Dariusz Żelasko orcid.org/0000-0001-5125-3647
dzelasko@pk.edu.pl
    Cracow University of Technology, Faculty of Physics, Mathematics and Computer Science

Ensuring the qos in computer networks through the use of the pay&require multi-agent system and electronic auctions

Zapewnianie jakości usług w sieciach komputerowych poprzez wykorzystanie systemu wieloagentowego Pay&Require i aukcji elektronicznych

Abstract

In modern computer networks, agent-based systems are widely used. The very fundamental usage of agents are for management systems e.g. supporting SNMP-based databases and multiple client-server communications. This paper describes the Pay&Require mechanism implementing a multi-agent approach for a QoS-enabled computer network. The unique features of the P&R system are its comprehensive approach to the cooperation of agents dedicated to traffic monitoring, the selective response to the QoS-oriented admission of user requests, event-driven reconfiguration and transmission quality brokerage. The brokerage in quality purchase was based on different models – from a simple reactive agent to an agent with learning capabilities. The presented approach uses auctions in which agents (brokers) can buy quality parameters according to customer requirements. The use of auctions allows the dynamic pricing of data transmission services.

Keywords: agent negotiations, market-based price modelling, auctions, computer networks, quality assurance, QoS, Pay&Require

Streszczenie

We współczesnych sieciach komputerowych bardzo często wykorzystywane są systemy agentowe. Podstawowym zastosowanie agentów jest zarządzanie systemami, np. SNMP i komunikacja klient-serwer. W artykule opisano mechanizm Pay&Require w którym zastosowano podejście wieloagentowe do zapewniania QoS w sieciach komputerowych. Cechą wyróżniającą mechanizm P&R jest kompleksowe podejście do współpracy agentów odpowiedzialnych za monitorowanie ruchu, reakcja na żądania użytkowników dotyczące QoS, rekonfiguracja na podstawie zdarzeń i pośrednictwo w zakupie jakości. Pośrednictwo to opiera się na różnych modelach – od prostego agenta reaktywnego do agenta z możliwością uczenia. Prezentowane podejście wykorzystuje aukcje, w których agenci (pośrednicy) mogą kupować parametry dotyczące jakości zgodnie z oczekiwaniami klienta. Wykorzystanie aukcji pozwala na dynamiczne kształtowanie cen usług transmisji.

Słowa kluczowe: negocjacje, metody rynkowe, aukcje, sieci komputerowe, zapewnianie jakości, QoS, Pay&Require

1. Introduction

The continuous development of both hardware (such as computing power, memory size and speed) and software can be observed in modern computer networks. More and more, techniques derived from IT solutions such as agent systems are found. The use of agent systems aims to improve the way in which software is designed and implemented. The design of the system using elements that are useful from the point of view of the development of modern software such as reactivity, proactivity and social behaviour, is characteristic of the agent-based approach [1, 2]. Reactivity is the capability to monitor the environment in which the agent is located and to respond to changes. Proactivity is the demonstration of initiative and goal-oriented behaviour. Social behaviour, in turn, means that the agent should interact with other agents in the environment. Another important issue is the agent's independence – it should be able to operate without external interference. A single agent is perceived as an intermediary, usually between the user and the environment in which it operates.

The classical approach in networks is to use agents in management systems (management agents) [7, 12, 13]. The task of such an agent is to provide the interface that enables management of the device while taking into account the received feedback and the implementation of the reconfiguration processes [11]. The operation of computer networks is based on traffic management, which consists of traffic stream classification, QoS qualitative analysis, route definition, and the definition and implementation of active traffic management methods in nodes.

Classical IP networks do not guarantee transmission quality – rather, they deliver a 'best effort' transmission service. IP networks with IntServ (not used due to the lack of scalability) or DiffServ [8] (providing great capabilities despite being used for more than 20 years) provide another step in the development of QoS traffic management. Techniques for traffic streaming in a connection mode are ATM (asynchronous transfer mode), MPLS (multiprotocol label switching) [9], GMPLS (generalised MPLS), or the latest SDN (software-defined networking) [10] concept provide QoS guarantees through centralised asset monitoring and the defining of control parameters. A multi-agent system, the primary role of which is to provide updates and distribution of control rules, can be used in each of these concepts. Using agents for network control and quality assurance is a non-classic and innovative approach.

The Pay&Require concept shown in this paper is an innovative approach to quality assurance in computer networks [15]. An agent-based approach to network management was used to achieve decentralisation of the solution. Electronic auctions play an important role in decision-making in the agent-based network management system. It is important to define the rules for the settlement of auctions and the value paid for acquiring the goods. We can distinguish two approaches – first-price and second-price [6]. In first-price auctions, the participant who made the best bid wins and receives the auction item for the bid amount. In second-price auctions, the client bidding the most wins, but pays as much as the next auction participant offered. Auctions can also be classified according to the openness of information and we can distinguish between open-cry and sealed-bid auctions. In open-cry auctions, the

participants have full knowledge of the actions of other auction participants. The participants do not have access to information about the activities of other participants in sealed-bid auctions. For auctions where one good is offered, the following different auction protocols are defined. The simplest protocols are first-price-sealed-bids, where the auction is held in one round and the participant who makes the highest bid wins. As the auction is held in one round, it is very important that users bid according to the maximum accepted amount from the very beginning. Another protocol is the second-price-sealed-bid, and in this case, the participant who made the highest bid wins but pays the second highest amount.

Auctions for multiple goods are more complex because many factors can affect their course. Participants can apply using several different bidding methods. The first of these is the XOR method. It consists of placing many different bids, and the user will only pay according to one of them. In situations where it is possible to meet several conditions at the same time, the user pays the highest amount of the individual bids. For example, when $d1$, $d2$, $d3$, $d4$ goods are available, the user can submit the bid according to the assumptions shown in equation (1).

$$Of = (\{d_3, d_4\}, 20)XOR(\{d_1\}, 10) \tag{1}$$

Such a notation means that the user can pay 20 if the user receives goods $d3$ and $d4$; the user pays 10 when receives item $d1$ only; but pays 20 when they receive goods $d1$, $d3$, $d4$. Another possibility is the so-called OR bids, in which the final bid is the sum of the component bids. For the example shown in equation (1) this means that the participant pays 20 when receiving goods $d3$ and $d4$, 10 when receiving item $d1$ only, and 30 when receiving goods $d1$, $d3$, $d4$.

2. Pay&require concept

the Pay&Require (P&R) concept is an alternative solution to quality assurance techniques in computer networks. Its main assumption is that data transmission takes place at the guaranteed quality level. Quality is defined by parameters such as throughput, transmission delay and number of lost packages. Obtaining the appropriate transmission quality is achieved by selecting such routing paths that the parameters meet the client's requirements. Quality is monitored at specified intervals to determine if the transmission quality has changed. This is achieved through active measurements performed by test transmission on each network link. This determines the current quality of each link. When quality satisfies client requirements, transmission takes place using the established paths. However, the network reconfigures if a deviation from the required parameters is found and this results in the changing of routing tables. Such a solution enables transmitting the data of different clients via different paths.

The concept separates the physical layer (network devices) from the management-control layer (Fig. 1). The devices responsible for the packet routing (R_x) operate in the physical layer. Agents responsible for the monitoring of transmission parameters and reconfiguring the network (Ag_x) operate in the control layer. Monitoring agents periodically check the current

quality. When parameters change, agents send this information to the agents responsible for reconfiguration.

This type of agent defines new paths and then performs the reconfiguration of physical layer devices based on quality and the client's requirements. Reconfiguration of this layer consists of the transmission of configuration commands which allow devices to route packages based on new rules. Agents responsible for the purchase of quality (market) comprise a separate layer. They are intermediaries between the client (Ca_x) and the environment where the auctions or negotiations are conducted. Another agent represents the service provider (Oa).
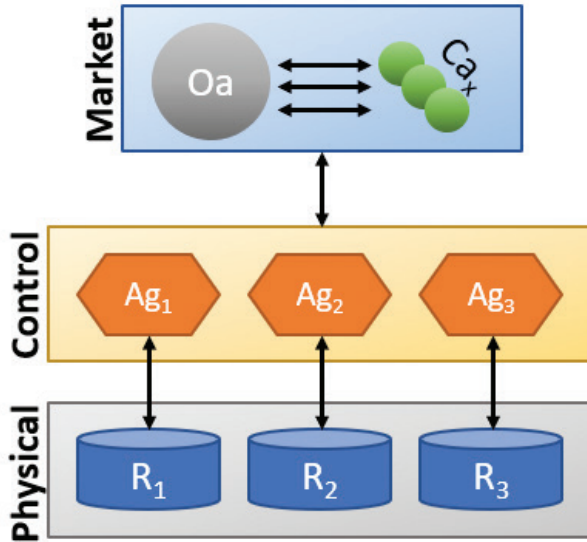
Fig. 1. Pay&Require layers

3. Architecture of agents

Among the numerous types of agents based on different architectures and with different algorithms [1, 3, 4], cognitive and reactive agents were used in this research. The simplest types of agents, the task of which is to mediate in operation without the developed learning and decision-making skills, are often used in computer networks. The P&R concept uses several types of agents.

3.1. Monitoring agent

The first agent is responsible for monitoring the transmission quality (the so-called monitoring agent). This agent belongs to the group of reactive agents, whose operation is based on the mapping of the situation in the environment to a particular action. There are one or more instances of an agent of this type within each active device on the network. The agent can monitor the entire device or its interfaces – in this case, multiple monitoring agents can operate as a part of one device. Each agent of this type is responsible for monitoring

the parameters of individual links. The agent can make decisions based on predefined rules or based on its own experience acquired during the operation. Qualitative parameters may be subject to a minimum change that does not noticeably affect the quality of the service. Therefore, the agent should act on the basis of parameter value ranges and should be able to learn the correct behaviour during its life.

3.2. Route reconfiguration agent

The second agent used in the P&R concept is responsible for the reconfiguration (the so-called reconfiguration agent); it is an example of a reactive agent. Once the monitoring agent has determined that the parameters excessively differ from the assumed values, it reports the need to change the route. The route reconfiguration agent starts the process of assigning new paths; a path is created between users based on both the quality information for each link on the network and the client information. The path must satisfy client requirements – the quality cannot be worse and should not be better. Subsequently, after assigning new paths, the agent will send the new configuration to a subordinate device. An agent can monitor one device or a group of devices.

The monitoring agent and the route reconfiguration agent may be discrete elements or be implemented as a single agent with both functionalities. Figure 2 shows the *Ag* agent model along with details of the communication between agents of the same type and a router (physical layer). The first step is the exchange of information regarding networks directly connected to the agent-supervised router. Subsequently, agents send the information regarding networks they have learned from their neighbours to one another. The exchange of messages ends when all agents have information about the network topology. Agents that monitor devices to which clients are connected have information about the quality required by each client. The transmission path is then selected which will be used for a given client. Agents configure the router(s) they monitor based on the received information.

The agent periodically verifies the parameters of the device links that it monitors. The test consists of sending a test stream of information through each link. Parameters such as throughput,
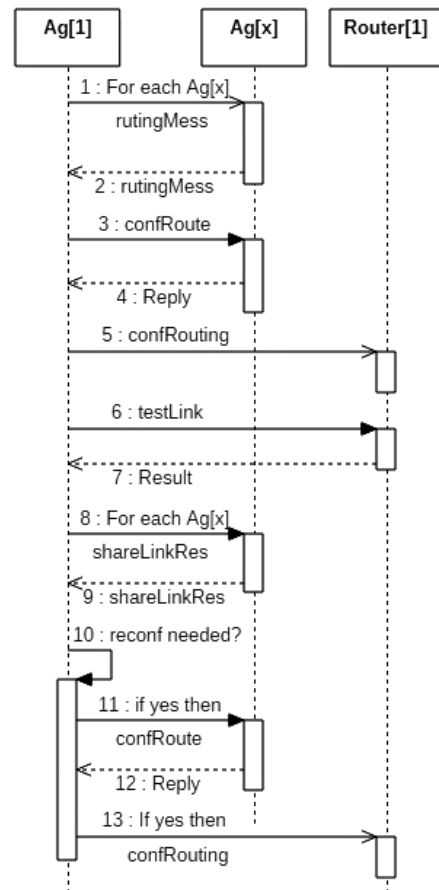

Fig. 2. Agent *Ag* operation

transmission time, delay, and the number of lost packages are determined. Information about measured parameters is sent to neighbouring devices. The agent evaluates the paths used for transmission by clients based on the received information. The routes are reconfigured when the parameters deviate from the assumptions.

3.3. Agent-trader

Agent-trader is the last type of agent. This agent is responsible for the quality trade such a type of agent may represent the provider or the client. In the simplest case, the user pays a certain amount for quality – this payment can be made for a specified interval (e.g. one month). This is not the only solution since it may happen that the user needs quality only for the duration of a specific transmission or for a particular service. The system then enables the user to temporarily change the quality. In the simplest terms, the agent system will act as an intermediary on the purchase. We can introduce various methods of market purchasing and negotiating here. Depending on the strategy of the agent, this can be classified as reactive – the simplest case being mapping of the situation to the decision. However, intelligent agents are used in more complex strategies where an agent uses historical data and other knowledge.

Each quality parameter can be a separate item – then the negotiations involve many goods at the same time, the combination of which will satisfy the client. It is also possible to translate a combination of qualitative parameters using a certain scale.

The auction mechanism can be used with regard to the allocation of goods. This allocation type is used when more than one party is interested in goods. The purpose of the auction is the allocation of goods to one participant. Each auction participant has an assigned strategy and the maximum amount that the agent is willing to pay for a given transmission quality (being its evaluation of the value of a given quality of service) is an important element of the strategy. The participants should not disclose their strategies. Auctions run according to certain rules – the auction protocol.

In the P&R concept, the agent representing the auction participant is not solely an intermediary but can make autonomous decisions based on the adopted strategy and the amount at its disposal. The agent can act carefully, either bidding only small amounts or bidding high amounts. Amounts may be fixed, random within a certain range or may result from the experience of the agent during previous auctions. Several agent action strategies have been adopted:

1. The agent has information about the quality sought by the client and the maximum amount that the client can pay. The bid (Of) is only made to a specified maximum. Equation (2) shows the method of bidding for this strategy, where q is quality and $max(c1(q))$ is the maximum amount the client i can assign for the purchase of quality q.

$$Of(q) \leq \max(c_i(q)) \qquad (2)$$

2. The agent has information about the maximum amount, expected quality and the possibility of deviation from quality within a certain range. This situation can be beneficial to the client, who wants transmission at an optimum price while maintaining

an acceptable level of quality. Equation (3) shows the bidding method. Qm is the margin of deviation from the assumed quality which is acceptable to the client.

$$Of(q \pm Qm) \leq \max(c_1(q + Qm)) \tag{3}$$

3. Where the same quality is offered successively in several different auctions (the provider can assure a certain level to several clients simultaneously), and the agent has information about the number of such auctions, it is possible to adopt a strategy where the user watches the results of subsequent games. In the last round, the agent takes part in the game by predicting its outcome based on previous games. Information received by the agent may be partial (final result of the auction only) or full (final result and bids submitted by each agent). In the case of partial knowledge, the agent can make predictions based solely on the results of previous games. Therefore, it may assume a certain probability that it will win the auction if it places a certain bid. There is a more complex model in which the agent has full information on the course of all games and bids submitted by other participants. With this approach, the agent can learn the behaviour of other players and learn about their strategies. A behaviour model can be created for each competitor on this basis. This model is used at the stage of submitting an offer such that the agent wins the auction with a certain probability while paying the optimum amount (not overpaying). The agent with knowledge of competitors can compare their models and then assume a strategy that will allow it to win. Whether or not an agent can have full or just partial information about previous auctions depends on the system configuration and the adopted auction protocol.

4. Findings

The research was conducted for both single-item auctions and combinatorial (multiple goods) auctions. In the case of single-item auctions, it is necessary to transform quality (resulting from many parameters) based on a certain mapping of parameters to transmission quality. With such a solution, a problem which affects many goods (e.g. throughput, transmission delay, package loss rate), can be reduced to a simpler decision-making problem.

4.1. One-time auctions of single items

The research was conducted for an agent whose job is to make a purchase for the client. The quality of data transmission service is defined within the range of 0 to 5. The research was conducted for both first-price and second-price auctions. Auctions are carried out in one round, i.e., agents bid simultaneously and only once. In both cases, the highest bid wins, but the final amount is the second largest of the submitted bids in the second-price auction. Ten clients were defined for the simulation. Client number 1 is analysed for the result of the game. Other clients are its opponents, but they do not exchange information about the

adopted strategy. For strategy 1, all clients are interested in the same quality. Table 1 shows the maximum amounts accepted by clients.

Table 1. Opponents for strategy 1

Client	Amount	Quality
K2	4	3
K3	4	3
K4	4	3
K5	14	3
K6	14	3
K7	14	3
K8	24	3
K9	24	3
K10	24	3

Figure 3 shows the results obtained for strategy 1. The measurement was performed for three different maximum amounts acceptable for client 1 – 10, 20, and 30 (measures 1, 2, and 3, respectively). The chart shows two values – the bid value, which is the amount the client 1 has offered, and the winning value, which is the winning amount. When the value is greater than or equal to the winning value, it means that the agent representing client 1 has won. Taking into account the strategies of other players, agent 1 wins only if its maximum is greater than the maximum of other players. This situation is based on the assumption that each agent will bid the maximum amount.

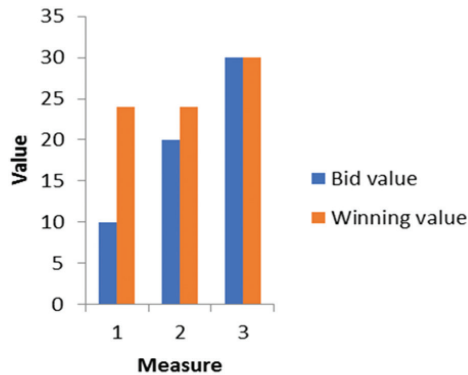

Fig. 3. Results for first-price strategy 1

For strategy 2, it is assumed that in addition to the maximum amounts, the clients are also interested in a specific quality that does not have to be the same to them. Client 1, for whom the outcome of the game is considered for strategy 2, has a defined quality acceptance threshold of ±1. Table 2 shows the adopted strategies for these measurements.

Table 2. Opponents for strategy 2

Client	Amount	Quality
K2	4	1
K3	4	2
K5	14	2
K4	4	3
K6	14	3
K8	24	3
K7	14	4
K9	24	4
K10	24	5

Figure 4 shows the results for strategy 2. Also in this case, three measurements were made according to the maximum amounts accepted by client 1. The situation was analysed depending on the expected quality (3 ± 1) for each measurement. When the maximum amount is 10, the agent does not win the auction despite the quality acceptance threshold. In turn, when the maximum amount is 20, the agent wins the auction for a quality level of 2 and lose it for a different amount. When the maximum amount of 30 is accepted, the agents win for each quality and pay that amount. Therefore, the agent should try to get the best possible quality by playing the high amount.
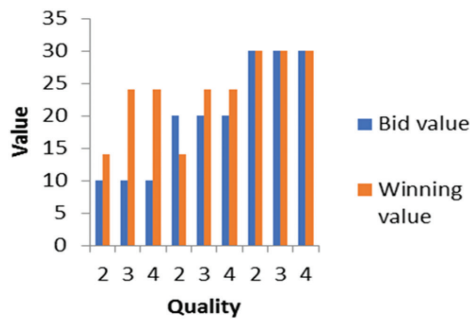
Fig. 4. Results for first-price strategy 2

4.2. Multiple auctions of single items

For strategy 3 and for a partial knowledge of the course of previous auctions, it is assumed that the purchase is possible in 10 rounds, where agent 1 watches the results for 9 rounds and then plays the amount in round 10 that is higher than the obtained average but lower than the maximum set by the client (variant 1) or such an amount that would enable it to win 90% of the previous auctions (variant 2).

$$\frac{1}{2} * \sum_{i=1}^{n} x_i < Of(q) \leq \max(c_1(q)) \tag{4}$$

Equation (4) shows the mode of operation of agent 1 when using variant 1. The bid depends on quality – $Of(q)$, and it is greater than the calculated average and less than or equal to the maximum acceptable to the client for a given quality.

Figure 5 shows the course of each round along with the average value observed by the agent after 9 rounds and the value estimation through which the agent would win 90% of the auctions. For a strategy where the agent plays a value of no less than the average of the previous games, one can note that for the strategies adopted by the remaining players, when agent 1 will play at least the amount equal to the average value in round 10, then it will win this round. This is due to the fact that the average was 23.89, and the maximum bid in round 10 was 22. However, agent 1 is not sure if its bid will win because the strategies of the remaining players may change in successive rounds. Therefore, another option is to submit a bid so that agent 1 would win 90% of the auctions. According to this approach, agent 1 would play the amount of 26. Assuming the well-known course of round 10 (the result of 22), agent 1 would win it by bidding 26, but it would pay more than in the strategy based on the average value. However, if the result of round 10 was greater than the average value, the agent would win by playing the value from variant 2.
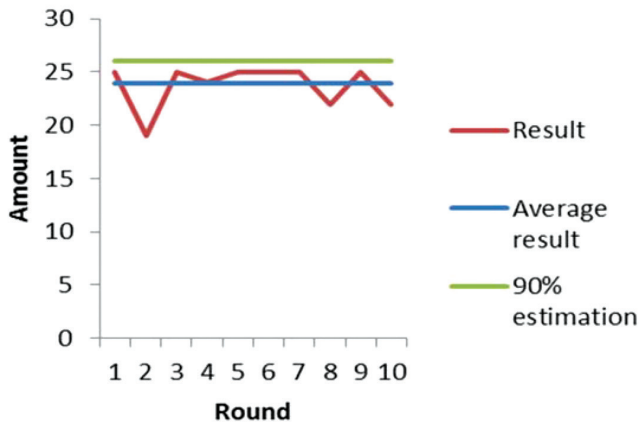

Fig. 5. Results for first-price strategy 3 – partial information

For strategy 3, assuming that the agent has full knowledge of all the auctions and bids submitted by competitors so far, it was assumed that all agents took part in 9 rounds. Agents 2, 5, 7, and 10 also take part in round 10 along with agent 1. With full knowledge of the submitted bids, agent 1 can determine with a certain probability what bid will be placed by each agent in the next round. Figure 6 shows bids submitted by agents in successive rounds and the result of each auction.

Based on 9 rounds, one can note that agent 10 submitted a maximum bid of 25 and a minimum of 6, agent 2 submitted a maximum of 23 and a minimum of 7, agent 5 submitted a maximum of 24 and a minimum of 6, agent 7 submitted a maximum of 25 and a minimum of 7. It can be assumed on this basis that the maximum values of submitted bids are very likely to be the thresholds for each agent.
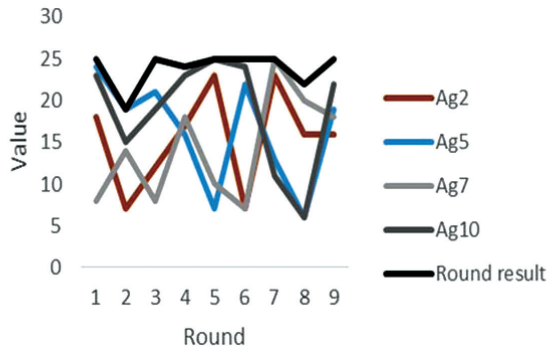
Fig. 6. Results for first-price strategy 3 – full information

Consequently, if agent 1 wants to win round 10, it should submit a bid of no less than the maximum of maximum bids of each competitor. In this case, the maximum is 25 and therefore agent 1 should bid higher than this value, but it should not be much higher in order to not overpay. In this way, agent 1 can learn the behaviour of other players and make a decision to get the expected result based on this knowledge. The more auctions the agent is watching, the more accurate its knowledge will.
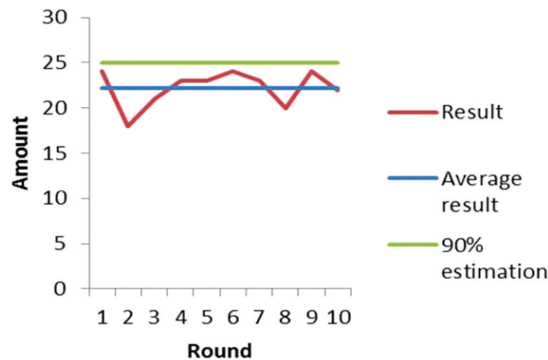
Fig. 7. Results for second-price strategy 3

4.3. Second price auctions

A number of experiments have been conducted with regard to the strategies discussed for second price auctions. The average result of 9 games is 22.22 for strategy 3, having a partial knowledge of the results of previous auctions agent 1 should bid no less than this value in round 10. It will pay the second largest amount; therefore, it should possibly play high. The second largest result in round 10 is 22, thus no matter how much higher client 1 plays, it will pay 22. Figure 7 shows the results for this strategy and assumptions. For variant 2, the agent should play no less than 25 to win in 90% of auctions. This is a minimum value, because it is not known exactly what bids other agents have submitted in the rounds – only the final amount, which is the second largest, is known. Therefore, agent 1 should play as high as possible and most likely will not pay more than 25 in the round where it will participate.

4.4. Combinatorial auctions

Auctions of this type apply to more than one item at a time. In the case of a data transmission service, there are quality parameters such as throughput, transmission delay, and the number of lost packages. Each of these parameters is understood as a separate item and their combination is the basis for the bid. Equation (5) shows the general rule for combinatorial (quality) auctions using logical operations. Op is the logical operator – XOR or OR for the purpose of study, q_n is the qualitative parameter, and amt_m is the bid for a given combination of qualities.

$$Of = (\{q_1, q_2, ..., q_n\}, amt_1)OP...OP(\{q_1, q_2, ..., q_n\}, amt_m) \tag{5}$$

In the study, the q_1 parameter is throughput, q_2 is the transmission delay, and q_3 is the packet loss factor. Client 1 can pay 15 when the parameters are {50 Mb/s, 4 ms}, 25 for {100 Mb/s, 2 ms, 0%} and 10 when only a throughput of 50 Mb/s is guaranteed. Equation (6) shows this strategy. The operator may be OR or XOR for the assumptions. In the case of OR operator, this strategy does not make much sense because it would mean that the user would pay 50 after receiving all parameters at the same time. If the user receives parameters {100, 2, 0}, it makes no sense to pay for worse parameters. Therefore, it is appropriate to use the XOR operator. In such a situation, the user pays the maximum amount if the user's requirements are met.

$$Of = (\{50,4\},15)OP(\{100,2,0\},25)OP(\{50\},10) \tag{6}$$

Unfortunately, it is hard to ensure a constant level of quality parameters. There are always changes that may not have a significant impact on the final quality. Consequently, an acceptance threshold should be defined for each parameter. This means that parameters within a given range are still acceptable to the client. In the simplest case, the client defines the acceptance threshold for each parameter. In a more complex case, it is possible to define the acceptance ranges for each amount separately. Another possible solution is to define whether the individual parameter values are minimum or maximum values. One can assume for the above example that the client specifies the minimum throughput, maximum delay, and the maximum package loss rate.

5. Conclusions

Agent systems in computer networks are still innovative concepts. They can be used both for monitoring and reconfiguring the network and to represent and act on behalf of the client, e.g. when purchasing quality of data transmission services. Purchases can be conducted using a variety of protocols and methods – one can define different strategies for the participation of agents in auctions on their basis of these protocols and methods. The most important assumption is maximising the profit, i.e. purchasing a certain quality for an effectively

calculated price. Strategies can work on the principle of a finite automaton (the simplest solution) or with learning elements based on the results of previous games. The results show that it is possible to use agents as intermediaries between clients and the provider.

The Pay&Require concept is a complex mechanism used for quality assurance in the computer network and dynamic pricing. The client pays for the quality that is guaranteed by monitoring the quality parameters and reconfiguration of transmission paths as needed – specific types of agents are responsible for monitoring and reconfiguring the network. In turn, the client can purchase quality by participating in the auction in which it is represented by an agent. This solution allows the entire network to be dynamically managed, which improves its operation.

References

[1]   Wooldridge M., *An Introduction to MultiAgent Systems*, John Wiley & Sons Ltd, 2002.
[2]   Franklin S., Graesser A., *Is it an agent, or just a program?: A taxonomy for autonomous agents*, International Workshop on Agent Theories, Architectures, and Languages, 1996.
[3]   Weiss G., *Multiagent systems*, Massachusetts Institute of Technology, 2013.
[4]   Russell S., Norvig P., *Artificial Intelligence A Modern Approach*, Pearson Education Inc., 2010.
[5]   Fatima S., Kraus S., Wooldridge M., *Principles of automated negotiation*, Cambridge University Press, 2015.
[6]   Wellman M. P., *Trading agents*, Morgan & Claypool, 2011.
[7]   Simple Network Management Protocol (SNMP) Applications (RFC3413).
[8]   New Terminology and Clarifications for Diffserv (RFC3260).
[9]   Multiprotocol Label Switching Architecture (RFC3031).
[10] Software-Defined Networking (SDN): Layers and Architecture Terminology (RFC7426).
[11] Mitrović D., Budimac Z., Ivanović M., Vidaković M., *Improving fault-tolerance of distributed multi-agent systems with mobile network-management agents*, Proceedings of the International Multiconference on Computer Science and Information Technology, 2010.
[12] Bogdanovic D., *Autonomic agent for transport networks*, Optical Fiber Communications Conference and Exhibition (OFC), 2015.
[13] Olfati-Saber R., Fax J.A., Murray R.M., *Consensus and Cooperation in Networked Multi-Agent Systems*, Proceedings of the IEEE, Vol. 95, issue 1, 2007.
[14] Cetnarowicz K., *Paradygmat agentowy w informatyce. Koncepcje, podstawy i zastosowania*, Akademicka Oficyna Wydawnicza EXIT, Warszawa 2012.
[15] Żelasko D., Cetnarowicz K., Wajda K., Koźlak J., *Pay&Require as concept of variable cost routing in dynamically reconfigured networks*, Technical Transactions, 1NP/2016.

Jakub Bernatt
Stanisław Gawron ORCID orcid.org/0000-0001-7219-9205
s.gawron@komel.katowice.pl

Tadeusz Glinka
Artur Polak
Institute of Electrical Drives and Machines KOMEL

Induction motors in traction drives, service tests

Silniki indukcyjne w napędach trakcyjnych, badania eksploatacyjne

Abstract

Electric multiple units (EMUs) EN57 are fitted with two cage induction motors to each bogie. Two motors driving one bogie are supplied from a common DC/AC inverter. These motors become damaged after a short service period; the end-rings start to break away, start to break away. The results of service tests conducted during normal train runs are presented in the paper. The investigation possibilities were limited to recording load currents and vibrations of four motors installed at two bogies of one car. It has been concluded that the reason for rotor winding damage may be traced back to the simultaneous impact of four factors: 1) transmission of load torque by mechanical gearbox; there is a backlash between the pinion mounted at the motor shaft and the toothed gear mounted at the drive bogie axle; 2) rigid assembly of the motor in the bogie frame and vibrations transmitted from the drive wheels to motor; 3) variable components of electromagnetic torque generated by higher harmonics of inverter voltage and current; 4) parallel operation of two unmatched motors supplied from common inverter.

Keywords: cage induction motors, traction drive systems, service tests, rotor winding failure.

Streszczenie

W zespołach trakcyjnych EN57 na wózkach jezdnych są zabudowane po dwa silniki indukcyjne klatkowe. Dwa silniki jednego wózka są zasilane z jednego falownika DC/AC. Silniki po krótkim okresie eksploatacji ulegają awarii, urywają się pierścienie zwierające pręty uzwojenia wirnika. W artykule przedstawiono wyniki badań eksploatacyjnych silników w czasie normalnej jazdy pociągu. Możliwości badawcze ograniczały się do rejestracji prądów obciążenia i drgań czterech silników zabudowanych na dwóch wózkach jezdnych jednego wagonu. Ustalono, że przyczyną uszkadzania się uzwojenia wirników jest równoczesne oddziaływanie czterech czynników: 1) przenoszenie momentu obciążenia przez przekładnię mechaniczną, która ma luz między kołem zębatym osadzonym na wale silnika i kołem zębatym sprzęgniętym z wałem kół jezdnych wózka; 2) sztywny montaż silnika na ramie wózka i drgania przenoszone z kół jezdnych na silnik; 3) składowe zmienne momentu elektromagnetycznego generowane przez wyższe harmoniczne napięcia i prądu falownika; 4) praca równoległa dwóch niesparowanych silników zasilanych ze wspólnego falownika.

Słowa kluczowe: silniki indukcyjne klatkowe, trakcyjne układy napędowe, badania eksploatacyjne, uszkadzanie się uzwojenia wirnika.

1. Introduction

Electric multiple units (EMUs) have been in operation for several decades, and nowadays, they are subjected to overhauls and modernisation – Fig. 1 [7]. In the drive car, DC drive units are replaced with AC drive units [1]. The motor car contains two drive bogies. Each bogie is fitted with two type LK 450 X6 cage induction motors. Motors M1 and M2 are mounted in the first bogie, and motors M3 and M4 in the second bogie. The pinions of the mechanical gearbox are mounted at motor shafts. The large toothed gears are mounted at drive wheels' axles. The two motors belonging to a single bogie are supplied from one common DC/AC power electronics converter, which is located below the car floor. After a relatively short service period, LK 450 X6 motors start to fail; the end-rings break away. Research has been undertaken at the KOMEL Institute in order to identify the reasons for damages of rotor windings [8].

Fig. 1. Electromotive unit EN57 [7]

2. Drive system of EN 57 EMU

The drive system is composed of: two inverters, four motors M1 ÷ M4 and four mechanical gearboxes. Three-phase squirrel cage induction motors LK 450 X6 are used, with the number of pole pairs $p = 3$. The rated data is [9]:

- ▸ nominal power/one-hour rating– 250/300 kW,
- ▸ rated voltage at 50 Hz – 2340 V,
- ▸ rated/maximum current – 78/160 A,
- ▸ rated/maximum frequency – 50/120 Hz,
- ▸ rated/maximum rotational speed – 987/2400 rpm,
- ▸ rated/maximum torque (at 50 Hz) – 2419/4400 N·m,
- ▸ breakdown torque (at 50 Hz) – 6600 N·m,
- ▸ efficiency ≥ 0.94,
- ▸ cos φ ≥ 0,84,
- ▸ forced cooling,
- ▸ Degree of Protection IP22,
- ▸ operating temperature– 30÷40°C.

A photo of the LK 450 X6 motor is shown in Fig. 2.

Fig. 2. Induction motor LK 450 X6 [8]

The motors are supplied from inverters converting the traction network 3 kV DC voltage into AC voltage by the pulse width modulation (PWM) method. Inverter FT-500-3000-UF is manufactured as HV IGBT 6.5 kV design – Fig. 3 [8]. The braking resistor is made of stainless steel. According to the manufacturer, the inverter fulfils the requirements set by UIC and EC standards (regulations) as to operational safety and electromagnetic compatibility. The AC voltage is controlled from a minimum value (train starting) to the rated value U_N = 2340 V. By changing the inverter's output frequency and voltage, two ranges of motor speed control are achieved (Fig. 4):

- ▸ control in the range from zero speed to rated speed (n_N = 987 rpm), torque is constant; this is obtained by a simultaneous change of the frequency and voltage ($f_{\min} \leq f \leq f_N$, $U_{1\min} \leq U_1 \leq U_{1N}$),

- ▸ control in the range from rated speed to maximum speed ($n_{\max}$ = 2400 rpm), power is constant; this is obtained by changing the frequency, while voltage is kept constant ($f_N \leq f \leq f_{\max}$, U_N).
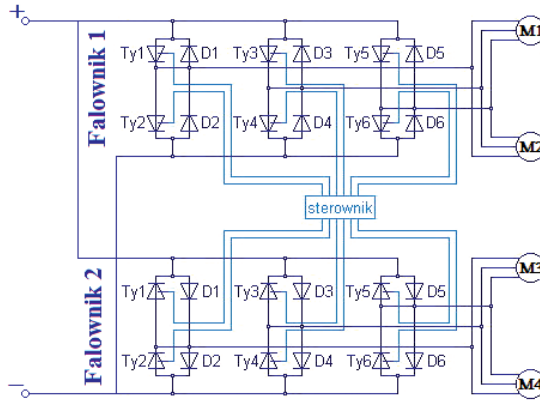
Ty - tyrystory, D - diody zwrotne, M - silniki trójfazowe

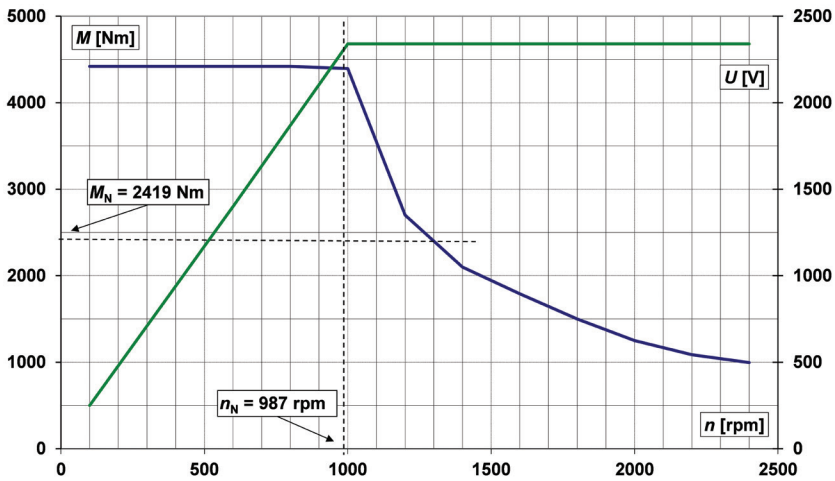Fig. 3. Electric scheme for drive car – supply circuit of LK 450 X6 motors

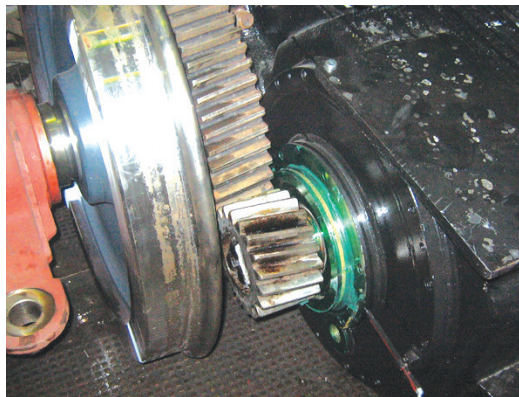Fig. 4. Torque and electric voltage vs. speed – motor curve

Fig. 5. Mechanical gear

The mechanical gear is simple and consists of a pinion and a large gear. The pinion with a number of teeth $Z_1 = 19$ is mounted at the motor shaft. The large gear with a number of teeth $Z_2 = 70$ is mounted at the bogie's drive wheel axle. The complete gear is shown in Fig. 5 [8].

3. Design of the LK-450 X6 motor

The traction motor is composed of three main parts:
- ▸ magnetic circuit, comprising the stator laminations, rotor laminations and the air-gap between these laminations,
- ▸ stator and rotor windings, placed in lamination slots,
- ▸ mechanical structure, i.e. shaft where rotor laminations are placed, body holding stator laminations, bearing plates and bearings.

The rotor winding is made of non-insulated copper bars placed in the slots of rotor laminations. Outside the core assembly, the bar ends are fast attached to copper short-circuiting end rings.

Different specimens of LK450 X6 motors are characterised by innate tolerance of the rated parameters. This tolerance is due to:
- ▸ differences in the magnetising curves of lamination steel,
- ▸ dimensional tolerance in winding wires,
- ▸ bearing slackness,
- ▸ working tolerances of mechanical working: laminations, shaft, bearing plates and body.

Magnetic circuits of LK-450 X6 are made of lamination steel M350-50A. In accordance with standard EN 10106:2007 (see Table 1), this steel is characterised by:
- ▸ maximum lossiness (total - at 50 Hz and 1.5 T): 3.50 W/kg,
- ▸ minimum magnetic polarisation (in AC magnetic field of 2500 A/m intensity): 1.5 T,
- ▸ maximum loss anisotropy (at 50 Hz and 1.5 T): ±12%.

Different batches of laminated steel may be characterised by even better parameters than the limits cited above. The magnetic circuits of motors where different batches of steels are used, will also differ from each other.

Moreover, bearing slacknesses are also present [10]:
- ▸ bearing D: minimum 0.145 mm, maximum 0.190 mm and
- ▸ bearing N: minimum 0.075 mm, maximum 0.110 mm.

The tolerances and backlashes are summed up in the airgap between stator and rotor; this also acts as a gap in magnetic circuit. The designed motor's air-gap is equal to 1.2 mm; if backlashes and tolerances are taken into account, then the real air-gap may range from 1.02 to 1.43 mm. Within this range, air-gaps in individual motors may differ from each other. The total tolerance of the magnetic air-gap determines the electrical and mechanical parameters' tolerances of individual motors. However, each motor's rated parameters are defined taking into account allowable tolerance. Allowable tolerances are specified in standard PN-EN 60034-1: 2011E, item 12, Table 20 [4]. In the case of machines with ratings above 150 kW, the tolerances are as follows:

- efficiency $\eta = -10\% \cdot (1 - \eta_N)$,
- total losses (-10%)
- $\cos\varphi = -\dfrac{1}{6}(1 - \cos\varphi_N)$,
- slip, at full load and when motor is heated ±20%,
- current when rotor is braked +20 %,
- rotational torque when rotor is braked: $(-15\%\ do\ +20\%)$,
- minimum rotational torque (-15%)
- breakdown torque (-10%).

The rated parameters of brand-new motors are contained within the tolerance limits given above. However, individual motors may differ as to their rated parameters. That is why motors dedicated to parallel operation should be matched, which means that their parameters should be nearly the same. A selection of motors for parallel operation may be done on the basis of no-load current, when motors are supplied with the rated voltage at a 50 Hz frequency. The measured values of no-load current are provided by the manufacturer (performance tests run at the manufacturing plant). The appropriate matching (coupling) of motors should be conducted by companies assembling motors in bogies.

LK 450 X6 motors are subject to numerous failures during operation. The failures are due to breakdowns of end-rings, short-circuiting the rotor bars. When the rotor is rotating, the torn ring damages the stator winding outhangs. Photos illustrating the points of junction of rotor bars to the end-rings, for a new motor and motor with a damaged ring, are shown in Fig. 6 [8].

Fig. 6. Junction of rotor winding bars to end-rings: in a brand-new motor (left) and a worn motor with a torn end-ring (right)

4. Operational tests of LK 450 X6 motors

Traction motors LK 450 X6 operating in EMUs EN57 were subjected to tests. The trains were operated by two regional companies, G and W [8]. The tests were conducted during normal commercial train operation. The following phase current waveforms were recorded:
- currents of motors M1 and M2, bogie #1, supplied from inverter 1, and
- currents of motors M3 and M4, bogie #2, supplied from inverter 2.

The transformation of DC voltage into AC voltage is achieved with the pulse width modulation (PWM) method. The inverter voltage is distorted; it contains a fundamental (1st) harmonic as well as higher harmonics. This is a natural effect. The fundamental current and

voltage harmonics generate useful electromagnetic torque. This torque is constant, and this corresponds to the conditions present in DC traction motors supplied with DC voltage. Higher harmonics of voltage and current generate variable torques [3], which have an adverse effect on the drive system. The torques at motor shafts were not recorded during the tests, since it was not possible. We were only able to record currents and mechanical vibrations of motors.

5. Current measurements

Examples of current waveforms are shown in Fig. 7. These were recorded for phases A, B, C of the M1 motor, train company W. The harmonic spectrum of the M1 motor phase A current is shown in Fig. 8. Fundamental harmonics of voltage and current generate useful electromagnetic torque; higher harmonics of voltage and current generate variable/ disturbance torques.
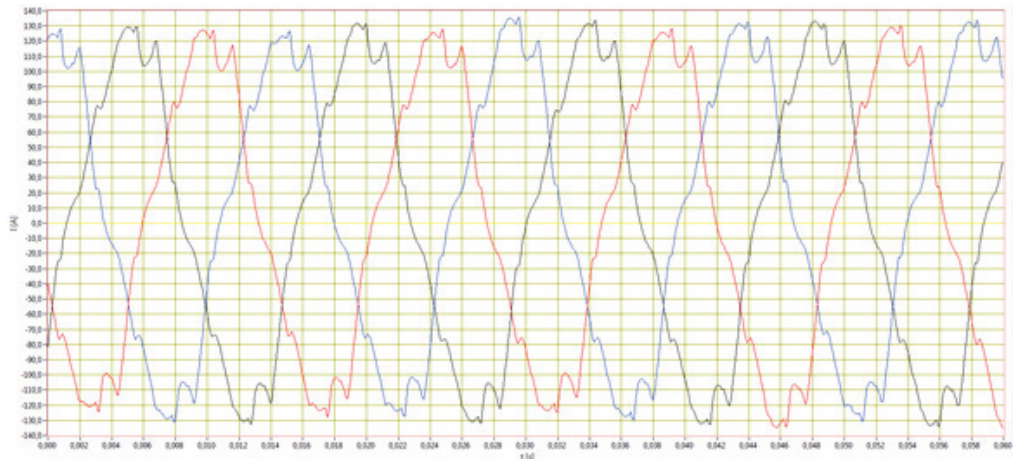

Fig. 7. Examples of phase current waveforms (phase A, B, C) for motor M1, train operator W. The fundamental frequency was f = 69.44 Hz, this corresponded to 58% of the train's maximum speed; the load current was 87A (RMS-value), i.e. 1.12 I_N
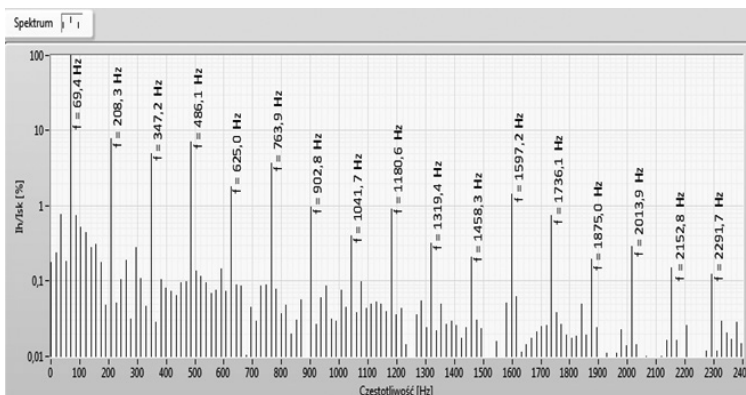

Fig. 8. Harmonic spectrum of motor M1 current, phase A (current waveforms are shown in Fig. 7)

When the AC frequency and load torque are changed, the motor current and voltage waveforms change, and their harmonic spectra change accordingly. The current distortion (deformation relative to sine wave) is much greater when the load current (torque) is small. This occurs when the train runs at a constant speed. Waveforms of M3 and M4 motor currents are shown in Fig. 9. These waveforms were recorded with the train running at a constant speed close to the maximum speed. It may be observed that motors M3 and M4 are loaded almost uniformly. This proves that these motors were adequately selected (matched).
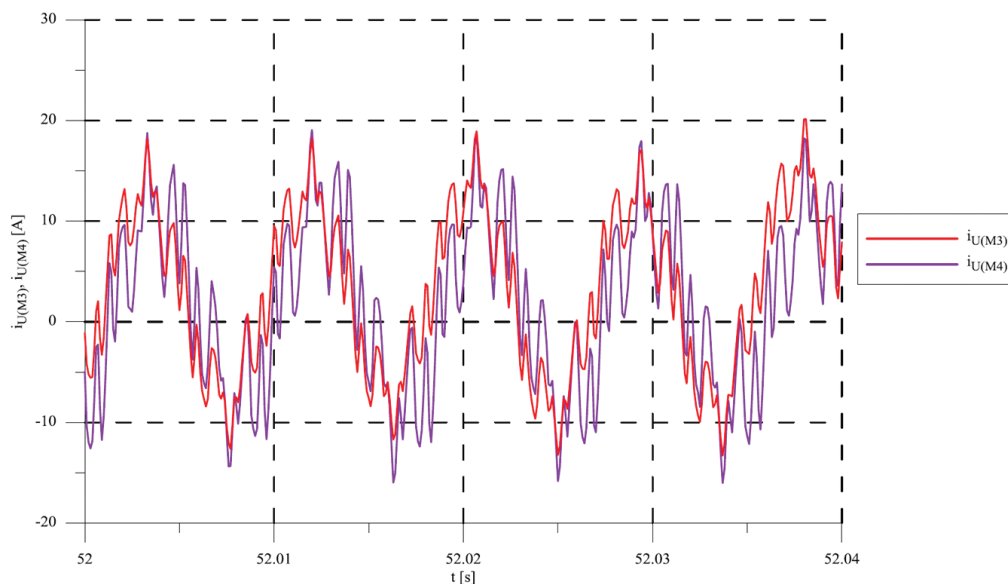
Fig. 9. Examples of phase current waveforms (phase A, B, C) for motors M3 and M4, bogie #2, train operator W. The fundamental frequency was f = 114.9 Hz, this corresponded to 96% of the train's maximum speed; load currents were I_{M3}=8.38 A; I_{M4}=8.49 A (RMS-values), i.e. 22% of I_N

Harmonic spectra of M3 and M4 motor currents are shown in Figs. 10 and 11.
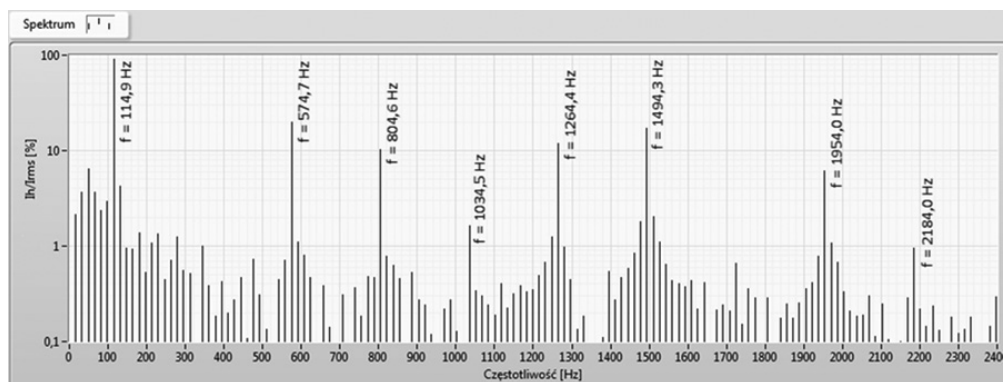

Fig. 10. Harmonic spectrum of the M3 motor current (current waveform is shown in Fig. 9)
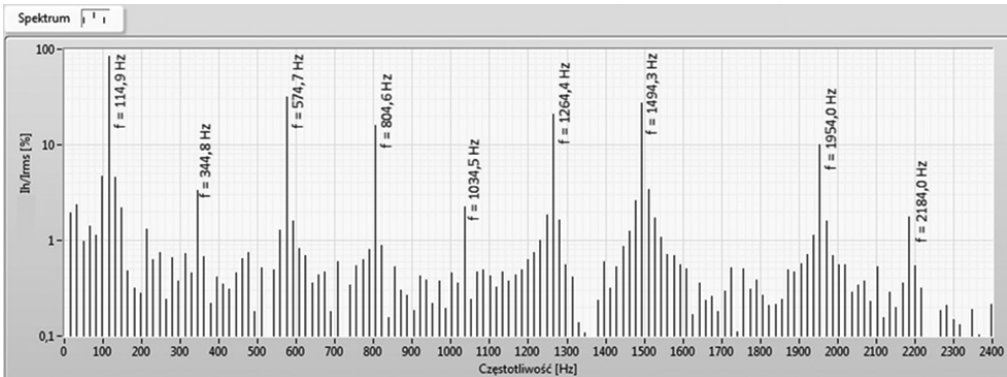
Fig. 11. Harmonic spectrum of the M4 motor current (current waveform is shown in Fig. 9)

In the harmonic spectrum of the M4 motor current, we may observe harmonic $f = 344.8$ Hz. This is not present in the harmonic spectrum of M3 motor current.

Voltage and current higher harmonics generate variable electromagnetic torques, which add up to useful torque generated by fundamental harmonics. Under load conditions, the motor currents are more distorted, which may result in negative instantaneous values of the torque. When torque is negative, the instantaneous value of the motor's rotational speed decreases. The pinion (mounted at motor shaft) gets out of contact with the large toothed gear (mounted at the wheel axle), since this large gear rotates at a constant speed. This constant speed of the large toothed gear is due to the car's inertial mass. When the instantaneous value of electromagnetic torque is positive, then the pinion accelerates and strikes at the large toothed gear. In this way, rotor elements, including end-rings which short circuit rotor bars, are subjected to sudden (surge) circumferential accelerations $\left(\dfrac{d\omega}{dt} \right)$.

Higher harmonic content in the load current of induction motors supplied from DC/AC inverters is normal. The beauty of power electronics converters lies in the fact that the generated variable voltage is distorted (non-sinusoidal), which results in distorted motor current waveforms (see Figs. 7 and 9) and the generation of higher harmonics of electromagnetic torque.

Motors in one bogie drive two separate bogie axles, and are connected by the track rails via the drive wheels. This is a parallel operation of motors supplied from a common converter and driving a common system of mechanical axles. If motor pairs M1 and M2, M3 and M4 are installed randomly, their parameters may differ within the allowable tolerance range. Differences in the motor parameters have an adverse effect on their parallel operation. This is the case observed in the investigated drive of bogie #1; it is confirmed by recorded courses of current RMS values of motors M1 and M2 operating in parallel. Here are some examples of RMS values of said motors M1 and M2:

▸ train accelerating under maximum load, M1 motor current attains 115 A, while M2 motor current is 87 A; the difference in load currents is 28 A, which is equal to 28% of the average current value,

- constant speed run, M1 motor current attains 110 A while M2 motor current is 15 A; the difference in load currents is 95 A, which is equal to 153% of the average current value,
- dynamic braking, M1 motor current attains 140 A, while M2 motor current is 25 A; the difference in load currents is c. 115 A, which is equal to 147% of the average current value.

These results prove that M1 and M2 motors are badly matched; the differences in load currents are very high. These large discrepancies may cause the occurrence of operational conditions where motor M1 should drive the bogie, while motor M2 would break the bogie. This phenomenon might be verified by load torque measurements; these were not possible during our tests. The load currents of M3 and M4 motors do not display such high disparities; the motors are matched correctly.

5.1. Backlash in the mechanical gearbox

The transmission of drive torque from the motor shaft to the drive axle is not elastic. The pinion is mounted at the motor shaft, and a large gear is mounted rigidly at the drive wheel axle; this is shown in Fig.5. The toothed gear is characterised by backlash. The induction motor supplied from the inverter generates a constant component of torque as well as variable torques; this is a normal effect of power electronics supply [3]. Variable components of electromagnetic torque affect the operation of gears. The pinion rotates in a non-uniform manner and tries to transmit this kind of motion to the large gear. The large gear, which is rigidly mounted at the drive wheel axle, maintains a constant speed due to high inertia of the car. The clearance between gear teeth causes clattering and mutual grinding of gear teeth; thus, the clearance increases with service time. Within the backlash range, the rotor of the motor will accelerate and decelerate due to variable components of the torque. When teeth come into contact, a surge-like braking of the rotor takes place. The derivative of angular rotor speed generates dynamic torque, which acts upon constructional elements of the rotor, including the end-rings, short-circuiting rotor winding bars. Shearing torque, which affects the junction of rings to bars, is equal to $J_p \dfrac{d\omega_m}{dt}$, where J_p is the moment of inertia of the end ring, and w_m is the angular speed of the rotor. This torque results in fatigue cracking of the junction between end rings and winding bars. The backlashes should be totally absent from the torque transmission path, and the toothed gear, together with the motor, should be elastically decoupled from the drive wheels and car mass [2, 3].

5.2. Vibrations transmitted to the motors by the bogie

On the outside of the motor body, there is a half-sleeve of a slide bearing; this contains the shaft of the bogie drive wheels – see Fig. 12. The motor is mounted to the bogie frame in the so-called axle hung nose suspended system. Moreover, it is affixed to the bogie frame via rubber pads with two ears and a special arm. The motor constitutes a partial load of the

wheelset axle, via an axle slide bearing. This impacts the motor operation unfavourably, since vibrations of the drive wheel are transmitted directly to the motor.

Standard PN-EN 61373 (IEC61373) [5] sets requirements as to resistance to mechanical shock and vibrations of mechanical, pneumatic, electric and electronic equipment of the rolling stock.
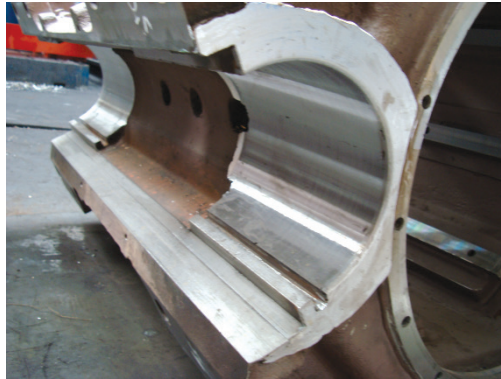

Fig. 12. Half-sleeve of a slide bearing – element of motor body

Technical requirements on the testing of railway vehicle equipment elements subjected to shocks and vibrations arising from the railway common operational conditions are defined in the standard. Maximum RMS-values of vibration accelerations occurring in service, in accordance with Appendix A.3 of the standard (category 3 – equipment mounted at wheelset axis) are [5]:

- in the vertical axis – 43 m/s^2 (*c.* 4.3 g),
- in the lateral axis – 39 m/s^2 (*c.* 3.9 g),
- in the longitudinal axis – 20 m/s^2 (*c.* 2.0 g).

From these requirements, we may conclude that during operation, the LK450 X6 motor may be subjected to maximum vibrations with an acceleration equal to 43 m/s^2 (*c.* 4.3 g). Under these conditions, the motor should be able to operate for 10 minutes without damage. During commissioning of the motors, the motor manufacturers run a test of the LK 450 X6 motor resistance to external vibrations as high as 50 m/s^2. The standard also provides regulations for the simulation test of durability at an increased vibration level. This simulation test should be conducted with the motor held at standstill, vibrations equal to 300 m/s^2 and a frequency range of 5÷150 Hz. The simulation test lasts 15 h (3 separate tests, each lasting 5 h, different directions).

The simulation tests of the motor's rotor construction have been conducted in at the KOMEL Institute. These tests included an investigation of the resistance to mechanical shock and vibrations. The stresses attained 50 MPa. Strength calculations for the rotor have also been run, as well as those for a portion of the rotor winding composed of a rotor bar and a segment of the short-circuiting end-ring, with the shock attaining an acceleration of 1000 m/s^2. This shock simulated the operating conditions set out in standard [5] and related to the equipment mounted on the

axle. The maximum value of stresses in the rotor attained 100 MPa, and in bars at the point of junction with the end-ring, it was equal to 120 MPa. These stresses did not exceed allowable values for the material used in the construction of the rotor winding. The displacement of rotor elements, due to these stresses, reached a maximum value of 0.2 mm. Results of calculations confirmed the resistance of the LK 450 X6 motor rotor construction to shock loading equal to 1000 m/s².

Measurements of the vibration acceleration of the LK450 X6 motor were conducted on trains belonging to train operator W, during commercial runs. An example of vibration acceleration waveform is shown in Fig.13. We may observe that, during normal operation, the motors are subjected to vibrations with accelerations of up to 150 m/s². The LK-450 motors fulfil the requirements set in the PN-EN 61373 standard; however, real vibrations acting upon the motor and caused by external conditions attain values of 150 m/s², which means that they are three times as high (43 m/s²) as vibration values given in the standard [5].
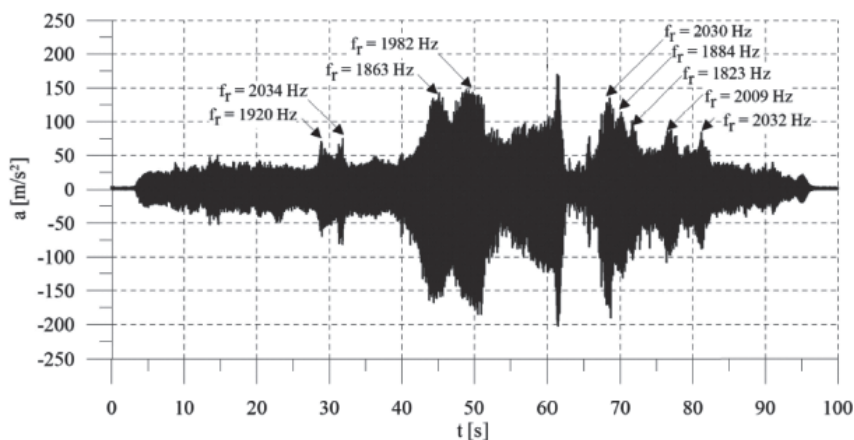
Fig. 13. Example of vibration acceleration, LK-450 motor, course recorded with train operator W

6. Conclusions

Exchanging the DC drive system present in electric multiple units EN57 for a drive system consisting of induction motors supplied from inverters is rational from the economic point of view, since AC drive is characterised by higher efficiency and lower energy consumption [1]. However, we must take into account the fact that apart from the constant torque, higher harmonic torques are also generated in induction motors supplied by inverters; this is an unavoidable natural effect [3]. Higher harmonic torques have not been generated in DC motors supplied by a constant voltage and controlled with resistors.

When the drive system was replaced, the mechanical structure of the bogie, composed of a mechanical gear and motor mounting, has not been changed. The toothed gears – a pinion at the motor shaft and a large gear at the drive axle, are mounted rigidly. The backlash of the toothed gear, together with variable components of motor torque, generates high dynamic torques.

The backlashes should be totally absent from the torque transmission path, and the toothed gear, together with the motor, should be elastically decoupled from the drive wheels and car mass.

LK 450 X6 motors are fitted with squirrel cage winding rotors consisting of copper bars short-circuited with copper end-rings. The end-rings are mounted on coil supports and they are protected from circumferential motion by wedges. The fatigue tearing of rings is due to circumferential acceleration.

At present, the mechanical structure of the bogie and harmonic components of motors' electromagnetic torque are the fundamental reasons for fatigue failures (breaking off) of end rings, which short-circuit rotor bars. The tearing away of the rings is accelerated by the fact that motors in the bogie are not matched (coupled) properly and that vibrations characterised by accelerations as high as 150 m/s2 are transmitted to the motor body via drive wheel axles and the bogie frame.

We have demonstrated that the ripping away of end-rings, short-circuiting rotor bars, is due to a simultaneous impact of four factors:

- variable components of electromagnetic torque generated by current's higher harmonics,
- parallel operation of two unmatched motors supplied from a common inverter,
- backlash in mechanical gearbox,
- vibrations transmitted to motors by the bogie.

Proposed changes in rotor winding.

The first proposed solution is to manufacture a rotor with a cast aluminium winding. Design calculations for such a motor have been conducted at the KOMEL Institute. It has been proven that it is possible to manufacture a motor with parameters identical to those of the LK 450 X6 motor, but with a cast aluminium winding. This sort of winding is compact, does not possess any clearances and hence it is more resistant to vibrations.

The second solution is to manufacture a rotor winding identical to the armature winding of a DC motor (without commutator and brushes). The rotor winding in slots is protected with wedges, and coil outhangs are secured with tapes [6]. This sort of protection works properly in DC motors, and therefore it might also be used in an induction motor. The electromagnetic calculations of such a motor have also been conducted at the KOMEL Institute and the motor's parameters have been proved to be identical to those of the LK 450 X6 motor.

References

[1] Biliński J., Frydrysiak R., Gmurczyk E., *Modernizacja systemu napędu elektrycznego zespołu trakcyjnego EN57 z zastosowaniem silników asynchronicznych.* Technika Transportu Szynowego. 12/2008.

[2] Lal Ganesh R.N., *Development of reliable designs of squirrel cage rotors for traction motors used in locomotives working in arduous operating conditions*, Published in IET Electric Power Applications Received on 5th December 2008 Revised on 17th March 2009; doi: 10.1049/iet-epa.2008.0284.

[3] Skarpetowski G., *Uszkadzanie klatki wirnika silnika trakcyjnego LK 450 X6*. Politechnika Krakowska. Em. Bombardier Transportation CH, 7/07/2014.

[4] PN-EN 60034-1: 2011E Maszyny elektryczne wirujące. Część 1: Dane znamionowe i parametry.

[5] PN-EN 61373 (IEC61373) Zastosowania kolejowe. Wyposażenie taboru kolejowego. Badanie odporności na udary mechaniczne i wibracje.

[6] Glinka T., Gawron S., Bernatt J., Poprawski W., *Uzwojenie wirnika silnika indukcyjnego trakcyjnego*. Patent claim P.418971 of 03/10/2016.

[7] https://upload.wikimedia.org/wikipedia/commons/3/30/EN57-2011_IMG_2900_filtered.jpg

[8] Bernatt J., Gawron S., Glinka T., Polak A., *Warunki pracy i awaryjność silników indukcyjnych lk 450 x6 napędzających zespoły trakcyjne EN57*, SEMTRAK 2016. XVII Ogólnopolska Konferencja Naukowa Trakcji Elektrycznej. Materialy konferencyjne, Wydawnictwo PiT, Krakow 2016.

[9] http://www.emit-motor.com.pl/Download/Katalogi,1.

[10] Calculations Institute of Electrical Drives and Machines KOMEL, 2015.

Zbigniew Drążek
zbigniew.drazek@ee.pw.edu.pl

Tadeusz Maciołek
Adam Szeląg
Marcin Steczek

Faculty of Electrical Engineering, Warsaw University of Technology

Energy efficiency of a railway line supplied by 3 kv supply system – a case study of the application of an inverter in a traction substation

Efektywność energertyczna linii kolejowej zasilanej napięciem 3 kv dc – studium przypadku zastosowania falownika w podstacji trakcyjnej

Abstract

Due to energy saving policy in the European Union and development of power electronics technology, one might expect an increase in the use of solutions, such as inverters in the substations of the 3 kV DC power supply system. The paper includes a study case of the analysis of traffic conditions on the use of inverters in 3 kV DC system traction substations so as to send back trains' braking energy from a DC traction power supply to an AC power supply network. The authors presented possible estimated energy savings for a selected railway line. Furthermore, the character of a power waveform and energy available for transferring from a DC to an AC power supply network was discussed as well. The effectiveness of this solution largely depends on the nature of train traffic, so prior to applying the inverters, a detailed analysis is required.

Keywords: energy efficiency, railway line, traction substation

Streszczenie

Polityka oszczędności energii prowadzona w krajach UE oraz rozwój technologii w energoelektronice zwiększa możliwości stosowania rozwiązań, takich jak falowniki w podstacjach systemu 3 kV DC. W artykule przedstawiono studium przypadku analizy wpływu warunków ruchu na zastosowania falownika w podstacji trakcyjnej 3 kV DC w celu zwrotu energii hamowania odzyskowego pociągów do zasilającej sieci elektroenergetycznej. Pokazano szacunkowo możliwe do uzyskania oszczędności energii dla wybranej linii kolejowej. Omówiono charakter przebiegu mocy oraz wartość energii możliwą do przesłania przez falownik do sieci zasilającej. Efektywność stosowanych rozwiązań i celowość stosowania falownika silnie zależy od charakteru prowadzonego ruchu, dlatego istotne jest przed jego zastosowaniem przeprowadzenie szczegółowych analiz.

Słowa kluczowe: efektywność energetyczna, linia kolejowa, podstacja trakcyjna

1. Introduction

In a DC railway traction supply system under conditions of frequent stops (suburban traffic), there is usually energy surplus (in comparison to energy consumed by vehicles) from regenerative braking. In order to use this energy, it has to be collected in an energy storage device on the DC side or sent to the power system. However, the basic condition is the presence of consumers on the AC side and a power supply system with appropriate technical parameters.

With development of technology of power electronics switching devices, one has started testing inverter solutions, especially those added to the existing rectifier traction substations. Solutions for urban traction developed by companies such as ABB or Alstom [1, 7] are already well-known and widely used, but in a 3 kV DC railway traction, apart from test solution, there is no information on the use of inverters or storage devices in substations [9, 20, 21].

A converter planned for application in the substation might be used, both as an inverter and as an active power filter. When used as an inverter, it converts and returns energy to AC network during a vehicle braking phase, and when it operates as an active power filter, it compensates harmonic distortion caused by a traction substation rectifier.

In case of a technical analysis related to the application of inverters, one should take into account a range of factors influencing the operation of an inverter traction substation, including, among others:

- ▸ optimization of traction substation equipment, including, its dimensions and location, so as to obtain the best possible conditions for regeneration with a considerably small number of converters;
- ▸ control and characteristics of converters that influence heavily on the parameters such as: system receptivity, power factor and higher harmonics content in AC voltage and equalizing currents in a rectifier-inverter circuit;
- ▸ power demand on the AC side.

    (1) Electric Traction Division, Electrical Eng. Faculty, Warsaw University of Technology
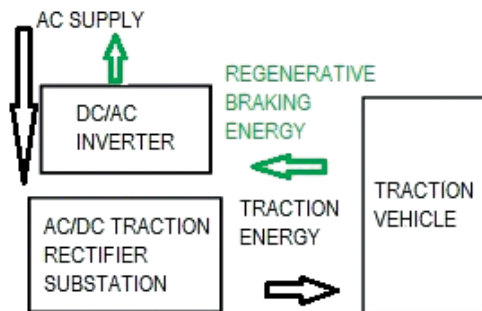   (2) Power Engineering Institute, Łódź University of Technology

Fig. 1. Diagram of energy flow in a DC traction system with the use of an inverter in a traction substation

2. The results of inverter application

Application of inverters in a power supply system provides the following results [2–6, 8, 10, 11, 15–19]:

- ▸ the use of energy that otherwise would be dissipated in braking resistors or dissipated into heat at brakes;
- ▸ an additional energy source for a power grid under conditions of considerable load of a grid (Fig. 1);
- ▸ the possibility of energy transfer through a MV network to the point of increased power consumption.

It was also considered whether elimination of resistors from the vehicles (providing that to all recuperation energy could be sent to DC network) with provision of braking energy transfer into a substation is a good solution. However, safety requirements do not allow for a vehicle's operation without braking resistors on-board due to fact that contact between current collector of the vehicle and catenary could be lost and current transfer to catenary during recuperation is not always possible).

When using inverters in a traction substation, the following should be taken into account:

- ▸ higher investments (devices, area, building);
- ▸ larger energy losses in a substation, increase of rectifiers' load;
- ▸ an inverter should have higher rated parameters than the respective rectifier;
- ▸ increase of distortion from higher harmonics and voltage fluctuations in a MV network, problems with electromagnetic compatibility in a traction system [14] and radio-eletrical interference;
- ▸ increase of reactive power consumption and lower power factor and voltage fluctuations in an AC network, which might require the use of filters of higher harmonics or reactive power compensators;
- ▸ requirements to use intelligent systems for control, monitoriong and protection;
- ▸ the requirement for a traction substation to have, at the inverter operation mode, higher voltage than an idle state of rectifier operation (e.g. so current flows only from braking vehicles and not from rectifier units to an inverter);
- ▸ the necessity for arrengements with local DNO (Distribution network operator) regarding the possibility of energy return to a grid.

With respect to a regenerative substation with grid energy return to AC supply, the Rail Infrastructure Manager with cooperation with the DNO has established the conditions for an AC traction substation – so as to fulfil the needs of the electricity market, and to enable feeding energy back into a public grid.

In Poland, Izba Gospodarcza Komunikacji Miejskiej [Urban Traffic Central Office] makes efforts [10] for regenerative braking energy return from the urban transport systems to the AC network to be included in Energy Law. However, certain legal problems regarding the following issues have not been resolved yet:

- ▸ lack of definition of "energy recuperation" in Energy Law and lack of determination of its source of origin, in particular, the need for special treatment of recuperation

energy as energy from the power system circulating in an electric traction system. Recuperation energy has to be used during a short period of a vehicle's regenerative braking, otherwise it is dissipated in a form of heat;

▸ lack of requirement of acceptance of the connected devices enabling recuperation energy return to an AC network imposed on the DNO;

▸ lack of appropriately defined manners for energy settlement;

▸ lack of legal intepretations regarding excise tax settlement;

▸ lack of support for the entities increasing energy efficiency of transport via increased recuperation efficiency.

In urban transport systems for many years inverters have been used in a thyristor technique, mainly the undergound systems (Brasil, ASingapur – powered by 750 V DC) and in Japan (1.5 kV DC). Current solutions of inverters with transistors allow for high efficiency, low harmonics content and a high power factor. In new substations, inverters are installed as rectifier and inverter units, and some additional inverter units [1, 7] are proposed for the existing substations.

3. Improving regenerative braking efficiency by means of additional equipment for a power supply system

During analyses of several solutions for recuperation efficiency improvement via application of an energy storage device or an inverter in a power supply system, the following should be taken into account [17]:

▸ traffic frequency;

▸ number of the required inverters or energy storage devices, their parameters and cost;

▸ scheme of sectioning and line power supply on the DC side;

▸ resistances in the DC circuits;

▸ an admissible voltage level in a catenary;

▸ amount of energy that can be taken over by other trains and the amount of energy that has to be received by an energy storage device / traction substation inverter;

▸ the additional costs of the equipment for rolling stock/a substation and savings that can be achieved – modern controlled rectifiers and inverters are equipped with the IGBT transistors [1, 7] that, due to PWM control, almost entirely eliminate the problem of harmonics and reactive power consumption, and the inverters connected to separate modules in parallel to classic rectifies may operate as filters of the current higher harmonics of rectifiers.

Introduction of regenerative braking is a new challenge and might cause the increase of disturbances from current and voltage higher harmonics under transient and steady states. The source of these disturbances includes both, a traction substation and a vehicle. When using rolling stock with DC and AC motors without recuperation, a substation constitutes an energy source with a variable component, and a vehicle is an energy consumer absorbing current distorted as a result of the operation of converters (choppers, inverters). In the case of recuperation, a vehicles becomes an energy source as well by generating, both, distorted current and voltage. In order to analyse this type of issue in a complex manner, one should take into account the mutual interaction

of a substation, vehicles drawing energy and regenerative braking vehicles together with a catenary. Due to the complex nature of the phenomenon, it is required to use modelling and simulation techniques, and the models of objects should take into account their parameters (variables in a frequency function) and different operating states as well as position changeability. In such a multi-source supplied circuit with changeable parameters might, under certain, unfavourable conditions, occur resonances increasing even the slightest disturbances to considerable values. From the point of view of the compatibility of a power supply system, vehicles and low-current systems of control and signalling, the following are of high importance [14]:

- ▸ traction substation's parameters;
- ▸ presence or absence of a filter on the DC side, and the type of a filter;
- ▸ sectioning schemes;
- ▸ parameters of a catenary;
- ▸ parameters of a vehicle's input filter (a vehicle's input impedance);
- ▸ symmetry of voltage supplying a substation.

4. Case study of efficiency – simulation analysis of energy balance regarding installation of an inverter in a 3 kV DC substation for suburban traffic

During research for the case study, a series of simulation calculations were conducted in order to prepare a case study of energy efficiency with the use of a program developed at the Electric Traction Division of the Warsaw University of Technology [14, 16, 17]. The analyses were based on a 2-track section of a railway line of 30 km long supplied with 3 kV DC voltage with substations equipped with rectifiers, and additionally, with the use of an inverter in one of the middle substations. No power limitation was assumed, that is, the whole power provided at the input of an inverter P_{fal} (at DC rails of a substation) might be transferred to the 3-phase AC side. One conducted a parametric analysis for a section with regular suburban railway traffic with 4 MW trains running on 2 tracks of a line (with 10 stops) and at a constant sequence dt = 3 min to 30 min.

As a result simulation, one determined instantaneous waveforms (analysis step – 1 s) for the following values:

P_{pt} – power drawn from all substations feeding the analysed section,
P_{poj} – power drawn from a catenary by all vehicles running on a section according to the set timetable,
P_{rek} – recuperation capacity of all traction vehicles,
P_{fal} – power available at the 3 kV DC rails of a substation equipped with an inverter.

The value of power P_{sr} for simulation time (equivalent to energy during simulation) and the maximum values of instantaneous power P_{max} were determined.

Fig. 2 shows waveforms from simulation of instantaneous power drawn from a substation for train operation for dt = 3.5 and 10 min, and Fig. 3 for dt =10 min. Average power drawn from a substation during simulation was respectively, 23 MW (for dt = 3 min), 17.6 MW (for dt = 5 min) and 9.3 MW (for dt = 10 min). Fig. 3 and 4 show, respectively, power waveforms P_{pt}, P_{poj}, P_{fal} and P_{rek} for dt = 5 and 10 min.
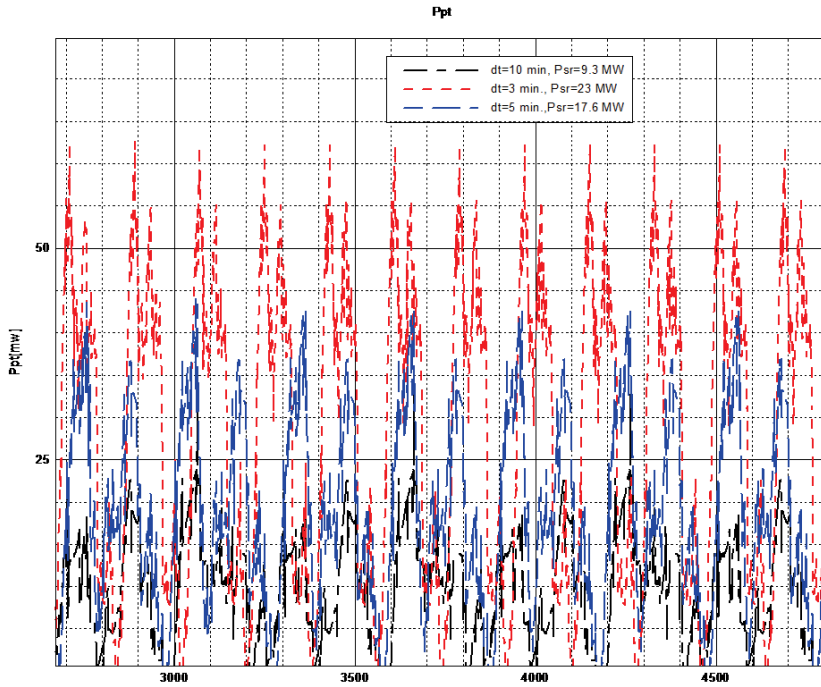
Fig. 2. Waveforms as a function of time of a substation's power P_{pt} for various times of a train sequence dt
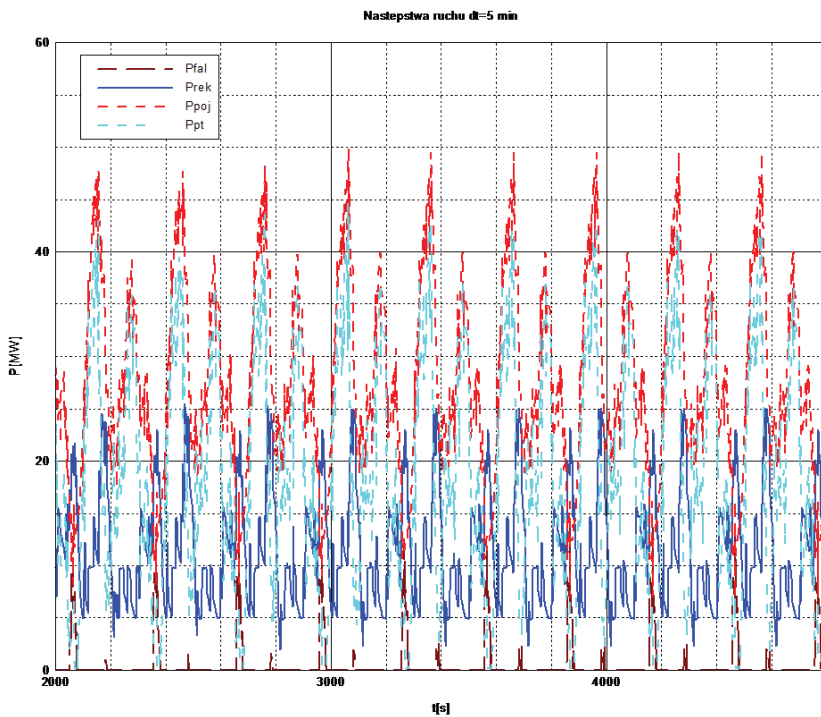
Fig. 3. Dependence of the waveform of power P_{pt}, P_{poj}, P_{fal}, P_{rek}, time intervals between trains $dt = 5$ min

Fig. 4. Dependence of the waveform of power P_{pt}, P_{poj}, P_{fak}, P_{rek}, time intervals between trains dt = 10 min.

Fig. 5. Dependence of the waveform of power supplied to the inverter P_{fal} as a function of time for various time intervals between trains dt = 3÷30 min

Average value of power supplied to an inverter P_{srfal} during simulation is not too high (Fig. 6 – from 0.53 MW at operation with a sequence every $dt = 5$ min up to 1.18 MW with sequence $dt = 15$ min). Assuming even a mini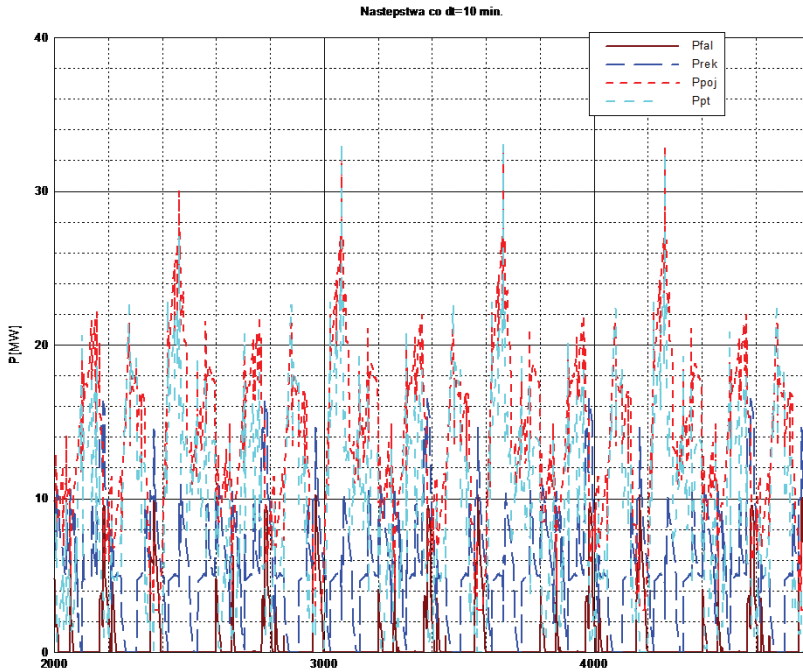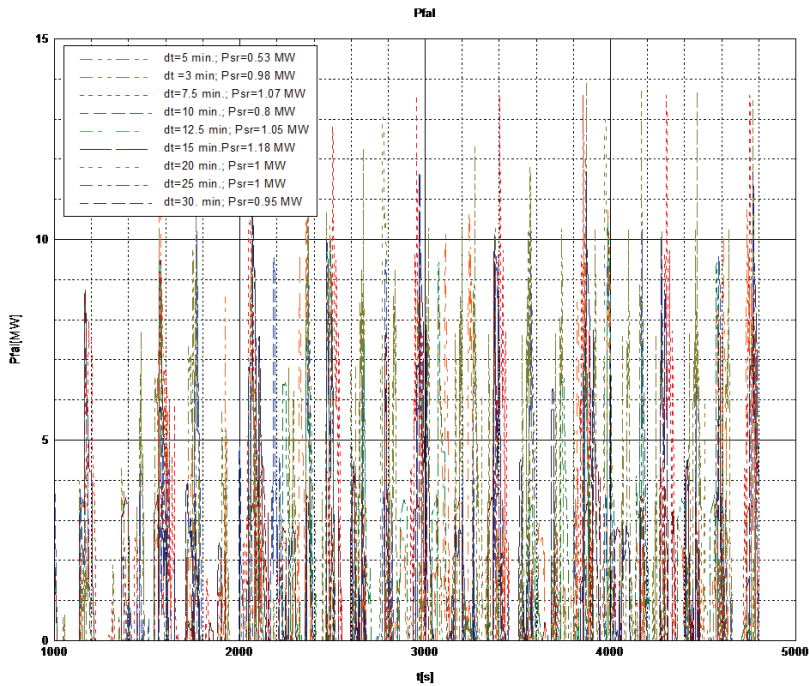mum value of average power $P_{srfal} = 0.5$ MW for 16 hours of traffic, one receives daily savings of 8 MWh and monthly of 180 MWh, taking into account only working days.
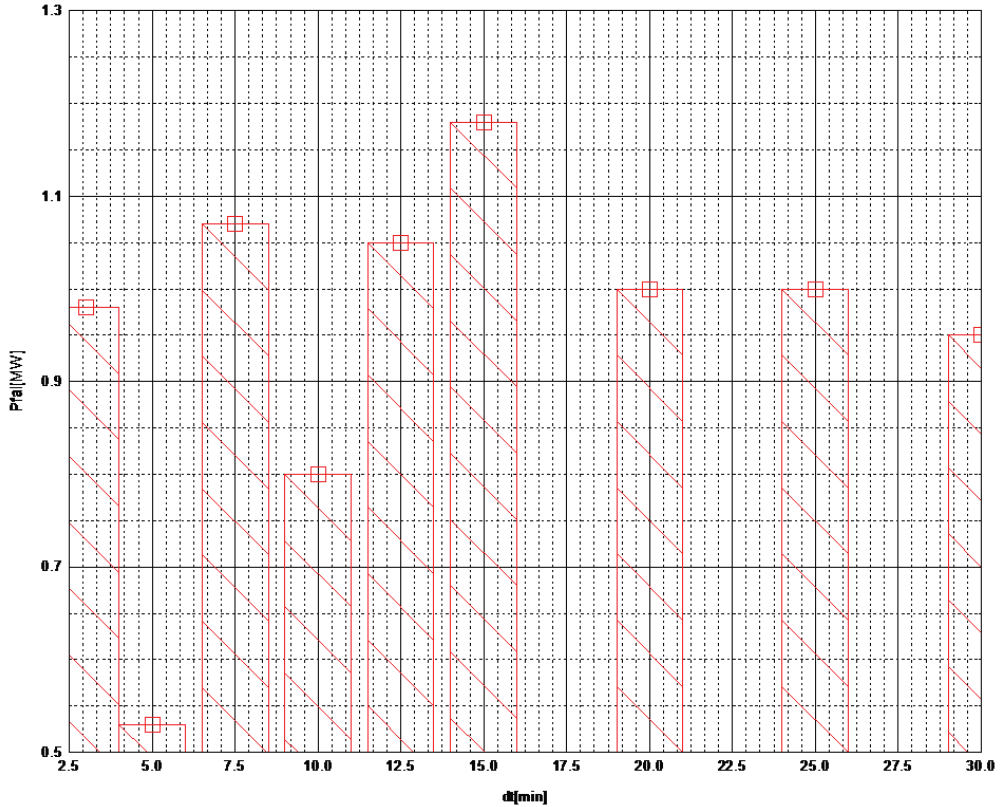
Fig. 6. Dependence of an inverter's average power P_{srfal} from time of train sequences dt

Energy efficiency of the application of an inverter will depend on the possibility of the AC power system to absorb pulse power P_{fal} reaching the inverter – power above 10 MW and duration time of several to a few dozens seconds (Fig. 7).

It relates to the change of receptivity of a 3 kV DC catenary (the possibility of exchanging energy between braking trains and trains taking energy) at the supply section and the overlap of braking processes of several trains. It is maximum power in particular P_{maxfal} that will determine the required rated power and overload capacity of an inverter, as well as influence its cost and financial profitability of the system. In order to receive power of up to 12 MW (except for the case for $dt = 5$ min power P_{maxfal} does not exceed this value – Fig. 8) at overload of 300% one should install an inverter with 4 MW rated power at average used power of up to 1 MW.

Fig. 7. Enlarged power waveforms P_{fal} from Fig. 5

Fig. 8. Dependence of the maximum power P_{maxfal} and average power P_{srfal} of an inverter and the ratio of $P_{maxfal}/P_{srfalod}$ to train sequence times dt

5. Summary

Assuming a specific timetable on a given line enables estimating certain energy performance, and consequently, economic effects fr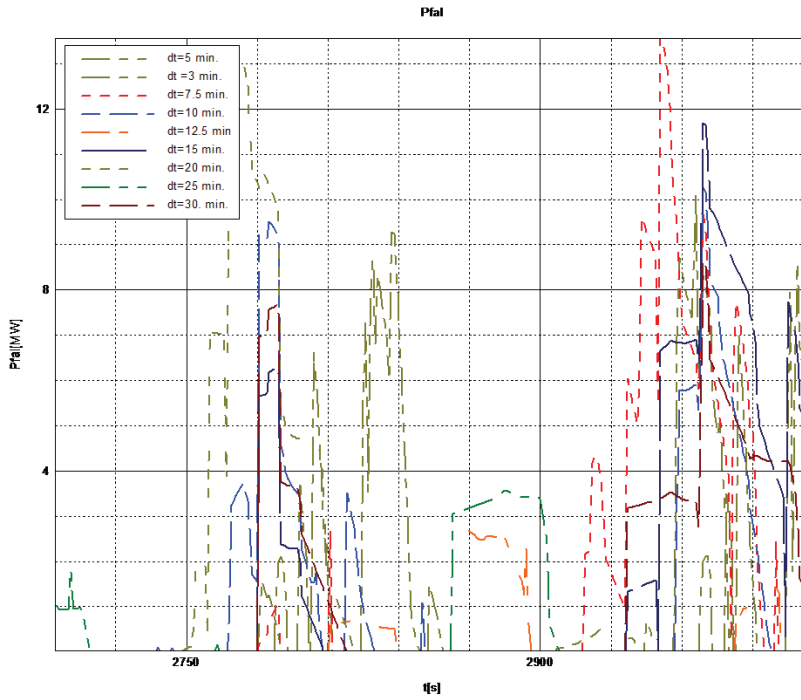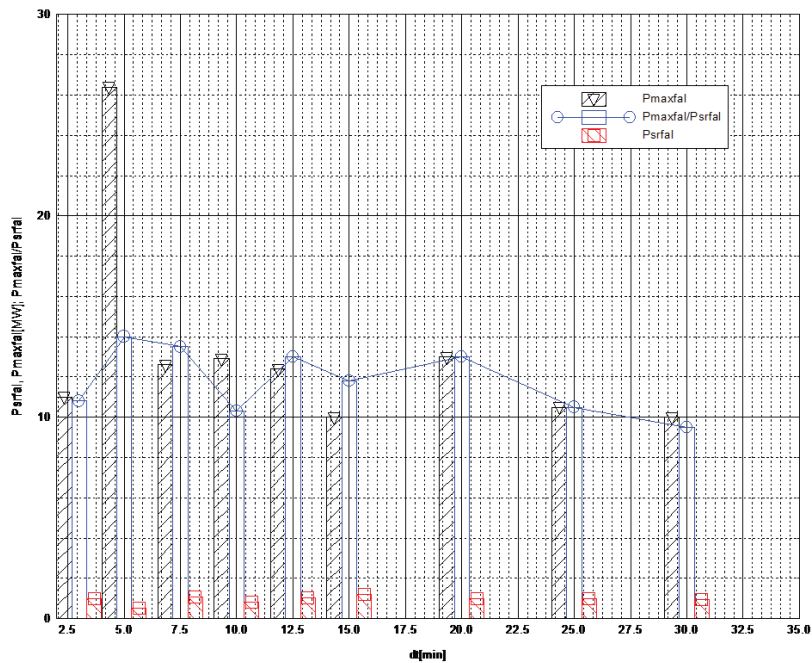om the application of an inverter for regenerative braking energy return to the power supply network in 3 kV DC railway substations. However, even the slightest changes in the timetable, especially traffic density and shift of traffic in both directions, will result in significant changes of energy performance. Relative share of additional energy saved due to the application of inverters is particularly sensitive to these changes. Even at the same traffic density and with trains running with a time shift, significant changes regarding the efficiency of inverter application will occur in traffic directions (a DC traction system changes its receptivity when changes in traffic flow occurs) [18]. When the receptivity of a system is increased (increased transfer of regenerative braking energy between the vehicles), the efficiency of inverter use decreases. Inverter dimensioning should take place on the basis of the expected waveforms of power supplied to the point of inverter connection, taking into account the following aspects:

▸ current (power) in an inverter is of pulse nature, and it is maximum peak current that influences power of an inverter and a transformer (operating simultaneously) due to low constants of semiconductor thermal elements and limitation of commutating circuit reactance (transformer),

▸ the values of equivalent power during peak hours of inverter load.

If each traction substation is equipped with an inverter system, the power supply system will be receptive at any time; however, it would not be economically feasible, since:

▸ usually, the value of braking current is lower than the train start-up current, and in the case a braking vehicle is at large distance from the substation and transfers a part of its energy to the vehicle starting at a given time, it is not justified to transfer a small amount of energy to the inverter,

▸ if all substations are equipped with inverters, energy used so far between the trains will be transferred to the substation, which will result in increased size of converters and larger losses.

The ratio of instantaneous power to rated power for an inverter may considerably exceed the value of this ratio for rectifiers (braking time is shorter than the time of energy consumption by a vehicle). This may mean that in order to reduce the costs, it is required to limit the value of admissible inverter current and failure to use maximum available regenerative braking power that is pulse in its nature. It is due to the fact that from the point of view of the amount of energy used in the AC side, sending a short-term high power pulse is not efficient, and it is very costly (inverter power, ensuring operation stability of the AC network receiving power). A solution limiting recuperation power pulses might consist in using, together with an inverter, a storage device receiving short power pulses (e.g. of supercapacitor) on the 3 kV DC side.

References

[1] ABB Review, ENVILINE™ ESS voltage support case study How can Rail Transit Authorities mitigate voltage issues due to increased power demand?, ABB edition 10.2014: https://library.e.abb.com/public/3f89a1a3b77dc59ac1257d73002dcde0/ ENVILIN%20ESS%20 voltage%20support%20case%20study%20ver2.pdf (access: 22.01.2017)

[2] Abe S., Fuimori H., Ito T., DC feeding system suitable for rolling stocks with re-generative braking system utilizing thyristor rectifier: http://ieeexplore.ieee.org/ document/264861/ (access: 12.12.2016).

[3] Bartosik M., Kamrat W., Kaźmierkowski M.P., Lewandowski W., Pawlik M., Peryt T., Skoczkowski T., Strupczewski A., Szeląg A., *Bezpieczeństwo elektroenergetyczne dla pokoleń*, Przegląd Elektrotechniczny, (92) 8/2016, 268–282.

[4] Cornic D., *Efficient recovery of braking energy through a reversible dc substation.* RailEnergy research programme results, Alstom Transport, IEEE 2010.

[5] Dolecek R., Dobrovolny M., *Traction converting substation from viewpoint of feeding interlocking plant At Czech Railways*, Advances in Electrical and Electronic Engineering.

[6] Henning P. H., Fuchs H. D., le Roux A. D., Mouton H. Du T., *A 1,5 MW Seven_Cell Series Stack Converter as an Active Power Filter and Regeneration Converter for a DC Traction Substation*, IEEE Trans. on Power Electronics, vol. 23, no 5, Sept. 2008.

[7] Hesop All in one Energy& Cost Saver; http://www.alstom.com/Global/Transport/ Resources/Documents/brochure2014/HESOP%20-%20Product%20sheet%20-%20 EN%20-%20LD.pdf?epslanguage=en-GB (access: 2.05.2017)

[8] Kondo K., *Recent Energy Svling Technologies on Railway Traction Systems*, IEEJ Transactions on Electrical and Electronic Engineering, 2010, 298–303.

[9] Maciołek, T., *Zastosowanie zasobników energii w trakcji kolejowej 3 kV DC–nieodległa perspektywa?*, TTS Technika Transportu Szynowego, 22, 2015.

[10] Majchrzycki A., Tuliński K., *Rekuperacja energii – klucz do optymalizacji kosztów czy dodatkowe problemy techniczne*, [w:] A. Szeląg (red.), *Trakcja elektryczna*, Prace Naukowe, Monografia II Kongresu Elektryki Polskie, Wyd. COSIW, SEP, Warszawa 2016.

[11] Mellitt B., Mouneimne Y.S., Goodman C.J., *Simulation study of DC transit systems with inverting substations*, IEEol. 131, Pt. B, No 2, March 1984.

[12] Mierzejewski L., Szeląg A., *Aktualne kierunki ograniczania zużycia energii elektrycznej w transporcie kolejowym*, Technika Transportu Szynowego 7-8/2004, 35–41.

[13] Pawełczyk M., *Rozwój systemów wykorzystujących akumulację energii w transporcie szynowym*, Pojazdy Szynowe 2/2011, 14–19.

[14] Steczek M., Chudzik P., Szeląg A., *Combination of SHE and SHM – PWM techniques for VSI DC-link current harmonics control in railway applications*, Transactions on Industrial Electronics, 2017: http://ieeexplore.ieee.org/document/7900369/ (access: 22.04.2017).

[15] Suzuki T., *DC-power supply system with inverting substations for traction systems using regenerative brakes*, IEE Proc., vol. 129, Pt B, No 1, January 1982.

[16] Szeląg A., Mierzejewski L., *Ground transportation systems*, [in:] Encyclopedia of Electrical and Electronic Engineering, Supplement I, John Wiley & Sons Inc., NY 1999, 169–194.

[17] Szeląg, A.,T. Maciołek., *Rozwiązania techniczne w układach zasilania poprawiające efektywność energetyczną transportu szynowego*, Pojazdy Szynowe 3/2015.

[18] Szeląg A., *Efektywność hamowania odzyskowego w zelektryfikowanym transporcie szynowym*, Pojazdy Szynowe, 4/2009, 9-16.

[19] Szeląg A., Maciołek T., Drążek Z., Patoka M., *Aspekty efektywności i energooszczędności w procesie modernizacji układów zasilania trakcji tramwajowej*, Pojazdy Szynowe, 3/2011, 34–42.

[20] Szeląg A., Maciołek T., *A 3 kV DC electric traction system modernisation for increased speed and trains power demand – problems of analysis and synthesis*, Przegląd Elektrotechniczny 3a/2013, 21–28.

[21] Szeląg A., *Wpływ napięcia w sieci trakcyjnej 3 kV DC na parametry energetyczno-trakcyjne zasilanych pojazdów*, Wyd. INW Spatium, Radom 2013, 58.

Marek Dudzik
marekdudzik@pk.edu.pl

Paweł Trębacz
ptrebacz@pk.edu.pl
Faculty of Electrical and Computer Engineering, Cracow University of Technology

Vasyl Hudym
gudymvi@ukr.net
Lviv State University of Life Safety, Ukraine

Modeling of contact wire's de-iceing phenomena using artificial neural networks

Modelowanie zjawiska odladzania przewodu jezdnego przy wykorzystaniu sztucznych sieci neuronowych

Abstract

The article presents results of iced wire's temperature approximation during process of heating this wire to melt ice. This approximation was implemented in Matlab using a two-layer feedforward artificial neural network (ANN). The results of the approximation are acceptable, but it is possible to improve them.

Keywords: melting of ice, iced wire, artificial neural network;

Streszczenie

W artykule przedstawiono wyniki aproksymacji temperatury oblodzonego przewodu podczas procesu jego nagrzewania w celu roztopienia osadu. Do aproksymacji wykorzystano sztuczną sieć neuronową (SSN) dwuwarstwową typu feedforward, zaimplementowaną w środowisku Matlab. Uzyskane wyniki aproksymacji są zadowalające, niemniej istnieje możliwość ich polepszenia.

Słowa kluczowe: topienie oblodzenia, oblodzony przewód, sztuczne sieci neuronowe;

1. Introduction

Railway malfunctions causes obstacles for people to reach the workplace which results people's change mean of transport to cars. Finally it increases traffic in cities and leads to traffic jams and wasting of time being inside. The winter is season in which probability of fault on railway is higher than during other seasons. Snow and rain fall in conjunction with gusts of wind can create hoarfrost or ice on the surface of contact wires which is a kind of electrical isolation. This isolation causes problem of electrical locomotive riding.

Exists a lot of methods to get rid of ice or hoarfrost from catenary lines which presents that icing problem is actual and could be solved based on different models of de-icing. Process of melting ice on catenary wires require contact wire – ice system's substitute thermal coefficient changes. During de-icing process coefficient will be decreasing from start value, depended of ice thickness, to value of wire's material thermal coefficient. Authors of this article want to present one of method to model processes of changing temperature according to substitute thermal coefficient value and melting time, during wire's de-icing. At the beginning of de-icing process, it will be heating of ice to temperature of zero degree, and then physical transformation ice into water. It will be the method based on artificial neural network analyzes. Wire's temperature calculations using substitute thermal coefficients let to obtain charts of contact wire's temperature as a function of time.

2. The use of an artificial neural network in the analysis of a selected overload

Artificial neural network (ANN) is a general name for mathematical structures and their software or hardware models, which perform calculations or signal processing by rows of elements called artificial neurons. Artificial neurons realize some basic operations on their input. The original inspiration for ANNs was the structure of natural neurons, synapses connecting the neurons and nervous systems, especially a brain [7, 9]. The neural network algorithms in traction research were used in: [2, 3, 6, 8].

2.1. Introductory information and input data

The calculations were performed using Matlab R2011B version. The input data for the ANN analysis were in this case 2102 pairs of numbers. In each pair one of the numbers (Input) was the time value and the other number (Output) was the temperature corresponding to the time.

Measurement data processing was performed using a two-layer feedforward neural network implemented in Matlab. Fig. 1 shows the neural network block created in the Simulink environment.

Fig. 2 depicts the created neural network structure. This structure had one hidden layer consisting of seven neurons. There were no delays implemented on the input for this layer. The activation function for the hidden layer was tangensoidal (tansig). Fig. 3 presents how the hidden layer looks like. The output layer had a linear activation function.
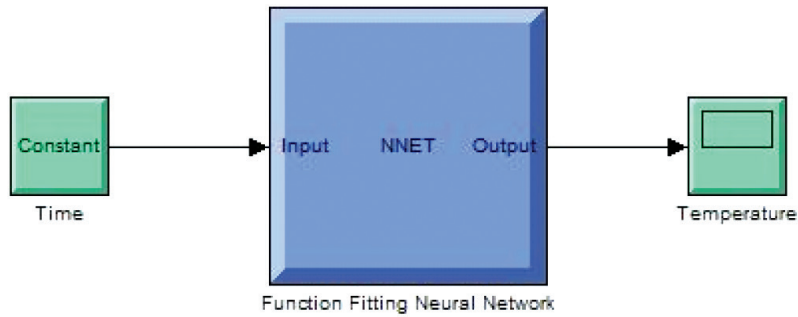
Fig. 1. The neural network block created in the Simulink environment. Own work
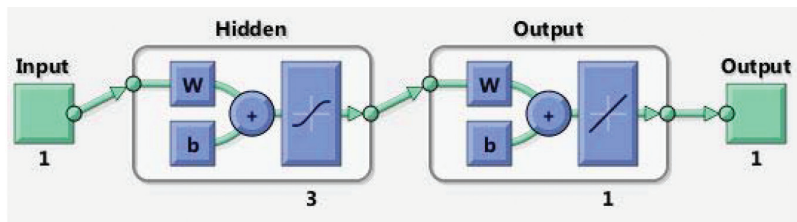
Fig. 2. The created neural network structure. Own work
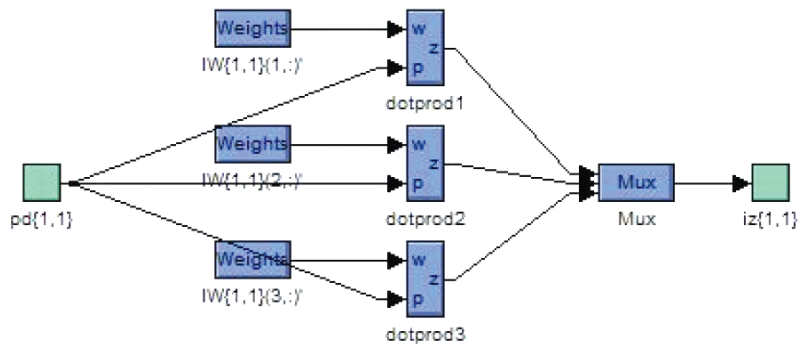
Fig. 3. The hidden layer of created neural network. Own work

The aim of the study was to fit a function between temperature variability phenomena corresponding to melting time.

The results shown below in Subsection 3.2. were obtained for the following ANN training settings [1]:

- ▶ maximum number of epochs to train: 10000;
- ▶ performance goal: 0;
- ▶ learning rate: 0,01;
- ▶ maximum validation failures: 12;
- ▶ momentum: 0,9;
- ▶ minimum performance gradient: 10^{-10};

113

▶ epochs between displays: 25;

▶ maximum time to train in seconds: infinite.

In order to teach the designed artificial neural network, the one-way network (up to 3 layers) training was used according to the Leveneberg-Marquardt algorithm.

2.2. Computation

Fig. 4 depicts results obtained from the training, validation and test of the ANN in the form of an error histogram.
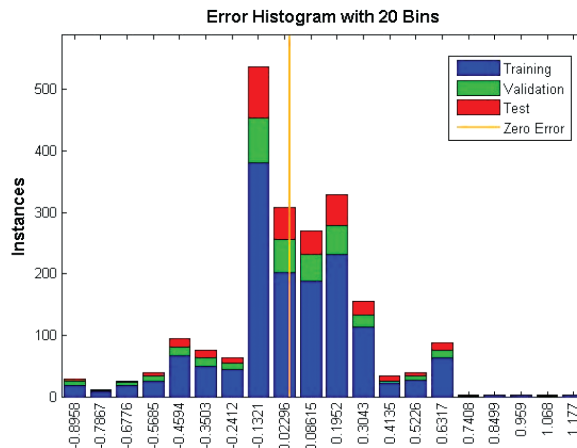
Fig. 4. Error histogram. Own work

Fig. 5 shows the illustration of performance of the ANN for successive learning epochs.

Fig. 5. Performance of the ANN. Own work

114

Fig. 5 presents the artificial neural network performance graph during its learning. The ordinate axis refers to the ANN performance function values. Mean square error (mse) was chosen as the performance function. The horizontal axis corresponds to learning epochs. The system reached the best neural network validation of the ANN performance for the 2176th epoch and it was equal to 0,094145. One can observe that the neural network system continued the learning algorithm for another 12 epochs in order to conf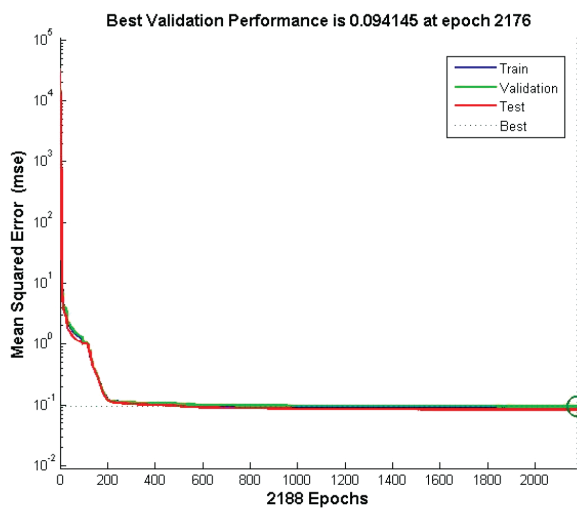irm the alleged local minimum for the goal set for the created network structure (Fig. 2). From epoch 1 to 2176, a downward trend in validation tests of the ANN learning can be seen.

Fig. 6 depicts the regression results for the training, validation and test and the regression for all data assigned to the ANN learning with a supervisor. Here, the ordinate axis represents the neural network output for the given input data. The abscissa axis shows values from the actual measurements (targets), to which the values returned by the ANN should be convergent.

The $R = 1$ regression result means that there is an unequivocal relation between the actual value (target; from measurement or simulation) and the neural network output value.

The regression results for the discussed case are as follows. The regression for the data assigned to the training reached $R = 0,99999$. The data constituted about 70% of all data assigned to the ANN learning with a supervisor. The regression for the validation was equal to $R = 0,99999$. The data used for this step were about 15% of all data. Lastly, the regression for the test was $R = 0,99999$. Consequently, the data used in this stage was about 15% of all data. One more regression value was calculated, for all data, and it was equal to $R = 0,99999$.

The training, validation and test are performed during the procedure of the neural network learning.
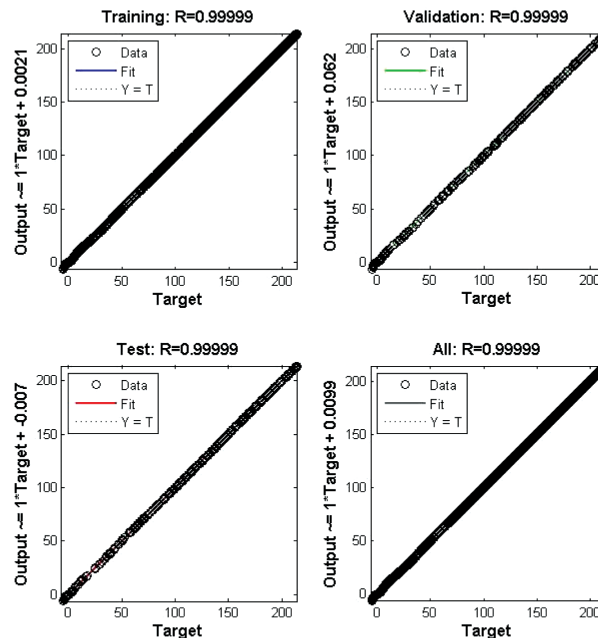
Fig. 6. Regression results for the training, validation and test and the regression for all data assigned to the ANN learning with a teacher. Own work

Figure 7 presents the results obtained from the approximation process (function fitting process) performed by the artificial neural network learning. In this figure, dots represent actual values of the substitute thermal factor obtained from measurements (targets), while cross marks represent results of the approximation. Vertical lines are absolute errors between actual values and the corresponding results obtained by the function fitting process. The solid line is the plot of the resulting approximating function.
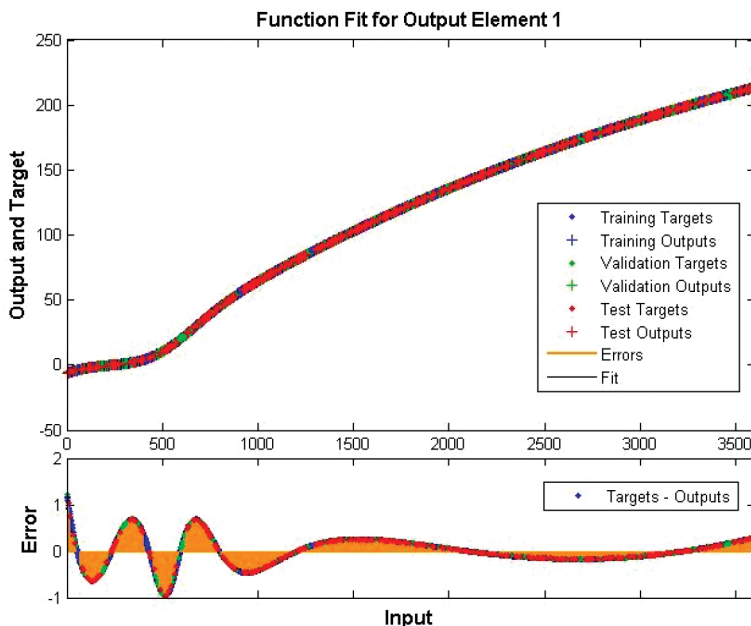
Fig. 7. Results of function fitting with the use of the ANN. Output – temperature, input – time. Own work

3. Conclusions

The calculation results shows that the described phenomena can be modeled with almost 100% precision. Getting to know the possibilities (specificity) of neural networks applied for studies of catenary lines de-icing. Results obtained during analysis presents that data using in calculations are correct. It is really important to confirm regularity of outcome, because it can simplify understanding of melting ice process on catenary lines and it is possible to use this knowledge during power circuits and emergency state protection designing. Authors agrees that it exists the potentiality to improve calculation to exactly 100% precision. Such studies will be continued.

References

[1] Bartman J., *Podstawowe funkcje biblioteki narzędziowej "Neural Network Toolbox. Version 5" pakietu MATLAB v.6*, Uniwersytet Rzeszowski, Zakład Elektrotechniki i Informatyki, online.

[2] Dudzik M., Drapik S., Prusak J., *Approximation of overloads for a selected tram traction substation using artificial neural networks*, Technical Transactions, 3-E/2016, 39–50.

[3] Dudzik M., Drapik S., Prusak J., Kobielski A., *Studium efektywności zastosowania sieci neuronowych w badaniach obciążeń kolejowych podstacji trakcyjnych*, MET'2013: 11th International Conference „Modern Electric Traction", Poland, Warszawa 2013, 176–180.

[4] Hudym V., Jagiełło A., Prusak J., Chrabąszcz I. Trębacz P., Kaczmarczyk A., *Metodyka usuwania oblodzenia z sieci trakcyjnej*, Logistyka 6/2015, 1055–1062.

[5] Hudym V., Jagiełło A., Prusak J., Chrabąszcz I. Trębacz P., *Preventing the formation of ice on the catenary lines*, Technical Transactions, 3-E/2016, 173–184.

[6] Kobielski A., Drapik S., Dudzik M., Prusak J., *Wstępne studium efektywności zastosowania sieci neuronowych w badaniach obciążeń kolejowych podstacji trakcyjnych*. TTS Technika Transportu Szynowego, 10/2014, 40–43.

[7] Korbicz J., Obuchowicz A., Uciński D., *Sztuczne sieci neuronowe. Podstawy i zastosowania.* Akademicka Oficyna Wydawnicza PLJ, Warszawa 1994.

[8] Malina A., Dudzik M., *Wykorzystanie algorytmów sieci neuronowych w celu zmniejszenia amplitud wahań momentu elektromagnetycznego silnika indukcyjnego w metodzie sterowania wektorowego DTC*, Elektrotechnika w zastosowaniach trakcyjnych, Kraków 2014, 281–294.

[9] Tadeusiewicz R., *Sieci neuronowe*, Akademicka Oficyna Wydaw. RM, Kraków 1992.

Denys Gutenko orcid.org/0000-0003-4160-724X
dgutenko@pk.edu.pl

Department of Automation and Information Technologies, Faculty of Electrical
and Computer Engineering, Cracow University of Technology

Selecting quasi-constant weight code parameters for systems
of automatics

Wybór parametrów kodu quasi-równoważnego w systemach
automatyki

Abstract

In this paper, the requirements of quasi-constant weight code parameters are considered for a certain
number of encoded messages and for various requirements of noise immunity. An algorithm is proposed for
choosing the optimal parameters of a quasi-constant weight code for a given number of encoded messages
and a level of noise immunity that would ensure maximum speed of control command transmission.

Keywords: quasi-constant weight codes, communication channel, noise immunity, speed of control command transmission

Streszczenie

W artykule uwzględniono wymagania dotyczące parametrów kodu quasi-równoważnego w odniesieniu
do liczby zakodowanych komunikatów dla różnych wymagań w zakresie odporności na szum. Został
zaproponowany algorytm wyboru optymalnych parametrów kodu quasi-równoważnego dla podanych
liczby zakodowanych komunikatów i poziomu odporności na szum, który zapewniłby maksymalną
prędkość przesyłu komunikatów.

Słowa kluczowe: kody quasi-równoważne, kanał komunikacyjny, odporność na hałas, prędkość przesyłu komunikatów.

Symbols

N, K – numbers of encoded messages (the number of control signals)

n – number of digits in a combination

k – number of units in a combination

α – half the width of the interval of the allowed values of the number of units in the combination

β – half the width of the segment of unacceptable values of the number of units in the combination

D, P – fractions of detectable errors

1. Introduction

In modern automation systems, the actual task remains to increase the speed of transmitted control signals with the required noise immunity. In control systems, communication channels are often asymmetric. For asymmetric channels, it is advisable to select constant weight codes since with an increase in the degree of asymmetry of the channel, the detectability of these codes increases. In an absolutely asymmetric communication channel, constant weight codes allow 100% of errors to be detected. In addition, for a given code word length, the chosen constant weight code usually has more resolved combinations than the separable code with the same detecting ability [1]. Another advantage of constant weight codes is the ease of detecting errors by counting the number of units in a combination. As a consequence, coding and decoding devices are simple; this is why these codes are widely used. For example, one of these codes is a five-digit code with two units and a seven-digit code with three units [2].

The main drawback of constant weight codes is their inseparability; therefore, in the code combination, it is necessary to convert input words into constant weight combinations. [1]. In addition, constant weight codes cannot detect errors when one or more units tend to zero at the same time and the same number of zeros tend to units in the transposed combination [2]. Additionally, constant weight codes should be selected for communication channels with a certain level of noise immunity. However, in some control systems over time, the requirements for noise immunity of the communication channel may change. This is why, in such cases, it would be useful to change the level of noise immunity of transmitted combinations, so we could obtain a gain in speed in cases where high noise immunity is not needed. In this paper, speed will be understood as the number of control commands sent per unit of time. To increase speed, it is necessary to encode a control command using a combination with the fewest number of bits since in this case, it would be possible to send less bits through communication channel for one control command. In standard constant weight code, it is impossible to change the length of code combination. A code in which the length of the code combinations changes with noise immunity is called the quasi-constant weight (code with quasi-constant weight) [3, 4, 5]. Therefore, the task emerges of developing an algorithm for selecting a quasi-constant weight code which provides maximum speed with changing requirements for noise immunity.

2. Choice of quasi-constant weight code

Let us suppose that there is a control system with a communication channel through which K different control commands can be transmitted. It is necessary to choose a quasi-constant weight code that could be used to transfer command data, satisfy the changing noise immunity requirements and at the same time, can provide the best possible speed for these requirements.

If the requirements for noise immunity are unchanged, the quasi-constant weight code becomes a normal constant weight code. This means that the quasi-constant weight code can be represented as a constant weight code on time intervals with unchanged requirements for noise immunity. This is why the operating time of the control device can be divided into a certain number of time intervals on which the requirements for noise immunity are constant. Thus, at each of these intervals, combinations of constant weight codes corresponding to the given noise immunity are sent. The parameters of the constant weight codes depend on the noise immunity requirements for the corresponding interval. In addition, the number of constant weight combinations must be greater than or equal to the number of control commands K:

$$N_p \geq K, \tag{1}$$

where N_p is the number of combinations.

In general, the number of combinations of the constant weight code is $[6]$

$$N_p = \frac{n!}{(n-k)!k!} \tag{2}$$

where n is the number of digits of the combination and k is the number of units.

By substituting (2) into (1), a new formula is obtained:

$$\frac{n!}{(n-k)!k!} \geq K \tag{3}$$

Therefore, for each constant weight code used in a quasi-constant weight code, the parameters n and k must have values with which inequality (3) is satisfied. From inequality (3), it is possible to get parameters n and k by analysing the corresponding graphs or by the method of selection. Figure 1 presents variants of the graphical solution of the inequality (3) for different n and k with the number of control signals $K = 35$.

In Fig. 1, continuous curves show the relationship between the number of allowed combinations and different k with some fixed parameter n for each curve. By the nature of the changes in this figure, one can see that the number of allowed combinations reaches the maximum value for $k = n/2$ and gradually decreases from this value to the minimum value for $k = 0$ and $k = n$. Since n and k can only take discrete values, it should be understood that the relationship between the number of allowed combinations and the parameter k is a collection of points that are connected in a continuous curve for easy perception.

The solution of inequality (3) is the collection of curve points that are on or above the line $K = 35$. As can be seen in Fig. 1, there is a minimum value of $n = n_{min}$ for which there are
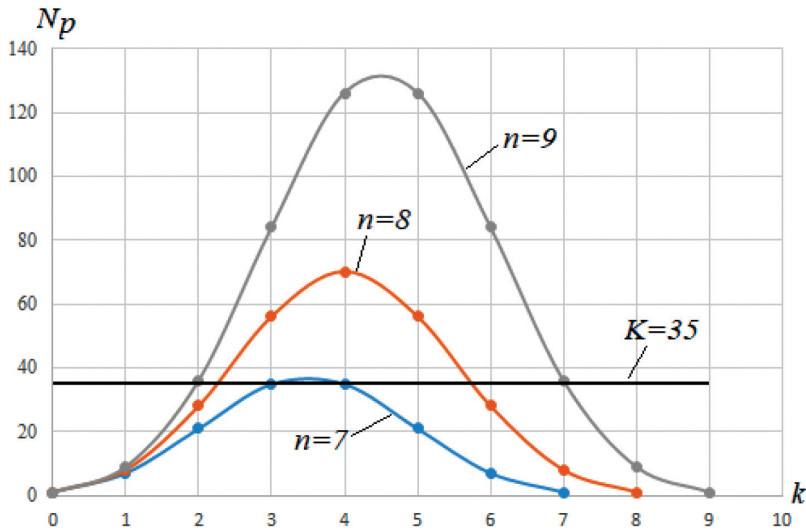
Fig. 1. Options for solving inequality (3) for different n and k for $K = 35$

solutions of this inequality. As n increases, the number of possible solutions increases. For $n < n_{min}$, the inequality has no solutions since there are no integer nonnegative k for which it is satisfied.

For a fixed n, the range of values of k at which the corresponding curve is above the line $K = const$ is symmetrical with the centre of symmetry at $n/2$. This means that the range of values of k at which inequality (3) is satisfied in the general case can be written in the form $k \in \left[\dfrac{n}{2} - \alpha_i ; \dfrac{n}{2} + \alpha_i \right]$, where α is a parameter that determines the width of the range of values of k for a certain $n = n_i$ if solutions of inequality (3) exist. As can be seen in Fig. 1, with increasing n value, the range of solutions of k also increases, so for $n_j > n_i$, $\alpha_j > \alpha_i$.

For the considered example, the minimum value of n for which inequality (3) would be satisfied is $n_{min} = 7$. The range of solutions k for a given n is in the range 3 to 4 and is symmetrical with the centre of symmetry at $n/2 = 3.5$. However, k cannot take such a value, since it must always be integer. In this interval, there are two non-negative integer values $k = 3, 4$ which are the solution of this inequality.

For $n = 8$, the range of solutions of k is symmetrical with the centre at $n/2 = 4$, and there are already three integer values $k = 3, 4, 5$ on this range, which are the solutions for this inequality. For $n = 9$, the range of solutions of k is symmetrical with the centre at $n/2 = 4.5$ and on this range, there are already six integer values k = 2, 3, 4, 5, 6, 7, which represent solutions for inequality (3). With increasing n, the number of possible solutions for k increase further.

It should be understood that despite increased numbers of decision for inequality, with increased length n of the combination the speed will be also reduced, because more bits must be transmitted for each control command. Therefore, with imposed noise immunity requirements and a certain number of control commands K, it is necessary to select a constant weight code with the minimum number of bits in combinations.

To estimate the noise immunity, the formula [1] of the fraction of detectable errors is used:

$$D = 1 - \frac{N_p}{N_B}, \tag{4}$$

where N_B is the number of all possible combinations.

The fraction of detectable errors is characteristic of the code itself and is not characteristic of the communication channel. Since the number of bits of the constant weight code is described by the parameter n, the number of all possible combinations N_B with this number of bits is equal to the number of combinations of the binary natural code 2^n. By substituting formula (2) into (4), the fraction of detectable errors for the constant weight code with n-bit combinations having k units is obtained:

$$D = 1 - \frac{\frac{n!}{(n-k)!k!}}{2^n}. \tag{5}$$

Let us assume that for the communication channel in the control system, there are requirements for the noise immunity level that can be expressed as the required fraction of detectable errors in the used code. Such a required fraction is described with the parameter P. As mentioned earlier, the operating time of the control system was divided into intervals in which the requirements for noise immunity are unchanged. This means that for each of these intervals $P = const,$ and for each of them, it is necessary to choose a constant weight code which satisfies the requirements of its noise immunity. This is why it is necessary to choose a constant weight code with parameters n and k for which the fraction of detectable errors (5) should be greater than or equal to the parameter P.

$$1 - \frac{\frac{n!}{(n-k)!k!}}{2^n} \geq P. \tag{6}$$

Inequality (6) can be solved either graphically or by the method of selection. Figure 2 shows the solutions for different n and k for the parameter $P = 0.85$.

Figure 2 shows the curves, each of which is the relationship between the fraction of detectable errors and the number of units k in constant weight combinations with fixed number of bits n. Since k takes only discrete values, this relationship can be expressed by a collection of points that are connected in continuous curves for easy perception of the figure.

The solution of inequality (6) is the collection of curve points that are above the line $P = 0.85$. As can be seen in the figure, in the general case for a fixed n, the solution of this inequality for parameter k is two intervals. The beginning of the first interval is always at 0 and the end of the second interval is always at n. The end of the first interval and the beginning of the second interval are symmetrically located with the centre of symmetry at point $n/2$. This is why, in the general case, the solution of inequality (6) for some $n = n_i$ can be expressed
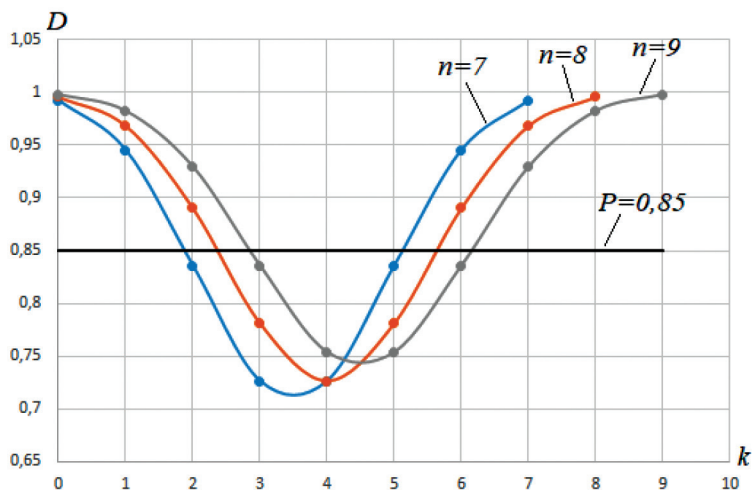
Fig. 2. Options for solving inequality (6) for different n and k for $P = 0.85$

as $k \in \left[0; \dfrac{n}{2} - \beta_i \right] \cup \left[\dfrac{n}{2} + \beta_i; n \right]$, where $\beta_i \geq 0$ is the parameter that describes the width of the interval at which inequality (6) has no solutions. As can be seen in Fig. 2, if n increases, the number of possible solutions for k also increases.

For this example, for $n = 7$, the range of possible solutions of k is at intervals $[0, 1]$ and $[6; 7]$. The end of the first interval and the beginning of the third interval are symmetrically located with a centre of symmetry at point $n/2 = 3.5$. Thus, solutions for inequalities (3) and (6) were obtained. The next step is to find a general solution for both inequalities (3) and (6) since such a general solution would correspond to the parameters of a quasi-constant weight code which satisfy all requirements. Such a solution is the intersection of two intervals obtained from the inequalities (3) and (6). Figure 3 a) shows the intersection of these intervals if $\beta < \alpha$.

The result of this intersection is two intervals $\left(\left[\dfrac{n}{2} - \alpha; \dfrac{n}{2} - \beta \right] \text{ and } \left[\dfrac{n}{2} + \beta; \dfrac{n}{2} + \alpha \right] \right)$ of k values.

At these intervals, it is necessary to choose the optimal k. Since the choice of k is made with fixed n, it will not affect the speed of the system. This is why the criterion of choice should be something else; for example, it could be additional noise immunity. Despite the fact that all values of k satisfy inequality (6), and thus the requirements for noise immunity, additional noise immunity is not superfluous, considering that other parameters do not suffer at the same time. This is why at these intervals, you can choose the best k for the noise immunity parameters. According to Fig. 2, the further k is from $n/2$, the higher the noise immunity is.

Since $\beta < \alpha$, the most distant from $n/2$ are the points $\dfrac{n}{2} - \alpha$ and $\dfrac{n}{2} + \alpha$.

If $\beta > \alpha$, there is no intersection between intervals, and the general solution for inequalities (3) and (6) is an empty set (Fig. 3b). If $\beta = \alpha$, then the solution is only two points $\dfrac{n}{2} - \alpha = \dfrac{n}{2} - \beta$ and $\dfrac{n}{2} + \alpha = \dfrac{n}{2} + \beta$.
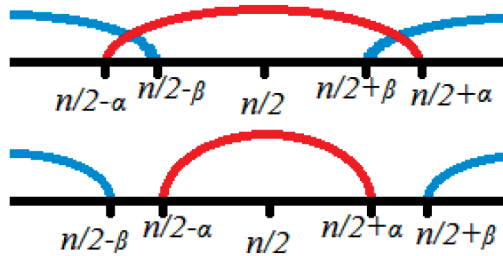
Fig. 3. Variants of general solution for inequalities (3) and (6)

By using the obtained results, it is possible to receive a general algorithm for selecting parameters n and k of the quasi-constant weight code at each time interval with a constant requirement for noise immunity determined by the permissible fraction of the detected error P and a given number of control commands K in order to obtain the maximum speed.

1. Set $n = 2$.
2. Set $k = n/2$ if n is even. If n is not even than set k to the closest integer value, which is less than $n/2$.
3. Check whether the inequality (3) holds with such parameters n and k. If inequality (3) doesn't hold, increase n by one and go to p. 2. If inequality (3) holds, go to p. 4.
4. Decrease k by one and check whether the inequality (3) holds with such parameters n and k. If inequality (3) doesn't hold, increase k by one and go to p. 5. If inequality (3) still holds, go to p. 4
5. Check whether the inequality (6) holds with such parameters n and k. If inequality (3) doesn't hold, increase n by one and go to p. 2. If inequality (3) still holds, go to p. 6.
6. Select current parameters n and k as parameters of quasi-constant weight code for transmission.
7. The end of the algorithm.

At the end of the obtained algorithm, the quasi-constant weight code with the minimum number of digits n of a combination is received, for which inequalities (3) and (6) are satisfied. This algorithm allows obtaining the maximum speed for a given number of control commands and noise immunity requirements for each time interval. Since this algorithm must be performed at each time interval with an unchanged noise immunity requirement, the number of bits change, adapting to the changing requirements of noise immunity while striving to maintain the maximum speed.

3. Conclusion

Thus, the proposed method allows a given set of control commands to select quasi-constant weight code parameters that provide the maximum speed at the required level of noise immunity. Such quasi-constant weight codes can be used for the control command transmission in systems of automatics [2].

References

[1] Berezyuk N.T., *Information encoding*, Kharkiv 1978.

[2] Tutevich V.N., *Telemechanics*, Moscow 1985.

[3] Tsymbal V.P., *Teriya information and coding*, 1992, 263.

[4] Peter Fenwick, *A Note on Variable-Length Codes with Constant Hamming Weights*, Journal of universal computer science, Vol. 21, issue 9, 2015.

[5] Kulik I.A., Skordina Ye.M., Posny S.N., *Error-detecting Ability of Quasi-Equilibrium Code of Sumy*, Bulletin of Sumy State University Series Technical Sciences, No. 1, 2012, pp. 100–111.

[6] Borisenko A.A., Berezhnaya O.V., Kulik I.A., *Estimation of the noise immunity of the data transmission system on the basis of equilibrium codes*, Sumy: Visnyk of Sumy State University, No. 1(12), 1999, pp. 79–82.

Wojciech Mazur
Waldemar Zając-Domański
pezajac@cyf.kr.edu.pl
Faculty od Electronical Engineering, Cracow University of Technology

High-frequency cascade converter for a dual-system locomotive

Konwerter kaskadowy wysokiej częstotliwości dla lokomotywy dwusystemowej

Abstract

This article presents the concept for using an LLC resonant converter equipped with a medium-frequency transformer to upgrade the existing EU 07 locomotive into a dual-system vehicle. The work was created which sets out the specification for such an upgrade, but the design was eventually rejected by the investor and it became the subject of a diploma thesis.

Keywords: LLC resonant converter, equipped with medium frequency, modernizing transformer

Streszczenie

W artykule przedstawiono koncepcję wykorzystania konwertera rezonansowego LLC wyposażonego w częstotliwość średnią transformatora modernizującego istniejącej lokomotywy EU 07 do pojazdu dwusystemowego. Praca określa specyfikację takiego ulepszenia, ale projekt został ostatecznie odrzucony przez inwestora i stał się przedmiotem pracy dyplomowej.

Słowa kluczowe: konwerter rezonansowy LLC, wyposażony w częstotliwość średnią, transformator modernizujący

1. Introduction

The development of semiconductor components, such as in particular isolated gate bipolar transistors, also known as IGBT, having the capacity to operate at voltages of up to 6.5 kV and frequencies in the range of 1 to 10 kHz, has enabled medium-frequency transformers (MFT) to be used in the main circuits of electrically powered locomotives supplied by 15 kV AC systems. One of the major downsides of overhead traction power supply was the need for a heavy transformer, due to the frequency of 16.7 Hz.

The design of a traction converter built with the aid of a medium-frequency transformer (MFT) has been attracting a growing interest thanks to the competitive edge that it offers, compared with systems equipped with heavy and relatively inefficient transformers operating at the power grid frequency. The proposed converter, thanks to its multiplied frequency, is characterized by a reduced size and weight as well as improved efficiency [1, 2].

A medium-frequency transformer is an integral part of an LLC resonant converter. It is designed in such a way that the leakage and magnetizing inductance of the winding are involved in resonance action, which is the reason for the double "L" in the name. The idea of the converter under discussion is based on modularity. Each module has an identical topology, allowing every vehicle to be equipped, for example, with an additional module which would normally be out of service but could be nevertheless switched on in the case of the other's failure or maintenance [4]. The modules on the alternating voltage side, where the fast switch and input choke are found, are connected in series and their number depends on the supply voltage of a given system and the blocking capability of semi-conductor components, such as IGBT transistors, as mentioned earlier on. On the rectified voltage side, the modules are connected in parallel [2].
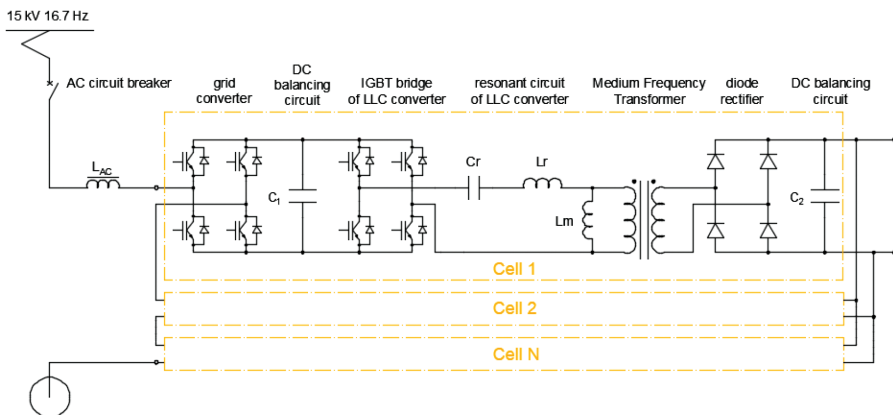
Fig. 1. Converter topology

In each cell presented in the Fig. 1, it is possible to distinguish:
- ▶ a four-quadrant grid converter, whose input terminals are connected in series with the terminals of a converter in the subsequent module,

- ▶ a DC balancing circuit,
- ▶ an LLC resonant converter, which operates in such a way as to prevent energy from returning to the traction grid, consisting of: an IGBT transistor bridge, a capacitor selected for the assumed resonant frequency, a MFT whose leakage inductance forms a resonant circuit in conjunction with the capacitor as well as a diode rectifier whose output terminals are connected to a DC balancing circuit common for all the cells.

2. Multi-level grid converter

A multi-level cascade converter is one of the most frequently used topologies in medium-voltage drives. It is composed of multiply connected single-phase bridges (Fig. 2) which are connected in series on one side to provide the required voltage level and reduce higher harmonics [3].

Fig. 2. The example of a seven-level grid converter with a design based on H-bridges

It is possible to generally classify methods of multi-level converter modulation into two categories: phase-shifted and level-shifted modulation. Both of them are applied in cascade converters [3].
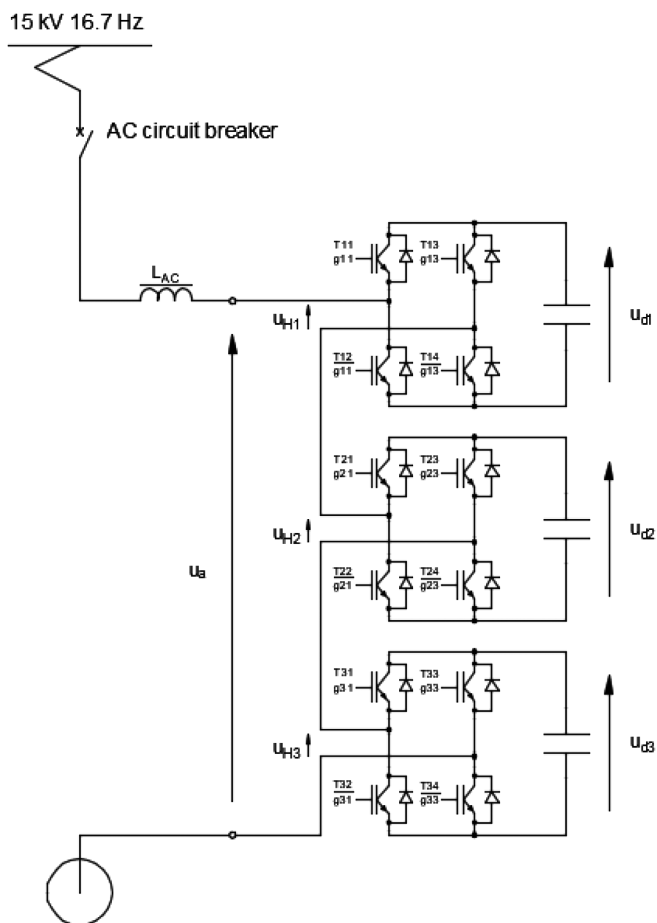
A multi-level converter with m voltage levels requires (m-1) triangle waveforms to generate gating signals. In phase-shifted carrier signal modulation, all triangle waveforms have the same frequency and amplitude, while the shift between the adjacent waveforms can be calculated as follows:

$$\theta = 360°/(m-1) \tag{1}$$

The modulating signal for a single phase is a sinusoid, while gating signals are triggered by a comparison of the modulating waveform u_s with triangle carrier waveforms u_{cr11} to u_{cr33}.

Fig. 3 presents the principle of phase-shifted carrier signal modulation for a seven-level cascade converter, whereby each of the 6 triangle waveforms is shifted by 60 degrees relative to the adjacent waveform. The frequency ratio of carrier wave to modulating wave is $m_f = f_{cr}/f_s = 3$, and the depth of modulation can be expressed as the amplitude ratio of modulating wave to carrier wave, i.e. $m_a = U_s/U_{cr} = 0.9$. The waveforms u_{cr11}, u_{cr21}, u_{cr31} (marked with solid lines) are used to generate gating signals for the upper valves of the left branch of each constituent bridge – T_{11}, T_{21}, T_{31}. The other waveforms: u_{cr13}, u_{cr23}, u_{cr33} (marked with intermittent lines), which are shifted each by 180 degrees relative to u_{cr11}, u_{cr21}, u_{cr31} serve to generate gating signals for the upper valves of the right branch of each constituent bridge – T_{13}, T_{23}, T_{33}. Not all signals for the lower bridges of the valves have been presented, because they operate in reverse to their corresponding upper valves. For example, the gating signal g_{31} for valve T_{31} is formed through a comparison of signal u_{cr31} against modulating signal u_s, whereas the gating signal g_{32} for valve T_{32} in the same branch is formed by negating signal g_{31}.

The instantaneous value of phase voltage may be expressed as the sum of instantaneous voltages for each separate bridge:

$$u_a(t) = u_{H1}(t) + u_{H2}(t) + u_{H3}(t) \tag{2}$$

where:

u_{H1}, u_{H2} and u_{H3} – the partial bridge voltages.

With the application of unipolar modulation, the voltage of each bridge may assume one of three values: $+U_d$, $-U_d$ or 0. A combination of three three–level bridges will produce a seven–level system, while the entire system's phase voltage will reach the following values: $+3U_d$, $+2U_d$, $+U_d$, 0, $-U_d$, $-2U_d$, $-3U_d$, as indicated in the figure below for the last waveform. As valves in different bridges are not operated simultaneously, the rise of phase voltage over time is only U_d, resulting in a considerable decrease in the rate of voltage rise dv/dt and reduction of electromagnetic interferences. Additionally, the combined switching frequency of the converter is related to the switching frequency of a single valve in a manner illustrated below:

$$f_{conv} = (m-1) * f_{val} \tag{3}$$

where:

f_{conv} –   converter switching frequency,

f_{val} –   valve switching frequency,

m –   number of levels.

This desirable feature means an increase in the converter's switching frequency accompanied by a relatively low switching frequency of individual valves and a shift of harmonics towards higher orders. Another benefit is the reduced switching losses related to a comparably low switching frequency of the valves [3].
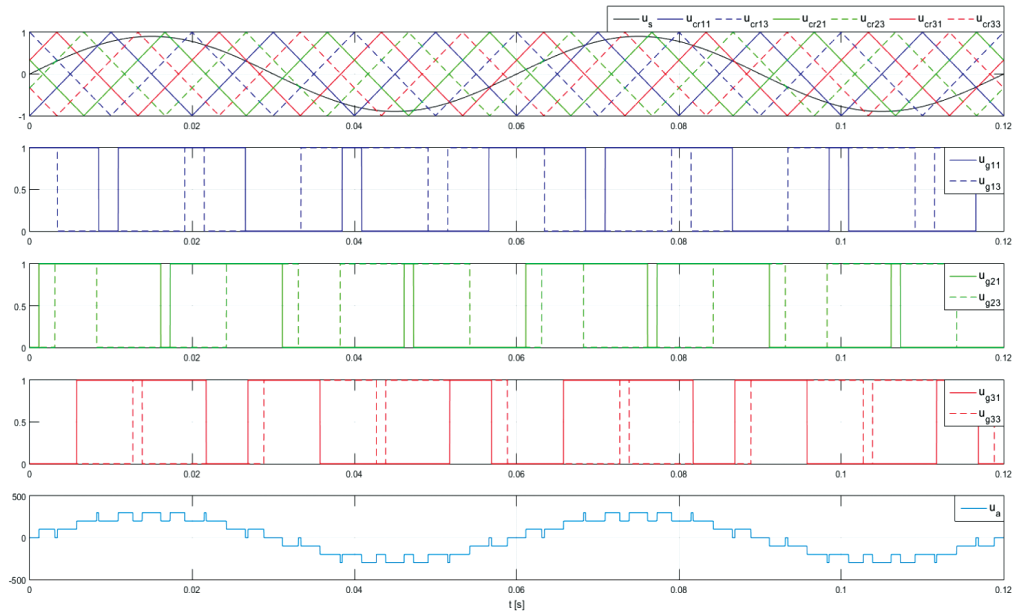
Fig. 3. Phase-shifted carrier signal modulation of a seven-level converter

In the top figure: black – modulating signal, lines marked in: blue, green and red – triangle waveforms for the upper valves of the left (solid lines) and right (intermittent lines) branches of each bridge. In the following three figures: control signals for the upper valves of the left (solid lines) and right (intermittent lines) branches of each bridge. The lower waveform: light blue – voltage generated at the converter input.

3. LLC resonant converter

The LLC converter finds numerous applications due to its benefits such as a wide range of loads, reduced switching losses thanks to zero-voltage switching and a low primary side valve shut-off current as well as secondary-side rectifier diode zero-current switching [4]. These soft-switching parameters could be obtained thanks to the transformer being in place and

having integrated such features of the resonant circuit as leakage and magnetizing inductance. Also, the transformer ensures that the voltage levels at the DC balancing circuit are galvanically separated and adjusted accordingly by selecting the appropriate gear ratio.

Fig. 4. LLC resonant converter topology

The Fig. 4 presents a typical topology of a full-bridge LLC resonant converter. The configuration features three basic parts:
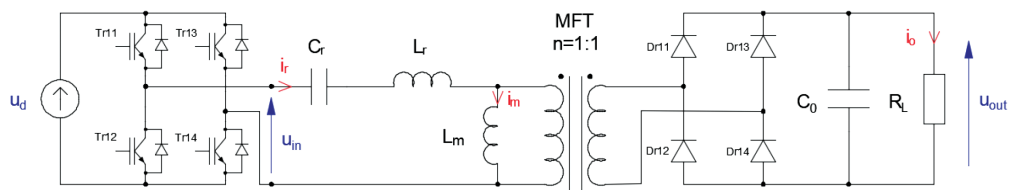
a) semi-conductor valves made from IGBT transistors which are triggered to generate a rectangular voltage waveform. The bridge produces a bipolar rectangular voltage wave by alternately operating valve pairs: Tr11, Tr14 and Tr12, Tr13 at a fill rate of 50%. The dead cycle time between switches is necessary to prevent short-circuits and to enable the system to perform zero-voltage switching (ZVS);

b) the resonant circuit is characterized by resonance capacity C_r and two inductances – serial (leakage) L_r and magnetizing L_m. The gear is designated as n. The current flowing through the circuit supplies energy to the load by means of the transformer providing galvanic separation and adapting with the aid of the gear the output voltage to the required value;

c) on the converter secondary side, the diode bridge converts alternating to direct voltage, thereby powering the load. The output capacitor smooths out the rectified voltage.

Unlike pulse converters, a resonant converter adjusts voltage not by transmission of pulse energy, for example, from the voltage circuit to the current circuit, but by changing the resonant circuit's impedance in conjunction with changes in the operating frequency. This has the effect of changing the amplification factor of the transition function and thereby also the direct output voltage value. The existing designs of resonant converters using parallel or serial resonance were burdened with a number of limitations related mainly to the need for operating above or below resonant frequency, a very high rise of frequency in the case of zero-load operation, as well as high overvoltage and overcurrent occurring in the semi-conductor valves at resonant frequencies. The LLC converter is practically free from these shortcomings.

For an LLC converter, it is possible to determine a standardized direct voltage amplification characteristic (nU_{out} / U_{in}) for relative frequency (f_s / f_0) with a variable parameter of Q_e, also known as the resonant system's quality factor representing the converter's load condition.

The quality factor Q of a resonant circuit relates to vibrating systems and is in proportion to the ratio of energy W_m stored in a resonating system to energy W_t lost in a single vibration period, as in the following formula:

$$Q = \frac{2\pi \cdot W_m}{W_t} \quad (4)$$

In an electric resonant circuit, the quality factor gives an idea of its selectivity, or in other words, its ability to filter out waves with frequencies differing from the resonant frequency, as well as indicating the fade rate of free vibrations.

a) A resonant system's quality factor Q_e representing the converter's load:

$$Q_e = \frac{\sqrt{L_r / C_r}}{R_{L\_eqv}} \quad (5)$$

b) basic resonant frequency f_0:

$$f_0 = \frac{1}{2 \cdot \pi \cdot \sqrt{L_r \cdot C_r}} \quad (6)$$

c) second resonant frequency f_p:

$$f_p = \frac{1}{2 \cdot \pi \cdot \sqrt{(L_r + L_m) \cdot C_r}} = \frac{f_0}{\sqrt{1 + \dfrac{L_m}{L_r}}} \quad (7)$$

d) converter amplification is a relationship between output and input voltage. Fig. 5 depicts that amplification M_g can be expressed with electrical parameters of equivalent circuit of LLC converter:
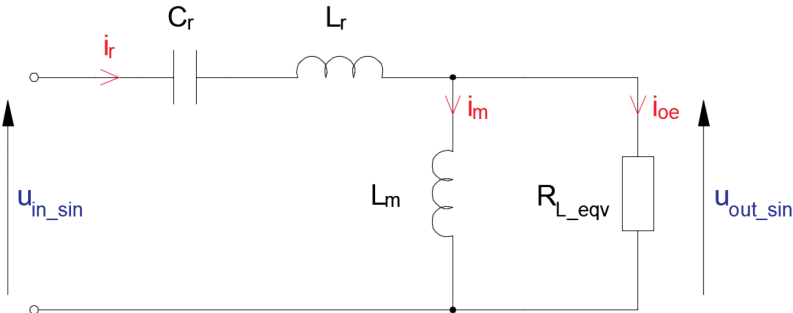
Fig. 5. Equivalent circuit of LLC converter

$$M_g = \frac{U_{out\_sin}}{U_{in\_sin}} = \left| \frac{jX_{Lm} \| R_{L\_eqv}}{(jX_{Lm} \| R_{L\_eqv} + j(X_{Lr} - X_{Cr}))} \right| = \left| \frac{(j\omega L_m) \| R_{L+eqv}}{(j\omega L_m) \| R_{L+eqv} + j\omega L_r + \dfrac{1}{j\omega C_r}} \right| \quad (6)$$

Equations 8.1 and 8.2 are valid only for sinusoidal waveform.
After transformations and entering variables, f_n, l_n, Q_e:

$$f_p = \frac{1}{2\cdot\pi\cdot\sqrt{(L_r + L_m)\cdot C_r}} = \frac{f_0}{\sqrt{1 + \dfrac{L_m}{L_r}}} \qquad (7)$$

where:

L_r — resonant inductance,

C_r — resonant capacitance,

L_m — magnet inductance,

$R_{(L-eqv)}$ — load resistance converted into the primary side, relative frequency,

$\dfrac{f_n = f_{sw}}{f_0}$ — switching frequency,

$L_n = L_m / L_r$ — relative inductance.
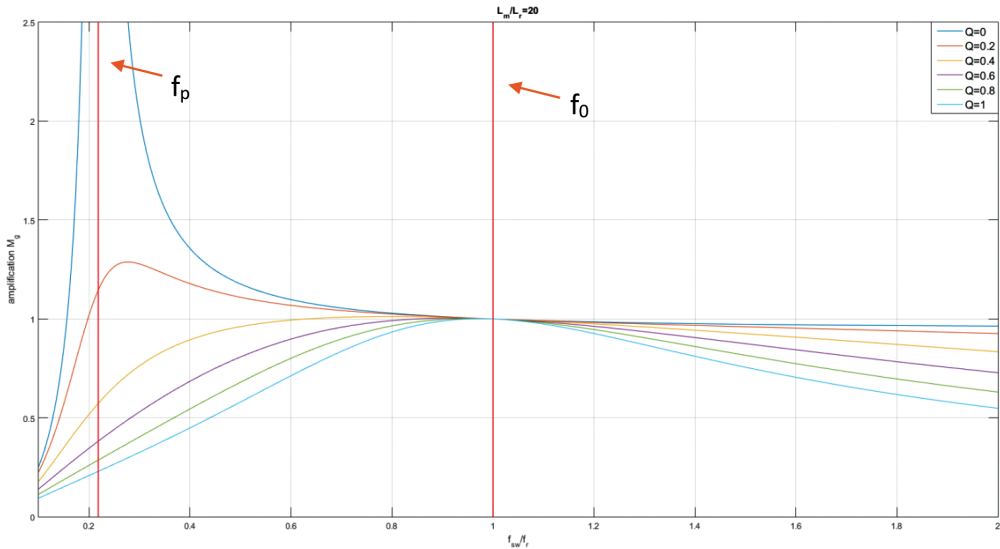
Fig. 6. Frequency amplification of the converter. $Q = 0$ to $Q = 1$ – quality factor of the resonant system, standing for converter load

The above characteristics shows a relationship between converter amplification and relative frequency for a range of loads, starting from idle represented by $Q = 0$, through increasingly greater loads represented by the rising value of Q, with magnetizing inductance 20 times greater than leakage inductance.

Bringing the inductance ratio down to 4, for example, means that for a wide range of loads (from $0.2 < Q_e < 1$), the operating (amplification) point is likely to change considerably in step with changes in frequency around resonant frequency. In this case, however, the converter supply voltage is balanced by a grid converter and so there is no need for amplification, leading to flattened amplification characteristics, as indicated in the figure below. Additionally, a high magnetizing inductance lowers the valve switch-off current.

Among the converter's most essential features is the fact that the generalized amplification value remains equal to 1 for a basic resonant frequency irrespective of the load applied. This means that a correctly designed unit will keep the LLC converter free from frequency fluctuations even where considerable variation of load is the case.

An LLC converter may operate in a (ZVS) area, in which transistors are switched on wherever the voltage at the transistor is zero, which eliminates power losses at switching. Also, a switch-off can be effected with a relatively low current, with the transistors capable of suppressing overvoltages unaided and helping to considerably reduce power losses occurring at transistor switch-off. Because of the resonating circuit current having sinusoid waveform, the current flowing through the diodes has a semi-sinusoid waveform, which means that for operation at resonant and sub-resonant frequencies, diode commutation takes place at zero-current. As a result, in this type of converter, power losses related to switching component commutation are kept to minimum across the effective operating range [4, 5].

4. Simulation

The simulation was carried out in a Matlab & Simulink environment. The main circuit and controls were built using a basic library and SimPower Systems library. The selected method (ode23s) of solving rigid differential equations was based on a modified Rosenbrok formula, in which the maximum step length was set at 10^{-6} s. Due to the complexity of the circuit, the multi-level input converter was simulated separately from the resonant converters. The system is not automatically adjustable; the parameters defining the power flow through the input converter were calculated beforehand for a specific operating point. This is part of the reason why a simplification was used by adding filters of the 2. harmonic at the output of each constituent bridge.

The simulation was carried out at both maximum and minimum supply voltage, the operation of the input converter was simulated at full load, while a single LLC converter was simulated at full power (corresponding to 1/8 of the total power) and at 10% of its rated power.

For both cases, the inverter operates correctly. The output voltage of each constituent bridge (violet) is 3300 V, the current flowing through the power line is in phase with voltage and its near-sinusoid wave points to a low THD. The green waveforms show voltage generated at the input terminals of the converter.

Output voltage (yellow) is 3 kV regardless of the voltage. Soft-switching conditions have been met, because the gating signal (green) is applied to the transistor when its voltage between collector and emitter (black) is equal to 0. The magnetizing current has a triangle waveform in both cases and turns off valves at approximately 40 A.

Fig. 9 presents a concept for the main circuit of the upgraded locomotive. The pulse controllers used in this application as traction converters and serial motors may be replaced with asynchronous inverters and motors. In a DC application, capacitor C_f forms together with choke L_f an input filter, while in an AC application, the same capacitor forms a common

balancing circuit for each constituent diode bridge. The number of serially connected modules on the input side is 8 and depends on the blocking capability of IGBT transistors. The systems are switched by the aid of specially designed contactors. No provisions have been made for a return flow of energy to the alternating current grid.

Table 1. Simulation parameters

Output voltage	13,500–18,000 V 16 2/3 Hz
AC choke inductance and resistance	15 mH 0.1 Ω
Switching frequency for a single bridge of the input converter	1 kHz
Capacity of a capacitor of a single bridge	1.5 mF
Initial charge of a capacitor of a single bridge	3300 V
Resonant frequency of 2. harmonic filter	33 Hz
MFT primary side resistance	0.04 Ω
Leakage inductance on MFT primary side	87.5 μH
Resonance capacity	16.08 μF
MFT gear	1.1 : 1
MFT magnetizing inductance	7.639 mH
MFT secondary side resistance	0.033 Ω
MFT secondary side leakage inductance	72.3 μH
Resonant frequency	3 kHz
LLC converter switching frequency	2.7 kHz
LLC converter's output capacitor capacity	0.924 mF

Table 2. MFT transformer parameters

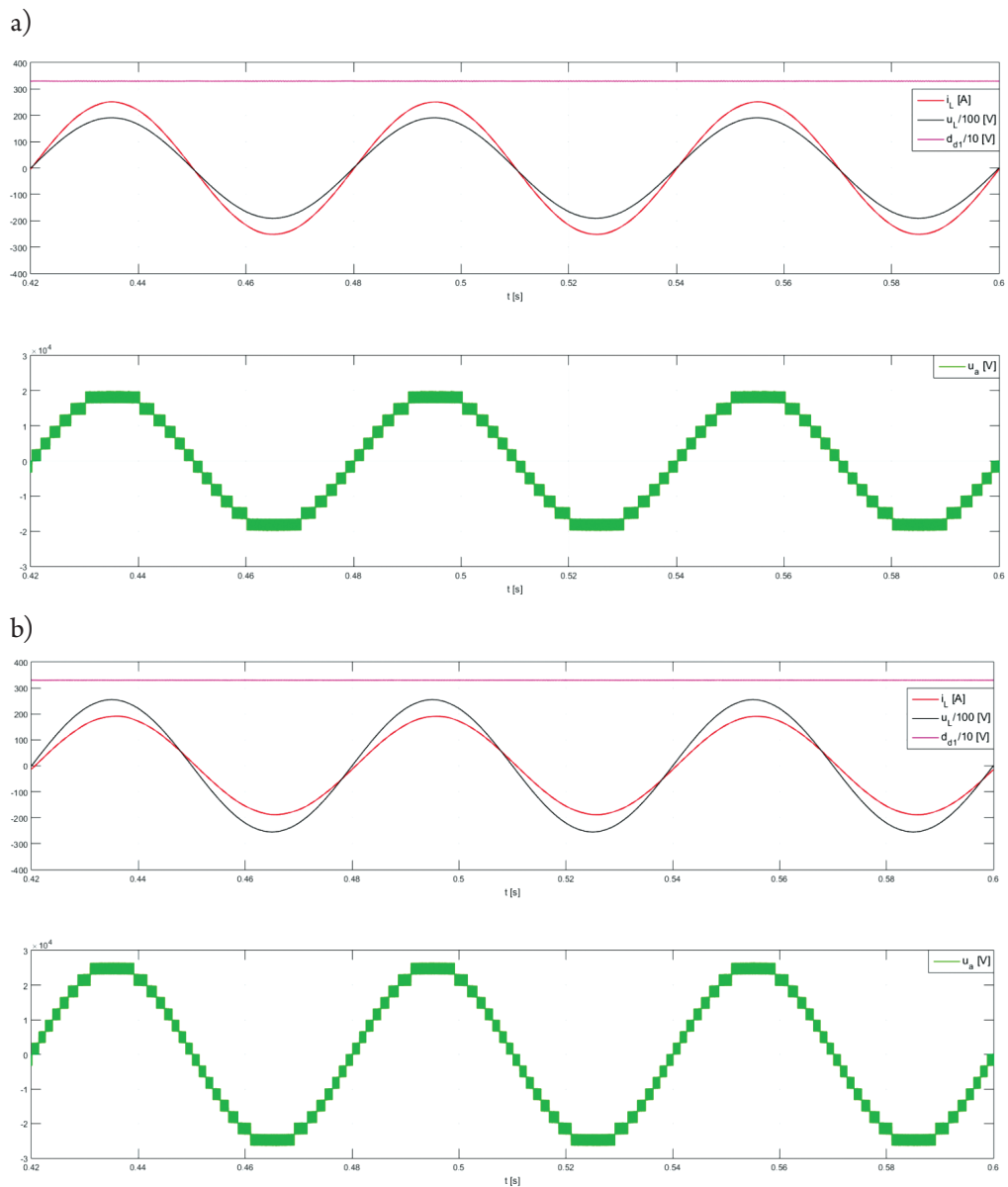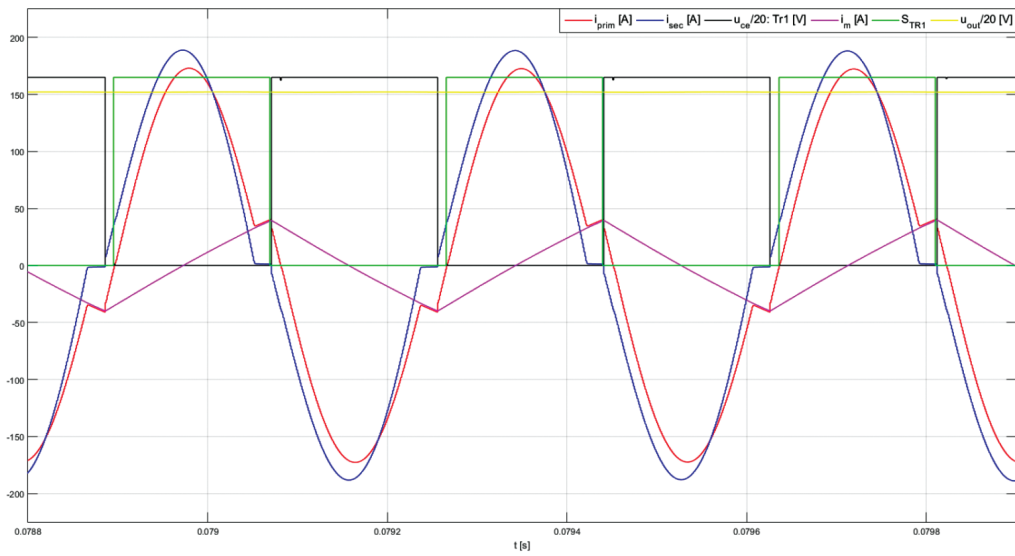| Rated power	300 kVA
Rated voltage	2971 V
Gear ratio	1.1 : 1
Power loss in the winding	800 W
Short-circuit voltage – absolute	0.1

a)

b)

Fig. 7. Multi-level inverter waveforms for: a) supply voltage of 13.5 kV; b) supply voltage of 18 kV
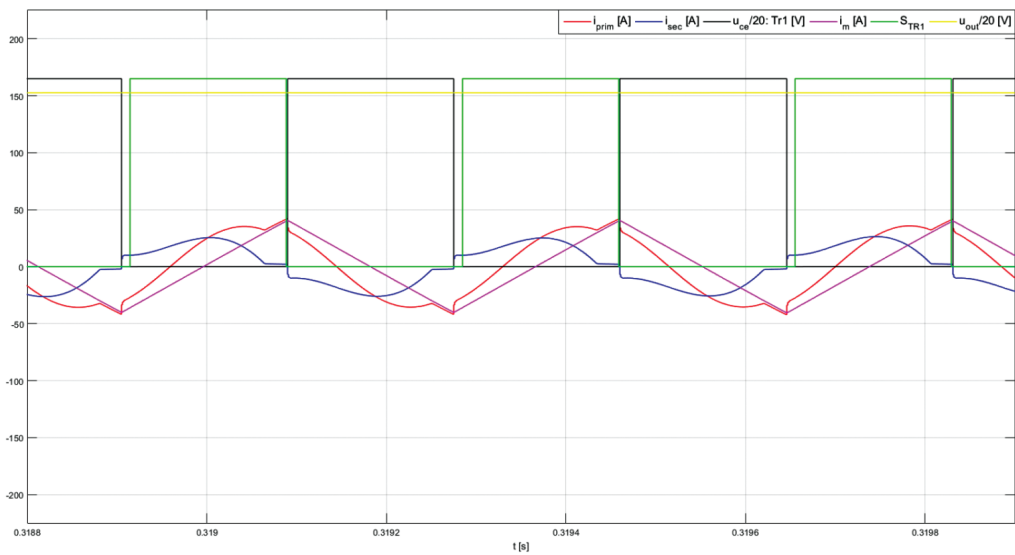
a)

b)

Fig. 8. Waveforms of a single LLC converter for: a) full load 300 kW; b) 10% of rated load – 30 kW
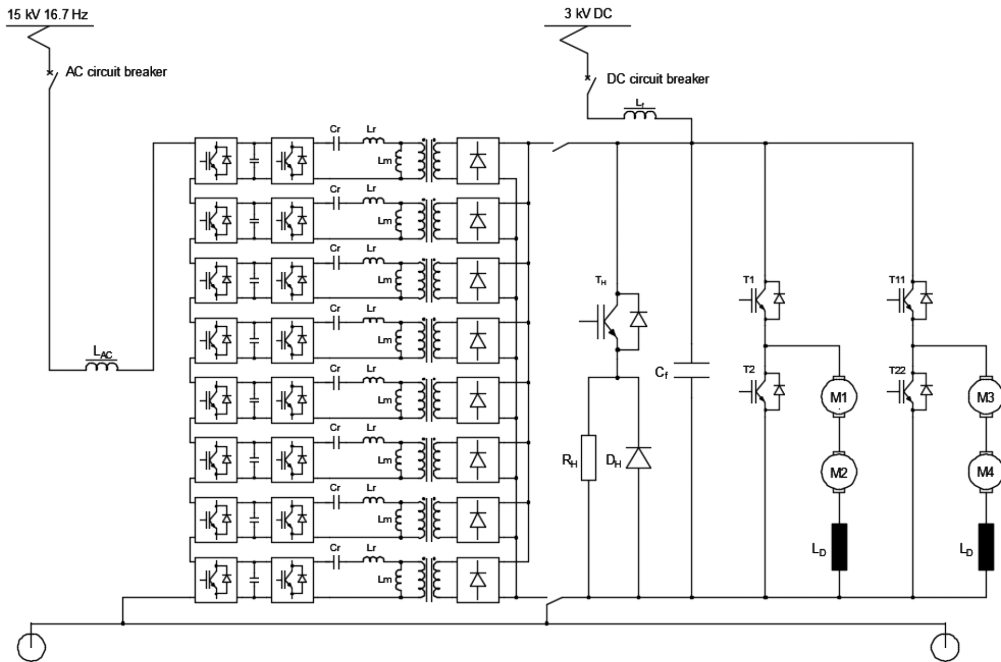
Fig. 9. The concept for the main circuit of the upgraded locomotive

5. Summary

This article presents the concept for upgrading the main circuit of EU 07 locomotive into a dual-system vehicle. The aim adopted herein was to develop a concept that would eliminate the need for using a traction transformer operating at grid frequency. A cascade converter system has been proposed, with medium-frequency transformers.

The simulations have shown that a multi-level input converter may be successfully built using IGBT transistors with a lower voltage rating, whereas the application of phase-shifted carrier signal modulation distributes the voltage evenly across each of the H-bridges, while also shifting the harmonics in the power grid towards higher orders as well as reducing electromagnetic interferences as a result of a decrease in the rate of voltage rise dv/dt. As a result, the input current is deformed to a small extent only. The system operates with a power coefficient approximating 1. The selected type of resonant converter enables reliable operation across a wide range of loads and good performance of valve commutation thanks to zero-load switching and low currents.

The benefits also include modularity and thereby extendibility to include additional modules in case of failure or the need for servicing or replacements. The disadvantages, on the other hand, include a large number of fully controllable components, complexity of the control system and a high price.

References

[1] Mazur W., *Modernizacja (części elektrycznej) lokomotywy EU 07 na dwusystemową przy założeniu minimum zmian*, Praca magisterska, Kraków 2017.

[2] Zhao C., Dujic D., Mester A., Steinke J. K., Weiss M., Lewdeni-Schmid S., Chaudhuri T., Stefanutti P., *Power Electronic Traction Transformer – Medium Voltage Prototype*, IEEE Transactions on Industrial Electronics, Vol. 61, No. 7, July 2014.

[3] Bin Wu, *High Power Converters*, IEEE Press, John Wiley and Sons, Inc., Hoboken, New Jersey, 2006.

[4] Hong Huang, *Designing an LLC Resonant Half – Bridge Power Converter*, 2010 Texas Instruments Power Supply Design Seminar, SEM1900, Topic 3, Texas Instruments Incorporated, 2010, 2011.

[5] Yang B., Ren Y., Lee F. C., *Integrated magnetic for LLC resonant converter*, IEEE APEC Proceedings, 2002.

[6] Skarpetowski G., Tułecki A., Zając W., *Studium wykonalności dla projektu modernizacji lokomotywy elektrycznej serii EU07 przeznaczonej do międzynarodowych przewozów towarowych*, Listopad 2015.

[7] Skarpetowski G., Zając W., *Oddziaływanie przekształtnikowych napędów trakcyjnych na infrastrukturę kolejową*, Politechnika Krakowska, Kraków 2012.

Bartosz Rozegnał
Zbigniew Szular
Witold Mazgaj
pemazgaj@cyfronet.pl
Institute of Electromechanical Energy Conversion, Faculty of Electrical and Computer
Engineering, Cracow University of Technology

Modifications of the soft switching system resistant to
disturbances in control systems of voltage sources inverters

Modyfikacje układu łagodnego przełączania odpornego
na zakłócenia w układach sterowania trójfazowych
falowników napięcia

Abstract

Reduction of the switching losses in three-phase voltage source inverters can be achieved by using of soft switching systems that not only increase the efficiency of the inverters, but they also reduce the size of the semiconductor cooling circuits, that is especially important in traction vehicles. The majority of existing soft switching systems have some drawbacks that could be danger for inverter operation in the case of disturbances in control systems. The paper briefly describes the structure, operation principles and results of laboratory tests of the proposed soft switching system. Particular attention has been paid to the specific features of alternative versions of the proposed soft switching system, that allow to improve operating parameters of the basic system.

Keywords: soft switching, switching losses, voltage source inverters, ZCZVS converters

Streszczenie

Zmniejszenie strat przełączania w trójfazowych falownikach napięcia można uzyskać, stosując układy łagodnego przełączania, które nie tylko wpływają na zwiększenie sprawności falownika, ale również pozwalają ograniczyć gabaryty układów chłodzących elementy półprzewodnikowe, co w napędach trakcyjnych ma istotne znaczenie. Zdecydowana większość istniejących układów łagodnego przełączania ma pewne mankamenty mogące zagrozić bezawaryjnej pracy falowników w przypadku wystąpienia zakłóceń w układzie sterowania. W artykule skrótowo opisano strukturę, zasady działania oraz wyniki badań laboratoryjnych proponowanego układu łagodnego przełączania tranzystorów. Szczególną uwagę zwrócono na alternatywne wersje proponowanego układu, które pozwalają polepszyć parametry eksploatacyjne układu podstawowego.

Słowa kluczowe: falownik napięcia, łagodne przełączanie, straty przełączania, przekształtniki ZCZVS

1. Introduction

A squirrel-cage induction motor is the most common solution to convert electrical energy into kinetic energy. This type of motors has gained great popularity in traction vehicles because of high reliability and lower price compared to other solutions. Traction vehicles in Poland are supplied by the DC network. Therefore, in order to use a three-phase induction motor it is necessary to transform the direct voltage into the alternating voltage with the adjustable frequency and RMS value, and the voltage source inverter (VSI) seems to be an indispensable device. Modern constructions of the traction vehicles impose large size limitation on drive systems which refer also to the inverters. It is necessary to ensure the proper operating temperature of semiconductor elements, and the cooling system applied in inverter largely determines dimensions of this device.

Due to the extreme operating conditions of the inverter, caused by various loads and different weather conditions (especially high temperatures during the summer months), cooling systems of the inverters have important meaning. Therefore, it is advisable to make attempts which can allow us to reduce energy dissipation during the inverter operation. This aim can be achieved by power loss reduction in the inverter transistors, especially when the voltage source inverter operates with the pulse width modulation method. Power losses in transistors are a sum of the conduction losses and the switching losses. The first type of these losses depends on the transistor current and on the collector-emitter voltage during the conduction state of the given transistor; user of inverters do not have influence on the conduction losses. On the other hand, the switching losses depend on changes of the transistor current and voltage during both the turn-on and turn-off processes and these losses can be reduced by using VSIs which operate with the so-called soft switching systems [1–6]. Figure 1 shows an example of waveforms of the transistor current, voltage, and power losses of the Insulated Gate Bipolar Transistor (IGBT) type IRG4PH50KD (1200 V, 24 A) during the hard switching processes in the three-phase laboratory voltage source inverter. The transistor
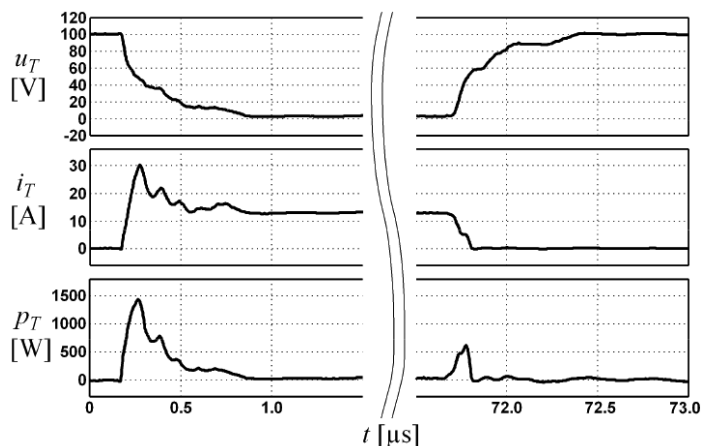

Fig. 1. Waveforms of the transistor current, voltage, and power losses during both the turn-on and turn-off processes in the three-phase voltage source inverter

current after the turn-on process was equal to 12 A, and the voltage at the end of the turn-off process reached a value of 100 V; the turn-on and the turn-off times of this transistor were equal to 72 ns and 390 ns, respectively. The transistor switching losses in a single cycle at the frequency of 3 kHz were approximately equal about 1.17 W for the assumed switching conditions. It is well known that the share of the switching losses in total power losses occurring in IGBTs rises with the switching frequency. In many cases, these losses are greater than the conduction losses at the switching frequency of a few kHz. An increase of these losses leads not only to a reduction of the inverter efficiency, but it can cause problems with proper cooling of IGBTs. It is worth underlining that the estimation of the total switching losses in VSIs needs to take into account the losses occurring in freewheeling diodes.

The pursuit of the reduction of the switching losses is to increase the efficiency of power electronic inverters; less switching losses lead to an improvement of cooling systems of IGBTs. The fulfilment of this requirement is often more important than an improvement of the efficiency, especially in inverters of medium and high power ratings. In order to reduce the switching losses, the voltage value or the current value of the switched transistor should be close to zero during the switching processes. A lot of soft switching solutions are described in scientific literature. Generally, these systems can be divided into two groups; the first one includes VSIs with one central auxiliary soft switching circuit [7–12] and the second group refers to the inverters with individual auxiliary soft switching circuit in each phase of the given inverter [13–19]. The majority advantages of the first group are small number of additional elements of the given soft switching circuit, and in result simple structure. However, control methods in these solutions of the transistor soft switching are quite complicated and the switching frequency can change in relatively narrow ranges. In the second group of the soft switching systems, each phase of the inverter has an own soft switching circuit. In this case the soft switching circuits have more complicated structures in comparison to the inverters with central auxiliary circuits, but the VSIs can operate with higher switching frequencies. In some individual solutions, the structure of auxiliary resonant circuits includes special transformers [20–22]. Figure 2 presents, for example, one of the most often soft switching system presented in literature [13, 16].
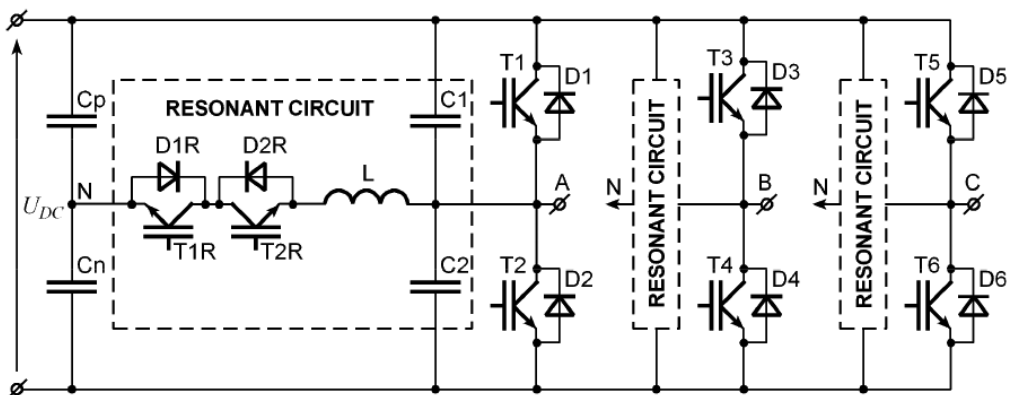

Fig. 2. Three-phase voltage source inverter with individual soft switching in each phase

In the majority of the existing soft switching systems, the auxiliary circuits consist of capacitors connected in parallel to the main transistors [8, 10, 20] and resonant coils which are connected in series to auxiliary transistors [7, 9, 10, 13, 16]. These connections are not recommended because the main or auxiliary transistor can be damaged during disturbances in control systems. For example, when the main transistor is turned on and the voltage of the capacitor connected in parallel to this transistor is higher than zero, then this capacitor discharges abruptly through the given main transistor; in second case when the auxiliary transistor is turned off at a non-zero current of the resonant coil then an overvoltage can appear in the given VSI. Due to these drawbacks the next part of this paper presents the patented solution, wherein the above disadvantages do not occur.

2. Basic soft switching system resistant to control disturbances

The basic soft switching system which is resistant to control disturbances is presented in Fig. 3 [23–25]. In this system do not occur previously mentioned connections which are characteristic properties of the majority soft switching systems existing up till now. The control method of the presented system is easier in comparison to other soft switching methods because the auxiliary transistors in the given VSI are switched with respect to the main transistors, not the other way round.
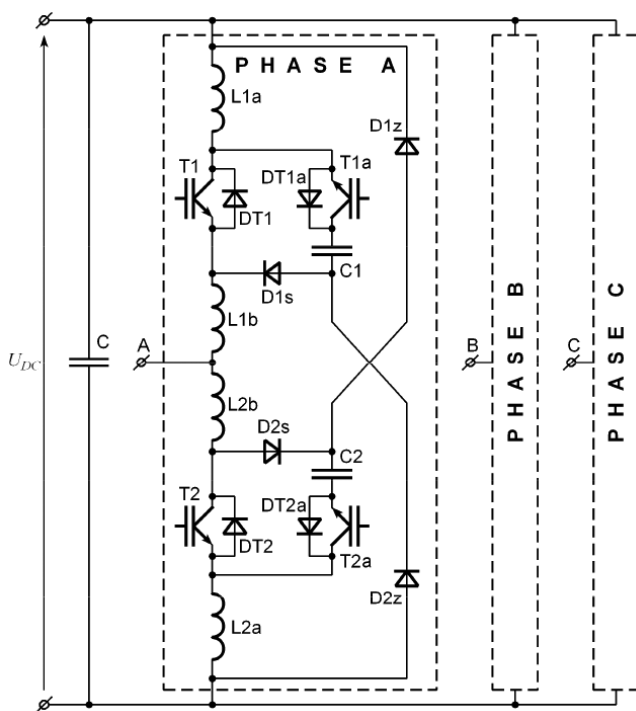

Fig. 3. Three-phase VSI with soft switching system resistant to control disturbances

In the presented solution, to the given main transistor $T1$ following elements are added: one auxiliary transistor $T1a$, two resonant coils $L1a$, $L1b$, one capacitor C1 and two diodes. So, the auxiliary circuit of one phase of the VSI includes six additional elements, what is typical of other VSIs equipped in individual soft switching systems. The key role of the additional coil $L1a$ is certain limitation of the increase of the main transistor current during the turn-on process. In turn, the capacitor C1 is applied to reduce the increase of the main transistor voltage during the turn-off process. Two additional diodes $D1s$ and $D2z$ should keep linearity of the load current when the main transistor is turned off. The coils $L1b$ and $L2b$ protect the VSI against short circuits when accidentally two main transistor in one phase may be turned on. The auxiliary transistors are turned on with a certain delays with respect to the main transistors and they are turned off after the end of the capacitor resonant discharge process, but not later than the corresponding main transistor is turned off. In the proposed solution the capacitors are not connected in parallel to the main transistors and the coils are not connected in series to the auxiliary transistors. These are significant advantages in comparison to the soft switching systems existing up till now. Simplified waveforms of chosen currents and voltages of the proposed soft switching system are shown in Fig. 4. The whole switching process has only six stages, unlike to many other proposals of the soft switching [12]. The operation principles and determination of the parameters of the proposed soft switching system are described in detail in [24, 25].
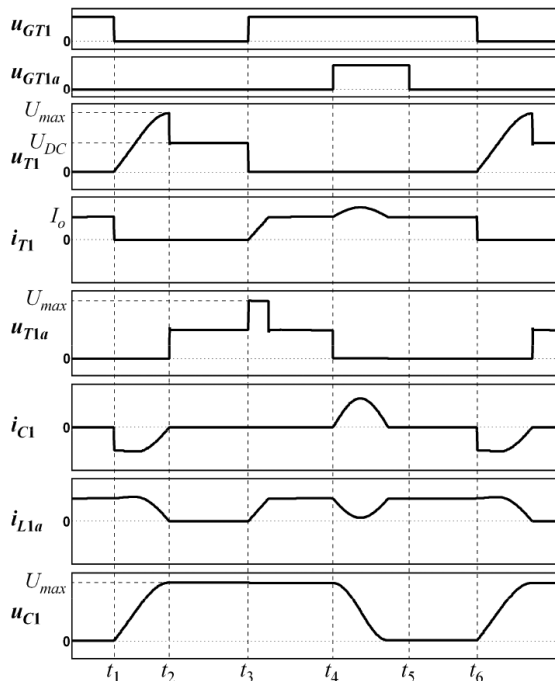
Fig. 4. Simplified waveforms in the proposed soft switching system: u_{GT1}, u_{GT1a} – control signals of the main transistor $T1$, and auxiliary transistor $T1a$, u_{T1}, i_{T1} – voltage and current of the transistor $T1$, u_{T1a} – voltage of the auxiliary transistor $T1a$, i_{C1}, u_{C1} – current and voltage of the capacitor C1, i_{L1a} – current of the coil $L1a$

Validation of the described soft switching system was performed with the use of the voltage source inverter with the power rating of about 3 kW. The value of the DC supply voltage was equal to 100 V and the maximum load current was not higher than 14 A. Figures 5 and 6 show waveforms of laboratory measurements for previously described full switching process.
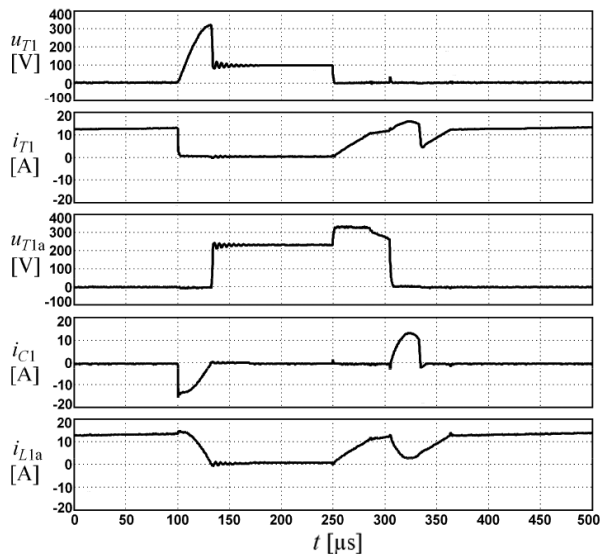
Fig. 5. Waveforms measured in the laboratory voltage source inverter with the proposed soft switching system: u_{T1}, i_{T1} – voltage and current of the transistor $T1$, u_{T1a} – voltage of the auxiliary transistor $T1a$, i_{C1} – current of the capacitor $C1$, i_{L1a} – current of the coil $L1a$, the capacity of the capacitors – 1 µF, inductance of all coils – 300 µH
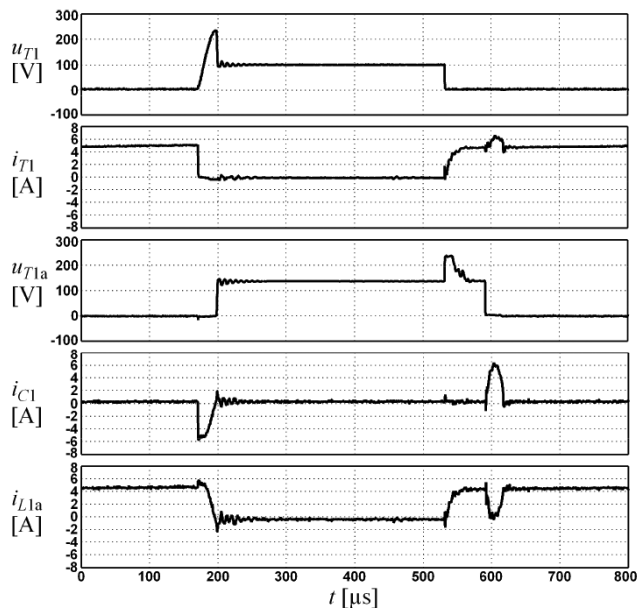
Fig. 6. Analogous waveforms as in Fig. 5 measured for inductance 100 µH of the coils $L1b$, $L2b$

The switching processes of both the main and auxiliary transistors have soft character. It allows us to reduce the switching losses even up to 70–80 per cent with respect to these losses occurring in the VSIs which operate without soft switching systems. The control method is simple because the control algorithm should determine only the value of the time delay between switching signals of the main and the auxiliary transistors.

It is worth underlining that the decrease of the inductance L_{1a}, L_{2a} leads to a certain reduction of the maximum value of the capacitor voltage that is equal to the maximum value of the voltage of the main transistor T1. However, for the correct operation of the proposed soft switching system, this voltage should be at least twice the voltage of the DC supply source.

3. Application of auxiliary thyristors in proposed soft switching system

The auxiliary transistors in the proposed basic soft switching system can be replaced by appropriate selected thyristors (Fig. 7) [26]. This proposal refers first of all to the voltage source inverters with high power rating. Operation principles of the system with thyristors are analogous as in the basic version and the waveforms of currents and voltages are similar to the analogous waveforms in the basic soft switching system. However, the control method is simpler because thyristor (e.g. Ty1) requires only turn-on signal and this thyristor turns off when the resonant discharging of the capacitor C1 ends. So, we do not have to determine the conduction time of the auxiliary transistor as in the basic solution.

Fig. 7. Basic soft switching system with the auxiliary thyristors

The auxiliary transistor as in the basic solution. It is worth underlining that thyristors are more resistant to overvoltages and overloads.

Due to the relatively high switching frequency (several kHz), in this proposal the so-called pulse thyristors should be applied, which have significantly shorter turn-off times with respect to "classical" rectifier thyristors. However, even the pulse thyristors have significantly longer turn-off times in comparison to IGBTs. For example, the turn-off time of the IGBTs applied in the laboratory soft switching system is equal to 0,39 μs, whereas these times of the pulse thyristors with the similar operation parameters have these values in the range from 15 μs to 25 μs, so it should be taken in the control algorithm of the soft switching of the given three-phase VSI with auxiliary thyristors. Figure 8 presents simplified waveforms of the transistor current i_{T1} and the capacitor current i_{C1} in the case when the auxiliary transistors are replaced by the pulse thyristors. The correct operation of the modified soft switching system occurs when the auxiliary thyristor regains forward blocking capacity before the next turn-on process of the main transistor. Therefore, the minimum time interval t_{Ton} between two successive turn-on processes of the main transistor should fulfil the following condition (Fig. 8):

$$t_{Ton} \geq t_{rise} + t_{dis} + t_q \qquad (1)$$

where

t_{rise} – time, when the transistor current reaches the maximum value of the load current,
t_{dis} – time of the resonant discharge of the capacitor,
t_q – turn-off time of thyristor.

The value t_{Ton} can be shorter by the time t_{char} which refers to the charge process of the capacitor after the turn-off process of the main transistor. If the relationship (1) is not fulfilled then the capacitor begins to discharge during the non-conduction state of the main transistor.
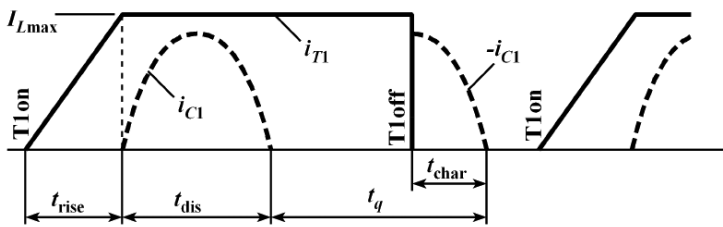

Fig. 8. Simplified waveforms of the transistor current i_{T1} and the capacitor current i_{C1} in the soft switching system with the auxiliary transistor: t_{rise} – time when the transistor current reaches the maximum value of the load current I_{Lmax}, t_{dis} – time of the resonant discharge of the capacitor, t_q – time when the thyristor regains forward blocking capacity, t_{char} – time of the charge of the capacitor

The minimum value of the time t_{Ton}, which describes a required time interval of the conduction state of the main transistor, influences the maximum admissible value of the amplitude modulation ratio m_{amax}:

$$m_{amax} = 1 - 2 f_i t_{min} \qquad (2)$$

where:

f_i – switching frequency.

It is necessary to stress that the values $m_{a\max}$ of the VSI operating with the auxiliary thyristors are smaller in comparison to these values concerning the VSI with the soft switching system based on the auxiliary transistors, and differences between these values depend strongly on the switching frequency. However, it should be noted that the switching times of IGBTs operating at a voltage of several kV are of the order a few μs, so the application of the auxiliary thyristors seems worthy of consideration, especially in VSIs of high power rating.

4. Alternative configuration of the basic soft switching system

In the proposed basic soft switching system, the signals turning on the auxiliary transistors have to be delayed with respect to the turn-on signals of the main transistors and this is a certain inconvenience in the control algorithm. Therefore, by way of further research it has been developed an alternative version of the basic soft switching system [27]. In the alternative proposal, the roles of the all coils differ in comparison to their roles in the basic system and the appropriate coils are coupled magnetically (Fig. 9). Numerical calculations have shown that the application of the magnetic couplings improves the basic system operation and allows us to simplify the control algorithm.
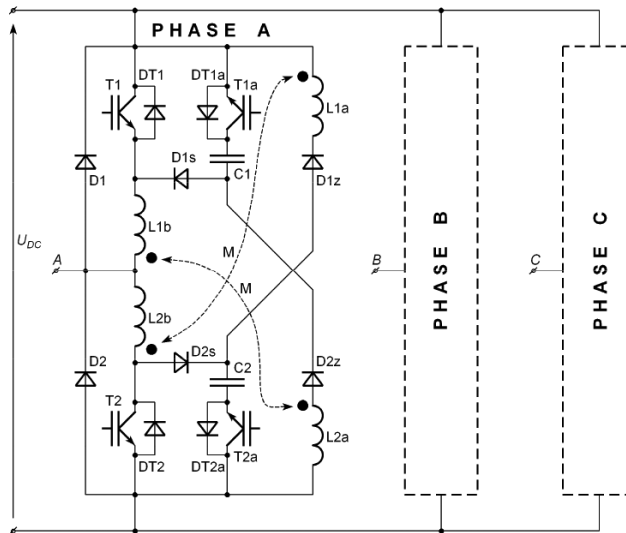

Fig. 9. Alternative configuration with magnetically coupled coils of the basic soft switching system

As previously mentioned, in the basic soft switching system it is necessary to set a certain time-delay between the turn-on signals of the auxiliary transistors with respect to the main transistors. Moreover, it is necessary to determine the conduction time of the auxiliary transistors. So, the control algorithm of the basic system has to generate two additional signals for the auxiliary

transistors. Appropriately chosen negative magnetic couplings between the coils $L1a$, $L2b$ and between $L2a$, $L1b$ allow us to eliminate the two extra signals of the auxiliary transistors. These negative couplings are designed to reduce to zero the currents of the coils $L1b$ and $L2b$ (connected to the load terminal) when the main transistors are turned off. Consequently, the auxiliary transistors can be switched using the same control signals as the main transistors.

The operation of the proposed alternative solution is described with the assumption that the cycle begins when the main transistor $T1$ and the auxiliary transistor $T1a$ are turned off. From this moment the current of the transistor $T1$ drops abruptly to zero whereas the current of the auxiliary transistor $T1a$ is equal to zero; the load current flows through the diode $DT1a$, capacitor $C1$ and coil $L1b$ and the capacitor $C1$ charges itself resonantly. When the resonant charging process of the capacitor $C1$ is finished, the load current flows from negative terminal of the DC source through diode $D2$. In the next stage of the considered cycle both the main and auxiliary transistors $T1$, $T1a$ are turned on simultaneously. The current of the main transistor $T1$ begins to increase with limited steepness to the value of the load current and also the capacitor $C1$ begins to discharge resonantly through transistor $T1a$, DC source, coil $L2a$ and diode $D2z$. Due to the occurrence of the coils $L1b$ and $L2a$ the turn-on processes of both the main and auxiliary transistors have soft character. In next time interval the current of the coil $L1b$ increases due to the negative magnetic coupling M between coil $L1b$ and $L2a$.

In the next stage the discharge current of the capacitor $C1$ and the current of the coil $L2a$ start to decrease; the voltage of the coil $L1b$ changes its sign. This causes that the current of the coil $L1b$ is reduced to the value of the load current. In the end stage of the operation cycle, the current of the auxiliary transistor $T1a$ decreases instantly to zero, whereas the collector-emitter voltage of this transistor is close to zero; so, the turn-off process of the auxiliary transistor $T1a$ has the soft character. The second transistors $T2$, $T2a$ of the given phase are switched similarly as the transistors $T1$, $T1a$.

The coils $L1b$, $L2b$ (Fig. 9) should reduce the current steepness of the main transistors $T1$, $T2$ during turn-on processes; inductance of these coils can be determined as follows:

$$L_{1,2b} = \frac{U_{DC}\, t_r}{m_r\, I_{T\max}} \tag{3}$$

where:

t_r – time when the current of the main transistor increases from 10% to 90% of its maximum value,

m_r – ratio of the transistor current at time t_r to the $I_{T\max}$ value ($m_r \leq 1$).

As previously mentioned, the resonant discharging process of the capacitor $C1$ occurs in the circuit $T1a$, DC source, $L2a$, $D2z$. Assuming that in the initial stage of this process the current of the coil $L1b$ rises linearly and the voltage change of the capacitor $C1$ is not significant, the inductance of the coils $L1a$, $L2a$ can be determined using the formula:

$$L_{1,2a} = \frac{U_{DC}\left(m_C - 1\right) t_r}{m_r\, I_{T\max}} \tag{4}$$

where:

m_C – ratio of the maximum capacitor voltage with respect to the UDC supply voltage.

The current of the coil $L1b$ flows through diode $DT1a$ after the turn-off process of the transistor $T1$ (Fig. 9); so the magnetic field energy associated with the coil $L1b$ is converted into energy of the electric field in the capacitor $C1$. Hence, the capacitance of the capacitors $C1$, $C2$ can be determined using the following formula:

$$C_{1,2} = L_{1,2b} \frac{I_{T\max}^2}{\left(m_C U_{DC}\right)^2}. \tag{5}$$

The value of the coefficient m_C depends on the DC supply voltage and on the maximum load current. It is necessary to stress that all IGBTs should be selected with respect to the maximum voltage that can occur on the capacitors, and the determination of the inductances $L_{1,2a}$, $L_{1,2b}$ is a bit simplified, because in reality the negative magnetic coupling between coils also should be taken into considerations.

As a result of the application of the negative magnetic couplings between appropriate coils, the current of the coil $L1b$ decreases to zero after the turn-off processes of both the main and auxiliary transistors. The current of the coil $L1b$ decreases to zero when the diode $D2z$ is in the reverse region; at the end of this process, the whole load current flows only through the diode $D2$. An equivalent circuit diagram of the given soft switching system for the considered process is shown in Fig. 10. It is assumed that the load current does not change its value, so this current can be replaced by a current source. On the basis of the second Kirchhoff's law we can write the following equation for the mesh consisting of the coils $L1b$, $L2a$, conducting diodes $D1s$, $D2$ and non-conducting diode $D2z$ (voltage drops on the diodes $D1s$, $D2$ are neglected):

$$L_{1b} \frac{di_{L1b}}{dt} + u_{D2z} - M \frac{di_{L1b}}{dt} = 0 \tag{6}$$

where:

u_{D2z} – voltage on the diode D2z,

M – mutual inductance $M = k\sqrt{L_{1b}L_{2a}}$,

k – mutual inductance ratio.

In the considered process the diode $D2z$ should be in the reverse region, so the voltage u_{D2z} on this diode has not to be higher than zero, and the derivative of the current i_{L1b} has negative values. By using the mentioned conditions and the equation (6) we can determinate the value of the mutual inductance ratio k:

$$k \geq \sqrt{\frac{L_{1b}}{L_{2a}}} \tag{7}$$

If this condition is fulfilled, the current of the coil $L1b$ decreases to zero after the turn-off processes of both the main and auxiliary transistors. The value of the mutual inductance ratio k depends on the previously determined inductances of the coils $L1a$, $L2a$ and $L1b$, $L2b$.
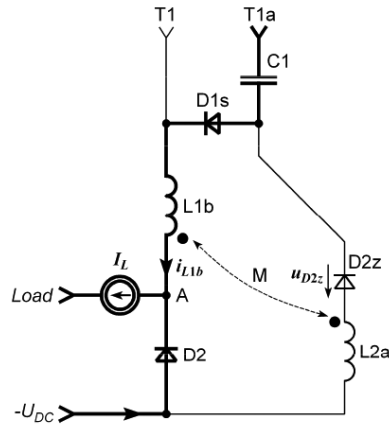
Fig. 10. An equivalent circuit diagram of the given soft switching system for the case when the current of the coil L1b decreases to zero; diode $D2z$ is in the reverse region

Numerical calculated waveforms of the currents and voltages in the alternative configuration of the proposed soft switching system for different value of the coupling coefficient k are presented in Figs. 11 and 12. The first figure shows the waveforms for the correct selection of the ratio k. In turn, the next figure presents analogous waveforms for the case when the coils are not coupled magnetically; however, it does not lead to inverter failure, only transistors are switched "hard".

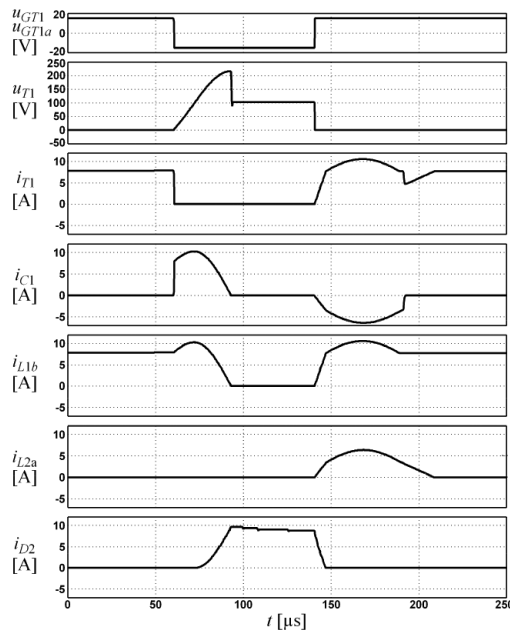Fig. 11. Numerical calculated waveforms in the system presented in Figure 9: (U_{DC} – 100 V, I_{max} – 8 A, frequency – 3 kHz, C1, C2 – 0.7 μF, $L1b$, $L2b$ – 550 μH, $L1a$, $L2a$ – 150 μH, negative coefficient of mutual inductance – 0.52; waveform description as in Fig. 4
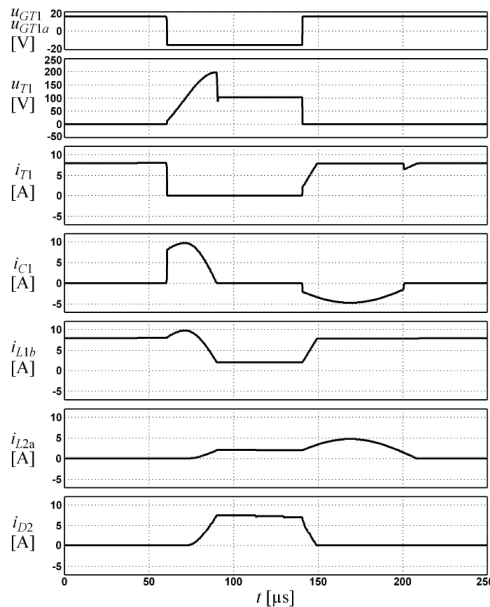
Fig. 12. Analogous waveforms as in Fig. 11 calculated for the case when the coils are not coupled magnetically

The presented research shows that for properly selected value of the mutual inductance ratio, the current of the coil $L1b$ reached zero before turn-on of the main and auxiliary transistors (Fig. 11), and in this case all transistors are soft switched using the simplest possible control algorithm; otherwise, the turn-on processes of the main transistors take place with increased losses because the turn-on process of this transistor begins at non-zero current (Fig. 12).

5. Conclusions

In the soft switching system, proposed in this paper, the capacitors cannot discharge rapidly through the main transistors and also it is impossible to interrupt the current of the coils when different control distortions appear. The control algorithm of the transistor switching is simple because the auxiliary transistors are turned on with a small time-delay with respect to the main transistors and the auxiliary transistors can be turned off at the same time as the main transistors. Laboratory research proofs that all transistors in the proposed soft switching system are switched softly.

The alternative solutions have several advantages with respect to the basic soft switching system. The application of the thyristors instead of the auxiliary transistors simplifies the control method, however, due to relatively long times of the thyristor turn-off process, the maximum switching frequency is lower in comparison to analogous value of the basic soft switching system. In turn, negative magnetic couplings between the appropriate coils allow us to use the same control signals for both the main and auxiliary transistors.

Acknowledgements

References

[1] Feix G., Dieckerhoff S., Allmeling J., Schonberger J., *Simple Methods to Calculate IGBT and Diode Conduction and Switching Losses*, 13th European Conference on Power Electronics and Applications, EPE '09, Barcelona, Spain, 8–10 September 2009, 1–8.

[2] Drofenik U., Kolar J.W., *A General Scheme for Calculating Switching – and Conduction-Losses of Power Semiconductors in Numerical Circuit Simulations of Power Electronic Systems*, 5th International Power Electronics Conference, IPEC-Niigata, Japan, 2005.

[3] Maswood A.I., *A switching loss study in SPWM igbt inverter*, 2nd IEEE International Conference on Power and Energy, PECon 08, Johor Baharu, Malaysia, 1–3 December 2008, 609–613.

[4] Rajapakse A.D., Gole A.M., Wilson P.L., *Approximate Loss Formulae for Estimation of IGBT Switching Losses through EMTP-type Simulations*, International Conference on Power Systems Transients, IPST'05, Paper No. 184, Canada, 19–23 June 2005, 1–6.

[5] Hiraki E., Tanaka T., Nakaoka M., *Zero-Voltage and Zero-Current Soft - Switching PWM Inverter*, 36th Power Electronics Specialists Conference PESC '05, Recife, Brazil, 12–16 June 2005,798–803.

[6] Martinez B., Li R., Ma K., Xu D., *Hard Switching and Soft Switching Inverters Efficiency Evaluation*, International Conference on Electrical Machines and Systems ICEMS 2008, Wuhan, China, 17–20 October 2008, 1752–1757.

[7] Amini M.R., Farzanehfard H., *Three-Phase Soft-Switching Inverter With Minimum Components,* IEEE Transactions on Industrial Electronics, vol. 58, June 2011, Iss. 6, 2258–2264.

[8] Khalilian M., Farzanehfard H., Adib E., *A novel quasi-resonant three-phase soft-switching inverter,* 3rd Power Electronics and Drive Systems Technology, PEDSTC, 2012, 471–476.

[9] Liu Y., Wu W., Blaabjerg F., Chung H.S., *A modified two-level three-phase quasi-soft-switching inverter*, Twenty-Ninth Annual IEEE Applied Power Electronics Conference and Exposition, APEC, 2014, 261–267.

[10] Panda B., Bagarty D.P., Behera S., *Soft-switching dc-ac Converters: A brief literature review,* Int. Journal of Engineering Science and Technology, vol. 2, 2010, 7004–7020.

[11] Wu W., Geng P., Chen J., Ye Y., *A Novel Three-Phase Quasi-Soft-Switching DC/AC Inverter,* IEEE International Symposium on Power Electronics for Distributed Generation Systems, PEDG, Hefei, China, 16–18 June 2010, 477–480.

[12] Hiraki E., Tanaka T., Nakaoka M., Zero-Voltage and Zero-Current Soft Switching PWM Inverter, 36th Power Electronics Specialists Conference PESC '05, Recife, Brazil, 12–16 June 2005, 798–803.

[13] Chandhaket S., Yoshida M., Eiji H., Nakamura M., Konishi Y., Nakaoka M., *Multi-functional Digitally-Controlled Bidirectional Interactive Three-phase Soft-Switching PWM Converter with Resonant Snubbers,* IEEE 32nd Annual Power Electronics Specialists Conference, PESC, vol. 2,Vancouver, Canada 2001, 589–593.

[14] Chao K.H., Liaw C.M., *Three-phase soft-switching inverter for induction motor drives Iyomori-Three*, IEE Proceedings – Electric Power Appl., vol. 148, Jan 2001, 8–20.

[15] Galea C., *New topology of three phase soft switching inverter using a dual auxiliary circuit*, 15th European Conference on Power Electronics and Appl., EPE 2013, 1–9.

[16] Karyś S., *Power loss comparison for the ARCP resonant inverter regard to control method*, Przegląd Elektrotechniczny, 84, nr 11, 2008, 64–68.

[17] Li Y., Lee F.C., Boroyevich D., *A Three-Phase Soft-Transition Inverter with a Novel Control Strategy for Zero-Current and Near Zero-Voltage Switching*, IEEE Transactions on Power Electronics, vol. 16, Sep 2001, 710–723.

[18] Martinez B., Li R., Ma K., Xu D., *Hard Switching and Soft Switching Inverters Efficiency Evaluation*, International Conference on Electrical Machines and Systems, ICEMS, Wuhan, China, 17–20 October 2008, 1752–1757.

[19] Keir A. S., *Soft switched Tyree-phase inwerter with staggered re sonant revovery system*, Patent US5576943, US 1996.

[20] Karyś S., *Three-Phase Soft-Switching Inverter with Coupled Inductors, Experimental Results*, Bulletin of the Polish Academy of Sciences – Technical Sciences, 59, Zeszyt 4, Warsaw, Grudzień 2011, 535–540.

[21] Zhang H., Chu E., Liu X., Wang Q., Hou L., , *Resonance electrode type three phase soft switch inverter circuit*, Patent CN101478258 (A), China 2010.

[22] Sun P., Lai J., Qian H., Yu W., Smith C., Bates J., *High Efficiency Three-Phase Soft-Switching Inverter for Electric Vehicle Drives*, IEEE Vehicle Power and Propulsion Conference, VPPC '09, Dearborn, USA, 7–10 Sept. 2009, 761–766.

[23] *Mazgaj W., Rozegnał B., Szular Z., Sposób łagodnego przełączania tranzystorów trójfazowego, dwupoziomowego falownika napięcia oraz układ łagodnego przełączania tranzystorów trójfazowego, dwupoziomowego falownika napięcia,* Polish patent PAT.226065, 2016.

[24] Mazgaj W., Rozegnał B., Szular Z., *Trójfazowy dwupoziomowy falownik napięcia z łagodnym przełączaniem tranzystorów odpornym na zakłócenia sterowania*, Przegląd Elektrotechniczny, R. 92, NR 3/2016, 148–153.

[25] Mazgaj W., Rozegnał B., Szular Z., *A novel soft switching system for three-phase voltage source inverter*, Czasopismo Techniczne, 2-E/2016, 3–15.

[26] Mazgaj W., Rozegnał B., Szular Z., *Sposób łagodnego przełączania tranzystorów trójfazowego, dwupoziomowego falownika napięcia oraz układ łagodnego przełączania tranzystorów trójfazowego, dwupoziomowego falownika napięcia*, Polish additional patent application P. 415597, 2016.

[27] Mazgaj W., Rozegnał. B, Szular Z., *Sposób łagodnego przełączania tranzystorów trójfazowego, dwupoziomowego falownika napięcia oraz układ łagodnego przełączania tranzystorów trójfazowego, dwupoziomowego falownika napięcia*, Polish additional patent application P. 418673, 2016.

Jan Szymenderski (iD) orcid.org/0000-0002-8771-4211
jan.szymenderski@put.poznan.pl

Wojciech Machczyński
Instytut Elektrotechniki i Elektroniki Przemysłowej, Wydział Elektryczny, Politechnika Poznańska

SIMULATION OF PIPELINE RANDOM RESPONSE TO STRAY CURRENTS
EFFECTS PRODUCED BY D.C. TRACTION SYSTEM

SYMULACJA LOSOWEJ ODPOWIEDZI RUROCIĄGU NA PRĄDY BŁĄDZĄCE
GENEROWANE PRZEZ TRAKCJĘ ELEKTRYCZNĄ PRĄDU STAŁEGO

Abstract

The paper presents a method of the simulation of the pipeline potential shift produced by D.C. traction stray currents which are stochastic in character. The calculation model presented is based on the deterministic model used in the earth-return circuit theory combined with the non-deterministic approach based on the Monte Carlo procedure. The model of the equivalent rail with current energization and the concept of superposition allow one to consider more complicated D.C. railway systems using a segmental approximation of the complex railway route and taking into account a number of substations and loads at any location. A locomotive position and a load current are assumed to be independent random variables in the non-deterministic approach. Using simulation program developed random characteristics of a pipeline response e.g. maximum, minimum, median and mean values can be obtained. Hence the pipeline regions more exposed to corrosion risk can be determined.

Keywords: D.C. traction, complex geometry, stochastic stray currents, earth return circuit, pipeline potential shift, simulation, Monte Carlo method.

Streszczenie

W artykule przedstawiono metodę symulacji potencjału rurociągu generowanego przez prądy błądzące o losowym kierunku przepływu i wartości. Przedstawiony model zrealizowano w oparciu o metodę deterministyczną w połączeniu z procedurą Monte Carlo. Model zastępczy szyn wykorzystuje zasilanie prądowe oraz zasadę superpozycji. Pozwala to rozważać złożone układy z zastosowaniem segmentowej aproksymacji trasy kolejowej i uwzględnieniu wielu podstacji i pojazdów w dowolnej lokalizacji. Zakłada się, że pozycja lokomotywy i prąd obciążenia są niezależnymi zmiennymi losowymi w podejściu niedeterministycznym. Wykorzystując zaprezentowaną metodę przedstawiono charakterystyki odpowiedzi rurociągu, tj. minimalne, maksymalne, medianę i wartości średnie potencjału. Na tej podstawie można wyznaczyć rejony rurociągów zagrożone korozją elektrochemiczną.

Słowa kluczowe: Trakcja prądu stałego, złożona geometria, stochastyczne prądy błądzące, obwód ziemnopowrotny, potencjał rurociągu, symulacja, metoda Monte Carlo.

1. Introduction

The electromagnetic compatibility of components of electric traction system is a criterion participating more and more in the decision of network planning and operation. D.C. electrified traction systems are a potential source of stray currents. The important problem, technically, is to evaluate the harmful effects (electrolytic corrosion) that an electrified railway has on nearby earth-return circuits (e.g. pipelines).

The stray currents from the D.C. rail-return circuit may flow into the earth and into the underground structure, returning to the rails or negative feeder taps in the vicinity of the substation or power plant. The general nature of the stray current problem is illustrated schematically in Fig. 1 [10, 16].
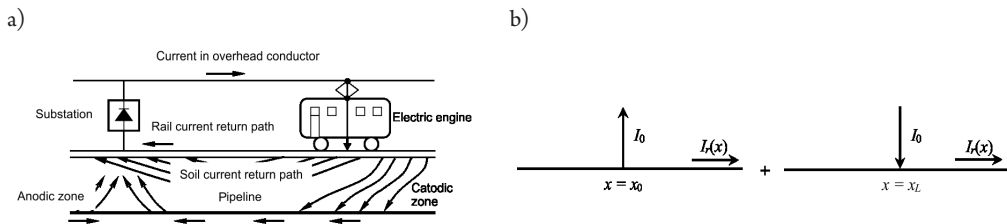

Fig. 1. Generation of stray currents: a) a railway system, b) railway system equivalents

When a metallic structure is electrically influenced by stray currents, the potential of the structure shifts in the positive or negative direction, where the current leaves or enters the metal surface, Fig. 1a. The key problem in the evaluation of the new foreign structure response to the stray currents interference consist in the determination of the potential shift of the structure with respect to the adjacent (local) earth.

To predict the potential shift due to the stray current influence, calculation methods/tools can be used, especially at design stage of new traction lines or pipelines. The existing simulation models presented in the literature are mainly based on the deterministic approach, e.g. an analytical method of calculation basing on the complete field method of solution of the transmission-line problem. The analysis is applicable to any D.C. railway system in which tracks can be represented by a single earth return circuit (equivalent rail) with current (shunt) energization [10, 11, 16]. The method, similarly to the "field approach" – e.g. the Boundary Element Method [1, 2, 13] is an alternative to the approximate method in which the equivalent rail with current energization is modeled as a large multinode electrical equivalent circuit with lumped parameters. This circuit is a chain of basic circuits, which are equivalents of homogenous sections of the rail [3, 4, 7, 9, 14, 15]. It should be pointed out, that the simulations presented by deterministic approach refer to the chosen point of time, i.e. at the time t = const. In reality flowing stray currents are stochastic in character, meaning that the current as well as the flow direction change at random. Different from the existing models, which are based on a deterministic approach, the paper [7] presents a non-deterministic approach to study of effects generated on buried pipelines located in stray currents area. The method bases on random and statistical aspects of stray current, which are captured by Monte Carlo approach.

The objective of the paper is to present problems of the modeling of stochastic stray currents effects generated by D.C. electrified railways forming geometrically complex routes. The model of the equivalent rail with current energization and the concept of superposition allow one to consider more complicated D.C. railway systems using a segmental approximation of the complex railway route and taking into account a number of substations and loads at any location. The special concern will be however given to the simulation of a pipeline response i.e. the pipeline potential shift produced by stochastic stray currents. The calculation model is based on the deterministic model combined with the non-deterministic approach based on the Monte Carlo procedure, in which a locomotive position and a load current are independent random variables.

The analysis described in the paper may be useful in understanding effects on metal installation buried in the stochastic stray current area. The non-deterministic simulation model presented can be especially useful in the design stage of new earth return circuit (pipelines) buried in the stray current area, when frequent alterations are made as the design progresses. The efficiency of the simulation program developed is demonstrated by illustrative calculations.

2. Current and potential excited in a rail by current energization

Solution for current and potential can be obtained using a rail modeled as a circuit with distributed parameters [10, 11, 16]. The system shown in Fig. 1b may be applied directly by superposition in building up electrified railway system. In this system tracks are represented by a single conductor – equivalent to a rail continuously in contact with the earth through the track ballast. The conductor is energized with the currents I_0 and $(-I_0)$ by a feeder station and a load at points $x = x_0$ and $x = x_L$, respectively.

The starting point for the analytical solution for current and potential along an equivalent rail located along the x – axis of the Cartesian coordinate system is, according to the multi-conductor line theory, the system of linear differential equations:

$$-\frac{dV_r(x)}{dx} = ZI_r(x) - E_s(x)$$

$$-\frac{dI_r(x)}{dx} = YV_r(x) - J_s(x)$$

(1)

where:

V_r – denotes the rail potential,
I_r – the rail current,
Z – the longitudinal impedance (resistance) per unit length (p.u.l.),
Y – the p.u.l. shunt admittance (conductance),
E_s, J_s – the p.u.l. external sources (longitudinal and shunt, respectively) driving the homogeneous line. The details of the circuit with earth return parameters can be found in the literature, e.g. [5, 6, 10–12, 16].

Consider the case of a finite rail extending from $x = x_1$ to $x = x_2$. The rail is energized with the current I_0 at $x = x_0$ and is open circuited on both ends. The solution of the eqn (1) for the current along the rail, taking into account the boundary conditions:

$$I_r(x_1) = I_r(x_2) = 0 \tag{2}$$

is given in the form:

$$I_r(x) = -\text{sign}(x - x_0)\frac{I_0}{2}e^{-\Gamma|x-x_0|} + A_1 e^{-\Gamma x} + B_1 e^{\Gamma x} \tag{3}$$

where:

A_1, B_1 – constants which are to determine from the boundary conditions,
Γ – the propagation constant and

$$\text{sign}(x - x_0) = \begin{array}{ll} -1 & \text{when} \quad x - x_0 < 0 \\ 1 & \text{when} \quad x - x_0 > 0 \end{array} \tag{4}$$

Finally the constants A_1 and B_1 become:

$$A_1 = -\frac{I_0}{2}\frac{ch\Gamma(x_2 - x_0)}{sh\Gamma L}e^{\Gamma x_1}, \quad B_1 = \frac{I_0}{2}\frac{ch\Gamma(x_0 - x_1)}{sh\Gamma L}e^{-\Gamma x_2} \tag{5}$$

where $L = x_2 - x_1$ denotes the rail length.
Potential along the equivalent rail can be calculate from the relationship:

$$V_r(x) = -\frac{1}{Y}\frac{dI_r(x)}{dx} \tag{6}$$

For the case of current energization of the rail by a vehicle at the point $x = x_L$ (Fig. 1b), currents and potentials are calculated from the equations (3, 5 and 6) with $I_0 = -I_0$ and $x_0 = x_L$, respectively.
It should be pointed out, that for the case of other kind of the boundary conditions, e.g. defined by impedances of finite value at rail both ends, the constants can be evaluated in similar way.
To demonstrate range of changes of rail potential and current values, sample results of a deterministic simulation are presented, Fig. 2. For a straight finite 10 km length rail two cases were considered. In both cases vehicle current was $I = 1$ A and the station was located at point $x_0 = 0$ km. In case 1 the vehicle was located at $x_L = 1$ km, whereas in case 2 the position of the vehicle was $x_L = 9$ km.
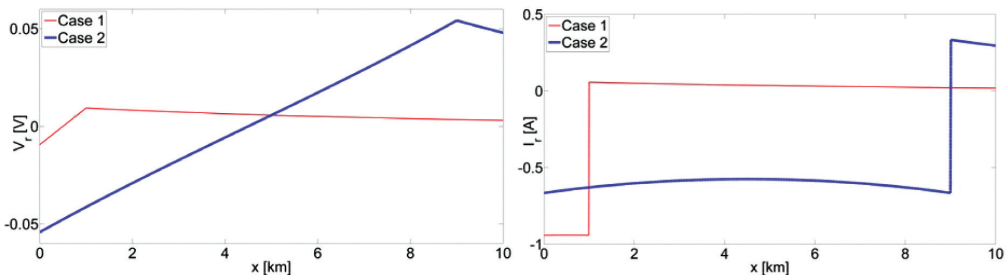

Fig. 2. Potential and current along the rail as a function of the vehicle position

Despite to the simple layout, the presented values have changed in wide range. It follows that the use of random algorithms for calculating stray currents effects on nearby earth return circuits and the estimation of the electrochemical corrosion risk due to the D.C. stray currents is justified.

3. Scalar potential in the earth due to current in the equivalent rail

The knowledge of the earth potential of the electric flow field in the vicinity of the tracks is required for the evaluation of stray currents effects on nearby structures. The potential (primary potential) can be obtained by the technique used in the earth return circuit theory, when the conductor with earth return carries a longitudinal current [8, 10, 11, 16]. The basic circuit for the calculation of the earth potential is shown in Fig. 3.
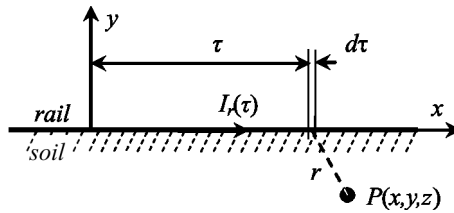

Fig. 3. Equivalent rail with longitudinal current flow on the earth surface

The equivalent rail is placed on the earth surface and is carrying the longitudinal current $I_r(x)$ which flows in the positive direction of the x axis lying along the rail. The rail can be regarded as a set of current elements of length $d\tau$. From each element an elementary leakage current $(-dI_r(\tau)/d\tau)$ flows into the earth with the conductivity γ, producing the elementary scalar potential. In the observation point $P(x, y, z)$ the scalar potential can be determined from the expression:

$$dV_e^0(P) = -\frac{1}{2\pi\gamma r}\frac{dI_r(\tau)}{d\tau} \tag{7}$$

where r is the distance from the current element (source point) to the observation point.

If a finite rail extending from $x = x_1$ to $x = x_2$, is energized with the current I_0 at $x = x_0$ and open circuited on both ends, the current along the rail is described by eqn. (3). Thus the scalar potential can be determined from the following expression:

$$V_e^0(x,y,z) = \frac{I_0\Gamma}{4\pi\gamma}\left[-e^{-\Gamma x_0}\int_{x_1}^{x_0}\frac{e^{\Gamma\tau}}{\sqrt{(x-\tau)^2+y^2+z^2}}d\tau - e^{\Gamma x_0}\int_{x_0}^{x_2}\frac{e^{-\Gamma\tau}}{\sqrt{(x-\tau)^2+y^2+z^2}}d\tau - \right.$$
$$\left.\frac{ch\Gamma(x_2-x_0)}{sh\Gamma L}e^{\Gamma x_1}\int_{x_1}^{x_2}\frac{e^{-\Gamma\tau}}{\sqrt{(x-\tau)^2+y^2+z^2}}d\tau - \frac{ch\Gamma(x_0-x_1)}{sh\Gamma L}e^{-\Gamma x_2}\int_{x_1}^{x_2}\frac{e^{\Gamma\tau}}{\sqrt{(x-\tau)^2+y^2+z^2}}d\tau\right] \tag{8}$$

For the case of current energization of the finite length rail by a vehicle at the point $x = x_L$ the scalar potential is calculated from the eqn. (8) with $I_0 = -I_0$ and $x_0 = x_L$, respectively.

4. Calculation of earth potential generated by D.C. traction of complex geometry

The models of the equivalent rail with current energization shown in Fig. 1b and the concept of superposition allow one to consider more complicated D.C. railway systems using a segmental approximation of the complex railway route and taking into account greater number of substations and loads at any location. The earth potential in the observation point has to be evaluated for each rail segment with leakage current applying each time a new coordinate system and transforming appropriately boundary conditions and coordinates of energization points.

Consider the arbitrary configuration of the D.C. railway system, as shown in Fig. 4a. For calculation purposes, the current path is divided into straight-line segments. For simplicity consider only the k-th segment of the current path. It is convenient to define two different Cartesian reference systems: the first one x, y, z is a reference system (external reference system), the second one x', y', z' is referred to the k-th segment, Fig. 4 b. It should be noted, that the reference coordinate system can be arbitrary located in the space, it is however reasonable to locate the xy plane on the earth surface.
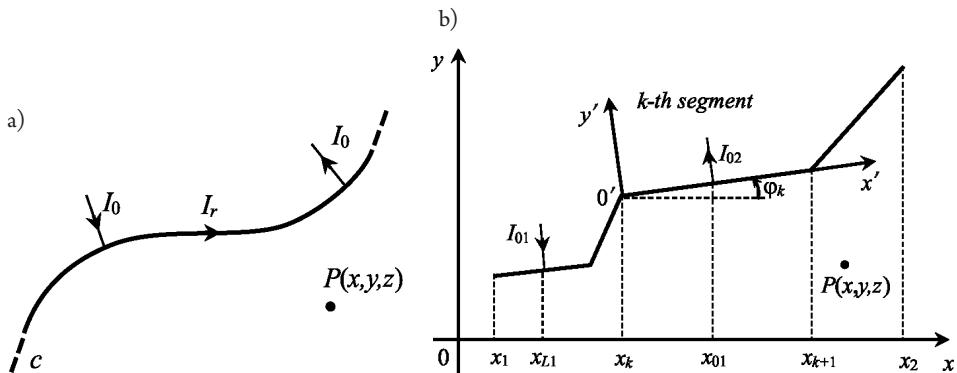

Fig. 4. a) Complex railway route (current path) generating the electric field in the earth, b) Reference systems and the k-th segment of the current path – top view

The terminating points of the k-th segment have in the reference (unprimed) system the coordinates (x_k, y_k, z_k) and $(x_{k+1}, y_{k+1}, z_{k+1})$ respectively. The segment lies in the xy plane, φ_k is the angle between the segment and the x – axis (angle measured anticlockwise), l_k is its length and taking into account that the circuit segment is parallel to the xy plane $(z_k = z_{k+1})$

$$l_k = \sqrt{\left(x_{k+1} - x_k\right)^2 + \left(y_{k+1} - y_k\right)^2} \qquad (9)$$

Assuming that the substation or the vehicle is located inside the k-th segment as shown in Fig.1b at points $x = x_0$ or $x = x_L$ in the reference system, the coordinates of the current

energization with currents I_0 or $(-I_0)$ should be transformed into the current – primed coordinate system giving:

$$x'_0 = (x_0 - x_k)\cos\varphi_k \quad x'_L = (x_L - x_k)\cos\varphi_k \tag{10}$$

Similarly the coordinates of the end points of the equivalent rail, given in the reference coordinate system, x_1 and x_2 after the transformation into the current coordinate system are

$$x'_1 = -\sum_{i=1}^{k-1} l_i \quad x'_2 = \sum_{i=k}^{n} l_i \tag{11}$$

where n denotes the number of segments the rail is divided into.

The current along the rail can be now determined in the primed coordinate system from the expression (3), whereas the constants A_1 and B_1 are defined by eqn. (5) with $L = \sum_{i=1}^{n} l_i$.

Taking into account the relation (8) the scalar potential in the earth due to current flowing in the k-th segment energized with the current I_0 at the point x'_0 (substation) can be determined from the following expression:

$$V_{ek}^0(P) = \frac{I_0 \Gamma}{4\pi\gamma}\left[-e^{-\Gamma x'_0}\int_0^{x'_0} \frac{e^{\Gamma\tau}}{\sqrt{(x'-\tau)^2 + y'^2 + z'^2}}d\tau - e^{\Gamma x'_0}\int_{x'_0}^{l_k} \frac{e^{-\Gamma\tau}}{\sqrt{(x'-\tau)^2 + y'^2 + z'^2}}d\tau + \right.$$

$$\left. -\frac{ch\Gamma(x'_2 - x'_0)}{sh\Gamma L}e^{\Gamma x'_1}\int_0^{l_k} \frac{e^{-\Gamma\tau}}{\sqrt{(x'-\tau)^2 + y'^2 + z'^2}}d\tau - \frac{ch\Gamma(x'_0 - x'_1)}{sh\Gamma L}e^{-\Gamma x'_2}\int_0^{l_k} \frac{e^{\Gamma\tau}}{\sqrt{(x'-\tau)^2 + y'^2 + z'^2}}d\tau \right] \tag{12}$$

On the other hand the earth scalar potential due to current flowing in the k-th segment with the current $(-I_0)$ at the point x'_L (vehicle) can be calculated from the eqn. (12) with $I_0 = -I_0$ and $x_0 = x_L$, respectively.

It should be noted that in order to calculate the earth potential in the observation point $P(x, y, z)$, the coordinate transformation (transposition and rotation) should be taken into account, i.e.

$$x = x'\cos\varphi - y'\sin\varphi + x_k, \quad y = x'\sin\varphi + y'\cos\varphi + y_k \tag{13}$$

where the origin O' of $x'y'$ coordinate system has coordinates (x_k, y_k) relative to the reference xy coordinate system and the x' axis makes an angle φ with the positive x axis.

Finally, when the number of current energizations (substations and loads) of the equivalent rail is N and the rail is divided into n segments the earth potential can be calculated from the relation:

$$V_e^0(P) = \sum_{k=1}^{n}\sum_{m=1}^{N} V_{ek,m}^0(P) \tag{14}$$

163

5. Current and potential along a pipeline buried in the d.C. Stray currents area

Current and potential along the pipeline located in an electric flow field $(E(x) = -dV_e/dx)$ due to stray currents can be calculated using a pipeline modeled as a circuit with lumped parameters [4, 7–9, 15].

Assuming a segment of the length l of the pipeline to be homogeneous (e.g. Z_p, Y_p = const.), it is possible to model the segment by a π – two port, as shown in Fig. 5 [4, 9] with the series impedance and the shunt admittance:

$$Z_p = Z_{0p}\sinh(\Gamma_p l), \; Y_p = \frac{2\tanh\left(\Gamma_p l/2\right)}{Z_{0p}} \tag{15}$$

where:

Z_{0p} – characteristic impedance,
G_p – propagation constant of the pipeline.

For direct current the electrical parameters of a pipeline segment can be defined:

$$Z_p = R_p \; Y_p^{-1} = G_i^{-1} + G_e^{-1} \tag{16}$$

where:

R_p – longitudinal pipeline resistance,
G_i – pipeline insulation conductance,
G_e – pipeline shunt conductance related to the soil conductivity.

The whole rail length can be subdivided into elementary cells which may have different lengths or different specific parameters.

If the pipeline is subjected to the electric field with the potential V_e^0, the passive model (Fig. 5 a) has to be completed by the voltage sources acting in shunt branches of the π – two port, Fig. 5 b.
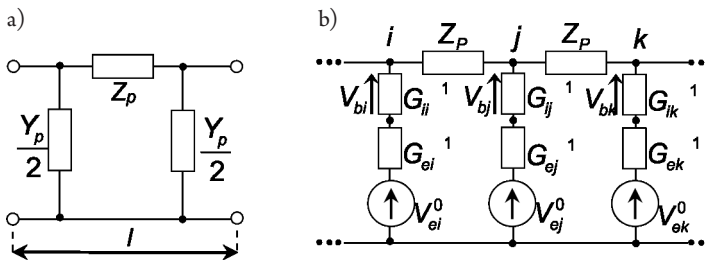

Fig. 5. a) π – two port model of an elementary homogeneous segment of a pipeline, b) chain of π – two ports modeling a pipeline with voltage sources representing the pipeline energization

After being divided into sections the pipeline can be composed of such basic two-ports which define the nodes and branches of the network model, which is well suited for computer - aided circuit analysis using simulation programs. The number of subdivisions of the pipeline can theoretically be as large as required, according to the wanted degree of discrimination in the potential and current computation.

The key problem in the evaluation of a foreign structure response to the stray currents interference consist in the determination the potential shift of the structure with respect to the adjacent (local) earth, which is described by equation:

$$V_b(x) = -\frac{1}{G_i'} \cdot \frac{dI(x)}{dx}$$

(17)

where:

G_i' – unit-length pipeline insulation conductivity.

To calculate this quantity the current flowing between pipeline and earth is required, Fig. 5b. To determine the current nodal analysis is used.

6. Incorporating Monte carlo procedure

An electrified D.C. railway system (producer of stray currents) and a nearby underground pipeline (victim of stray current interference) create a conductively coupled system of earth return circuits. Almost all parameters of the system present random characteristics. The outflow of stray currents into the ground depends on the properties of electric traction return circuits: the actual load of traction circuits i.e., the load of each electric locomotive, their number and position on the route, type and quality of rails and subgrade, and also the structure and conductivity of the surrounding environment, etc. Similarly, such parameters as conductance of pipeline insulation, soil structure and conductivity (seasonal changed), groundings along the pipeline route, insulating flanges, etc. influence electrical parameters (mutual conductance, series and shunt resistances, propagation coefficients) of the coupled earth return circuits. It is assumed in the paper, as in [7], that two stochastic quantities: locomotive position and a load current are most useful, as independent random variables characterized by suitable probability distribution, for the estimation of stochastic stray currents effects on affected pipelines.

The method proposed is intended as a tool for estimation of location of anodic/cathodic zones along a pipeline buried in stochastic stray current area. The calculation model is based on the deterministic block of models described in sections 2-5 combined with the non-deterministic approach based on the Monte Carlo procedure, in which the independent random variables are treated as input parameters for calculation of random characteristics of pipeline responses (output parameters of deterministic block) e.g. potential shift along an affected pipeline. The values of the pipeline responses compose statistical distributions and each of them can be suitably processed, thus obtaining significant parameters like maximum, minimum, median and mean values. Hence the pipeline regions more exposed to corrosion risk can be estimated. The application of the method presented shall be illustrated by an example in the sequel. Calculation algorithm developed is shown in Fig. 6.

The first step is insertion the parameters of pipeline, electric traction and simulation geometry. On this basis are next calculated rail and pipeline mathematical models. These models are used to calculate output quantities in a static state for one drown position of the vehicle and load current. For this purpose is used a random number generator, which is available in the development

environment MATLAB. Numerous tests have shown that the distribution of random numbers is evenly in the search range. Repeating many times calculations for static system, taking into account different current values and the position of the vehicle results in obtaining the entire spectrum of the results of a given size including information on the incidence of specific values (earth potential, pipeline potential to the adjacent earth, leakage current).
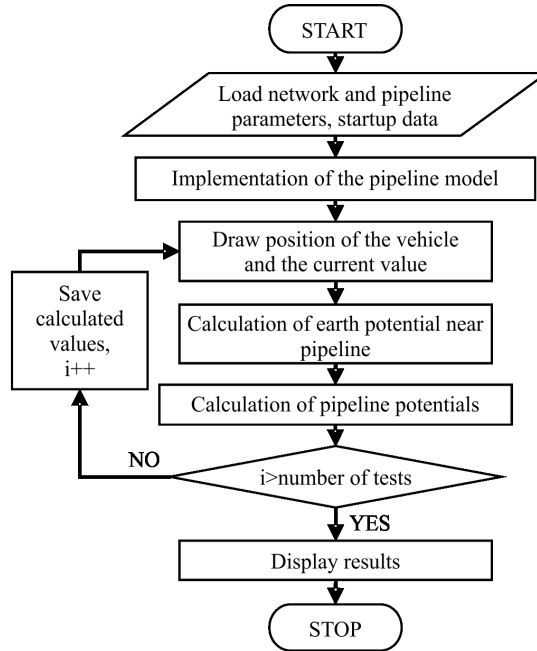

Fig. 6. Flowchart with algorithm of the proposed stochastic method

7. Examples of calculation

The following case has been proposed to present the algorithm developed. A rail section is modeled by equivalent finite 10 km length earth return circuit with parameters $Z' = 0.02\ \Omega/$km and $Y' = 0.76$ S/km. A substation is located at point $x_0 = 0$ km. Two vehicles are running along the rail section. A pipeline with the diameter 355.6 mm has a length of 1.0 km, and its electrical parameters are: $Z'_p = 0.02\ \Omega/$km, $Y'_p = 0.011$ S/km. The pipeline is buried in the soil with conductivity 0.01 S/m at 1.0 m depth, and its center is located 10 meters away of the rail middle section central point. The pipeline is open circuited at its both ends. The angle between pipeline and the rail is $\alpha = 45°$, Fig. 7. Calculations of the pipeline potential to the adjacent earth have been curried out for $n = 1000$ samples with randomly chosen load $I_0 \in (0, \dots 1000\text{ A})$ and the position of the vehicles $x_L \in (0, \dots, 10\text{ km})$, assuming that the calculation points are located at 0, 250 500, 750 and 1000 m from the left end of the pipeline. The histograms of the pipeline potentials are shown in Fig.8, and minimum, maximum, average and median values of pipeline potential to the adjacent earth are summarized in Table 1.

y [km]

vehicle 2

0,50

vehicle 1

0,25

station
$2I_0$

pipeline

rail

x_{L2}

α

x_p

x_{L1}

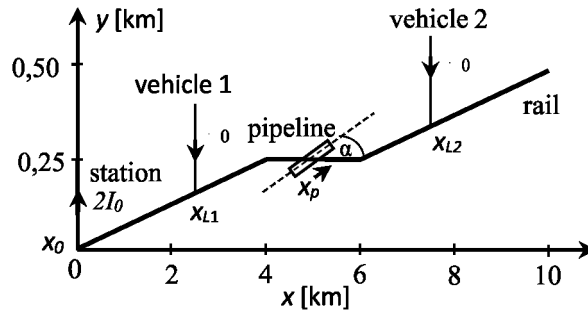x_0

0   2   4   6   8   10

x [km]

Fig. 7. The pipeline location relative to the rail – top view (no scale)

Table 1. Summary of minimum, maximum, average and median values of pipeline potential to the adjacent earth, calculated at points located along the pipeline

Location of the calculation point x_p [m]	Min value [V]	Max value [V]	Average [V]	Median [V]
0	0,000	1,295	0,365	0,329
250	0,000	0,643	0,187	0,170
500	−1,880	0,013	−0,383	−0,307
750	−0,336	0,088	−0,068	−0,052
1000	−0,566	0,682	0,021	0,031

The calculations have been performed to estimate the anodic and cathodic zones along the pipeline. On the basis of the histograms and the results shown in the Table 1, it can be determined that the positive pipeline potential to the adjacent earth values occur at end points of the pipeline. Along sections of the pipeline lying between points $x_p \in$ (0–350 m) and $x_p \in$ (900–1000 m) the anodic zones can be expected. The highest and positive values of the potential average and median values are obtained at point located nearest to the substation (x_p = 0 m). As one would expect the negative potential occurs at the middle point of the pipeline, and the cathodic zone spreads between points $x_p \in$ (350 m–900 m).

For the above calculation example, it was proposed to change the parameters of the insulation of the central pipeline segment (from 400 to 600 m). The initial conductivity value of the insulation was reduced a ten times. The rest of the pipeline insulation value remains unchanged. Calculations of the pipeline potential to the adjacent earth have been curried out for n = 1000 samples with randomly chosen load $I_0 \in$ (0, … 1000 A) and the position of the vehicles $x_L \in$ (0, … , 10 km). The average value of the potential to the adjacent earth decreased both at the beginning and at the end of the pipeline. In the end section of the pipeline the mean values changed the sign to negative, which resulted in the conversion from anode to cathode zone. The result was presented in Fig. 9.
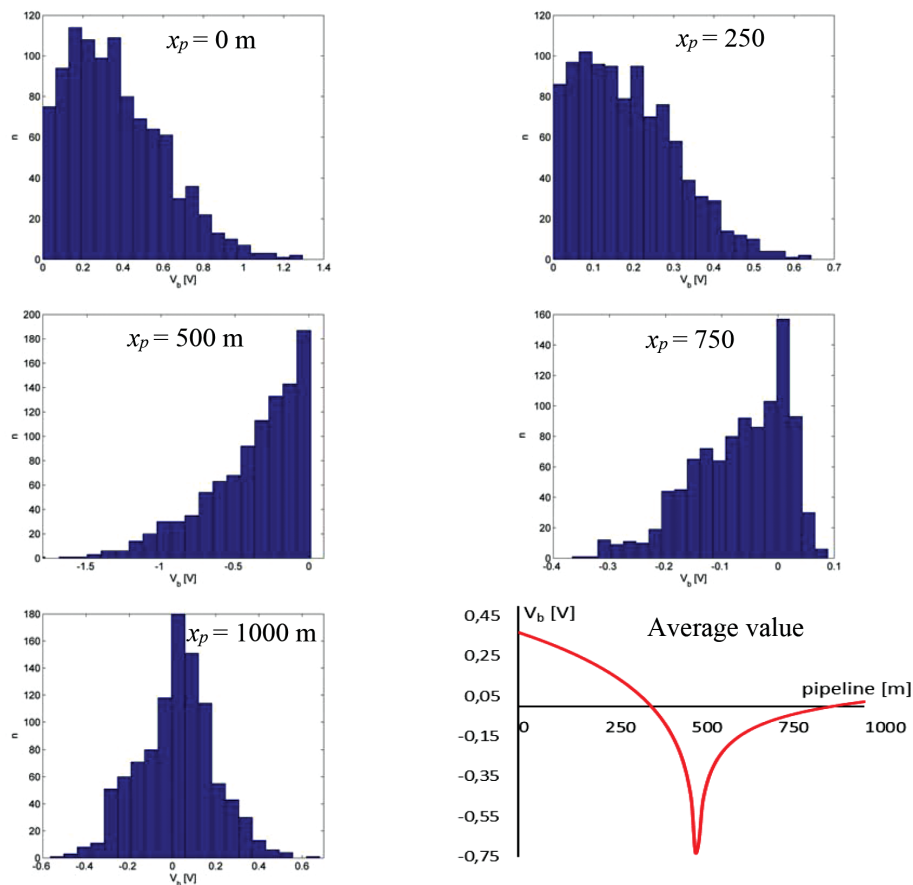
Fig. 8. Histograms and average value of the pipeline potential to the adjacent earth at points located along the pipeline
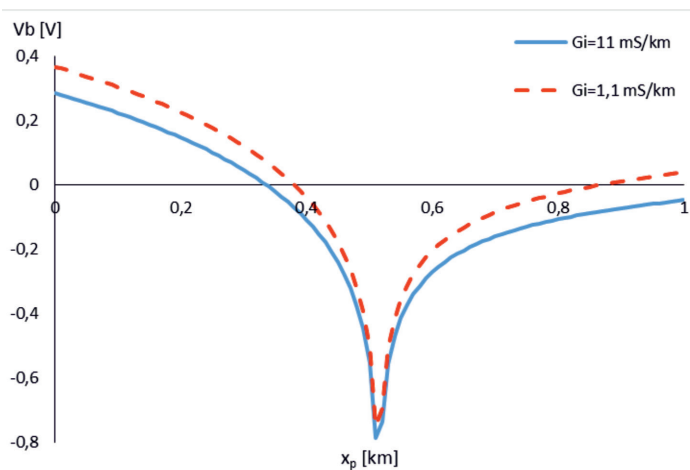

Fig. 9. The average value of the pipeline potential to the adjacent earth as a function of the insulation conductivity

8. Final remarks

The method proposed is intended as a tool for estimation of location of anodic/cathodic zones along a pipeline buried in stochastic stray current area. The calculation model is based on the deterministic block of models combined with the non-deterministic approach based on the Monte Carlo procedure, in which the independent random variables are treated as input parameters for calculation of random characteristics of pipeline responses (output parameters of deterministic block) e.g. potential shift along an affected pipeline. The values of the pipeline responses compose statistical distributions and each of them can be suitably processed, thus obtaining significant parameters like maximum, minimum, median and mean values. Hence the pipeline regions more exposed to corrosion risk can be estimated.

The formulas derived and program developed allow to manage cases with any complex geometry of the system D.C. traction route – underground pipeline. The necessary data for calculations are: the number of substations and vehicles, the magnitude of current energizations, coordinates of energization points, electrical parameters of the equivalent rail, the number of segments the equivalent rail is divided into and the coordinates (x_i, y_i, z_i) and $(x_{i+1}, y_{i+1}, z_{i+1})$ of terminating points of each segment, coordinates of the observation point along the pipeline and its electrical parameters, earth conductivity. It should be noted that all coordinates refer to the reference system, which can be arbitrary located in the space.

The analysis described in the paper may be useful in understanding effects on metal installation buried in the stochastic stray current area. The simulation models presented can be especially useful in the design stage of new earth return circuit buried in the D.C. stray current area, when frequent alterations are made as the design progresses.

References

[1]   Bortels L., Dorochenko A., Van den Bossche B., Weyns G., Deconinck J., *Three-Dimensional Boundary Element Method and Finite Element Method Simulations Applied to Stray Current Interference Problems, A Unique Coupling Mechanism That Takes the Best of Both Methods*, Corrosion, Vol. 63, No. 6, June 2007, 561–576.

[2]   Brichau F., Deconinck J., *A Numerical Model for Cathodic Protection of Buried Pipes*. Corrosion, Vol. 50, No. 1, January 1994, 39–49.

[3]   Charalambous C.A., Cotton I., Aylott P., *A Simulation Tool to Predict the Impact of Soil Topologies on Coupling Between a Light Rail System and Buried Third-Party Infrastructure*, IEEE Trans. Veh. Technol., Vol. 57, No. 3, 2008, 1404–1416.

[4]   Czarnywojtek P., Machczyński W., *Computer simulation of responses of earth-return circuits to the a.c. and DC external excitation*, European Trans. on Electrical Power, ETEP Vol. 13, No. 3, May/June 2003, 173–184.

[5]   Hill R.J., Brillante S., Leonard P.J., *Railway track transmission line parameters from finite element field modeling: Shunt admittance*, Proc. IEE Elect. Power Applicat., Vol. 146, No. 6, 1999, 647–660.

[6]   Hill R.J., Brillante S., Leonard P.J., *Railway track transmission line parameters from finite element field modeling: Series impedance*, Proc. IEE Elect. Power Applicat., Vol. 147, No. 3, 2000, 227–238.

[7]   Lucca G., *Estimating stray currents interference from DC traction lines on buried pipelines by means a Monte Carlo algorithm*, Electrical Engineering, DOI 10.1007/s00202-015-0333-6, published online: 05 April 2015.

[8]   Machczyński W., Budnik K., Szymenderski J., *Assessment of D.C traction stray currents effects on nearby pipelines*, The International Journal for Computation and Mathematics in Electrical and Electronic Engineering, vol. 35, iss 4, 2016, 1468–1477.

[9]   Machczyński W., Czarnywojtek P., *Computer simulation of a protection of underground conductors against stray currents*, 16th International Corrosion Congress, September 19 – 24, 2005, Beijing, China, paper 21-03, 1–8.

[10] Machczyński W., *Simulation model for drainage protection of earth–return circuits laid in stray currents area*, Electrical Engineering, Vol. 84, No 3, July 2002, 165–172.

[11] Machczyński, W., *Currents and potentials in earth return circuits exposed to alternating current electric railways*, Proc. IEE, Part B, Vol. 129, 5, 1982, 279–288.

[12] Mariscotti A., Pozzobon P., *Determination of the electrical parameters of railway traction lines: Calculation, measurements and reference data*, IEEE Trans. on Power Delivery, Vol. 19, No. 4, 2004, 1538–1546.

[13] Metwally I.A., Al-Mandhari H.M.,Nadir Z., Gastli A., *Boundary element simulation of DC stray currents in oil industry due to cathodic protection interference*, European Trans. on Electrical Power, Vol. 17, Sept./Oct. 2007, 486–499.

[14] Ogunsola A., Mariscotti A., *Electromagnetic Compatibility in Railways, Analysis and management*, Springer – Verlag, Berlin Heidelberg 2013.

[15] Ogunsola A., Mariscotti A., Sandrolini L., *Estimation of stray current from a dc-electrified railway and impressed potential on a buried pipe*, IEEE Trans. on Power Delivery, Vol. 27, No. 4, 2012, 2238–2246.

[16] Sunde E.D., *Earth conduction effects in transmission system*, New York, Dover 1968.

Piotr Lipiec
  lipiec@mech.pk.edu.pl

Magdalena Machno

Sebastian Skoczypiec
  Institute of Production Engineering, Faculty of Mechanical Engineering, Cracow University of Technology

Experimental research on electrodischarge drilling of high aspect ratio holes in ti-6al-4v alloy

Badania elektroerozyjnego drążenia głębokich otworów w stopie tytanu ti-6al-4v

Abstract

The drilling of small cylindrical (D < 1 mm) holes with a high ratio of length to diameter (L/D > 10) in difficult-to-cut materials is significantly beyond mechanical drilling capabilities. Electrodischarge machining (EDM) is a good and cost effective alternative in such situations. The machinability of electrodischarge machined material is determined by its thermal and electrical properties; therefore, the high electrical resistivity, the relatively high melting point and low thermal conductivity of Ti-6Al-4V alloy cause problems during the machining of parts made of this material. In this article, the results of experimental research on electrodischarge microdrilling in Grade 5 Ti-6Al-4V alloy are presented. The influence of various machining parameters (pulse time, discharge voltage, current amplitude, dielectric pressure, electrode-tool rotation speed) on key technological factors such as hole depth, side gap, linear tool wear, mean drilling speed and hole taper angle was analysed.

Keywords: EDM, holes with a high ratio of length to diameter, drilling, titanium

Streszczenie

Drążenie cylindrycznych otworów o małych średnicach (D < 1 mm) charakteryzujących się dużą smukłością (L/D > 10) w trudnoskrawalnych materiałach wykracza poza możliwości konwencjonalnych metod wiercenia. Obróbka elektroerozyjna jest dobrą i efektywną alternatywą dla tego typu zastosowań. Obrabialność w EDM jest zdeterminowana przez właściwości związane z przewodnością cieplną i elektryczną obrabianego materiału oraz dielektryka. Wysoki opór elektryczny i relatywnie wysoka temperatura topnienia, przy niskiej przewodności cieplnej stopu tytanu Ti-6Al-4V, powodują pewne problemy podczas jego obróbki, co stwarza konieczność poszukiwania jej optymalnych parametrów. W artykule przedstawiono wyniki badań doświadczalnych procesu mikrodrążenia elektroerozyjnego stopu tytanu Ti-6Al-4V. Badano wpływ parametrów obróbki takich jak: czas impulsu, wartość napięcia pracy i amplitudy prądu, ciśnienia dielektryka, prędkości obrotowej elektrody roboczej na podstawowe wskaźniki technologiczne oraz dokładności wymiarowe i kształtowe.

Słowa kluczowe: EDM, drążenie, tytan, głębokie otwory

1. Introduction

Over recent years, a progressive tendency for the production of miniaturised parts can be observed – this is compliant with the principle: smaller, faster, cheaper. This trend has now become a primary object of interest in many industries, such as aviation, automotive, and electronics (area of the MEMS (microelectromechanical system) production). In the abovementioned branches of industry, along with progressing miniaturisation, one can notice an increasing demand for effective techniques of micro-hole production with diameters from 8 to 500 μm and aspect ratios above 20: 1. For example, during the production of jet engines, a lot of holes are made (20,000–40,000) in the turbine, combustion chamber and stator units. Often, as in the case of turbine blades that are cast, internal cooling channels are created by placing special ceramic cores in the moulds. However, improving the quality of the surface obtained in such a manner requires the use of special abrasive pastes, which results in a longer production cycle. Unconventional methods (e.g. electrodischarge machining, laser beam machining, electrochemical machining) are used for the production of holes.

In addition to the growing demand for effective and efficient micro-production techniques, there are increasing requirements for the quality of the internal surface of drilled micro-holes and their dimensional and shape accuracy. Very often items that require drilling are made of difficult-to-cut materials.

For the construction of aircraft components, turbine engines mainly use materials such as titanium alloys, nickel alloys, steels, nickel-based superalloys. Physical and strength properties of these materials (high ductility, high specific strength, tendency to strengthen during machining, higher hardness) make it impossible to effectively drill micro-holes in them using conventional machining [1].

During electrodischarge machining (EDM), material is removed from the workpiece as a result of the energy of pulsed electrical discharge between two electrodes immersed in a liquid dielectric medium. During this process, the material melts and evaporates in the discharge. Machinability in the EDM process does not depend on the mechanical properties of the workpiece, but only on its electrical and thermal conductivity; this causes this type of machining to be often used for hard-to-cut materials [2–5].

Disadvantages of spark erosion machining include electrode wear, deformed shape of the obtained hole (conical shape), and heat-affected top layer of the workpiece surface [6–9]. In some cases, additional finishing operations are also required [10]. High temperature in the discharge zone causes a heat-affected zone, which can lead to a change in the mechanical properties of the surface layer (formation of microcracks, additional stresses or porosities) [11].

During the drilling of holes using EDM, the working electrode moves towards the material and also rotates (Fig. 1). The dielectric is supplied into the machining area through a channel in the electrode which enables better removal of the products of erosion. Various types of oil-based liquids or deionized water are used as a dielectric; however, in the case of deep hole drilling, deionised water is preferred.
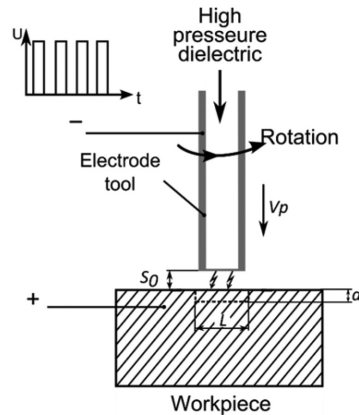
Fig. 1. Scheme of the EDM drilling process

EDM is a technology used in the machining of titanium and its alloys, especially in the case of microdrilling. Due to the mechanical, thermal and chemical properties of these materials, conventional machining is difficult; therefore, EDM is good alternative to other machining methods, especially when complicated or when a shape with a high ratio of length to diameter has to be machined [12–15].

This paper concerns electrodischarge drilling of Grade 5 Ti-6Al-4V alloy. This material is characterised by its high temperature and corrosion resistance, high strength factor and excellent mechanical properties and is commonly applied in the aircraft and space industry. However, due to its high level of chemical reactivity low thermal conductivity, conventional machining of Grade 5 alloy is difficult; EDM is therefore a good machining alternative [1, 16, 17]. It is worth stressing that in comparison to the materials most commonly machined using EDM, Ti-6Al-4V alloy has high electrical resistivity (five times larger than common steel), a relatively high melting point and low thermal conductivity [17, 18, 19]. It is also important that the electrical resistivity of Ti-6Al-4V alloy be highly dependent on the temperature. On the basis of the abovementioned features, one can state that machining of this material is characterised by rapid heat generation (because of low electrical conductivity) and problems with heat dissipation. This results in low productivity and poor surface integrity.

The results of previous research concerning EDM drilling in Grade 5 highlight the following problems: obtaining of high aspect ratio *see above note* hole for diameters less than 1 mm, hole taper, white layer formation and microcracks [18].

In this article, the results of experimental research on electrodischarge microdrilling in Grade 5 Ti-6Al-4V alloy are presented. During the experiment, the influence of following machining parameters were applied: voltage pulse time, discharge voltage, current amplitude, dielectric pressure and electrode-tool rotation speed. The impact of these parameters on hole depth, side gap, linear tool wear, mean drilling speed and hole taper angle was analysed.

2. Research methodology

The research was carried out on a machine tool designed and built at the Institute of Production Engineering of Cracow University of Technology (Fig. 2). Titanium alloy Ti-6Al-4V was used as the machined material. This is an alloy often used in the aerospace and biomedical industries, characterised by very good mechanical properties, relatively low density, high corrosion resistance and high strength at high temperature. The test stand consists of several components of which the most important are:

▸ mechanical part of the machine with servo drives, electrode, sample grip and electrode guide,
▸ pulse generator with power supply,
▸ high pressure system for dielectric circulation,
▸ drive control system.

An important element was the electrode guide (Fig. 3), which allowed minimising the impact of electrode vibrations and clamping eccentricity on the drilling process.

The main goal of the research was to examine the impact of process parameters on efficiency, accuracy, electrode wear and drilling speed. The research was performed according to the design of the experiment. Table 1 shows the input and output parameters used during the tests.

Table 1. Research input and output parameters

Input parameters	min	max
Time of the pulse t_i [μs]	100	999
Current amplitude I [A]	2.00	4.65
Discharge voltage U [V]	60	120
Dielectric inlet pressure p_{in} [bar]	50	90
Electrode rotation speed ω [1/min]	100	500
Output parameters		
Linear tool wear (TW) [%]		
Side gap(S) [μm]		
Taper angle(α) [deg]		
Drilling speed (v) [μm/s]		
L/D ratio		

The shape, dimensions and material of the tool electrode were kept constant throughout the testing (single channel, 0.4 mm diameter, made of copper); similarly, the dielectric fluid was deionised water for the duration of the experiment. Each sample had a thickness of 10 mm and the holes were drilled through the entire depth of the samples. To avoid problems with through drilling, an additional technological pad was applied on the underside of sample

(Fig. 2). Full quadratic (constant, linear, interaction, and squared terms) polynomial was selected in order to statistically fit experimental data. Matlab software was used to calculate the polynomial coefficients and perform a regression analysis.
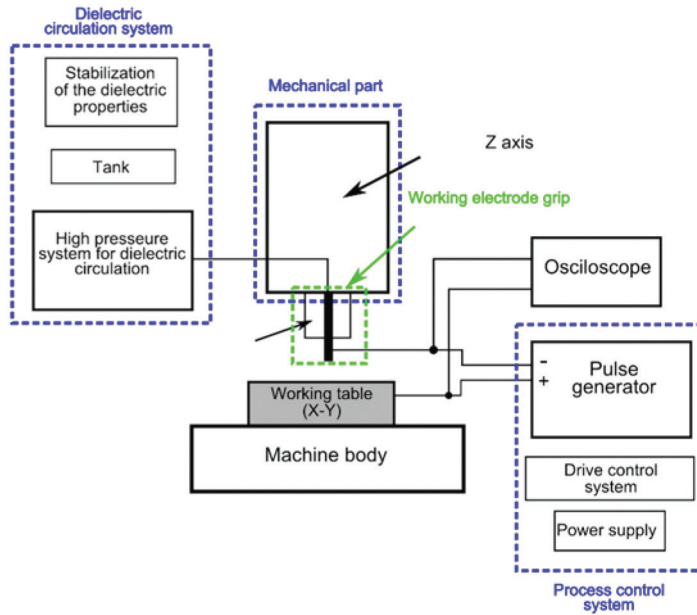

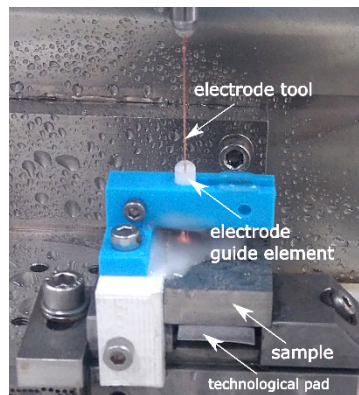Fig. 2. Scheme of the test stand and its main functional units

Fig. 3. Photography of the electrode guide system

3. Results analysis

During the research, the influence of five input parameters on technological factors was investigated. This allowed testing which factors – apart from the most important parameters such as current amplitude and pulse time (Fig. 4) – affect the efficiency of the electrodischarge drilling process.

The electrical parameters have the largest impact on drilling speed and side gap thickness (Figs. 4, 5 and 6); however, optimal selection of rotation speed and dielectric inlet pressure gives the possibility to obtain much better results of selected technological factors.
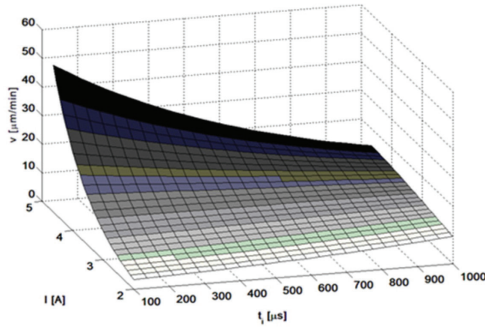

Fig. 4. Relationship of drilling speed v, current amplitude I and pulse time t_i, discharge voltage $U = 100$ V, dielectric inlet pressure $p_{in} = 70$ bar, electrode rotation speed $\omega = 300$ rpm

Fig. 5. Relationship of drilling speed v, current amplitude I and discharge voltage, pulse time $t_i = 550$ µs, dielectric inlet pressure $p_{in} = 70$ bar, electrode rotation speed $\omega = 300$ rpm

Fig. 6. Relationship of side gap S, current amplitude I and pulse time t_i, discharge voltage $U = 100$ V, dielectric inlet pressure $p_{in} = 70$ bar, electrode rotation speed $\omega = 300$ rpm
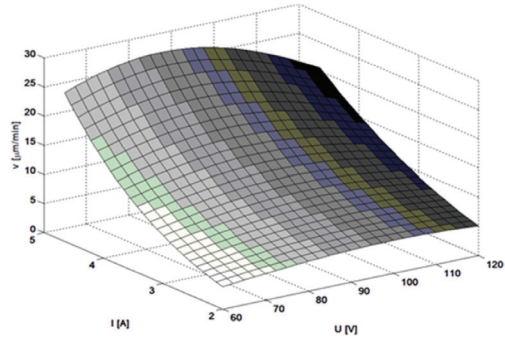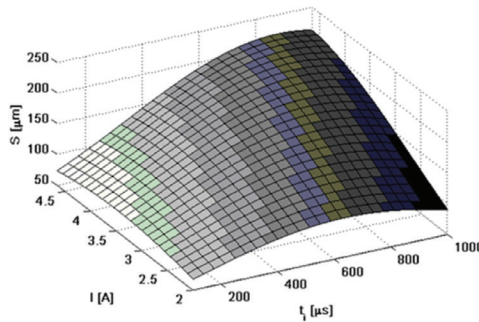
Results relating to the relationship between L/D ratio and dielectric inlet pressure (Fig. 7) indicate that, when other machining parameters are kept constant, increase of dielectric pressure improves the L/D ratio. Taking into account that each hole depth was 10 mm, this means that hole diameter decreases. Better frontal and side gap flushing means that erosion products from the discharge area are removed more efficiently (dielectric is 'fresh') and a smaller gap is necessary to initiate the discharge.

In Fig. 8, the relationship between drilling speed v and electrode rotation speed ω is presented. With increase of ω – when other machining parameters are kept constant – drilling speed also increases. Rotation of the electrode tool improves the evacuation of the machining products from the gap and also gives the possibility to obtain a hole with better circularity (see Fig. 11d); however, this effect is connected with the improvement of electrode stiffness. For an electrode diameter of D = 0.4 mm and a L/D ratio higher than 10, the eccentric

effect becomes significant. Increase of electrode tool rotation speed gives the possibility to minimalise the eccentric effect.

It is worth emphasising that drilling speed decreases with increases to dielectric pressure (Fig. 9). This is due to a loss of dielectric continuity and the dielectric-air mixture which occurs and in the gap. This results in a decrease of the frequency of effective discharges and their efficiency; as a result, machining speed decreases. Contrastingly, increase in dielectric inlet pressure and an increase of discharge effectiveness cause a decrease of tool wear.

The amount of removed material depends on single pulse discharge which is related to discharge current amplitude, discharge voltage and pulse time. Results observable in Figs. 11a, 11b and 11c indicate that an increase of these technological factors significantly affect the hole diameter and quality. Change of dielectric pressure and electrode-tool rotation speed influences flushing efficiency.

It is worth mentioning that because the hole depth was 10,000 μm, the mean taper angle calculated for the drilled holes was 0.4 of a degree.
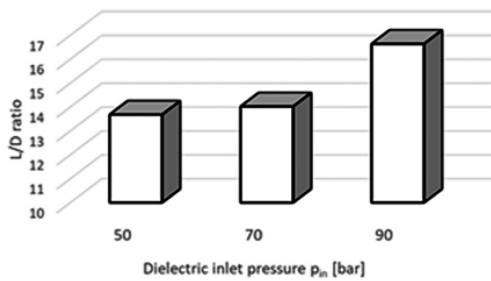

Fig. 7. Relationship of L/D ratio and dielectric inlet pressure; t_i = 550 μs, I = 3,33 A, U = 100 V, ω = 300 rpm

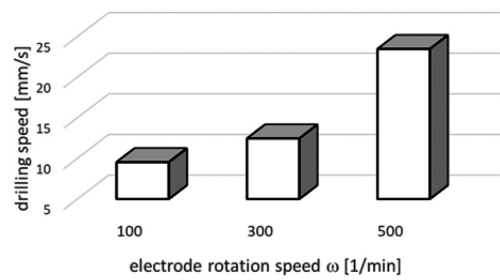
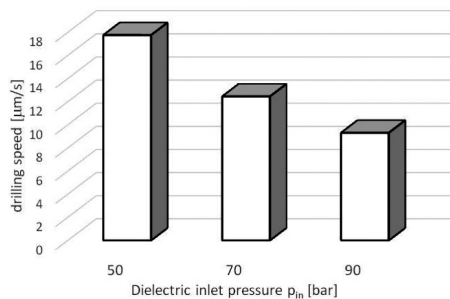Fig. 8. Relationship of drilling speed and electrode rotation speed ω, t_i = 550 μs, I = 3,33 A, U = 100 V, p_{in} = 70 bar

Fig. 9. Relationship of drilling speed and dielectric inlet pressure; t_i = 550 μs, I = 3,33 A, U = 100 V, p_{in} = 70 bar
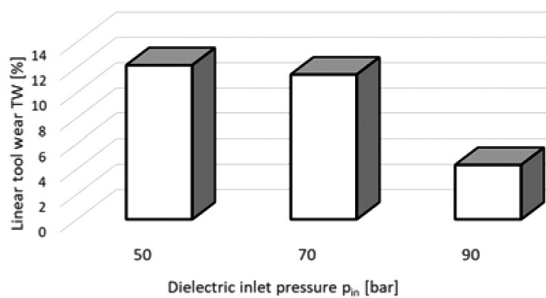
Fig. 10. Relationship of linear tool wear and dielectric inlet pressure; t_i = 550 μs, I = 3,33 A, U = 100 V, ω = 300 1/min
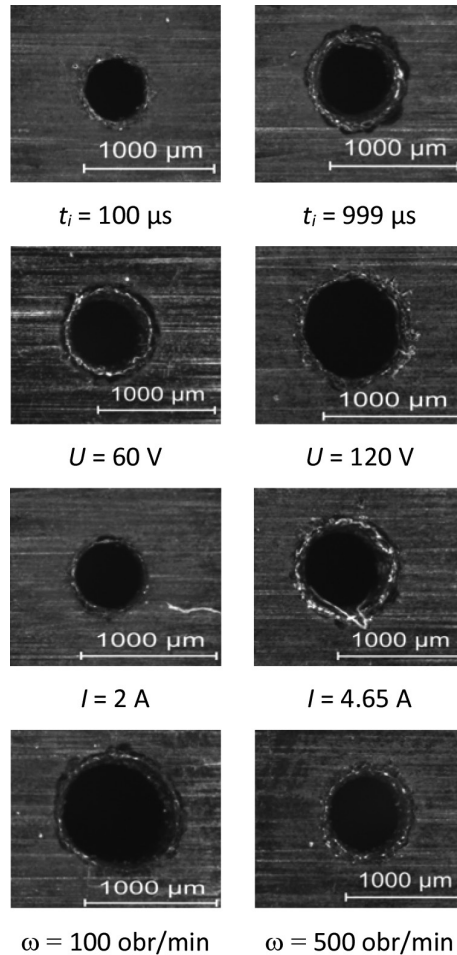
Fig. 11. Photographs of entrance hole for extreme values of pulse time t_i (a), discharge voltage U (b), current amplitude I (c) and electrode-tool rotation speed (d); other input parameters are from the centre of the research plan (t_i = 550 μs, I = 3,33 A, U = 100 V, p_{in} = 70 bar, ω = 300 rpm)

4. Summary

The conducted research proved that electrodischarge machining is a good alternative for conventional methods when drilling high aspect holes in Grade 5 Ti-6Al-4V alloy. It gives the possibility to drill through holes (L/D ratio above 15) with relatively high efficiency (the drilling speed reaches 3 mm/min). The analysis of the results allows formulation of the following conclusions:

▶ Dielectric inlet pressure and electrode rotation speed have significant influence on hole depth. Increase of dielectric inlet pressure leads to better gap cleaning, which results in a decrease of tool electrode wear and in a decrease of drilling speed. This can be explained by a decrease of discharge energy, despite of increase of the process

effectiveness. Therefore, one can state that the selection of optimal dielectric pressure is a compromise between machining speed and tool wear.

▶ Increase of electrode tool rotation speed leads to an increase of drilling speed. Electrode rotation with a relative high speed (ω = 500 1/min) results in the efficient cleaning of the machining area, which directly contributes to an increase in process efficiency. Tool rotation also improves axial symmetry, but in the case of eccentricity, it can increase hole diameter.

▶ Due to the thermal and electrical properties of the machined material, the quality of the inlet and outlet holes is not perfect; thus, further research focused on surface integrity is needed.

References

[1]   Percina M., Aslantas K., Ucuna I., Kaynakb Y., Cicekc A., *Micro-drilling of Ti–6Al–4V alloy: The effects of cooling/lubricating*, Precision Engineering, Vol. 45/2016, 450–462.

[2]   Rajurkar K.P, Sundaram M.M., Malshe A.P., *Review of Electrochemical and Electrodischarge Machining*, Procedia CIRP, Vol. 6/2013, 13–26.

[3]   Skoczypiec S., Machno M., Bizoń W., *The capabilities of electrodischarge microdrilling of high aspect ratio holes in ceramic materials*, Management and Production Engineering Review Vol. 6-3/2015, 61–69.

[4]   Plaza S., Sanchez J.A., at all, *Experimental study on micro EDM-drilling of Ti6Al4V using helical electrode,* Prec. Eng. Vol. 38/2014, 821–827.

[5]   Skoczypiec S., Ruszaj A., *A sequential electrochemical-electrodischarge process for micro part manufacturing* Prec. Eng., Vol. 38/2014, 680–690.

[6]   Hasan M., Zhao J., Jiang Z., *A review of modern advancements in micro drilling techniques* Journal of Manufacturing Process, Vol. 29/2017, 343–375.

[7]   Kliuev M., Baumgart C., Wegener K., *Fluid dynamics in Electrode Flushing Channel and Electrode-Workpiece Gap During EDM Drilling*, "Procedia CIRP", Vol. 68/2018, 254–259.

[8]   Li J., Yin G., Wang C., Guo X., Yu Z., *Prediction of aspect ratio of a micro hole drilled by EDM* "Journal of Mechanical Science and Technology", Vol. 27/2013, 185–190.

[9]   Kamal K., Rawalb S.K., Singha V.P., Anu B., *Experimental Study on Diametric Expansion and Taper Rate in EDM Drilling For High Aspect Ratio Micro Holes in High Strength Materials*, "Materials Today: Proceedings", Vol. 5/2018, 7363–7372.

[10] Risto M., Haas R., Munz M., *Optimization of the EDM drilling process to increase the productivity and geometrical accuracy,* "Procedia CIRP" Vol. 42/2016, 537–542.

[11] Mowwer T.D., *Degradation of titanium 6Al–4V fatigue strength due to electrical discharge machining,* "International Journal of Fatigue", Vol. 64/2014, 84–96.

[12] Manjaiah M., Narendranath S., Basavarajappa S., *A review on machining of titanium based alloys using EDM and WEDM,* "Rev. Adv. Mater. Sci." Vol. 36/2014, 89–111.

[13] Antar M., Chantzis D. et al., *High Speed EDM and Laser Drilling of Aerospace Alloys*, "Procedia CIRP", Vol. 42/2016, 526–531.

[14] Hasçalık A., Çaydas U., *Electrical discharge machining of titanium alloy (Ti–6Al–4V)*, "Applied Surface Science", Vol. 253/2007, 9007–9016.

[15] Sanchez J. A., Plaza S., et al., *Electrode set-up for EDM-drilling of large aspect-ratio microholes*, "Procedia CIRP" Vol. 6/2013, 274–279.

[16] Ezugwu E.O., Wang Z.M., *Titanium alloys and their machinability – a review*, "Journal of Materials Processing Technology", Vol. 68/1997, 262–274.

[17] Hascalik A., Caydas U., *Electrical discharge machining of titanium alloy (Ti–6Al–4V)*, "Applied Surface Science", Vol. 253/2007, 9007–9016.

[18] Wansheng Z., Zhenlong W., Schichun D., Guanxin C., Hongyu W., *Ultrasonic and electro discharge machining to deep and small hole on titanium alloy*, "Journal of Materials Processing Technology", Vol. 120/2002, 101–106.

[19] Fonda P., Wang Z., Yamazaki K., Akutsu Y., *A fundamental study on Ti–6Al–4V's thermal and electrical properties and their relation to EDM productivity*, "J. Mater. Process. Technol", Vol. 202/2008, 583–589.

Izabela Pliszka
Norbert Radek
    Faculty of Mechatronics and Mechanical Engineering, Kielce University of Technology

Aneta Gądek-Moszczak
Renata Dwornicka
dwornick@mech.pk.edu.pl
    Institute of Applied Informatics, Faculty of Mechanical Engineering,
    Cracow University of Technology

Jozef Bronček
    Faculty of Mechanical Engineering, University of Žilina, Slovakia

Microstructure of laser-modified electro-sparking coatings

Mikrostruktura powłok elektroiskrowych modyfikowanych

Abstract

The article summarizes research on a method used to improve tribological properties. The paper presents possibilities of using laser surface modification by means of EDM. The performed research confirmed that the concentrated laser beam stream can effectively modify the state of the ESD coating layer, WC-Cu and improve their usability. The work aims to assess the properties of coatings after laser treatment, based on the observation of the newly created structure of the material, the measurement of adhesion and microhardness measurement.

Keywords: WC-Cu coating, laser treatment, electrospark deposition, surface

Streszczenie

W artykule podsumowano badania nad metodą poprawy właściwości tribologicznych. Przedstawiono możliwości zastosowania modyfikacji laserowej powierzchni na drodze obróbki elektroiskrowej. Wykonane badania potwierdziły, iż skoncentrowanym strumieniem wiązki laserowej można skutecznie modyfikować stan warstwy powłok elektroiskrowych, WC-Cu i wpływać na poprawę ich właściwości użytkowych. Artykuł ma na celu ocenę właściwości powłok po obróbce laserowej przeprowadzonych na podstawie obserwacji nowo powstałej struktury materiału, pomiaru przyczepności oraz pomiaru mikrotwardosci.

Słowa kluczowe: powłoki WC-Cu, modyfikacja laserowa, obróbka elektroiskrowa, powierzchnia

1. Introduction

Due to new market demands, it is advisable to create new protective layers for machine parts if their fragments or surface layer are worn, and if the surface layer requires other features than the core. Currently, there is a growing role of machining using a concentrated energy stream, which is used primarily in the machining of components from difficult-to-machine construction plastics, as well as for parts with very complex shapes, which would be too labor-intensive and time-consuming to use as traditional methods. In this group of treatments, those that use broadly understood erosion, often supported by electrical energy, such as electro-erosion machining, can be mentioned.

The electrospark deposition (ESD) process is a surface treatment technique used to produce hard and wear resistant coatings on various metallic materials. It uses high current/low voltage electrical pulses of short duration to coat electrode material (anode) with a substrate (cathode) [1]. During the process, energy stored from high voltage capacitors is discharged through an electrode of the material to be deposited. Thus, a small molten part of the material is removed from the electrode and coated to the substrate in the form of a sudden spark [1, 2].

Electrospark deposition is a cheap and efficient way to improve the usable properties of metal. The use of a laser beam to smoothen the coatings applied by the spark erosion method should ensure a reduction of surface roughness and change in the shape of the unevenness profile. The purpose of laser compaction is to reduce the porosity of the coating and to eliminate cracks, delaminations and cracks in the surface of the coating, which results in a significant improvement in the integrity of the coating [1-4].

2. Materials

Based on literature and our own experiences, we have developed a powder blend, which has been produced by powder metallurgy methods for coating electrodes ESD. The tests were performed on the WC-Cu (50–50%) coating produced on the normalized C45 grade steel specimens by electrospark deposition. The coatings were deposited in the argon atmosphere with the use of an EIL-8A pulse generator for triggering spark gaps, with manual electrode displacement [5–7].

The following parameters were established in compliance with the manufacturer's guidelines and previous experience of the authors:

- ► voltage $U = 230$ V;
- ► capacitor volume $C = 150$ μF;
- ► current intensity $I = 0.7$ A;
- ► deposition time $\tau = 2$ min/cm^2.

The coatings were subjected to laser treatment at the Centre for Laser Technology of Metals. A BLS 720 Nd:YAG laser capable of generating 150 W maximum average power was used, operating in the pulse mode, manufactured by Baasel Lasertechnik. The laser treatment was performed in the ambient air atmosphere. The tests used a focusing head. The TEM$_{00}$ beam defined the radiation energy distribution. The parameters used were as follows:

- ▸ spot diameter $d = 0.7$ mm;
- ▸ laser power $P = 60$ W;
- ▸ specimen movement rate $v = 250$ mm/min;
- ▸ nozzle-workpiece distance $\Delta l = 1$ mm;
- ▸ pulse duration $t_i = 0.4$ ms;
- ▸ pulse repetition frequency $f = 50$ Hz;
- ▸ beam shift jump $S = 0.4$ mm.

2.1. Adhesion and microhardness tests

Measurements of the adhesion of WC-Cu coatings (50% WC and 50% Cu) before and after laser treatment were made using the scratch test method. A REVETEST device from the Swiss company CSEM was used for the measurements. The measurements were carried out with the following scratch test parameters: load growth rate – 103.2 N/min; speed of table advance with the sample – 9.77 mm/min; crack length – 9.5 mm; Diamond Rockwell cone with rounding radius – 200 μm.

The scratch test consisted in making the scratches with a properly selected penetrator (in this case a diamond cone – Rockwell) with a gradual increase in normal force (loading the penetrator) with simultaneous measurement of the resistance force of the material (tangential force) and recording of acoustic emission signals which informed about the formation damage to the layer in the form of cracks or peeling of the layer. The lowest normal force causing a loss of adhesion of the coating with the substrate is called the critical force and is taken as a measure of this adhesion.

To assess the value of the critical force, the change of acoustic emission and tangential force signals as well as microscopic observations (optical microscope built into the REVETEST apparatus) is used. In the tests that were carried out, values of critical forces were evaluated on the basis of microscopic observations of the resulting scratches after passing of the penetrator, which were referred to the course of acoustic emission signals. The sample results are presented in Table 1, which contains the values of critical forces from three measurements of a given sample and their average values calculated.

 Electro discharge coatings had comparable adhesion. The average value (from three measurements) of the WC-Cu coating's critical force was 7.70 N. The laser treatment improved the adhesion of the WC-Cu coating to 24% without this treatment. Higher adhesion of laser treated coatings may be caused by limiting their porosity and thus improving their tightness. However, detailed arrangements regarding this problem will be implemented in the next stages of the research.

The microhardness was determined using the Vickers method. The measurements were performed under a load of 0.4 N. The indentations were made in perpendicular microsections in three zones: the white homogeneous difficult-to-etch coating, the heat affected zone (HAZ) and the substrate. The test results for the ESD WC50-Cu50 coating before and after laser treatment are shown in Table 2. The laser treatment of the ESD coating caused a slight decrease in the microhardness of both the coating and heat affected zone.

Table 1. Results of adhesion measurements

Coating	Critical power [N]			Average value [N]
	Number of the measurement			
	1	2	3	
WC-Cu	8.19	8.56	6.34	7.70
WC-Cu+laser (P = 60 W)	9.56	10.17	8.86	9.53

Table 2. Results of microohardness tests

Coating	Microhardness HV0.4		
	Coating	HAZ	Substrate
WC-Cu	643 ± 54	438 ± 23	278 ± 18
WC-Cu+laser (P = 60 W)	617 ± 21	407 ± 22	279 ± 7

2.2. Microstructure testing

Microscopic examinations were carried out on samples made in a plane perpendicular to the applied surface, which gives the possibility of observing the characteristic areas of the material to be tested, its structure and enables measurements of the thickness of applied coatings. The photo (Fig. 1) presents an example of the microstructure of the WC-Cu coating (50% WC and 50% Cu) applied by electro-discharge treatment on steel C45.
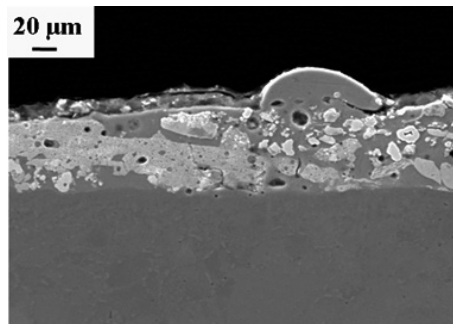

Fig. 1. Microstructure of the WC50%-Cu50% coating

The photo shows an example of a microstructure of the WC-Cu coatings coated electro-spark deposition. Based on the obtained results, it was found that the thickness of the obtained layers was from 36 μm to 60 μm, while the range of the heat affected zone (SWC) into the ground material was from about 20 μm to 30 μm. In the photo of the microstructure shown, there is a clear boundary between the coating and the substrate, and pores and microcracks can be observed.
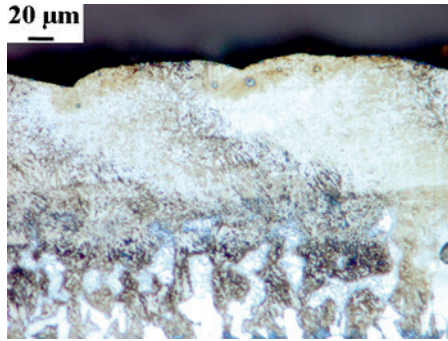
Fig. 2. Microstructure of WC50%-Cu50% coating after laser treatment with P-60W

As a result of the laser beam modification of the WC-Cu coatings applied with electro eroding and the subsequent coagulation, their chemical composition has changed. Laser treatment has homogenized the chemical composition of the coating (Fig. 2). There was also fragmentation of the structure and crystallization of highly supersaturated phases due to the occurrence of significant temperature gradients and obtaining high cooling rates. The TWP produced as a result of laser treatment did not have microcracks and pores and discontinuities at the boundary layer – substrate. The thickness of laser-treated WC-Cu coatings ranged from 40μm to74 μm. The SWC, created as a result of laser irradiation, had a range of 30–45μm and this is related to the higher density of laser processing power in relation to EDM.

3. Conclusions

Based on the research carried out so far and after analyzing their results, we can conclude that:
- ▸ A concentrated beam of laser beam can effectively modify the state of a material layer and thus improve the performance.
- ▸ The use of WC-Cu coatings imposed on electro-sparking increased the operating properties, in particular, increased their usability
- ▸ Laser irradiation of coatings assists in healing of micro-cracks and pores.
- ▸ The laser treatment of the ESD coating caused a slight decrease in microhardness of both the coating and heat affected zone.

References

[1] Radek N., *The influence of laser treatment on the microstructure and properties of the tungsten carbide electrospark coatings,* Adv. Manuf. Sci. Tech., 35, 2011, 59-71.
[2] Thamer A.D., Hafiz M.H., Mahdi B.S., *Mechanism of building-up deposited layer during elektro-spark deposition,* Journal of Surface Engineered Materials and Advanced Technology, 2, 2012, 258-263.

[3]   Jahan M.P., Rahman M., Wong Y.S., *A review on the convetional and micro-electrodischarge machining of tungsten carbide,* International Journal of Machin Tools & Manufacture 51, 2011, 837-858.

[4]   Radek N., Antoszewski K., Pliszka I., Shalapko J., *Properties and applications of carbide and ceramic coatings applied with erosio*n, Mechanik Nr 4/2015, 163-167.

[5]   Chang-bin T., Dao-xin L., Zhan W., Yang G., *Electro-spark alloying using graphite electrode on titanium alloy surface for biomedical applications,* Applied Surface Science, 257, 2011, 6364-6371.

[6]   Ozimina D., Scholl H., Styp-Rekowski M., *Forming of anti-wear surface layers by EDM treatment. Selected issues of machining with a concentrated energy beam,* chapter 2, 2003, 104-109.

[7]   YI W., Dang-Sheng X., *The effect of laser surface texturing on frictional performance of face seal,* Vol. 197 Journal of Materials Processing Technology, 2008.

Jolanta Radziszewska-Wolińska
jradziszewska-wolinska@ikolej.pl

Danuta Milczarek
Materials and Structure Laboratory, Railway Institute

Norbert Radek
Faculty of Mechatronics and Mechanical Engineering, Kielce University of Technology

Łukasz Pasieczyński
Firma Handlowa BARWA Jarosław Czajkowski

Michal Petru
Institute for Nanomaterials, Advanced Technologies and Innovations, Technical University of Liberec

Influence of composition of anti-graffiti coating system used in rolling stock on fire end structure properties

Wpływ składu systemu powłokowego antygraffiti na właściwości ogniowe i strukturalne

Abstract

The paper discusses fire parameters of individual layers of anti-graffiti coating systems proposed for use in rail transport. Modifications and their effect on flammable properties of these coatings have been described. Performed tests included, first of all, parameters such as lateral spread of flame over the surface and heat emission, whose fulfillment proved the most difficult in the previous studies. For this purpose, polyester putties were tested on an epoxy primer. Then, fire parameters for different anti-graffiti systems containing a swelling layer as an additional protective layer were determined.

Keywords: fire tests of railway materials, critical heat flux at extinguishment, lateral spread of flame on products, cone calorimeter, maximum average rate of heat emission, fire safety

Streszczenie

W artykule omówiono parametry ogniowe poszczególnych warstw systemu malarskiego antygraffiti proponowanego do zastosowania w transporcie szynowym. Opisano modyfikacje systemu i ich wpływ na właściwości palne tej powłoki. Przeprowadzone badania obejmowały przede wszystkim takie parametry, jak rozprzestrzenianie płomieni na powierzchni i emisję ciepła, których spełnienie w poprzednich badaniach okazało się najtrudniejsze. W tym celu przeprowadzono testy szpachli poliestrowej na podkładzie epoksydowym. Następnie określono parametry ogniowe dla różnych systemów antygraffiti zawierających warstwę pęczniejącą jako dodatkową warstwę ochronną.

Słowa kluczowe: badania ogniowe materiałów kolejowych, krytyczny strumień ciepła podczas gaszenia, boczne rozprzestrzenianie się płomienia po powierzchni, kalorymetr stożkowy, maksymalna średnia szybkość emisji ciepła, bezpieczeństwo przeciwpożarowe

1. Introduction

An important effect of the existing fire (posing a deadly threat to passengers and impeding evacuation) is the spread of flames on the surface as a result of combustion of materials used in railway vehicles. European Standard EN 45545-2 [1] introduced the need to meet new requirements in terms of fire properties for paint systems too. This requirement proved difficult to reconcile with physical and mechanical requirements of coatings in the functional scope, i.e. allowing ease of application and maintaining protective and decorative properties as long as possible. The above has become a challenge for the paint industry, trying to develop new or modify existing products. The works were started by testing the impact of different variants of the anti-graffiti coating on properties of the entire paint system. However, the values of the specified CFE and MARHE parameters were significantly different from the admissible criteria. However, due to the fact that the coating had a negligible thickness in relation to the thickness of the entire system subjected to combustion as part of laboratory tests, no significant influence of the applied anti-graffiti layer on the test results was demonstrated [2]. Therefore, in the next stage of the work, the effect of the thickness of the putty layer on the properties of the entire system was determined, and then an additional protective layer was introduced into the system.

2. Laboratory tests of fire properties

To assess fire resistance, fire parameters were selected that characterize the material's resistance to external fire sources, i.e.:
1. CFE – critical heat flux, kW/m^2 (the lower its value, the greater the fire hazard) according to ISO 5658-2 [3] (Figs. 1 and 2),
2. MARHE – maximum average rate of heat release kW/m^2 – (the higher its value, the greater the fire hazard), according to ISO 5660-1 [4] (Fig. 3).
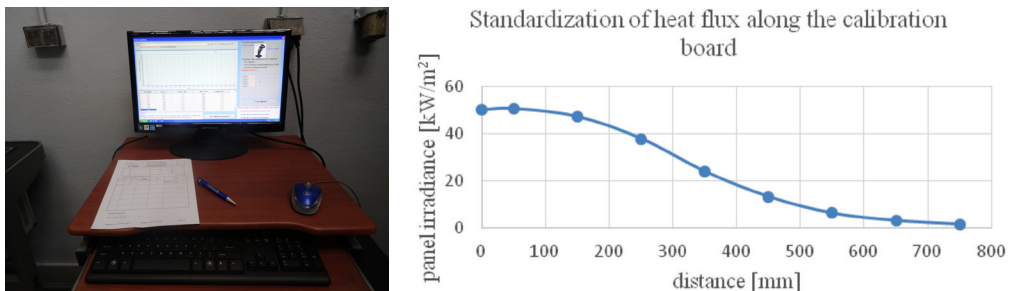

Fig. 1. Standardization of flux along the calibration board

All the tested coatings were applied to 1 mm thick S355 steel plates. Paint systems for rolling stock must also fulfill mechanical and qualitative properties to protective and decorative properties maintenance longer on the vehicle. These requirements include

adhesion, resistance to weather conditions (humidity, UV, corrosion) as well as hardness and specialized properties such as anti-graffiti. Coating systems intended for rolling stock ,in addition to the above-mentioned requirements as well as ease of application and operation, must also have adequate fire performance [5, 6].
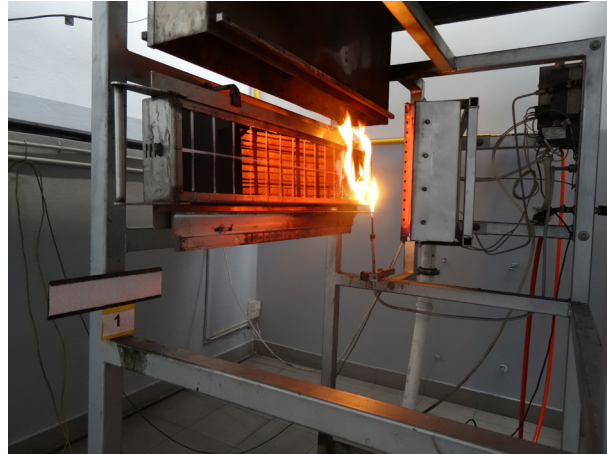

Fig. 2. The sample during test in Railway Institute according to ISO 5658-2

Fig. 3. The sample during test in Railway Institute according to ISO 5660-2

The quality of the putty affects the parameters of the entire system, and especially its flexibility, resistance to extrusion, scratching and impact, as well as the flammable and smoke

properties. As a preliminary study aimed at directing further modification work, the impact of the thickness of the putty on its fire properties in terms of flame propagation was determined. LongLife polyester putties with a thickness of 1000 μm, 2000 μm and 3000 μm were prepared on an 80 μm thick epoxy primer SPR91001.

In the next stage of the work, an intumescent layer was introduced into the system in order to limit the impact of the ignition source operation on the lower layers, especially on the putty. The first CFE tests were carried out for the system with anti-graffiti XPC 60036 in two variants, i.e. using a 200 μm intumescent paint placed as the third or as the fourth layer. In both cases, a putty thickness of 2000 μm was assumed.

Then, further research was undertaken to determine the required thickness of the intumescent layer, placed as the third layer in the system, to meet the requirements for CFE. The tests were carried out for the thickness of 200 μm, 400 μm and 600 μm. As a protective layer against graffiti, BO-100AGR varnish with the best physical and chemical properties was used in all samples.

3. Results and discussion

A microstructure analysis was conducted for anti-graffiti coating systems using a JEOL JSM-7100F scanning electron microscope with field emission and a Hirox KH-8700 light microscope.
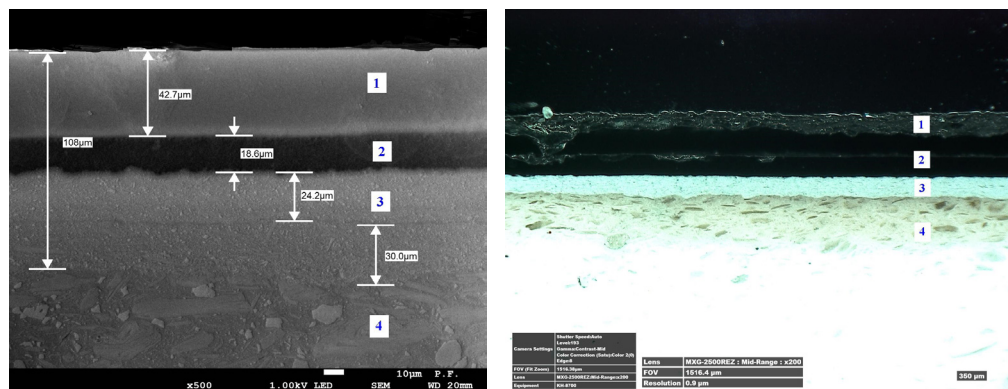

Fig. 4. SEM (left) and LM (right) micrographs of the polished cross-section through an anti-graffiti O-100AGR coating system on S355 carbon steel substrate: 1 – anti-graffiti layer, 2 – base layer, 3 – undercoat layer, 4 – putty

The thickness of the obtained coating systems was from approx. 2350 to approx. 2450 μm. There are clear boundaries between the individual layers (Fig. 4). Fig. 4 shows a clear boundary between the varnish layers and the putty. Also, the varnish layers are free of pores and microcracks.

A putty is the thickest layer in the coating systems applied to the external walls of rail vehicles. The above results from the desire to hide all inequalities and obtain the maximum flatness of the painted surface of the wagon body shells. The research began with the first two parameters, whose fulfillment in the previous studies proved the most difficult. The obtained impact of the polyester putty on an epoxy primer is presented in Table 1.

Table 1. The results of fire tests for sample of polyester putty

No of sample	Coating system layer	Layer thickness, [μm]	CFE, [kW/m²]	MARHE, [kW/m²]
A8/16	SPR91001	80	8.9	126.6
	LongLife	1000		
A9/16	SPR91001	80	8.6	158.6
	LongLife	2000		
A10/16	SPR91001	80	8.2	161.1
	LongLife	3000		
Requirement according to EN45545-2			> 20	< 90

The carried out tests confirmed the high impact of putty on the negative results of entire paint systems. At the same time, it was found that the effect of the layer thickness on the determined parameters from 2000 μm is reduced.

The obtained results of the paint system with a swelling layer are presented in Table 2 and Table 3.

Table 2. CFE test results for system sample with XPC 60036 and intumescent layer

No of sample	Coating system layer	Layer thickness, [μm]	CFE, [kW/m²]
A180/16	SPR91001	80	15.1
	LongLife	2000	
	Intumescent layer	200	
	XPP40003	60	
	XPB710	40	
	XPC60036	60	
A180.1/16	SPR91001	80	13.9
	LongLife	2000	
	XPP40003	60	
	Intumescent layer	200	
	XPB710	40	
	XPC60036	60	
Requirement according to EN45545-2			> 20

As can be seen in Table 2, more favorable values were obtained for the first variant, i.e. at the intumescent layer placed lower.

Table 3. CFE test results for system sample with BO-100AGR and intumescent layer

| No of sample	Coating system layer	Layer thickness, [µm]	CFE, [kW/m²]
A209/17	SPR91001	80	16.3
	LongLife	2000	
	Intumescent layer	200	
	XPP40003	60	
	XPB710	40	
	BO-100AGR	60	
A210/17	SPR91001	80	17.5
	LongLife	2000	
	XPP40003	60	
	Intumescent layer	400	
	XPB710	40	
	BO-100AGR	60	
A211/17	SPR91001	80	20.3
	LongLife	2000	
	XPP40003	60	
	Intumescent layer	600	
	XPB710	40	
	BO-100AGR	60	
Requirement according to EN45545-2			> 20
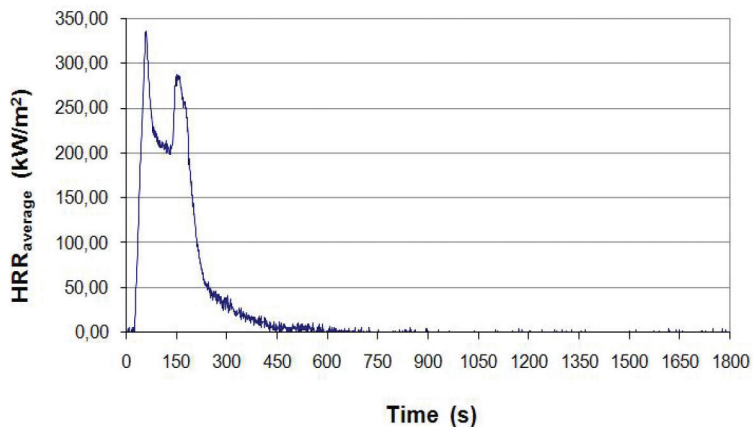
Fig. 5. HRR$_{average}$ heat releasing curve for anti-graffiti BO-100AGR

As a result, the thickness of the swelling layer of 600 μm allowed for obtaining a borderline, positive CFE value. Figure 5 shows an example of $HRR_{average}$ heat releasing curve for tested sample. You can see that bigger thickness of intumescent layer delays ignition and causes less heat emission.

4. Summary

The laboratory tests carried out allow us to state that the introduction of the swellable paint test as the 3rd layer of the coating into the paint system is the right direction of modification in order to protect the system against fire spread.

References

[1] PN-EN 45545-2: Railway applications – Fire protection on railway vehicles – Part 2: Requirements for fire behaviour of materials and components.
[2] Pasieczyński Ł., Radek N., Radziszewska-Wolińska J., *Operational properties of anti-graffiti coating systems for rolling stock*, Advances in Science and Technology Research Journal, 12, 1, 2018, 127–134.
[3] ISO 5658-2:2006 Reaction to fire tests – Spread of flame. Part 2: Lateral spread on building and transport products in vertical configuration.
[4] ISO 5660-1:2015 Plastics – Reaction-to-fire tests-Heat release, smoke production and mass loss rate – Part 1: Heat release rate (cone calorimeter method) and smoke production rate (dynamic measurement).
[5] Radziszewska-Wolińska J., *Fire properties of anticorrosion coatings to rolling stock*, Czasopismo Techniczne, 3-M/2016, 79–86.
[6] Radziszewska-Wolińska J., *Development of requirements for fire protection of rolling stock in Poland and its comparison with EN 45545*, Problemy Kolejnictwa, 57, 160, 2013, 109–119.

Robert Ulewicz
robert.ulewicz@wz.pcz.pl
    Department of Production Engineering and Safety, Czestochowa University
    of Technology, Poland

František Nový
    Faculty of Mechanical Engineering, University of Žilina, Slovakia

Influence of laser treatment on properties of high speed tool

Wpływ obróbki laserowej na własności stali szybkotnącej

Abstract

The paper presents the results of heat treatment tests of HS6-5-2 high speed steel with laser working in continuous mode. The tests used steel in the delivery state as well as steel after fluid treatment aimed at diffusion enrichment of the surface layer with carbon and nitrogen. The aim of the research is to determine changes in the structure of steel enriched with carbon and nitrogen and then subjected to the impact of the laser beam.

Keywords: laser heat treatment, high-speed tool steel

Streszczenie

W artykule przedstawiono wyniki badań obróbki cieplnej laserem pracującym w trybie ciągłym stali szybkotnącej HS6-5-2. W badaniach wykorzystano stal w stanie dostarczenia, jak również stal po fluidalnej obróbce mającej na celu wzbogacenie dyfuzyjne warstwy wierzchniej w węgiel i azot. Celem badań jest określenie zmian struktury stali wzbogaconej w węgiel i azot, a następnie podanej oddziaływaniu wiązki lasera.

Słowa kluczowe: obróbka laserowa, stal narzędziowa szybkotnąca

1. Introduction

The use of laser machining for parts of machines and tools, e.g. cutters or drills, creates a number of possibilities for improving their functional properties. The demand for new, more durable and harder tools has resulted in the increased interest in new methods of heat treatment [1–3]. One of the methods of obtaining more supersaturated structures with a higher than in the conventional grain refining processing, which arise as a result of the action on high energy material in a short time is laser treatment. Moreover, low costs, the possibility of full automation and high accuracy contributed to the use of lasers for industrial purposes. By using laser, we obtain a hard, abrasion-resistant surface layer of steel while maintaining the ductility of the core [4–7]. In case of laser processing, the power density and duration of laser radiation on the material have a decisive influence on the thickness and structure, and thus the properties of the surface layer [10–12]. The diffusional enrichment of the surface layer with carbon and nitrogen applied earlier is aimed at improving the functional properties of the surface layer of high-speed steels [8, 9]. The purpose of the work is to determine the effect of diffusion and laser treatment on the structure and hardness of the top layer of HS6-5-2 high speed steel tool.

2. Material and methodology of research

The HS6-5-2 high speed tool steel with the chemical composition shown in Table 1 constituted the test material.

Table 1. HS6-5-2 steel chemical composition

C	Mn	Si	Cr	W	Mo	V	P	Co	Cu	Ni	S
0.88	0.40	0.49	4.33	6.61	4.82	2.05	0.03	0.07	0.015	0.15	0.02

Plate-shaped samples with dimensions of 120 x 15 x 8 mm were prepared for the tests. The samples were then subjected to diffusion in coal and nitrogen in a fluidized bed, with the following parameters:

- nitrocarburizing temperature 1153 K,
- time 3.6 ks,
- air excess coefficient α_p 0.22,
- addition of ammonia to the atmosphere of 2.5%.

The sample after diffusion enrichment after being removed from the furnace is cooled in the air. As a result of diffusion enrichment, an enriched layer with a carbon content in the range of 1.1 to 1.3% and nitrogen 0.15% was obtained.

Molecular CO_2 laser was used for the tests, where the active medium is a mixture of gases composed of CO_2, helium and N_2. It emits infrared radiation with a wavelength of 10.63 µm. It is created as a result of the return of CO_2 particles to the basic level.

Laser processing was performed by increasing the focusing size Δf. The laser treatment parameters are shown in Table 2.

Table 2. Parameters of laser treatment

No.	Δf [mm]	Power Q [W]	Speed shift [mm/s]	diameter beam d [mm]	Power density g [10^3 W/cm^2]
1.	12	800	12	2.8	13
2.	16	800	12	3.73	7.3
3.	24	800	12	5.6	3.3
4.	28	800	12	6.53	2.4
5.	32	800	12	7.46	1.8

In order to characterize the structure obtained after hardening, tests were carried out using optical and scanning microscopy as well as x-ray examinations. The measurements of the microhardness distribution in the hardened layer of the Vickers method at 100 G load were also made. Metallographic smudges were made in planes perpendicular to the lines (paths) defined by the laser beam. In order to reveal the structure of the zone affected by laser radiation and the structure of the matrix, 5% of nital was used.

3. Results and discussion

The purpose of the work is to determine structural changes of HS6-5-2 steel resulting from the modification of its surface by diffusion enrichment in C and N, followed by laser hardening with a beam of different power density. The size and distribution of microhardness in the hardened layers was also determined. Figure 1 shows the distribution of microhardness of the surface layer enriched with carbon and nitrogen without affecting the laser beam. Figure 2 shows the distribution of microhardness after laser treatment with the power of:
- sample 1 – 13 · 10^3 W/cm^2,
- sample 2 – 7.3 · 10^3 W/cm^2,
- sample 3 – 3.3 · 10^3 W/cm^2,
- sample 4 – 2.4 · 10^3 W/cm^2,
- sample 5 – 1.8 · 10^3 W/cm^2.

In case of sample 1, a hardened layer consisting of four zones was obtained:
- the first zone is made of remelting material,
- second zone – melted,
- third zone – laser hardening,
- fourth zone laser remission.

All zones together have a thickness of 415 µm, assuming, as a criterion, hardness higher than the hardness of the core. The thickness of the melted zone is 190 µm. On this basis, the hardness of this zone was obtained at 750 HV. As we approached the second laser hardening zone, the hardness increased reaching a maximum of 1270 HV at a distance of 260 µm from the surface. The thickness of the third zone is estimated at approximately 100 µm. Then the hardness decreases, but it is higher than the hardness of the core. The hardness of the core is
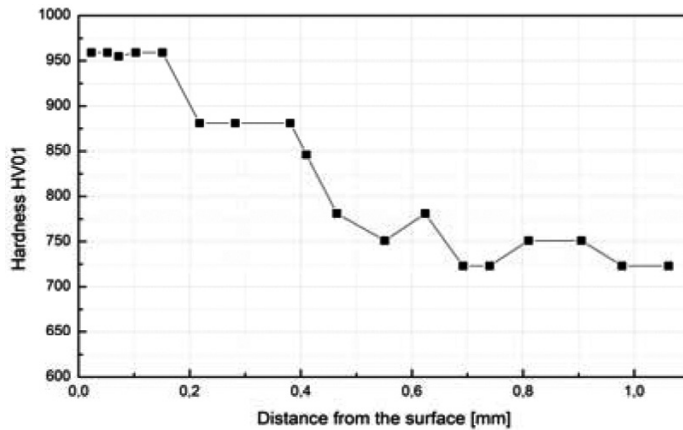
Fig. 1. Distribution of microhardness in the layer enriched in C and N without laser treatment
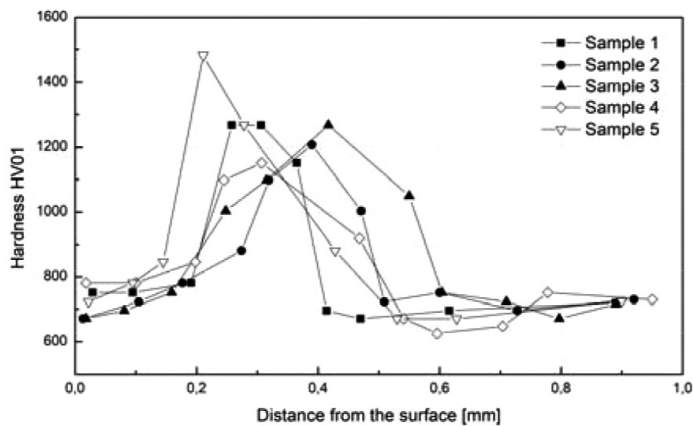

Fig. 2. Distribution of microhardness in the layer enriched in C and N after laser treatment

variable because it reaches values of 670–720 HV, which is related to the bandwidth of the parent material.

The effect of the laser beam on the surface of the sample is related to the change in beam diameter and power density. For sample 1, the beam width was 1.523 mm and affected a depth of 415 μm. For sample 2, the width of the beam impact path was 1.958 mm and the impact depth was 508 μm. Sample No. 3 impact field, the beam width was 2.50 mm and depth was 615 μm. Sample No. 4, the applied power density was $2.4 \cdot 10^3$ W/cm^2, and the resulting hardened area has a width of 2,831 mm and a depth of 692 μm. The last 5 sample using the $1.8 \cdot 10^3$ W/cm^2 beam power was acting in an area which was 3.107 mm wide and 246 μm deep. The reduction of hardness in the laser tempering zone is most probably caused by the decay of martensite and the coagulation of carbides. As a result of the conducted treatment, it was found that carbitic type M_4C_3 (V_4C_3) carbides exist in the nitro-nitrided layer. The amount of M_3C and M_2C carbides also increased. In this layer, large quantities of MoC carbide and the Mn_4C type phase of varying composition were formed, while the amount of $M_{23}C_6$ carbide decreased.

4. Summary

The thermo-chemical treatment in a fluidized bed assured obtaining a surface layer with fine-grained martensitic structure with a large number of coagulated alloy carbides formed during cooling due to the decreasing solubility of carbon in the austenite as well as those formed during the carburizing process. As a result of cooling of the samples in the air, the thin surface layer was decarburized. This is confirmed by the reduced amount of carbides compared to deeper situated zones. Saturation with carbon and nitrogen is variable at the thickness of the layer, which manifests itself in the microhardness distribution of this layer (Fig. 1, 2). Microhardness and microstructure testing confirm that along with the change of beam parameters, the width of the hardened layer increased, the depth grew in samples from 1 to 4, while in sample 5 the depth of the hardened zone decreased as compared to other samples. In sample 5, the applied power density turned out to be insufficient to cause a further increase in the depth of the hardened zone. This state of affairs, however, is beneficial.

References

[1]   Radek N., Antoszewski B., Pliszka I., Świderski J., Pietraszek J., *Production of heterogeneous surfaces by ESD and LBM*, Production Engineering Archives 13, 2016, 44–48.

[2]   Lipinski T., Wach A., *Influence of outside furnace treatment on purity medium carbon steel*, in. Conf. 23rd International conference on metallurgy and materials, Brno 2014, 738–743.

[3]   Scendo M., Trela J., Radek N., *Influence of laser power on the corrosive resistance of WC-Cu coating*, Surface & Coatings Technology 259, 2014, 401–407.

[4]   Bramowicz M., Kulesza S., Lipiński T., Szabracki P., Piątkowski P., *Fractal analysis of AFM data characterizing strongly isotropic and anisotropic surface topography*, Solid State Phenomena 203, 2013, 86–89.

[5]   Radek N., Pietraszek, B, Antoszewsk A., *The Average Friction Coefficient of Laser Textured Surfaces of Silicon Carbide Identified by RSM Methodology,* Advanced Materials Research 874, 2014, 29–34.

[6]   Radek N, Bartkowiak K., *Laser treatment of electro-spark coatings deposited in the carbon steel substrate with using nanostructured WC-Cu electrodes,* Physics Procedia 39, 2012, 295–301.

[7]   Zhang YC, Yang L., Chen TY., Zhang WH., Huang XW., Dai J., *Investigation on the optimized heat treatment procedure for laser fabricated IN718 alloy*, Optics And Laser Technology, 97, 2017, 172–179.

[8]   Lago J., Bokuvka O., Novy F., *The weld toe improvement of advanced HSLA steel by laser remelting,* Materials Today-Proceedings, 3/4, 2016, 1037–1040.

[9]   Sebek M., Falat L., Kovac F., Petryshynets I., Hornak P., Girman V., *The Effects Of Laser Surface Hardening On Microstructural Characteristics And Wear Resistance Of Aisi H11 Hot Work Tool*, Archives Of Metallurgy And Materials, 62/3 (2017) 1721–1726.

[10] Przybyłowicz K., Depczyński W., Konieczny M., *Wpływ gęstości mocy promieniowania laserowego na strukturę i własności lanej stali szybkotnącej*, IM, nr 5, 1999.

[11] Preece C. M., Draper C. W., *The effect of laser quenching the surfaces of steels on their cavitation erosion resistance*, Wear 1981, Vol. 67, 321–328.

[12] Mierzewiński D., Walter J., *Laser Surface layer modification*, Technical Transaction, 2-M/2009, 53–58.

Wojciech Żórawski
ktrwz@tu.kielce.pl

Szymon Kowalski
Center for Laser Technologies of Metals, Kielce University of Technology

Janusz Mądry
Jarosław Sienicki
PZL Mielec A Sikorsky Aircraft Company

Anna Góral
Institute of Metallurgy and Materials Science, Polish Academy of Sciences, Kraków

Medard Makrenek
Faculty of Management and Computer Modelling, Kielce University of Technology

Additive manufacturing of titanium with application of cold spray process

Technologia przyrostowa tytanu z zastosowaniem procesu natryskiwania zimnym gazem

Abstract

Cold spraying is a new technology which can be used in the area of additive manufacturing. This method is suitable for oxygen-sensitive materials, such as titanium. In this paper the microstructure and mechanical properties of cold sprayed titanium deposit were characterized.

Keywords: additive manufacturing, cold spraying, titanium

Streszczenie

Natryskiwanie zimnym gazem jest nową technologią, która może być wykorzystana również w technologiach przyrostowych. Ta metoda jest odpowiednia dla materiałów łatwo utleniających się takich jak tytan. W artykule scharakteryzowano mikrostrukturę i właściwości mechaniczne natryskanej zimnym gazem tytanowej struktury.

Słowa kluczowe: technologie przyrostowe, natryskiwanie zimnym gazem, tytan

1. Introduction

New low-cost manufacturing technologies are the base for further development for many branches of industry. Titanium with high strength to weight ratio and excellent corrosion resistance in many media including seawater is an irreplaceable material for many applications in aerospace [1, 2]. Currently used technologies for manufacturing titanium components which involve casting, forging, extrusion and machining are expensive and labor-consuming. Moreover, production process of many parts leads to significant losses of material that can reach up to 60%. Therefore, direct producing of titanium is crucial in aviation industry. Additive manufacturing technology allows for manufacturing parts of machines based on a layer by layer deposition. This process allows for producing components with complex shapes and additionally significantly lower time and cost. Recently, cold spraying has joined the group of applied additive technologies as selective laser sintering (SLS) or direct metal deposition (DMD) [3–5].

Cold gas spraying technology was developed in the mid-1980s by a team of prof. A. Papyrin at the Institute of Theoretical and Applied Mechanics in Novosibirsk. The principle of the cold gas injection process is to compress and heat the gas to 1373 K and then accelerate it to supersonic speed (2–4 Ma) in a de Laval nozzle. As the gas flows through the divergent part of the nozzle, it decomposes to a significant temperature drop, even below the ambient temperature, hence the name "cold gas spraying" [6]. The powder coating material is coaxially injected into the gas stream and reaches a velocity of 300 to 1200 m/s (Fig. 1) at the moment of impact.
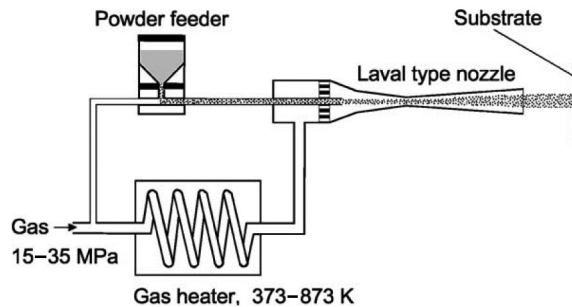

Fig. 1. Principle of cold spraying [7]

In the current operating systems for cold gas spraying, it is compressed to a pressure of 5 Pa at an output of 90 m³/h [8, 9]. The applied powders have different granulation ranges from 1 to 50 μm. As a working gas, nitrogen, helium, air or their mixtures are used. A lower cost is the advantage of nitrogen, but if higher speeds are required, helium is used. Because of its much higher cost, it is added to nitrogen to achieve the desired velocity of the gas stream, and when used alone, systems for recovering thereof are installed.

The objective of the presented studies is to analyze the microstructure and mechanical properties of cold sprayed titanium structure for application in additive manufacturing technology.

2. Methodology

Commercially available Ti angular powder with grain size 15 ± 65 µm was used as a starting material. Titanium structure was sprayed on a flat Al 7075 aluminium alloy bar with dimensions of 400 x 30 x 5 mm. The surface of the sample was cleaned to remove contaminations and grit blasted with corundum grit with size 30. During deposition, titanium particles were accelerated in a convergent-divergent nozzle located in the gun of cold spraying system Impact Innovation 5/8 equipped with the Fanuc M-20iA robot at Kielce University of Technology (Fig. 2).

Fig. 2. Impact Innovation 5/8 cold spray system

Nitrogen was applied as the process gas to obtain 4.3 mm thick titanium deposit. The microstructure of the Ti powder and cold sprayed coatings were analysed with the SEM Jeol JSM 7100F and SEM Quanta 3D. Phase composition of the sprayed coatings was studied using D8 Discover Bruker. Porosity of the coatings was evaluated on the base of image analysis according to ASTM-E2109. The Vickers hardness HV0.3 was measured by means of micro-hardness tester Innovatest Nexus 4000. The micromechanical testing of coatings was carried out with the use of the nanoindentation technique (Nanovea) with a Berkovitz indenter (the Olivier and Pharr methodology). Forty nine identations were carried out for titanium structure.

3. Results and discussion

3.1. Microstructure of cold sprayed Ti structures

Figures 3a and 3b show a cross-section of a cold sprayed titanium structure with different magnifications. Despite wide particle size distribution of powder, the microstructure presents a very good bonding between deformed titanium grains (Fig. 3a). Traces of boundaries between strongly deformed particles under impact with high velocity onto substrate are visible (Fig. 3b). Moreover, small pores as a result of incomplete filling of surface irregularities by particles striking surface are well seen.
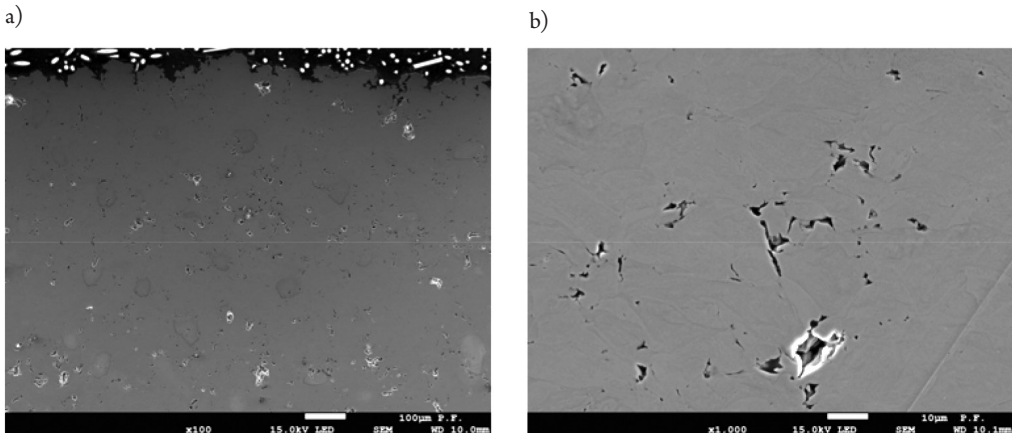
a)   b)

Fig. 3. Cross-section of cold sprayed titanium structure: a) 100x, b) 1000x
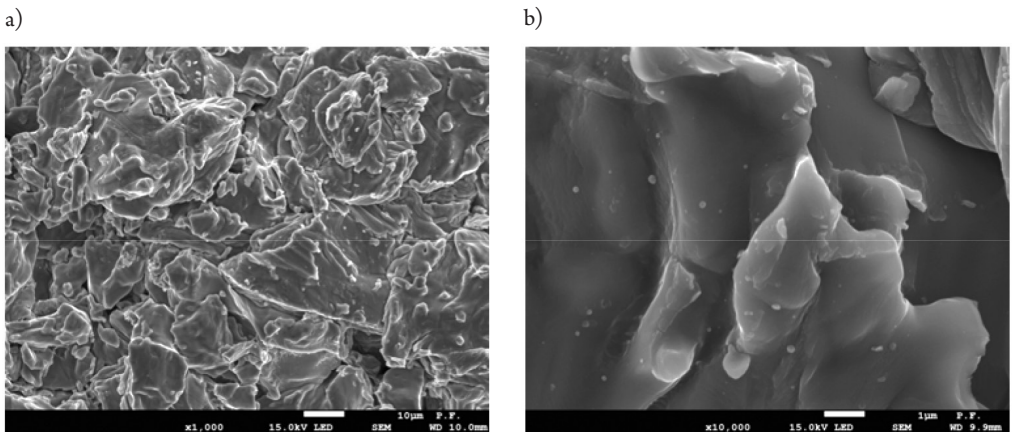
a)   b)

Fig. 4. Surface geometry of cold sprayed titanium structure: a) 1000x, b) 10000x

The microstructure of the surface of cold sprayed titanium structure consists of adjoining plastically deformed titanium particles which form an area with high roughness. Between deformed Ti grains, small voids are present indicating negligible porosity of coatings (Fig. 4a). The porosity of Ti structure estimated on the basis of forty images of cross-section was 2.6±0.8%. Severely flattened grains may be metallurgically bonded (Fig. 4b), which is mainly attributed to the high local temperature increase at the interface due to low thermal conductivity and resultant thermal diffusivity of titanium [10].

3.2. Phase composition

XRD analysis (Fig. 5) showed that the titanium powder and sprayed structure did not contain additional phases in the form of oxides or nitrides which can be formed in high temperature of the spraying stream.
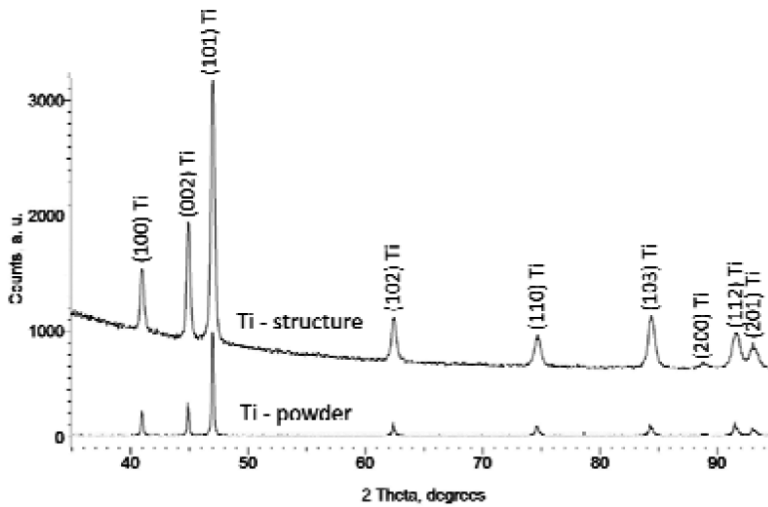

Fig. 5. XRD patterns of Ti powder and cold sprayed

3.3. Mechanical properties

The distributions of the nanomechanical properties were plotted as histogram distributions and maps of surface where each hardness and Young's modulus result was shown on the charts with the same dimensions and locations as in the investigated areas. Histograms and probability distributions of the hardness and Young's modulus of all cold sprayed titanium coatings are shown in Fig. 6.
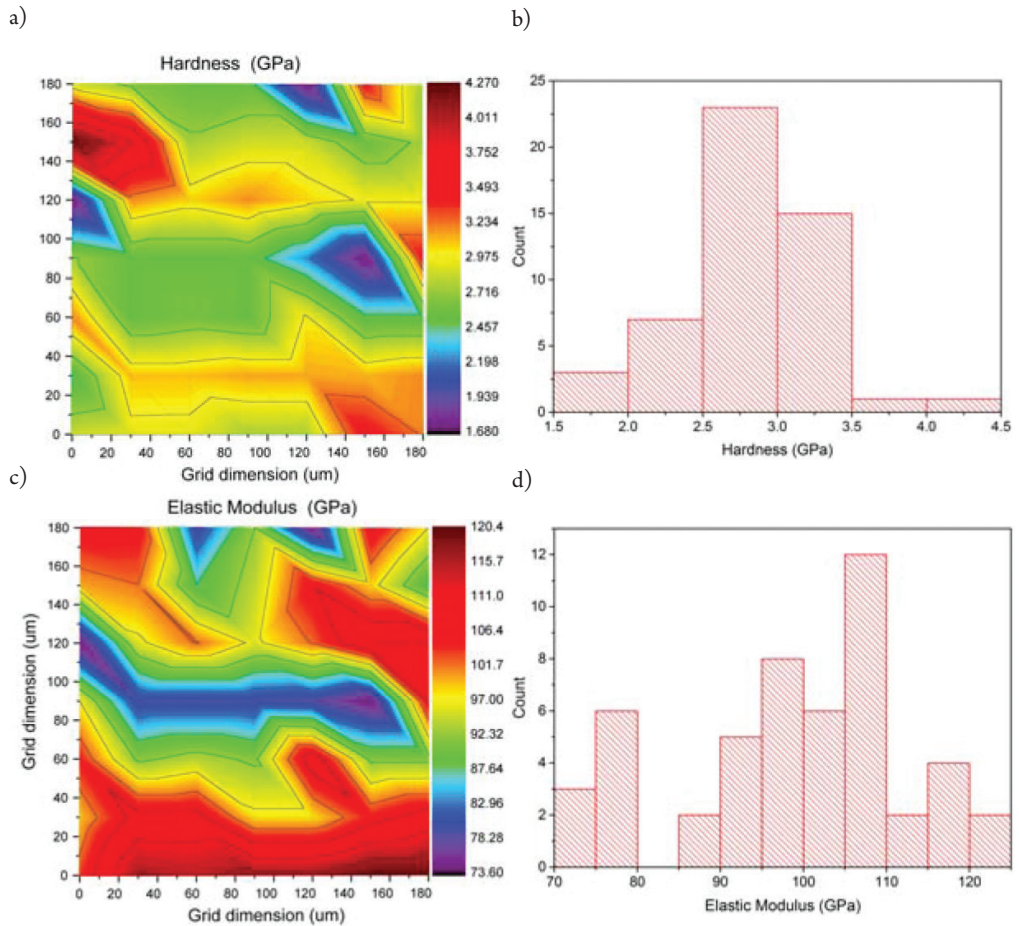
a)

b)

c)

d)

Fig. 6. Distribution of Ti structure coating: a) hardness map, b) hardness histogram and probability, c) Young's modulus map, d) Young's modulus histogram and probability

The nanoindentation tests showed the distribution of mechanical properties (hardness and Young's modulus) related to different areas of titanium structure. Mechanical properties and porosity of cold spayed titanium coatings are presented in Table 1.

Table 1. Properties of cold sprayed Ti structure

Property of Ti structure	H (GPa)	ΔH (GPa)	E (GPa)	ΔE (GPa)
	2.8	0.5	98.8	12.9

4. Conclusions

Microstructures of titanium deposits present a very good bonding between deformed titanium grains and negligible porosity. Severely flattened grains may be metallurgically bonded, which results from high local temperature at the interface. XRD analysis revealed that the titanium powder and sprayed structure did not contain additional phases. The nanoindentation tests showed the distribution of mechanical properties (hardness and Young's modulus) related to different areas of a titanium structure.

References

[1] Hussain T., McCartney D. G., Shipway P. H., Marrocco T., *Corrosion Behavior of Cold Sprayed Titanium Coatings and Free Standing Deposits,* J. of Thermal Spray Technology, 260, Volume 20(1-2), January 2011.

[2] Cinca N., Barbosa M., Dosta S., Guilemany J.M., *Study of Ti deposition onto Al alloy by cold gas spraying,* Surface & Coatings Technology, 205, 2010, 1096–1102.

[3] Raoelison R.N., Verdy Ch., Liao H., *Cold gas dynamic spray additive manufacturing today: Deposit possibilities, technological solutions and viable applications,* Materials and Design, 133, 2017, 266–287.

[4] Villafuerte J., *Considering Cold Sprayfor Additive Manufacturing,* Advanced Materials & Processes 50, May 2014, 50–52.

[5] Blochet Q., Delloro F., N'Guyen F., Jeulin D., Borit F., Jeandin M., *Effect of the Cold-Sprayed Aluminum Coating-Substrate Interface Morphology on Bond Strength for Aircraft Repair Application,* J. of Thermal Spray Technology, 26, 2017, 671–686.

[6] Papyrin A., *Cold Spraying,* Elsewier Ltd. 2007.

[7] Stoltenhoff T., Voyer M., Kreye H., *Cold Spraying – State of the art and applicability,* Proceedings of the ITSC 2002, Essen, 366–374.

[8] Kay C. M., J. Karthikeyan, *High Pressure Cold Spray,* ASM International 2016.

[9] Assadi H., Kreye H., Gartner F., Klassen T., *Cold spraying e A materials perspective,* Acta Materialia, 116, 2016, 382–407.

[10] Bae G., Kumar S., Yoon S., Kicheol K., Na H., Kim H., Lee C., *Bonding features and associated mechanisms in kinetic sprayed titanium coatings,* Acta Materialia, 57, 2009, 5654–5666.

If you want to quote this article, its proper bibliographic entry is as follow: Żórawski W., Mądry J., Sienicki J., Góral A., Makrenek M., Kowalski Sz., *Additive manufacturing of titanium with application of cold spray process,* Technical Transactions, Vol. 10/2018, pp. 201–208.

207